1-1-2007

Rehabilitation of reinforced concrete slab-column system using CFRP sheets.

Wafa Polies
University of Windsor

Recommended Citation

Polies, Wafa, "Rehabilitation of reinforced concrete slab-column system using CFRP sheets." (2007).
Electronic Theses and Dissertations. 6975.
https://scholar.uwindsor.ca/etd/6975

REHABILITATION OF REINFORCED CONCRETE SLAB-COLUMN SYSTEM USING CFRP SHEETS

By

WAFA POLIES

A Thesis
Submitted to the Faculty of Graduate Studies and Research
through Civil Engineering
in Partial Fulfillment of the Requirements for
the Degree of Master of Applied Science at the
University of Windsor

Windsor, Ontario, Canada

2007

© 2007 WAFA POLIES

Canada

ABSTRACT

Flat slabs are commonly used in the construction of buildings and parking structures. Usually, these components are subjected to large shear forces and bending moment. For several reasons, cracks are inevitable in concrete structures, they decrease the structural capacity. In addition, these cracks usually accelerate corrosion of the structure's reinforcement. Due to the high cost of new construction, the need for rehabilitation and upgrade of concrete structures has increased.

This research focuses on the use of carbon fiber reinforced polymer (CFRP) sheets as a competitive technique to reinforce and restore the capacity of a cracked flat-plat slab. Particular attention is paid for the slab-column connection. A series of tests were conducted on six slab-column connections specimens. The effect of the load eccentricity is selected as the main design parameter for this study.

Results show that the ultimate load capacity of the rehabilitated structures increased by an average of 88%. However, the effectiveness of the rehabilitation reduces with the increase of the eccentricity.

DEDICATION

To the candle that burned to brighten our way

To the first who taught me how to search

To my parents

God bless their souls in peace

iv

ACKNOWLEDGEMENTS

Thanks to God, who gave me strength and patience, without his blessing this research work could not have been completed.

This project has been carried out under the supervision and guidance of Dr. Faouzi Ghrib to whom I am profoundly grateful for his kindness, endless constructive commentary and valuable suggestions, continuous support, and encouragement throughout my studies. Dr. Ghrib devoted his time and sincere efforts to provide all necessary research facilities for this work.

In addition, I would like to thank and gratitude my co-advisor, Dr. Khalid Sennah for his guidance, time, and efforts to make this study a success.

I would like to express my appreciation to the committee members: Dr. W. Altenhof, Dr. S. Das and Dr. B. Budkowska for their constructive suggestions to improve this thesis.

Part of this acknowledgment goes to all technical staff: Pattric Seguen, Laucian Pop, Louis Beaudry, and Matthew St. Louis for their assistance in laboratory work.

I would like also to thank my fellow graduate students and friends, for their assistance: Mohamad Abd El-Aziz, Guo quan, and Sami Jasim. Deep appreciation to Anthony Mandarino for his beyond words help.

A special thanks also goes to the faculty and staff of the Department of Civil and Environmental Engineering; the Faculty of Graduate Studies and Research; Academic Writing Centre represented by Mr. Dave Owen; and Leddy Library at the University of Windsor.

Also I would like to thank Stantec Consulting Group Ltd, represented by Stephen Tsui, and Oliver Ng for providing information about the Windsor Dewatering Building project. Finally, I would like to express my grateful thanks and sincere appreciation to my husband, Laith, for his help, and encouragement; and to my lovely children: Rita, Riva, and Ryan for sacrificing many hours while I was away from them.

To all of those people, I would like to say God bless you.....

TABLE OF CONTENTS

CHAPTER

I. **INTRODUCTION**

II. **BACKGROUND AND LITERATURE REVIEWREVIEW**

III. EXPERIMENTAL PROGRAM

IV.   EXPERIMENTAL RESULTS AND ANALYSIS

V.   CONCLUSIONS AND RECOMMENDATIONS

LIST OF TABLES

TABLE

LIST OF FIGURES

FIGURE

xiv

xviii

xix

xxii

CHAPTER I

INTRODUCTION

1.1 General

Structural concrete refers to all types of concrete used in structural applications. Concrete has its first modern record as early as 1760. In 1796, J. Parker discovered Roman natural cement, and 15 years later Vicat burned a mixture of clay and lime to produce cement. In 1824, Joseph Aspdin manufactured Portland cement in Wakefield, Britain. In 1854, W. B. Wilkinson of England obtained a patent for a concrete floor reinforced by twisted cables. The Frenchman Francois Cignet obtained his first patent in 1855 for a system he used of iron bars, embedded in concrete floors that extended to the supports. Joseph Monier registered a patent to use it in beams and columns. In the United States, Thaddeus Hyatt conducted flexural tests on 50 beams that contained iron bars as tension reinforcement and published the results in 1877. He used prefabricated slabs in his experiments and considered that prefabricated units were best cast of T-sections placed side by side to form a floor slab [Hassoun, 2002]. It is not clear who built the first flat slabs. In their excellent review of the history of slabs, Sozen and Siess claim that the first American true flat slab was built by C. A. P. Turner in 1906 in Minneapolis [Mete A. Sozen and Chester P. Siess, 1963].

Reinforced concrete is composite of two basic materials, steel and concrete. The two materials work in a synergistic fashion when constructed properly to provide components with desired structural characteristics. Reinforced concrete is commonly used in structures designed for heavy use and long life, such as governmental, institutional buildings and public works structures. Concrete has a great capacity to

1

support compressive loads. However, it has only a limited capacity to support tensile loads. Steel has a great capacity to carry both compressive and tensile loads but it is relatively expensive material. Therefore, in order to construct structural elements which are long lasting, economical, and have both compressive and tensile capacity, steel is combined with concrete to harness the compressive strength of concrete and the tensile strength of steel. Reinforced concrete, as a structural material, is widely used in many types of structures. It is competitive with steel if economically designed. The advantages of reinforced concrete can be summarized as follows: relatively high compressive strength, better resistance to fire than steel which is (1-3 hours fire rating), a long service life with low maintenance cost, the ability to be cast to take a required shape, and a yield rigid member with minimum apparent deflection.

Concrete is relatively brittle and lacks adequate resistance to tension. Flexural cracks are one of the most common defects observed in reinforced concrete, and they occur for several reasons which will be explain later. The presence of cracks in a concrete structure generally causes serious concern to the building owner or occupants; furthermore it is important to establish their long-term effect on durability, i.e. the ability of the floor to perform the function for which it was originally intended or for any proposed change in use.

As the infrastructures deteriorate with time and due to the high cost of new construction, rehabilitation of damaged buildings is still structurally and economically worth saving. Rehabilitation, therefore, is a major challenge to civil engineers which is needed to restore the structural capacity of the distressed elements. It was estimated that in 1982, the value of repairs and maintenance to buildings in the UK amounted to some

2

$17 x 10^9 and if civil engineering structures were included this would rise to $20 x 10^9 [Perkins, P. H., 1997]. The US Army Corps of Engineers completed the Repair, Evaluation, Maintenance, and Rehabilitation (REMR) Research Program. The primary objective of six-year, $35 million research effort was to develop effective and affordable technology for maintaining and extending the service life of the existing Corps civil works structures. Savings of over $40 million, or more than four times the funding, have already been reported from the use of technology developed in the concrete portion of REMR [McDonald, J., 1991]

Composite materials have gained acceptance among civil engineers. Fiber Reinforced Polymers (FRP) for their outstanding properties such as high tensile strength could be used as external reinforcement to increase the flexural strength of existing reinforced concrete (RC) structures; they have been used for civil engineering applications in Canada since the 1980s. Historically, composites were first applied as flexural strengthening materials for RC bridges [Meier 1987; Fostasy 1987].

Structural concrete slabs are constructed to provide flat surfaces, usually horizontal, in building floors, roofs, bridges, parking garages, and other types of structures. The slab system may be classified as: one-way slab, two-way slab, waffled slab, and flat slab with drop panel and column capital or without these features namely a flat-plate slab (Figures 1-1 to 1-4).

Flat-plate is a special type of flat slab which has uniform thickness throughout, supported directly on columns without drop panels or column capitals. Flat-plate systems are widely used throughout the world because they have several advantages such as providing architectural flexibility, easier form-work, shorter construction time, lower

3

building height and more clear space (parking garage). The cost of a flat plate floor is generally less than that for one-way slab-and-beam floor by 19% [MacGregor, J. G. & Bartlett F. M., 2000]. However, despite its simplicity this system has low stiffness which may cause noticeable deflection. The flat-slab construction system has been widely used for a long time; the existence of cracks and other damage is the main cause of structural fatigue and a reduction of the capability of the structure to sustain its design load which affects the safety of the structure. Damage assessment and rehabilitation of civil structures is one of the most important and recently-emerging fields in engineering.

1.2 Problem Definition

Buildings and parking structures are usually composed of flat-plate slabs that are subjected to large shear and bending moment forces. Due to the transfer of these forces to the supporting columns the connection between the slab and column is an extremely critical area, where severe bending and shear forces are concentrated.

A failure can be considered as occurring in a component when that component can no longer be relied upon to fulfill its principal functions. Limited deflection in a slab which caused a certain amount of cracking/distortion in partition could reasonably be considered as a defect but not a failure.

The presence of cracks is playing an important role in indicating that the structure or parts of the structure are suffering from structural distress and structure disorder. If cracks extend up to the steel reinforcement they provide access for moisture, carbon dioxide, sulphur dioxide, oxygen, and aggressive liquids. This will result in corrosion of

4

the steel reinforcement and is the most serious durability problem affecting concrete structures, which in turn can cause the member affected to become structurally unsafe.

Due to the high cost of new construction, the need for maintenance and upgrade of concrete structures has increased considerably over the last decade and this trend will continue. Therefore, damage assessment and rehabilitation of structures is one of the most important and recently-emerging fields in structural engineering. It should be noted that the investigation, diagnosis and subsequent specification for remedial work are quite different to the design of a new structure. Thus, the first and most important step in rehabilitation of a deteriorated structure is to decide whether structural repair is working and, if so, whether the result is likely to be cost-effective.

1.3 Future Work on Standards and Codes

The need for specialized standards and codes for FRP materials arises because of their substantially different mechanical and physical properties in comparison to conventional construction materials. The development of standards and codes for the use of FRP reinforcement with concrete structures is ongoing and is expected to continue in the next several years. Much of this activity is motivated by immediate, obvious needs for improved, economical materials for the repair and retrofit of structures that are obsolete, degraded, or located in seismic zones. FRP and bridge decks suffer from the least amount of development of standards and codes. Future research efforts on standards and codes should therefore be increasingly concentrated in these areas (Bakis C. E. et al., 2002).

From 1967 to approximately 1990, strengthening of building components by adhesive bonding of flat-rolled steel was the dominant principle. Today, this principle has almost been replaced by strengthening with fiber composites. Recently, a number of researchers investigated the use of FRPs to repair or strengthen corrosion-damaged beams and columns (Lee et al. 2000; Sherwood and Soudki 2000; Soudki and Sherwood 2000; Debaiky et al. 2001; Masoud et al., 2001). Also as it will be discussed in chapter II, traditional methods have been used for rehabilitation of cracks in slabs while CFRP sheets have been used as repair material for punching shear failure, and for flexural strengthening of undamaged slabs. However, no information was found in the literature on the confining effects of CFRP on the flexural cracked slab-column system.

1.4 Research Objectives and Scope

Major factors responsible for deterioration are: structural changes, faulty design, poorly drafted specifications, unsuitable materials, improper workmanship, overloading, physical damage and exposure to an abnormally corrosive environment (Figure 1-5). The deterioration in concrete is usually manifested in the form of corrosion of reinforcing steel, cracking, spilling, excessive deflection.

The existence of cracks is the main cause of structural fatigue and a reduction of its capability to sustain its design load which will affect the safety of the structure. Furthermore, cracking is of concern for three main reasons: appearance, leakage, and corrosion.

Cracks on the slab around the connection may appear for the aforementioned reasons. To avoid demolition of the entire structure, these damaged connections must be

6

at least restored. Previous studies on slab-column connections have been conducted using traditional methods, studying other types of failure, and/or strengthening undamaged system.

The rehabilitation of reinforced concrete structures is a major challenge to civil engineers. The FRP composite is the external reinforcement for repair and upgrade of the structural capacity and stiffness. The purpose of rehabilitation is to improve the function and performance of the structure, restore and increase the strength and stiffness, improve the appearance of the concrete surface, increase water tightness, prevent access to corrosive materials (steel reinforcement), and improve the overall durability of the structures. The main purpose of this research is to study the efficiency of using CFRP sheets for rehabilitation of a flexural cracked RC flat-plate slab-column connection, and also evaluate their effectiveness on service behaviour and ultimate capacity.

1.5 Contents and Arrangements

This thesis is organized in five chapters:

Chapter II presents a comprehensive literature review relevant to the topic of this thesis, theoretical background of the cracking phenomenon, history and development of using FRPs in construction (strengthening and rehabilitation). This chapter discusses the methodology of this research.

Chapter III describes in detail, the experimental and test program that was carried out in order to obtain the required data, in addition to the rehabilitation scheme of slab-column connections, configurations of the tested specimens, instrumentation, and the material properties that had been used.

Chapter IV focuses on the analysis and observations of cracking propagation; response of each specimen under concentrated and/or eccentric monotonic loading. Failure mechanism are also described and analyzed in this chapter. The summary and the assessment of the experiments and results are also reported in this chapter.

The conclusions of this research and recommendations for future studies are presented in chapter V.
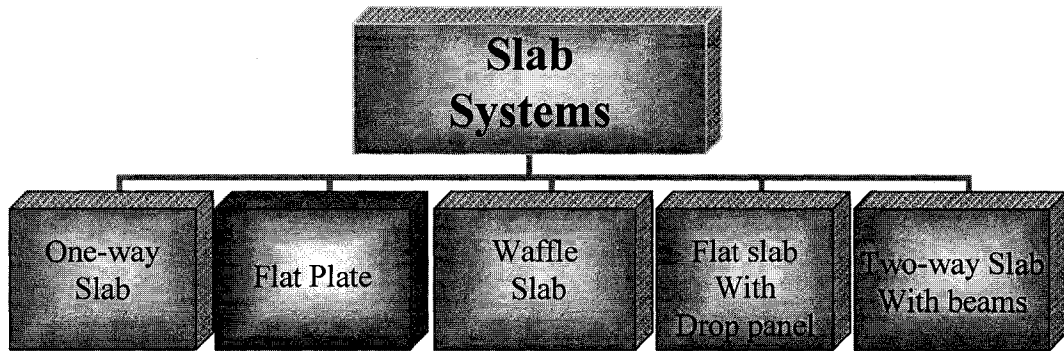
Fig. 1-1: Classification of Slab systems
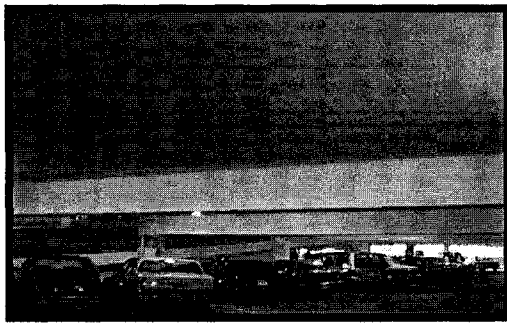
One-way slab
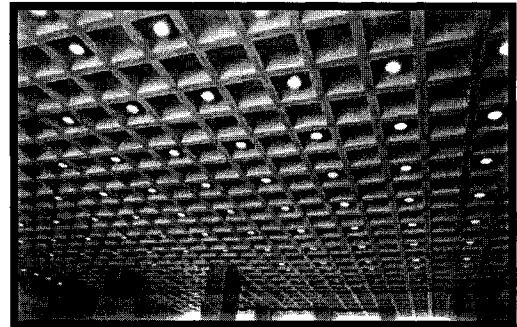
Waffle slab
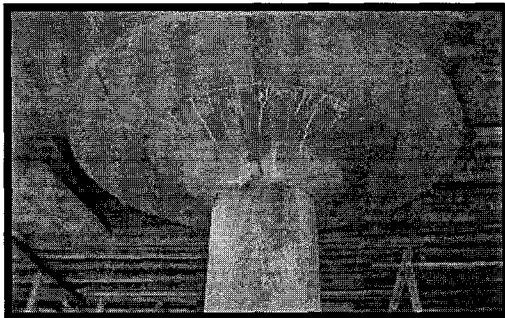
Flat slab with drop panel and column capital
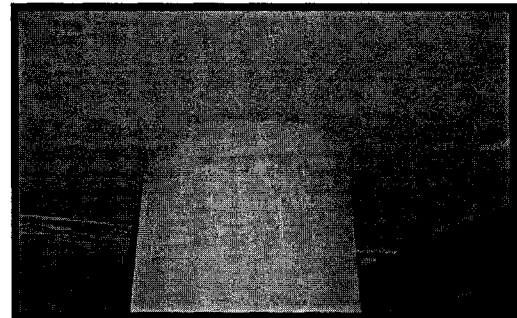
Flat plat slab

Fig. 1-2: Different types of slabs for RC structures

9
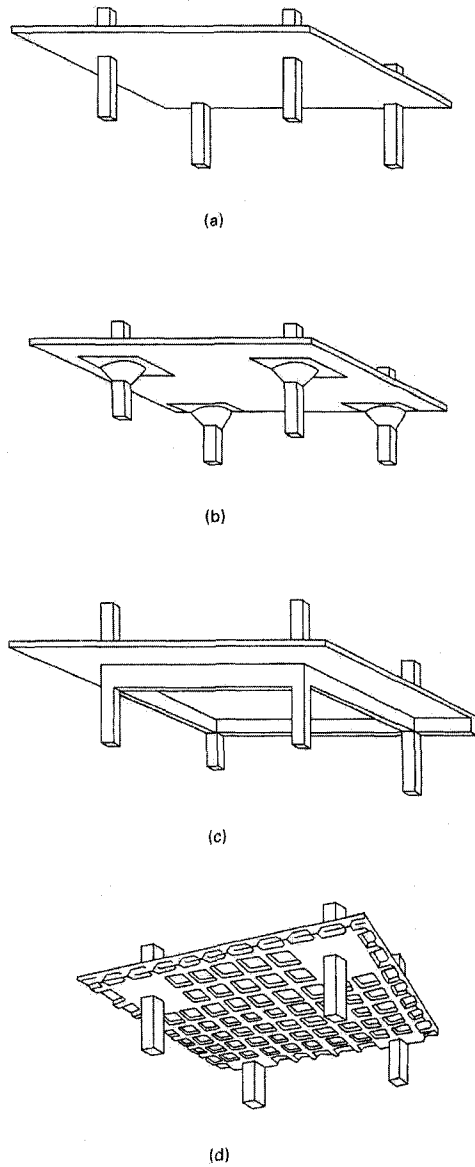
Fig. 1-3: Different types of slabs for RC structures

(a) Flat-Plat slab (b)Two-way slab with column capital
(c) Two-way slab with beams (d) Waffle slab

(Concrete Design Handbook, 1995)

10
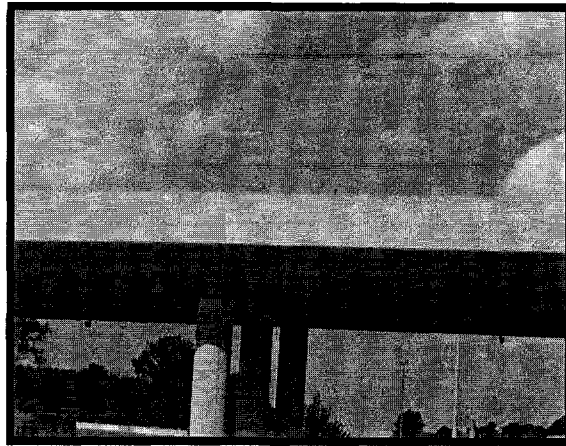
One-way-flat plate bridge slab
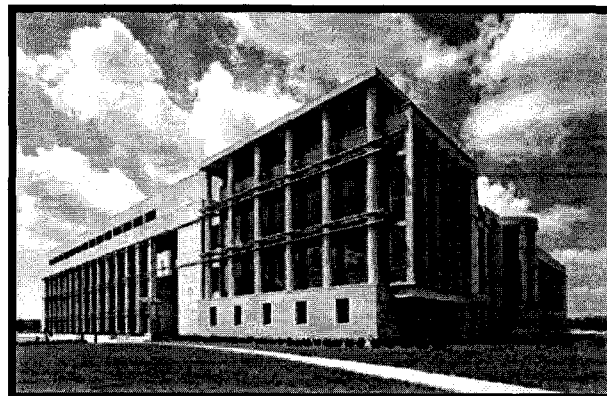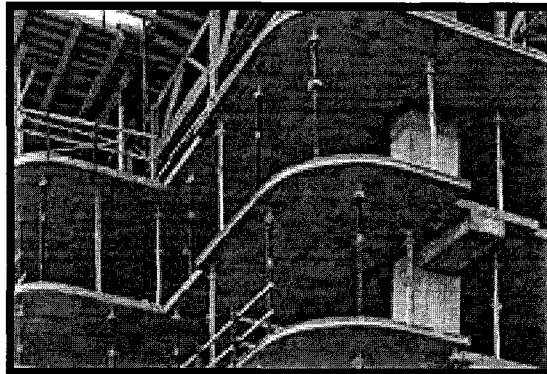
Fig. 1-4: Flat-plate slabs RC structures

11
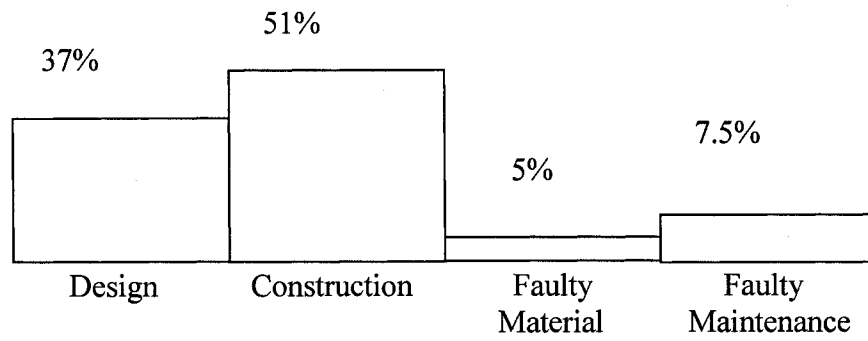
Fig.1-5: Where problems arise in RC structures. After (Hewlett, P. C., Materials and

Techniques, Keynote paper, Structural Faults and Repair, London, 1987, 24)

12

CHAPTER II

BACKGROUND AND LITERATURE REVIEWREVIEW

2.1 Introduction

Buildings and construction are an important symbol of civilization. Different materials have been used throughout the ages. Earth was the first material used for this purpose, the oldest civilization; Sumer, Iraq, (3500BC - 1792BC) had few natural resources, but Sumerians used what they had wisely; they built with earth and water to make bricks of clay. Straw (fiber) was added to clay as reinforcement material to protect clay bricks from cracking. Through the history, the usage of earth became less common as new materials such as wood, stone, concrete, steel and finally Fiber Reinforced Polymers (FRP) were introduced (Figure 2-1).

A typical RC slab has different failure modes: brittle mode (punching shear, compression) and ductile mode (flexural) which is the preferable mode of failure since it allows enough time for intervention rehabilitation of the structure (Figures 2-2, 2-3). Interior slab-column connections may exhibit flexural failure in the form of flexural crack emergence (Figure 2-4).

Several major national and international research programs were launched to investigate the feasibility of using aerospace technologies of polymer composites in the rehabilitation and upgrade of structural systems made of reinforced concrete. All studies have shown that FRPs increase the strength of flexural members significantly.

This chapter presents, in addition to the methodology of this study, the state of knowledge concerning the cracking mechanisms of reinforced concrete members and

13

theoretical background for explaining the cracking phenomenon of reinforced concrete members under external loads. The history and development of using FRPs in construction, their types and properties are also summarized in this chapter. Existing related research and several applications of rehabilitated concrete structures are also reviewed.

2.2 Flexural Cracking in Reinforced Concrete

2.2.1 General

Cracking is difficult to avoid for normally reinforced concrete (RC) structures have cracks. It is usually accepted that tensile cracking will occur in an economical design. Tensile cracks develop when concrete, with a limited capacity for elongation, tends to deform with the tensile reinforcement due to bonding action; however, the structures are designed so that the inevitable cracking of the concrete is restricted such that no cracks at the surface should exceed a prescribed limit. For several reasons, cracking in excess of the design accepted limits occurs during the service life of the structure. If such cracks are not sealed or structurally bonded, further deterioration may occur. Before deciding the most appropriate methods/materials for repairing/sealing cracks, it is imperative to establish the cause of the cracking and, where a permanent structural bonding of the crack is required, to carry out any other strengthening which may be necessary.

14

2.2.2 The field investigation

Before any repair is carried out, the causes of the damage must be identified. There may be more than one factor involved, and the probable sequence of events leading up to the damage must be established. Once the cause of damage has been determined, the objective of the proposed repair must be considered. The repair of this damage may be one or more of the following: restoration of durability, restoration of structural strength, increase of structural strength, restoration of improvement of appearance, and restoration of fitness for use.

It should be noted that the investigation, diagnosis and subsequent specification for remedial work are quite different than the design of a new structure. In reinforced concrete structures three main items should be checked [Hassoun, 2002]:

- The safety of the structure, which is maintained by providing adequate internal ultimate strength capacity.

- Deflection of the structural member, which must be limited (usually specified as a factor ratio of the span).

- Cracks, which are the main concern of this study, blight the appearance of the structure, and permit humidity to penetrate the concrete causing corrosion of steel and weakening the reinforced concrete member by decreasing the effective cross section of the member. The *ACI Code* and the *CSA23.3* implicitly limits crack widths for interior and exterior exposure to 0.40 mm and 0.33 mm, respectively.

15

2.2.3 Classification of cracks in RC structure

Cracking in RC structures can be due to many causes, and they can be classified in two main categories: (i) Structural cracking which indicates that the structural members were not able to support the loads they had to carry. (ii) Non-structural cracking is due to all other causes than lack of resistance capacity such as creep and shrinkage. The repair of existing cracks has the objective to correct this problem. When repair is completed, the existing load-carrying capacity will not increase neither for the individual members nor for the whole structure [Perkins, 1997].

If repairs do not need to be carried out immediately, observation over a period of time will enable cracks to be classified and will assist the diagnosis of the cause. The best suitable method of repair will depend on the classification and diagnosis. When cracked concrete need to be rehabilitated, changes in the crack width with time are important in determining the choice of rehabilitation technique. Therefore, it is practical to divide cracks into the following classes: [*DANSK standard*, 2004]

- Passive ('dead') crack, i.e. the crack is not moving and the cause of cracking is no longer there, i.e. old shrinkage cracks, accidental overload

- Active ('live') crack, i.e. the crack is still moving and the crack width changes. The cause of cracking persistent. This type of crack will be the focus of the present study

- Latent ('dormant') cracks, i.e. cracks which appear to be passive but may become active after rehabilitation.

Table 2-1 illustrates the characteristics and the causes of cracks.

16

2.2.4 Cracking phenomena

Due to shrinkage of the cement paste, micro cracks occur in concrete even before external loads are applied. Cracks initiate at critical locations where the limiting tensile properties of the concrete have been exceeded due to weak material and/or high stress and strain. More cracks are randomly located through the concrete and propagate to the surface of a reinforced concrete member under relatively low external loads. Only the tensile cracks arising from the application of external loads will be considered in this study.

The incidence of flexural and direct tension cracking that occurs at various stages is defined in relation to the stresses in the reinforcement at the cracked section

1.   First stage of cracking (primary cracks)

Cracks in this stage form at critical sections. Then more initial cracks propagate to the surface of the member under relatively low external flexural loads. These cracks are characterized by the fact that they are widely spaced in comparison to the lateral dimension of the member, so that the presence of one crack does not influence the formation of others. The initial cracks affect only the outer layer of the concrete. After crack appearance, the stress distributions in the reinforcement and the concrete adjacent to the reinforcement assume shapes similar to those shown in Figure 2-5, in which a tension member represents that part of a flexural member located symmetrically around the reinforcement and between two primary cracks. Experimental observations, shows that the steel stresses in this stage are usually below 97 MPa (14,000 psi). This stress level delimits the boundary between first stage and second stage cracking.

17

2. Second stage of cracking (secondary cracks)

This stage is concerned with the formation of secondary cracks between the random primary cracks. It is associated with cracks which are caused by the difference in extensibility between the concrete and steel and the bonding forces that exist between the two. Concrete tensile stresses are present between the primary cracks because of a bonding action as the concrete tends to deform with the reinforcing steel. Distribution and magnitude of the bond stress between the concrete and the reinforcement will determine the distribution of concrete stress and steel stress between the primary crack sections.

3. Third stage of cracking (equilibrium stage)

This stage occurs when no further secondary cracks form during increases of the external load, and existing secondary cracks continue to widen. The steel stresses during this stage are usually greater than 207 MPa (30,000 psi).

2.2.5 Flexural cracking mechanisms [ACI Committee 224, 1968]

Two cracking mechanisms are discussed in terms of simple model of a reinforced concrete member with the reinforcement loaded in direct tension, as shown in Figures 2-5, 2-6, and 2-7. This model has been proposed in various cracking studies.

A) Uniform concrete stress

The study of cracking was based on cracking patterns as observed at the surface of reinforced concrete members and has proposed or implied a cracking mechanism based on a "strength of materials" assumption that the concrete tensile stress is uniformly

18

distributed over an effective area of concrete and that a certain distribution of bond stresses exists along the reinforcement. Crack formation in the simple model (Figure 2-5.b) is assumed to occur when the external load increases gradually as follows:

1. Primary cracks form at random critical sections of RC member when the uniform tensile stress exceeds the tensile strength of the concrete.

2. A slip occurs between the concrete and the reinforcing bar at the primary crack section.

3. Concrete surfaces at the crack sections are free of stress, and the force in the reinforcement equals the external load.

4. The stress in the concrete decreases from a maximum value to zero as the reinforcement sustains all the tensile forces at the crack.

5. Concrete tensile stresses are present between the primary cracks because of a bonding action that takes place as the concrete tends to deform with the reinforcing steel.

6. A new crack may form as the external load increases and the uniform concrete stress exceeds the concrete tensile strength.

7. Cracking will continue to take place between existing cracks until the concrete stress does not again exceed the concrete strength because of excessive slip and reduced distance between cracks to transfer stress to the concrete.

B) Redistribution of concrete stress (Based on elasticity analysis of concrete stresses)

Concrete stresses are function of lateral dimensions and cracking spacing, a redistribution of concrete stresses occurs when a new crack formation alters the geometry

19

of the member. High tensile stresses will be present within a circular area located between two adjacent cracks as illustrated in Figure 2-6. Outside this circulate area; compression stresses or small tensile stresses will be present. When a set of cracks forms approximately halfway between existing primary cracks (Figure 2-7.a), the new cracks will spread laterally until they reach the periphery of the corresponding stress circles where the intensity of the average axial tensile stress is low. If the primary crack space is less than the double distance from the level of the reinforcement to the neutral axis, then the length of the new cracks will be less than that of the original primary flexural cracks (which extend to the neutral axis) and the new flexural cracks will become secondary flexural cracks.

The secondary flexural cracks, shown in Figure 2-7.b, will cause stress redistribution in the immediate vicinity of the reinforcement. A new set of cracks, secondary flexural cracks, develops when the maximum tensile stress in the concrete exceeds the tensile strength of the concrete. The lengths of these new tensile cracks will be governed by the diameter of the corresponding stress circles (the distance between two adjacent tensile cracks). If the crack spacing for adjacent cracks is less than the double thickness of the bottom cover of the flexural member, then the corresponding stress circles and the new set of tensile cracks will not reach the bottom face of the member as shown in Figure 2-7.b.

20

2.3 Rehabilitation of RC Slab Using Traditional Methods

2.3.1 Literature review

There are several traditional techniques by which the strength or stiffness of existing structures can be enhanced.

Alcocer (1991) studied experimentally the effectiveness of *concrete jacketing* of frame elements and developed some guidelines for its design to assess the effectiveness of this method. The program was aimed at studying the behaviour of beam-column-slab joints rehabilitated by jacketing. Four large-scale reinforced concrete frame connections were built to represent a prototype structure designed in the 1950s, which consisted of a joint with weak columns and strong beams. The structures were tested by applying a bidirectional cyclic loading. This research concluded that jacketing of frame elements was effective for the rehabilitation of existing structures, either damaged or undamaged prior to jacketing. Analysis of test results led to the identification of the effect of jacketing on performance of a damaged column prior to rehabilitation, the arrangement of the longitudinal reinforcement in the column jacket, and the jacketing of both beams and columns. Design recommendations for joint shear strength can be used to design well-confined interior joints rehabilitated by jacketing.

Farhey et al. (1995) studied experimentally the behaviour of repaired two-thirds-scale internal flat-slab-column subassemblages using *steel plate* and compared their performance with their response before being repaired. Four specimens were constructed and subjected to quasistatic, reversed, horizontal loadings. The experimental variables considered in the repair study were the repairs geometric parameters, such as the overall

21

dimensions of the steel plates, and their thickness. The deteriorated slab was repaired using commercial, ready-to-use powder, adding gravel and water, epoxy, and threaded bars to hold the steel plates. Different sizes and surface-treated steel plates had been used. The first cracks in the repaired specimens formed during an early stage of loading along the polyester glue at the edges of the steel plates around the column and then propagate gradually at the far edges glued to the slab, outlining the circumference. As the load increased, transverse-flexural cracks emerged in straight lines parallel to the supports, running toward the sides. At about two third of the failure load a noisy cracking was heard in the shear epoxy layer between the steel plates and the slab. The results of the repair technique showed very satisfying performance, restoring and amplifying strength, stiffness, and the energy-dissipation capacity.

NAHB Research Center, Inc. (2002) investigated the performance of *epoxy injection* crack repair for slabs-on-grade. Different width of flexural cracks were observed (0.76 – 6.35) mm. Cracks were initiated in the specimens by applying a single load at mid-span. Once the cracks were initiated, 0.375 mm diameter threaded rods were inserted into the conduits and tightened to prevent further degradation of the specimens. Then two component epoxy resins of various viscosities were injected into cracks. Flexural tests were then performed on repaired specimens to determine the performance of the repaired specimens. All of the repaired slab specimens with 0.76 mm and 6.35 mm cracks failed by development of a new crack parallel to the original one (Figure 2-8). A variety of viscosities and methods were used for repair of the 3.2 mm wide cracks, several of which were successful. Unsuccessful repairs were the result of epoxy seeping

out of the cracks into the sand bedding. The variability of results for the 3.2 mm wide crack repairs illustrates the need for quality assurance (QA) under current practice for repair of cracks with limited access to fully seal the crack surface against seepage of injected epoxy. More specific guidance on epoxy selection for this type of repair should help to prevent the problems experienced in this study. Crack repairs were completely effective for less than 0.76 mm crack widths, because the epoxy viscosity selection appears straight-forward.

2.3.2 Summary of using traditional method for RC slab rehabilitation

Several researchers had investigated different methods to rehabilitate cracked slabs. The concept of using *epoxy resin injection* systems as a means of repairing cracked concrete, so that after being repaired, the concrete acts monolithically again, has been established for over 30 years (from 1950's to 1980's). During this period many major structural rehabilitation projects using this technology have been carried out [Shaw, J.D.N., 1987]. This method is most frequently used when the repair is being performed in order to restore structural integrity, and to protect reinforcement from corrosion [Allen et al., 1993]. It is possible to restore the cracked concrete structure to the original tensile strength of the un-cracked one. As a result filling live cracks without gaining additional tensile resistance is not enough when the same cause of cracks still persist. Therefore, the problem could be generated by the appearance of new cracks almost parallel to the original ones as shown in Figure 2-8. Based on a paper represented at the 'International Conference on Structural Failure ICSF 87' Singapore Concrete Institute found that epoxy

injection is an excellent bonding coat. However, in such cases, separation cracks at the interface can be seen.

Concrete jacketing is an addition of a concrete shell surrounding a member which is reinforced. It is often seen that the new concrete/mortar mass separates from the old concrete. This obviously happens due to the dissimilar behaviour patterns of the old, already set concrete, and the subsequent new concrete which is undergoing stresses and strains while stiffening, mainly due to shrinkages [Manjrekar, 1995].

One of the most popular techniques for upgrading RC elements has traditionally involved the use of externally epoxy-bonded *steel plates*. This method has been established for more than 40 years. From the published literature, it would appear that the concept was developed almost simultaneously in South Africa and France in about the year 1965. In South Africa, resin-bonded reinforcement was used for the rapid emergency repair of a road overbridge damaged by the impact of a mobile crane which ruptured some of the steel reinforcement in several beams. This technique is simple, cost-effective, and efficient, but it suffers from major drawbacks such as the deterioration of the bond at steel-concrete interface cause by the corrosion of steel, difficulty in manipulating the heavy steel plates at the construction site, need for scaffolding, and limited delivery lengths of steel plate [Bakis et al. 2002]. Another common strengthening technique involves the construction of RC, shotcrete, or *steel jackets*. Jacketing is quite effective as far as strength, stiffness, and ductility are concerned; however, it increases the cross-sectional dimensions and dead loads of the structure.

Ferrocement is a type of thin composite material made of cement mortar reinforced with uniformly distributed layers of continuous, relatively small diameter wire

24

meshes. Furthermore, it is labour intensive, obstructs occupancy, and provides RC .elements with a potentially undesirable stiffness increase. Although the wire mesh helps to distribute shrinkage stresses evenly, it may introduce additional corrosion problems.

Although traditional techniques are simple, cost-effective and efficient in restoring the cracked concrete structure, they could be problematic as explained. Therefore, the need for structural rehabilitation of concrete structures all over the world is well known, and a great deal of research is being undertaken in this field.

Compatibility is a measure of the matching of physical, chemical, electrochemical and dimensional properties between the repair materials and the substrate. The correct choice and proper use of repair materials is therefore critical to the achievement of long service life for rehabilitated structures [Mailvaganam, 2001]. Composites have gained widespread use as strengthening materials for RC structures in applications. For example, as an alternative, the steel plates can be replaced by FRP strips or sheets. Furthermore, FRP sheets may be wrapped around RC elements instead of jacketing, resulting in considerable increases in strength, and confinement. It also helps to keep the conditions around the exposed steel and exposed concrete generally alkaline, thereby preventing corrosion of steel and carbonation of the adjacent concrete.

2.4 Rehabilitation and Strengthening of RC Structures Using FRPs

Extensive research across the world has led to a better understanding of properties and behaviour of the FRPs. Several major national and international research program were investigated the feasibility of using FRPs for rehabilitation and strengthening RC structures.

25

2.4.1 Literature review of slab strengthening using FRPs

The following researchers investigated the use of FRPs for strengthening RC slab structures.

Abdilrahman (2001) summarized the use of CFRP unidirectional laminates in strengthening a RC multi-story flat-slab structure which was originally designed as a residential building, and the owner of which requested the use of two floors for commercial purposes. CFRP plates were used to strengthen the structure. A total of 2200 m length of CFRP plates was bonded at the top and bottom surfaces in both directions to reduce the stresses in the longitudinal steel bars. The flexural capacity of several sections of the concrete slab increased by up to 35% to allow for the additional live load; the punching shear capacity of the slab was checked and found to be sufficient without strengthening the slab in shear. The maximum spacing between plates was kept five times the slab thickness, while with minimum spacing of 100 mm. The piping system and light fixtures were not removed during the application of CFRP. The CFRP plates which bonded to the top surface of the slab did not have enough length to transfer forces to the concrete; therefore, steel angles anchored to the concrete slab with steel bolts were used as mechanical anchorage for the CFRP plates which can transfer 60% of the maximum force of the plates. The design criteria covered the strength, serviceability, ductility, and the risk of loss of CFRP plates due to fire. Loading of the strengthened slabs was performed after installation of the laminates, and the residual deformation was only 6%. The strengthening did not require closing the working area during application and also reduced the estimated time of construction from one month (using concrete Jacketing) to ten days using CFRP.

26

Binici and Bayrak (2003) reported the test results of a punching shear strengthening method using (CFRP) as external shear reinforcement. They considered reinforced concrete flat plate subjected to concentrically applied shear forced strengthened with various configurations and amounts of CFRP. Their experimental results showed that the use of externally installed CFRP stirrups was effective and promising on increasing punching shear strength and deformation capacity of slab-column connections with negligible stiffness increases. The punching shear strength of test specimens increased by up to 51% compared to the control specimens.

Abou El-Enein, (2004) studied experimentally the change in strength and behaviour of the slab-column connections in a flat-plate system when reinforced with CFRP sheets. Three cases of column position were investigated: central column, eccentric column and edge column. Two specimens of each case were studied: the first one as control specimen, while the second one was strengthened with CFRP. As a result of the comparison between control and strengthened specimen for central-column specimen, the deflection at failure was decreased by 7%, the ultimate load carrying capacity increased by 32%, and the increase in cracking load was 23%.

2.4.2 Literature review of slab rehabilitation using FRPs

The need for structural rehabilitation of RC structures is well known. Number of researchers studied the use of FRPs for repair of deteriorated concrete slab.

27

Teng et al. (2000) investigated the feasibility and effectiveness of bonding glass fiber reinforced polymer (GFRP) strips/sheets on the top surface (the tension side) of deficient RC cantilever slabs as a strengthening measure. The experimental work of this study included seven tests on cantilever slabs supported on a short wall segment. In all tests, the RC specimen was fixed on a stiff support erected on the floor. A line load was applied near the free end of the slab and was 600 mm from the fixed end. The slab was strengthened by two GFRP strips with epoxy. The first specimen was a control specimen without strengthening. Specimens two to four were strengthened with GFRP strips adopting different anchorage systems to the wall, where as specimens five to seven were strengthened with GFRP strips with different anchorage details to the slab in addition to a horizontal slot anchorage to the wall. The test results had demonstrated that a significant increase in the ultimate load and ductility can be achieved if the slot anchorage system is used to anchor the strips into the supporting wall. The effect of this strengthening method is even better if fiber anchors are installed or the free ends of GFRP composite strips are wrapped around the free edge and onto the soffit of the slab. The ultimate strength of one of the strengthening specimens was almost four times that of the control specimen. For specimen III, the failed model slab from Test II was reused; the concrete slab was already damaged, and a major crack already existed along the fixed end of the slab before strengthening. The first two specimens collapsed in a brittle mode of failure where the rehabilitated specimen was ductile and the ultimate load was more than double that of the control specimen.

28

Vatovec et al. (2002) described a project in the United States where CFRP was effectively used to address design deficiencies of a concrete garage structure. The garage consists of four parking levels. Typical garage decks are 203 mm (8 inch) thick, post-tensioned cast-in-place concrete flat slabs with drop panels supported by concrete columns. During the construction of the garage, it was discovered that the post-tensioning system in the east-west (E-W) direction of the slab was inadequately designed. A remedial repair was developed by the original designer of the garage from 1984 to 1995 using different methods. In 1984, a Gunite beam between drop panels with supplemental column had been added, the limited load testing was performed and it was concluded that the design was adequate. In late 1984, the first delamination between the Gunite beams and the slab was noted. They investigated that 30% of the Gunite beam was up to 40% delaminated. In 1989, a Gunite beam debonded from the underside of the fourth level slab and fell to the slab below because of the poor surface preparation. Over the next several years following the failure, a number of nondestructive testing (NDT) and isolated epoxy-injection repairs were performed, but no overall remediation plan was implemented. The garage has changed owners several times since the original construction. In 1995, Simpson Gumpertz & Heger (SGH) identified a number of other garage problems including excessive deflection of end garage bays and flexural cracks. After the last change in ownership (1999), (SGH) developed and implemented a comprehensive garage repair program using FEA. Moment redistribution in typical garage bays was used to eliminate or reduce the negative-moment region deficiencies; since CFRP repair to the top-side of the slab (negative-moment) is undesirable, the mid-span demand moment on the slab in the E-W direction was higher than the slab's ultimate

29

strength by 83% and in the N-S direction was 56%. The demand moment on the slab at mid-span and at the face of the first interior column was higher than the slab's ultimate strength by 125 and 63% respectively. The load tests showed that the Gunite beam system works adequately where bonded. In addition, the load tests showed that the slab repaired with CFRP performed well. Based on test results, an additional nineteen slab spans, where delamination of Gunite beams was evident, were strengthened with CFRP. Further monitoring of the performance of Gunite beams is required, and additional CFRP strengthening will be done periodically. Typical garage bays were repaired using additional steel-framing supports. The steel framing is used instead of CFRP, due to the fact that structural deficiencies that were larger than acceptable for CFRP repair were found in the end bays. Large deflections of cantilevered end bays were mitigated with the insertion of additional steel supports.

Mosalams (2003) investigated the effectiveness of using FRP composites in the repair and retrofit of un-reinforced and reinforced concrete slabs. Ten full-scale destructive tests were conducted. In addition, two more specimens were tested to 85% of the expected ultimate load for subsequent repair. All tested slabs were simply supported on all four sides undergoing two-way action. Uniformly distributed pressure was applied to tow-way slab specimens using a high-pressure water bag. Both carbon/epoxy and E-glass/epoxy composite systems were used. The maximum laminate strain at the ultimate load was 0.78% which is 65% of the rupture strain of the Carbon/epoxy system. The FRP systems have succeeded in upgrading the structural capacity of the slab. For repair application, test results indicated that both FRP systems were effective in increasing

30

appreciably the strength of the repaired slabs to approximately five times capacity. The authors claimed that the composite system restored not only the original capacity of the damaged slabs but also resulted in an appreciable increase in the strength of the repaired slabs to an average increase of more than 540% of the original capacity of the slab. For retrofitting applications, the authors also declared that the use of FRP systems resulted in an appreciable upgrade of the structural capacity of the as-built slabs up to 500% for unreinforced specimens and 200% for steel reinforced specimens.

Binici and Bayrak (2004) extended their study of the upgrading a procedure proposed previously [Binici 2003] to slab-column connections transferring shear forced and unbalanced moments. Four slabs were tested: two reference specimens and two of which were strengthened with CFRP stirrups acting as shear reinforcement around the slab-column connection area were used with two patterns of CFRP arrangements. One of the control specimens was loaded concentrically, and the other was loaded with an eccentricity equal to the column size by using a steel column with an overhang; strengthened specimens were loaded with the same eccentricity as was used for control specimens. The ultimate load carrying capacity compared to control specimens increased by about 45 and 60% depending on the strengthening pattern. As a result, CFRP used as shear reinforcement around the slab-column connection area for both patterns can be successfully used to increase the punching shear resistance of the system subjected to monotonic transfer of shear and unbalanced moment.

31

Robertson and Johnson (2004) presented the results of cyclic testing of three half-scale models reinforced concrete of slab-column connections subjected to punching shear. Each of the specimens was a half-scale model of an interior slab-column connection common to flat-slab buildings including three different types of shear reinforcement. While supporting a slab gravity load equivalent to the dead load and 30% of the live load, the specimens were subjected to an increasing cyclic lateral loading up to 5% lateral drift. The specimens were subjected to the same loading after they were repaired with gravity-fed epoxy crack sealers and CFRP sheet on the surface of the slab. The repair on the top surface of the slab was able to restore both initial stiffness and ultimate strength of the original specimen. Cracking of the specimen with epoxy only repair, proceeded similarly to the original specimen. However, fewer cracks formed in the epoxy repair area with these cracks opening slightly wider than the original specimen. In specimens with epoxy and CFRP, cracks outside of the CFRP area, which had not been repaired, reopened, but did not propagate into the CFRP-covered area; instead, these cracks extended as new cracks along the edge of the CFRP. Debonding of the CFRP around the slab-column connection was noted at drift levels in excess of 5%. In the specimen that have CFRP at the top and bottom face of the slab, a 40 mm long rupture occurred across the CFRP fibers adjacent to one corner of the column at the 7.5% drift level, indicating that the full capacity of the CFRP had been reached at this location. This confirmed the expectation that reinforcement of the bottom surface would not result in a substantial improvement in performance. The expensive and difficult task of soffit application of CFRP was therefore considered unnecessary to restore adequate connection performance.

Thanoon et al. (2005) investigated the structural behaviour of a cracked reinforced concrete one-way slab, which was repaired using different techniques. Five different techniques were used for the purpose of repair in the cracked concrete slab, namely cement grout, epoxy injection, ferrocement layer, carbon fiber strip and section enlargement. These techniques had been selected for their potential to either increase the structural capacity of members or to restore its original capacity. Furthermore, this study focused on the serviceability, strength and ductility performance for each of the repair techniques to ascertain their potential application in cracked reinforced concrete slabs. The slabs were loaded to failure stage and the slab specimens had been predicted in terms of deflection, variation of strain in concrete and steel, collapse loads and the failure modes. Six full-scale one-way reinforced concrete slabs were cast. Both crack and ultimate loads for all slabs indicate that the repaired slabs had a high degree of integrity.

2.4.3 Literature review of rehabilitation of RC beam using FRPs

The following researchers investigated the feasibility of using FRPs for rehabilitation purpose of RC beam.

Wang et al. (2004) evaluated the effectiveness of combining the corrosion protection and FRP strengthening techniques. Three different groups of beams were repaired according to the state of their corrosion damage. The RC beams were first corroded. All the corroded specimens with cracks more than 0.2 mm wide were sealed by first injecting an epoxy before being patched with FRP strips then externally bonded FRP unidirectional sheets were formed on each of the corrosion-damaged beams. Various

33

arrangements of FRP were applied; seventeen RC beams were repaired using 100 mm wide FRP sheets on the tensile side of the beam. The FRP sheets were patched by U-shaped FRP strips of 100 mm wide spaced every 200 mm along the sides of the beams to prevent shear or flexural failure due to corrosion of the tensile reinforcement material. The results show that both the rigidity and the ultimate load capacity were reduced as the degree of corrosion damage was increased. The analytical study demonstrates that a reduction in the steel reinforcement cross-sectional area due to corrosion is not the only factor that affects the load carrying capacity of corroded beams. The application of FRP patches can effectively overcome the reduction of the bonding strength between the corroded steel/concrete interfaces and improve the loading capacity of a corroded concrete beam. The equally spaced U-anchorage strips together with the longitudinal strips form an external reinforcing system for the corroded RC beam. This type of arrangement can improve the load carrying capacity of cracked and corroded RC beams and provides the space for coating the corrosion protection materials. However, the use of equally spaced U-anchorage strips to hold longitudinal strips constrains the extension of the fiber in the longitudinal direction in the intersection area. The strain value is higher at this site, but it enables the full usage of the fibrous composite material's strength.

El Maaddawy and Soudki (2005) studied the viability of using externally bonded CFRP laminates to extend the service life of corroded reinforced concrete (RC) beams. Fourteen beams were divided into two groups: The first group had six specimens, three of which were not corroded; two were strengthened by CFRP laminates using schemes I and II, but continuous wrapping around the specimen cross section over the middle was

34

replaced by an intermittent wrapping in scheme II; while the third one was kept as a virgin, the remaining three specimens of this group were subjected to 50 days of corrosion exposure without load, two of which were repaired using scheme I and II whereas the last one was not repaired. The second group consisted of eight specimens that were subjected to corrosion exposure under a sustained load for various times to simulate service conditions. Following corrosion, the specimens were repaired using scheme I. The remaining four beams were not repaired. All specimens were tested to failure under four-point bending. Corrosion of steel reinforcement significantly reduced the yield and ultimate loads of RC beam because of a reduction in the cross-sectional area of the steel bar, which it was almost proportional to the reduction in the steel mass loss. CFRP repair consisting of one flexural laminate along with U-shaped transverse strips effectively increased the strength of corroded beams at all levels of corrosion damage to 31% higher than the strength of the virgin un-corroded beam. Besides the increase of capacity, the CFRP repair reduced significantly the deflection capacity relative to that of the corroded and un-repaired beams on average about 46%. Finally, the beams repaired with flexural strengthening with a continuous wrapping showed a higher stiffness but a lower deflection capacity than those of the beams repaired with flexural strengthening with an intermittent wrapping, which improved the bond at the steel-to-concrete interface and thus increased the beam stiffness but reduced the deflection capacity. The ultimate load capacities for all repair techniques used in the study were capable of restoring the ultimate capacity of the defected slab except the specimen repaired by epoxy injection; the capacity of slabs repaired by CFRP and section enlargement, respectively, show 77.4% and 130% higher ultimate load capacities compared to the control slab. Concrete

35

strain decreased in the range between 30% and 50% for grout pouring; for epoxy injection and ferrocement layer specimens; while in CFRP and section enlargement specimens, the reduction in compressive strain of concrete was recorded at 65% and 85%, respectively.

2.4.4 Rehabilitation and strengthening RC structures using FRPs (case studies)

Within the field of RC structures, some companies in Canada and United States used FRPs materials for strengthening and repair existing RC structures.

- Stanley Consulting Group (1998), Windsor Dewatering Building

In this project, CFRP sheets were used to strengthen specific beams, columns and slab to achieve the required nominal shear and moment resistances. The surfaces were sealed with rigid materials prior to application of CFRP to leveled uneven surfaces. At the end, topcoat was applied as a decorative and protective coating in environments where moderate to severe corrosive conditions exist, and where long maintenance-free service life is required. As a result, the flexural and shear resistance were increased up to 17%, and 38% respectively (Figure 2-9).

- QuakeWrap, Inc. had been using FRP to strengthen different projects:

In 1997, at I–40 Bridge in Oklahoma many of the piers were damaged by corrosion. A traditional rehabilitation, which would increase column diameters, was not acceptable because the wider columns would interfere with the railroad right-of-way.

36

Glass fiber was wrapped around the piers, adding only 6.3 mm. The project took only three days (Figure 2-10).

In 1999, at Arizona State Hospital; corrosion of reinforcing steel had reduced the strength of the walls in the utility tunnel. Biaxial CFRP was used to strengthen the walls and the ceiling of the tunnel. The flexibility of the fibers allowed it to be wrapped around the limited space between the pipes (Figure 2-11).

In 2003, soon after the construction of a 26-story residential tower in an exclusive suburb of St. Louis, Missouri as shown in Figure 2-12 was completed, it was discovered that the columns in the lower 15 stories did not have sufficient reinforcing steel. Many columns were covered in wooden panels that were too expensive to discard. Repair of the columns had to be conducted while the units remained occupied, requiring minimal disturbance to the residents. Columns were wrapped using two layers of a unidirectional CFRP. The small thickness of the fabrics allowed the wooden panels to be re-installed around the columns after repair was completed.

In 2004, St. Joseph's Medical Center was adding new cath lab equipment and high density filing cabinets in separate locations. CFRP plates were bonded to the top surface of the slab to achieve the desired strength for the floors. The entire job took only 2.5 hours (Figure 2-13).

In 2005, at the City Court Garage located in Arizona inverted T-beams were damaged by corrosion. The beams were wrapped with a single layer of glass fibers (Figure 2-14).

In 2005, at Oran M. Roberts Elementary in Texas, seven double-tee beams required flexural and shear strengthening to support the weight of the heavy air

37

conditioning that was being placed on the roof. Biaxial glass fabric was used, allowing for both flexural and shear strengthening of the beams in a single application. Then an intumescing coating was applied to the strengthened beams to provide fire resistance (Figure 2-15).

In 2005, the installation of a high-density filing system with a live load of 15 kN/m2 necessitated that the floor of Providence Hospital in Alaska must be strengthened. CFRP plates were used while the hospital was in service (Figure 2-16).

In 2006, the parking structure of the Oceans One Condominium in Florida, was experiencing corrosion damage and shear cracking in many of its beams threatening its integrity. CFEP was used to wrap the beam which had been painted after being wrapped to match the rest of the structure (Figure 2-17).

2.5 Composite Materials

2.5.1 General

Historically composite meant any product made from a combination of two or more materials. In general, a composite is manufactured in an attempt to obtain the best properties of a set of materials or at least to capture a specific property of each material that is potentially better in the composite. It is also possible for the composite to have a particular property that neither component exhibit individually. According to Holmes and Just, a true composite is where distinct materials are combined in a non random manner to produce overall structural characteristics superior to those of the individual components. The concept of composite materials is not a new idea. Nature has provided us with several excellent examples of composite materials. Wood is a composite of

38

cellulose fibers contained in a matrix of lignin. Bone is composed of the protein collagen and the mineral apatite. In all these materials, the result is a product that is lighter and stronger than either of the components individually.

Composite materials have been used for centuries: bricks reinforced with straw, laminated iron-steel swords and gun barrels, linoleum, plasterboard, and concrete. Today industrial innovation, improved energy planning and uncertain availability have increased the interest in composites. Now that increasingly severe performance requirements are taxing many conventional monolithic materials to the limit, the engineer's traditional approach of fitting the design to the properties is changing into one of finding materials with the right properties to meet the demands of design, service, and economics.

2.5.2 Fiber reinforced polymers composite (FRPs)

Fiber-Reinforced Polymer composites provide a number of important benefits to the construction industry. In its basic form, FRP composites are a "family" of materials comprising a variety of polymeric resin matrices that are reinforced with various types of fibers. Fiber Reinforced Polymers (FRPs) have been used successfully for decades in the aerospace, shipbuilding, and sport goods industries. The function of the resin is to protect the fibers and to distribute the loads evenly among them. Conventional materials like FRPs are naturally orthotropic and their using needs to take into account this fundamental property, i.e. FRPs have physical properties that are different when measured along different directions. By orienting the fibers in a desired direction, one can direct the strength in an indented orientation. FRPs for structural strengthening are available in the form of precured strips or uncured sheets. The fibers in the composite represent the

39

principal load carrying component. Since the first research efforts in the mid-1980s the development of FRP technology has been tremendous.

2.5.3 History of FRPs

The earliest FRP materials used glass fibers embedded in polymeric resins that were made available by the burgeoning petrochemical industry following the World War II. Aided by the growth in research and demonstration projects funded by industries and governments around the world during the late 1980s and throughout the 1990s, FRP materials are now finding wider acceptance in the characteristically conservative infrastructure construction industry.

The use of FRP for civil engineering applications in Canada began in the 1980s when the Canadian Society for Civil Engineers created a Technical Committee on the Use of Advanced Composite Materials in Bridges and Structures [Bakis et al., 2002]. In 1995, the Canadian federal government established the Network of Centers of Excellence on Intelligent Sensing for Innovative Structures (ISIS). One area of focus of ISIS is the use of FRP materials for new structures and the rehabilitation of existing structures. ISIS published several design guidelines on externally bonded and internal FRP reinforcements, participated in several Code and Standards committees, and sponsored several national and international conferences. In 2000, Canadian Highway Bridge Design Code section 16, "Fiber Reinforced Concrete," was completed by the Canadian Standard Association (CSA, 2000). CSA also approved the code, "Design and Construction of Building Components with FRP in 2002" (CSA, 2002).

40

The United States has had a long and continuous interest in fiber-based reinforcement for concrete structures. Accelerated development and research activities on the use of these materials started in the 1980s. In 1991, the ACI established Committee 440, "FRP Reinforcement." The committee published a state-of-the-art report on FRP reinforcement for concrete structures in 1996 (ACI Committee 440, 1996). Committee 440 produced two documents approved by the Technical Activities Committee for publication in the year 2001. The documents are (1) "Guide for the design and construction of concrete reinforced with FRP bars"; and (2) "Guide for the design and construction of externally bonded FRP systems for strengthening concrete structures." (ACI Committee 440, 2001)

State-of-the-art strengthening and retrofit techniques increasingly utilize externally bonded FRP composites, which offer unique properties in terms of strength, lightness, chemical resistance, and ease of application. Such techniques are most attractive for their fast execution and low labour costs. Developments since the first research efforts in the mid-1980s have been remarkable. The range of applications has expanded to include masonry structures, timber, and even metals. The number of applications involving composites as strengthening/repair or retrofit materials worldwide has grown from just a few 10 years ago to several thousand today (Figure 2-18).

Various types of structural elements have been strengthened, including beams, slabs, columns, shear walls, joints, chimneys, vaults, domes, and trusses.

2.5.4 Carbon fibers reinforced polymers (CFRPs)

Carbon fiber, as shown in Figure 2-19, is produced by the controlled oxidation, carbonization and graphitization of carbon-rich organic precursors which are already in fiber form. The most common precursor is polyacrylonitrile (PAN), because it gives the best carbon fiber properties, but fibers can also be made from pitch or cellulose. Variation of the graphitization process produces either high strength fibers (2,600°C) or high modulus fibers (3,000°C) with other types in between. Once formed, the carbon fiber has a surface treatment applied to improve matrix bonding and chemical sizing which serves to protect it during handling.

When carbon fiber was first produced in the late sixties the price for the basic high strength grade was about $400/kg. By 1996 the annual worldwide capacity had increased to about 7,000 tonnes and the price for the equivalent (high strength) grade was $30-80/kg. Carbon fibers are usually grouped according to the modulus band in which their properties fall. These bands are commonly referred to as: high strength (HS), intermediate modulus (IM), high modulus (HM) and ultra high modulus (UHM). The filament diameter of most types is about 5-7 mm. Carbon fibers have the highest specific stiffness of any commercially available fibers, very high strength in both tension and compression and a high resistance to corrosion, creep and fatigue. Their impact strength, however, is lower than glass and aramid, with particularly brittle characteristics being exhibited by HM and UHM fibers. Carbon Fibers are conductive, have chemical resistance, they are non sensitive to UV-radiation; The Japanese standard does not prohibit the use of carbon fiber strips near live wires by railway tracks, for example, as they should be insulated from the steel reinforcement, the synthetic resin used for adhesive bonding between carbon fiber strips and reinforcement normally provides an

42

adequate insulation. The compressive strength is close to their respective tensile strengths. The coefficient of elasticity corresponds to that of steel (Figure 2-26). For some types, however, it is significantly higher. In atmospheric air, carbon fibers will start oxidizing at approximately 650 °C. CFRP strips are relatively stiff and are therefore not applicable for building components of complicated geometry. For such purposes carbon fiber sheets are more appropriate. Today there are three types of texture as illustrated in Figure 2-20: texture with uniaxial fibers, texture with fibers in two directions intersecting at right angles, and texture with fibers in three or more directions (multiracial texture) which is the latest development within fiber cloth; this kind of cloth is especially applicable for shear reinforcement. Also the sheets have ability for absorption of cracking tendency, preparation of anchorage, alkali reaction, and reinforcement for circular cross-section columns with reduction of the expansion by total encapsulation (jacketing).

Other types of FRPs are glass fiber (GFRP), and aramid fibers (AFRP). Glass fibers (GFRPs) are available in two types: E (electrical)-glass fibers and S (silica)-glass fibers. S-glass has a higher strength and stiffness than the E-glass; however, its high cost puts it as a second option for use in structural applications. Also many types of glass fiber will be attached by an alkali environment (ph $\geq$ 11), but not acid; furthermore, they are not conductive. The compressive strength is close to their respective tensile strengths. The modulus of elasticity is significantly lower than that of steel. Therefore, the use of an E-glass/epoxy system requires several layers to fulfill the creep rupture requirements, especially with damaged specimens where excessive deformation is expected. GFRP maintain their tensile strength up to the melting point, which is approximately 1000 °C (fire resistance).

43

Aramid fibers reinforced polymers (AFRP) are a trade name for organic fibers. AFRP consist of polymer fiber made of carbon, oxygen, and hydrogen molecules. Its good impact resistance makes it the best material for impact resistance applications regardless of low compressive resistance. Aramid fibers (AFs) have chemical resistance, and may absorb moisture which is assumed to harm the adhesive bond between fibers and synthetic resin. When AFs are exposed to direct sunlight their colour will be changed and their tensile strength will be reduced. AFRP are not conductive. The coefficient of elasticity is lower than that of steel; for some types, however, it is significantly higher. The compressive strength is significantly lower than that of steel, and they are not applicable at temperatures above 200 °C.

Fiber of carbon, glass and aramid are not injurious to health in normal use. However, protective measures should be taken when composite materials are formed, for example, cut by sawing machine or angle grinder. The fine fiber dust may irritate eyes, mucous membranes and the skin.

Fibers of carbon, glass and aramid are not poisonous substances and they are inactive so that they do not liberate harmful substances to the ground water or the atmosphere, therefore. There is no toxic waste. However, synthetic resin within or for gluing on to fiber composites may present a problem by combustion, since certain synthetic resins may develop toxic fumes.

2.5.5 Matrices

The continuous part in composite material is the matrix that binds the fibers. There are two types of resin forming the matrix in composites: epoxy and polyester

44

resins. The epoxy is the most commonly used for high load bearing applications, whereas the polyester is used in other applications with low bearing level.

The roles of a matrix in a composite are twofold. It serves as a binder that encapsulates the reinforcing fibres, transforming the load among them; it also protects the fibres from the environment and mechanical damage. The matrix must not damage the reinforcement and it must transmit any stresses to the reinforcement. Ideal unidirectional fiber reinforced composite material would have straight fibers running exactly parallel to each other, with fibers completely embedded in a strongly adhering, uniform matrix material.

2.5.6. Epoxy resin

Epoxy resins consist of a reactive resin which can, in much simplified terms, be considered as a material with a reactive "hook", and a hardener (also called curing agent) with reactive "eyes" (Figure 2-21). To achieve the full properties of the cured resin system, the right number of "hooks" must be intimately mixed with the right number of "eyes" so that in the pot of mixed resin a "hook" is immediately adjacent to an "eye".

The properties required for a specific application are achieved by careful attention to the chemistries of both the resin and the hardener which are influenced by the precise chemical nature of the chemical grouping structures between the chemical "hooks" and "eyes". The nature of these structures and also the nature of the other additives in the formulation will influence the ultimate strength, and rate of cure at different temperatures. Correct proportioning and thorough mixing are, therefore, imperative when using epoxy resin systems. The change in volume between the mixed uncured epoxy

45

resin/hardener and the fully-cured polymer is low and, if the material is carefully formulated, mixed and applied according to the formulator's instructions, can often be considered to be negligible. However, temperature of mixed resin system and cure temperature all need to be carefully considered to avoid shrinkage due to thermal contraction [Allen et al., 1993].

2.6 Methodology for Rehabilitation RC Slab Using CFRP Sheets

External forces such as shear and bending moment are caused by applied loads to the structure. The section of the member is designed in such a way that its internal ultimate capacity (resistance) is equal or greater than the external ultimate forces acting on the member.

The tensile strength of concrete is much lower than its compressive strength (about1/10), and hence concrete is subject to cracking in the tension zone. This is overcome by using reinforcement, to carry tensile forces and limit crack widths within acceptable values.

Flexural mode of failure in RC structures is the preferable mode that controls the design, (Figure 2-22). Unless care is taken in design and construction or for any other reasons explained previously, structure (live) flexural cracks may be appeared in the tension zone of interior slab-column system as a warning before failure (Figure 2-23), decreasing the effective cross section of the member, and allowing penetration of water, leading to corrode the steel reinforcement which declines its cross section. As a result, the internal ultimate flexural capacity will be reduced. If the ultimate flexural resistance

46

become less than the external acting forces which is the main reason of structural failure, rehabilitation will be needed.

In order to increase the ultimate flexural capacity of the system, additional external reinforcement must be added to the tension zone. The flexural (or bending) capacity of structural members can be easily enhanced by bonding a layer of FRP to the tension face of the element. In the case of a reinforced concrete structure, for example, the CFRP resists tension forces that supplement the tension force carried by the existing reinforcing steel. Thus, the moment capacity of the member can be calculated by taking into account the contributions of both steel and CFRP.

Figure 2-24 shows the variation of the strain and stress at the tension zone of the slab after the application of CFRP sheets to the tension (cracked zone); as seen the tension capacity of the section increased after adding the CFRP resistant tension force (T_f). The result of applying CFRP sheets to the tension zone of the slab will be:

- Increase in the flexural capacity of the slab (Uomoto et al., 2002)

- The system will exhibit a larger deformation capacity compared to the original system and will gain more stiffness.

2.7 Failure Modes of Flexural Strengthen RC Member with CFRP Sheets

Flexural strengthening of RC members using CFRP sheets may be provided by epoxy bonding materials to portions of the elements in tension, with fibers parallel to the principal stress direction. Well-established strengthening procedures for RC structures may be followed, provided that special attention is paid to issues related to the linear-elastic nature of FRP materials and the bond between the concrete and FRP.

47

Central to the analysis and design of FRP-strengthened RC structures is the identification of all of the possible failure modes as shown in Figure 2-25, which include the following:

(a) Steel yielding followed by FRP fracture;

(b) Steel yielding followed by concrete compressive crushing (while the FRP is intact);

(c) Concrete compressive crushing;

(d) FRP peel-off at the termination or cutoff point, due to shear failure of the concrete;

(e) FRP peel-off initiating far from the ends, due to inclined shear cracks in the concrete;

(f) FRP peel-off at the termination point or at a flexural crack due to high tensile stresses in the adhesive; and

(g) Debonding at the FRP-concrete interface in areas of concrete surface unevenness or due to faulty bonding.

Of the above, mode (b) is the most desirable. Modes (d) and (e) will be activated when the element's shear strength is approached; hence, they may be prevented by providing shear strengthening. Mode (f) can be suppressed by limiting the tensile strain in the FRP to a value of roughly 0.008. Finally, mode (g) May be avoided by proper quality control. Slip at the concrete-FRP interface may be ignored in the design [Bakis et al. 2002].

2.8 Summary

This chapter showed that the need for rehabilitation of building components is growing. By the nature of concrete its durability not always satisfactory and the need for repair will be necessary when the environmental effects appear. Rehabilitation often

presents the unique challenge of carrying out the repairs safely and efficiently while keeping the facility open to normal use.

An interior slab-column system may exhibit flexural cracks at the tension zone according to flexural failure design mode control. The proper repair of deteriorating structure is based on the careful evaluation of the causes, extent, and consequences of the deterioration, and the repair techniques, procedures, and materials necessary to remedy the situation. The cost of application and the efficiency of the repair process are major considerations in choosing the materials and techniques.
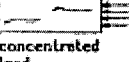
Composites have gained widespread use as strengthening materials for RC structures in applications, where traditional repair techniques may be problematic. Extensive research across the world during the last 25 years has led to a better understanding of properties and behaviour of the FRPs under different conditions.

As previous studies have shown, CFRP are competitive material having a high ability to increase flexural strength and stiffness which are important in controlling the deflection, reducing of cracking tendency, and crack's width; therefore, CFRP were chosen over other types of composites such as glass and aramid fiber (Figure 2-26). Furthermore, many studies have shown that CFRP has many advantages such as its resistance to electrochemical corrosion, favourable fatigue behaviour, high strength to weight ratio. Furthermore, FRPs can be easily bonded to the concrete surface without the use of extensive scaffolding and jacks, requiring a minimum amount of support equipment, they are easy to use and cost effective.

49

The current literature is limited to the strengthening of non damaged slab, rehabilitation of slab using traditional methods, and rehabilitation of slab exhibited punching shear failure. For economical benefits, innovative repair techniques is need to be developed so that the damage to the slab will be tested, and the ability of CFRP sheets to repair the flexural cracked zone at the slab-column connection which has been subjected to combined shear and unbalanced bending moment will be investigated; then the durability of the concrete structure can be improved and the service life prolonged.

So, the overall effectiveness of using CFRP sheets for rehabilitation of flexural cracked RC slab-column system subjected to shear and unbalanced moment has not been investigated.

50

Table 2-1: Characteristics and causes of cracks

Cause	Time of formation	Manifestation		Remarks
Plastic settle-ment (slump cracking)	First few hours after casting	Cracks along lines of reinforcement Cracks at changes in shape of section		Cracks can be large (> 1mm)
Plastic Shrinkage	First few hours after casting	'map' cracking or long cracks on surface of slabs cast in drying conditions		Cracks can be large (2-4 mm not uncommon)
Early thermal cracks	Not till after several months or years from construction	Large cracks at construction joints in wall. Other cracks depending on nature of restraints		Can be controlled by rein-forcement (<0.4 mm) by limiting pore sizes or control of temperature
Shrinkage	Not till after several months or years from construction	Similar to bending or tension cracks	See below	Usually small if reinforcement present (<0.4 mm)
Corrosion	Not till after several months or years from construction	Cracking along lines of bars, developing into spalling		Initially small (0.2 mm), increasing with time; rust staining may be visible in wet conditions
Alkali-aggregate reactions	Not till after several months or years from construction	Occurs in wet conditions frequently as 'map' cracking. Only occurs with certain types of aggregate		Cracks can be large (>1 mm)
Loading in service	Depends on usage of structure	flexure tension shear torsion bond		Generally small (<0.4 mm) if design for strength is satis-factory. Large cracks are generally an indication of mis-understanding of the response of the structure at the design stage
Restraint	Depends on external influences settlement etc.	bond flexural concentrated load		Usually small (<0.4 mm) if sufficient reinforcement present

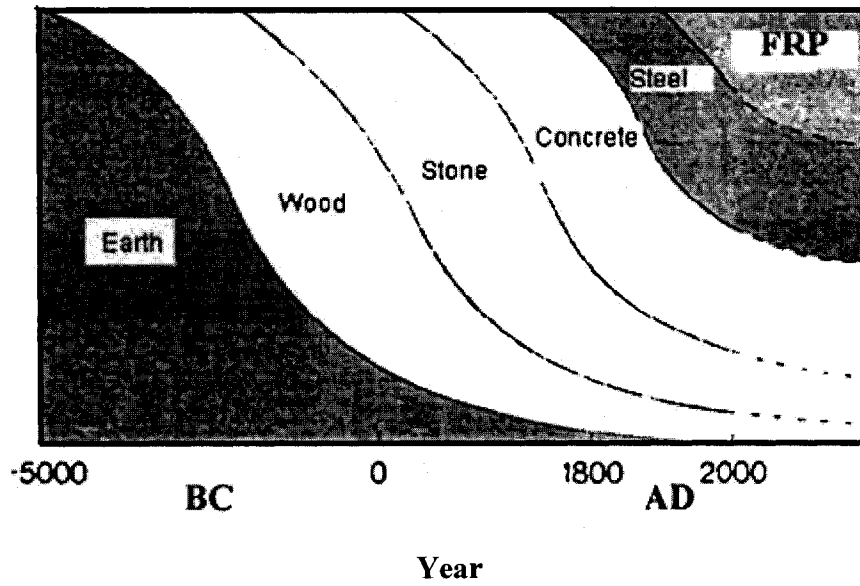After (Mailvaganam, N. P. "Repair and Protection of Concrete Structures." 1991)

51

Fig. 2-1: Construction materials in different ages
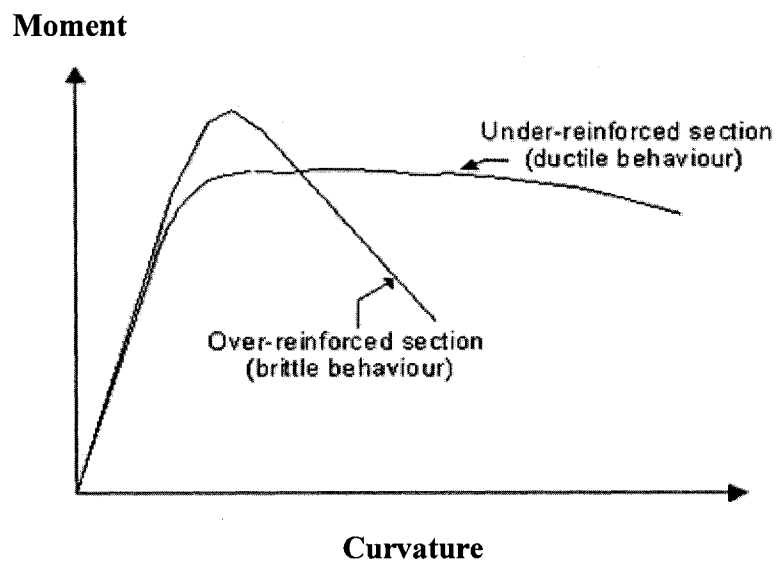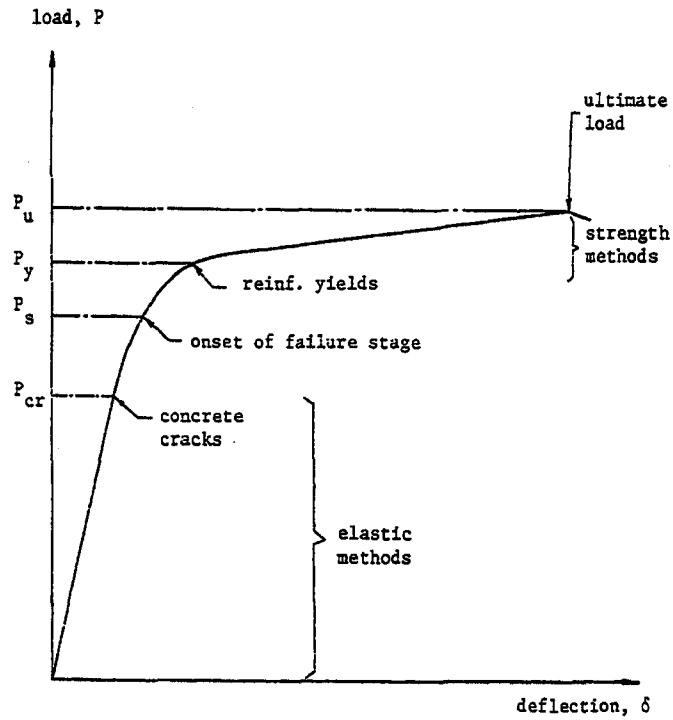
[Uomoto et al. 2002]

Fig. 2-2: Moment Curvature Relationship

(Concrete Design Handbook, 1995)

52

Fig. 2-3: Load-deflection curve for flexural control design

P_{cr} = flexural cracking load

P_s = Shear-cracking load

P_y = load at which reinforcement Yields
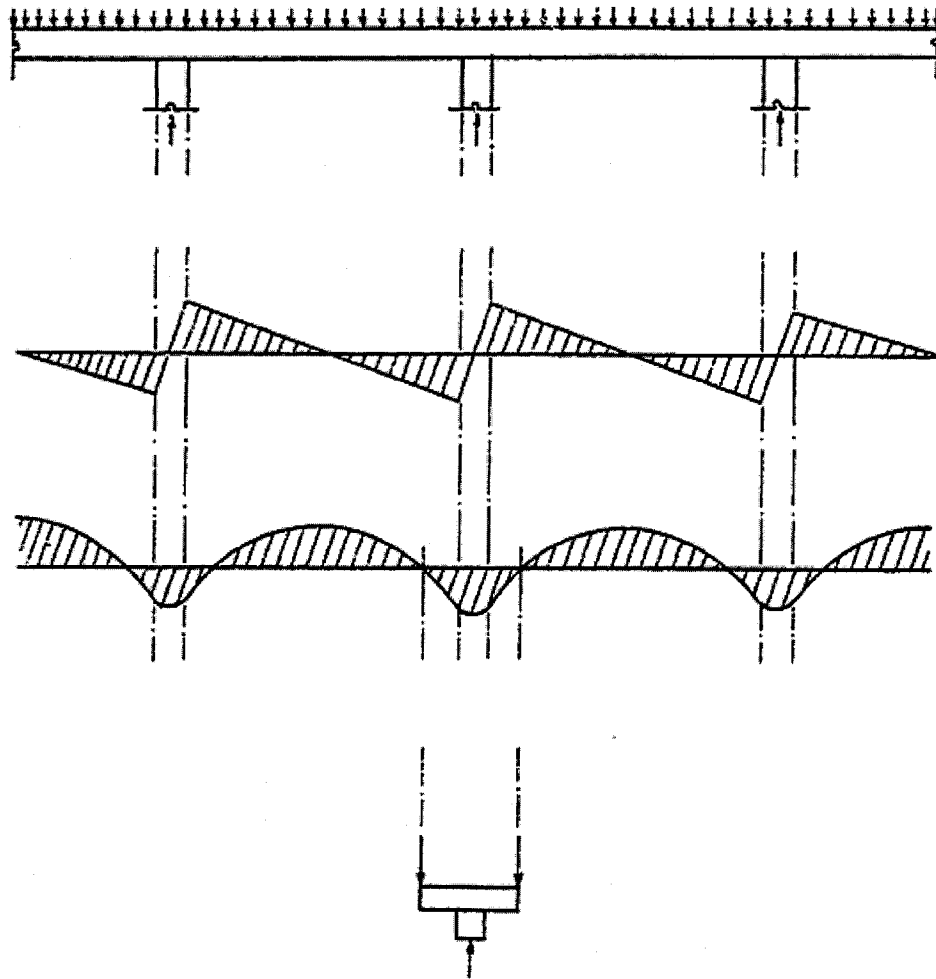
P_u = ultimate load

53

Fig. 2-4: Section at interior slab-column connection

(Shear and moment diagram)

Bending and shear forces are concentrated at Slab-column connection area
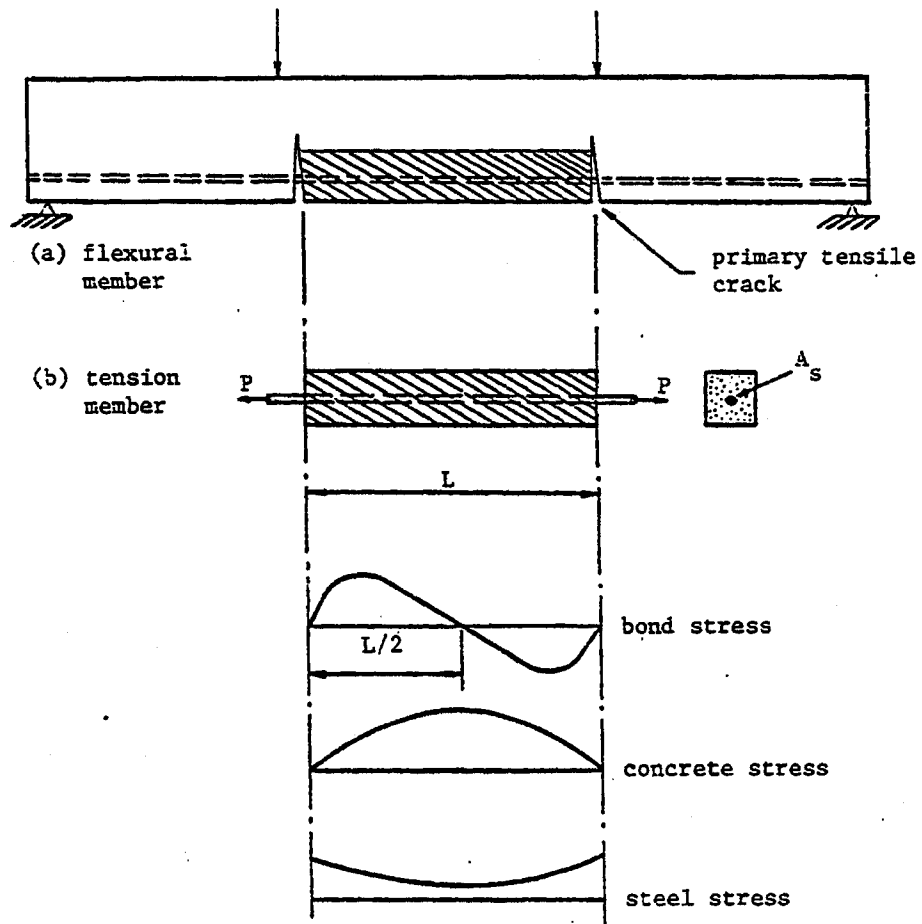
54

Fig. 2-5: Flexural and tension members after cracking

[ACI Publication SP-20, 1968]

55
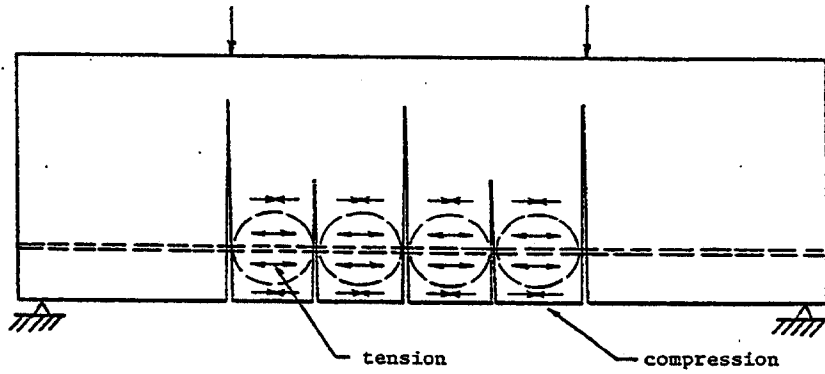
Fig. 2-6: Flexural member – stress redistribution

(a)

secondary
tensile crack
(first order)

primary tensile
crack

(b)

secondary tensile crack
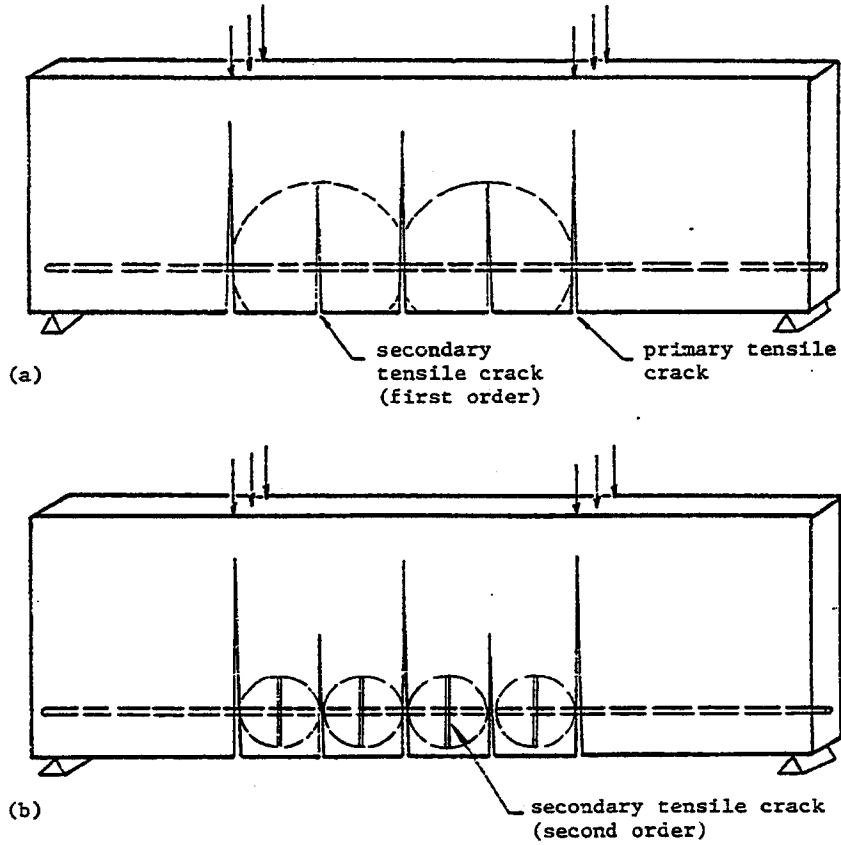(second order)

Fig. 2-7: Mechanism of tension cracking in flexural member
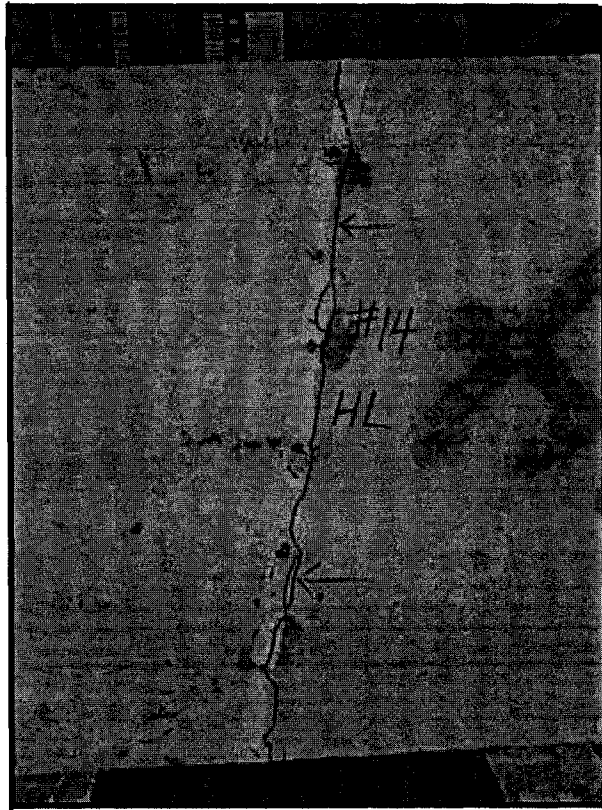
[ACI Journal, 1965]

56

Fig. 2-8: Typical failure of slab specimens after repaired

(New crack adjacent to the original but outside of repaired crack)

(NAHB Research Center, Inc.)

57
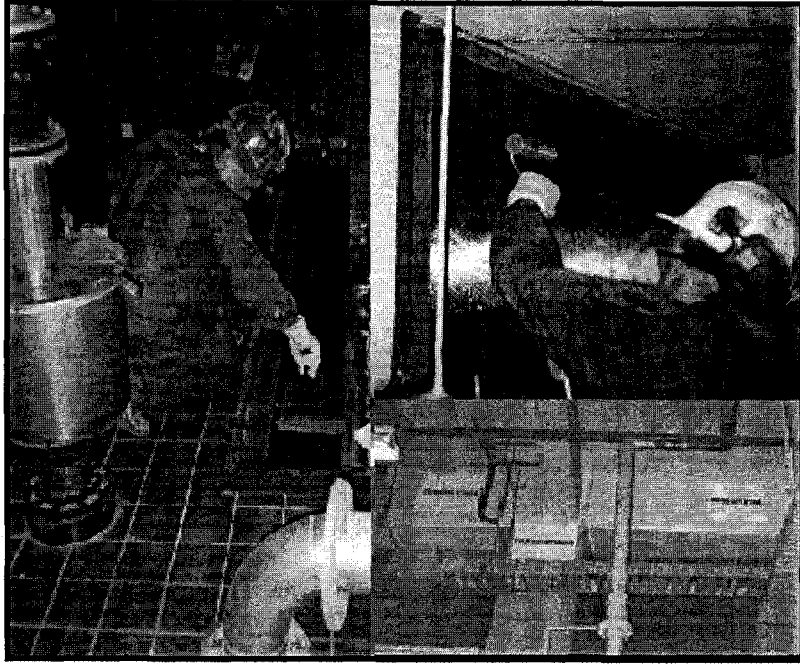
Fig. 2-9: Windsor Dewatering Building (Stanley Consulting Group, 1998)

Before repair

After repair
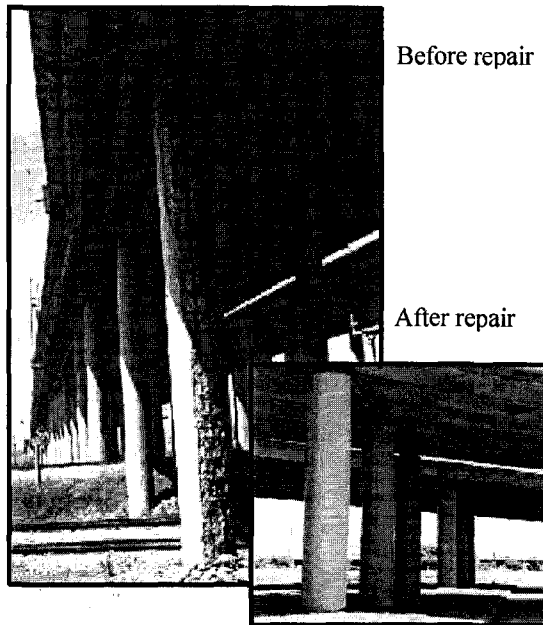
Fig. 2-10: I-40 Bridge, Oklahoma (repair of corrosion damaged piers)

58

Fig. 2-11: Arizona State Hospital (repair of walls and ceiling's tunnel)
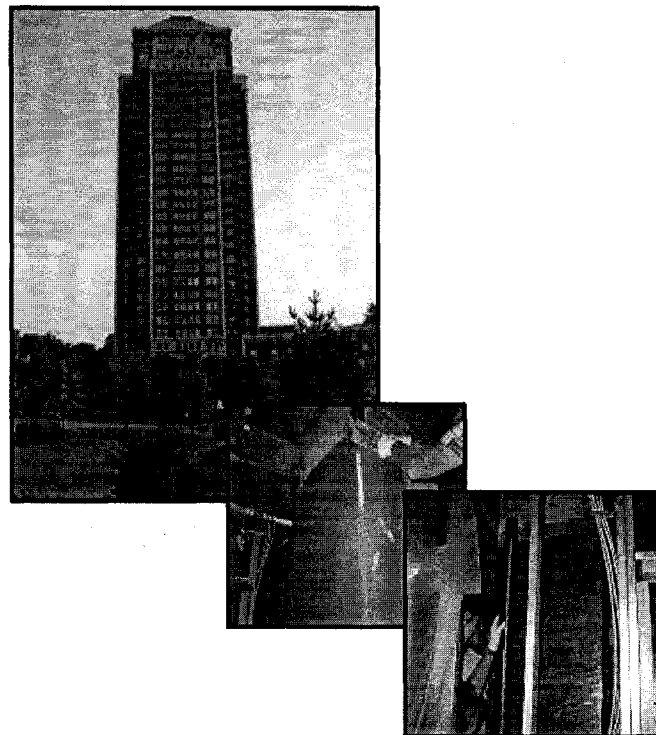
Fig. 2-12: St. Louis residential tower, Missouri

(Wrapping columns with CFRP sheets)

QuakeWrap, Inc. (http://www.quakewrap.com)

59

Fig. 2-13: St. Joseph's Hospital, Arizona

(Strengthening of the floors with CFRP plates)
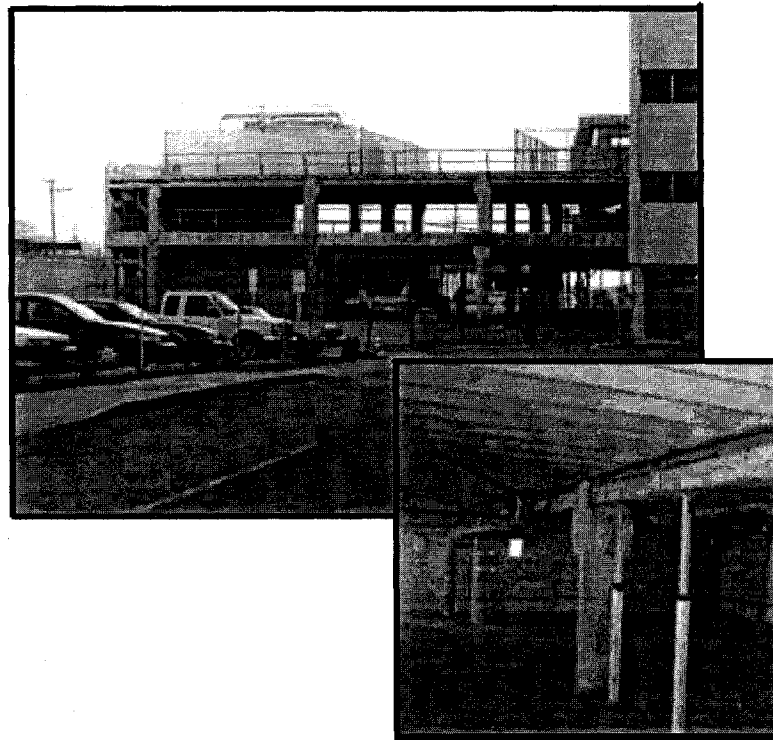
Fig. 2-14: City Court Garage, Arizona

(Repair of corrosion damaged T-beams using GFRP)

QuakeWrap, Inc. (http://www.quakewrap.com)

60

Fig. 2-15: Oran Roberts, Texas
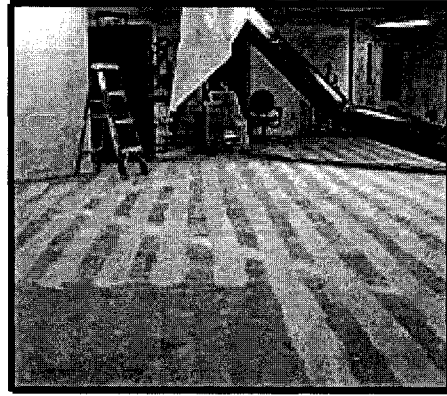
Fig. 2-16: Prov. Hospital, Alaska

(Strengthening of double T-beams with GFRP) (Strengthening of the floor with CFRP)
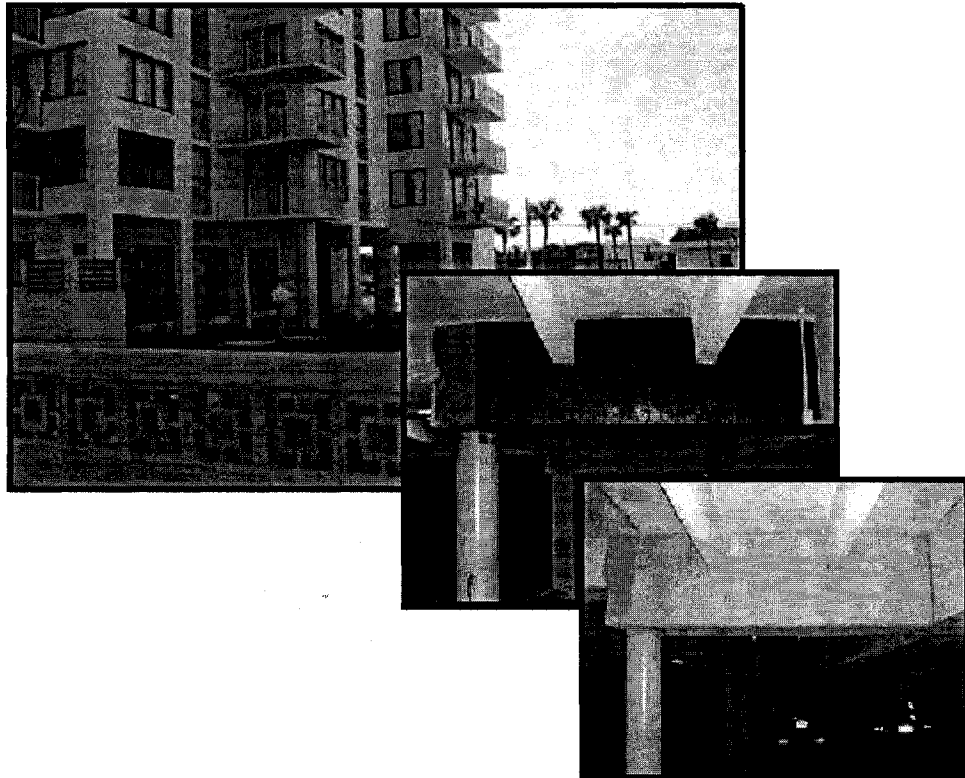
Fig. 2-17: Parking structure of the Oceans One Condominium

(Repair of corrosion damaged and shear cracking beam with CFRP)

QuakeWrap, Inc. (http://www.quakewrap.com)

61
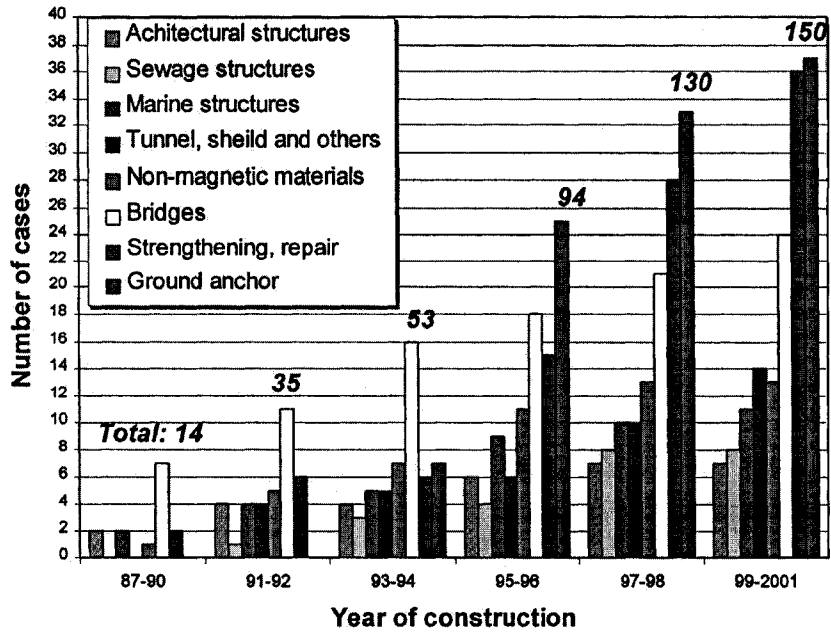
Fig. 2-18: Growing applications of fiber reinforced polymer composites in construction

industry
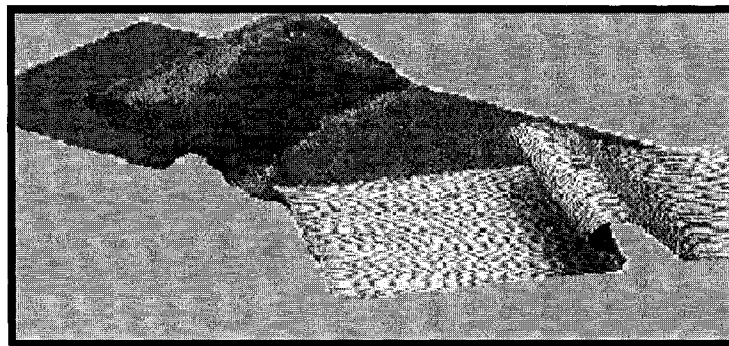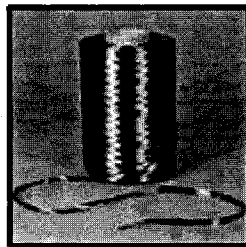
Fig. 2-19: Carbon Fiber Reinforced Polymer sheets

62
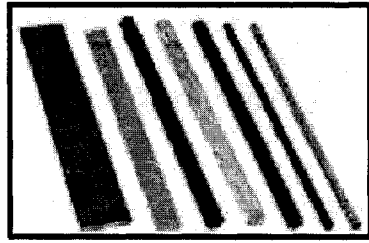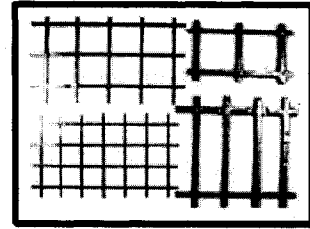
One dimension

Two dimension

Three dimension

Fig. 2-20: Common types of texture available fiber reinforced polymer composites
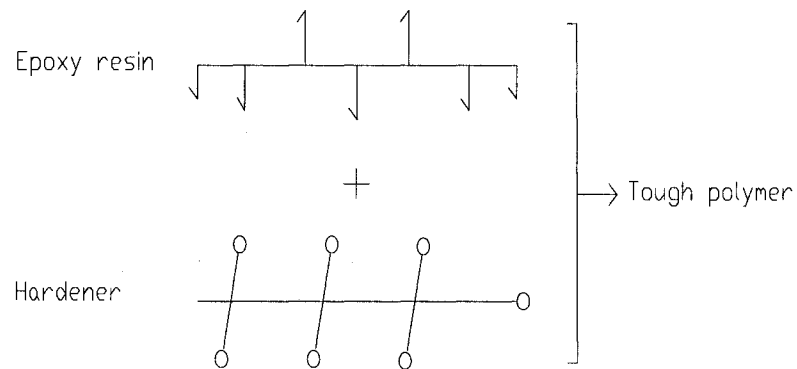
Fig. 2-21: Reactive hooks and eyes for Epoxy resins

63

Cross-Section **Strain Distribution** **Stress Distribution**
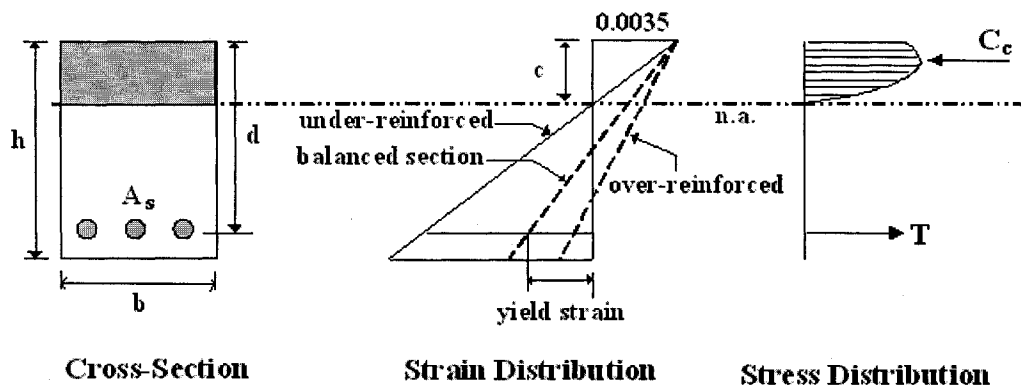
a) Plane Section Analysis

Cross-Section **Strain Distribution** **Stress Block**
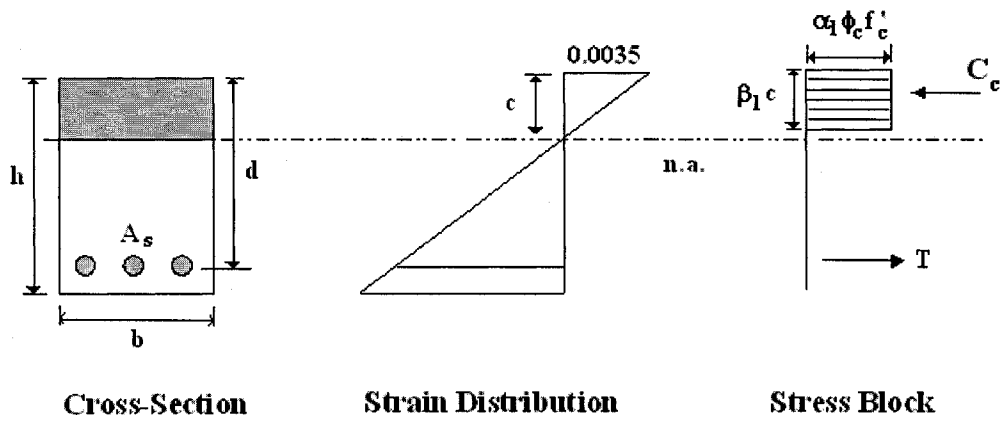
b) Rectangular Stress Block

Fig. 2-22: Flexural Analysis of Reinforced Concrete Sections

(Concrete Design Handbook, 1995)

64
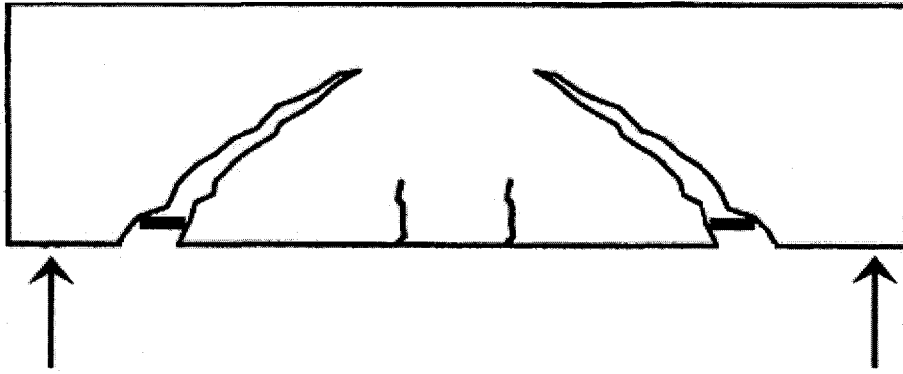
Fig. 2-23: Flexural cracks at tension zone of RC slab
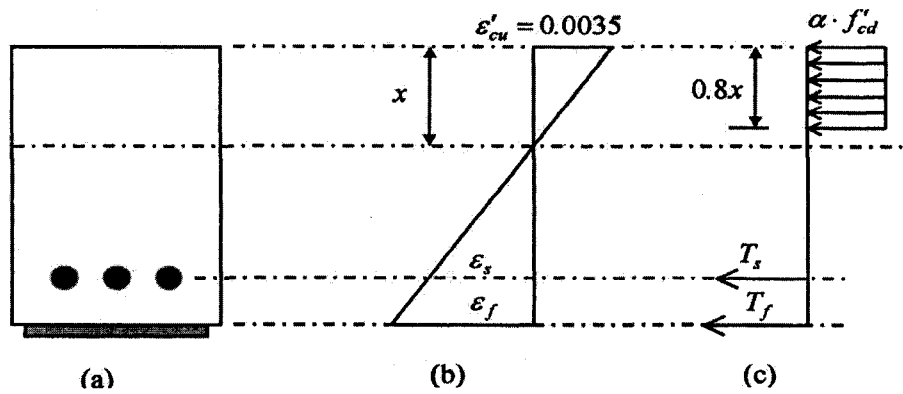
Fig. 2-24: Flexural Analysis of Reinforced Concrete Sections with CFRP

65
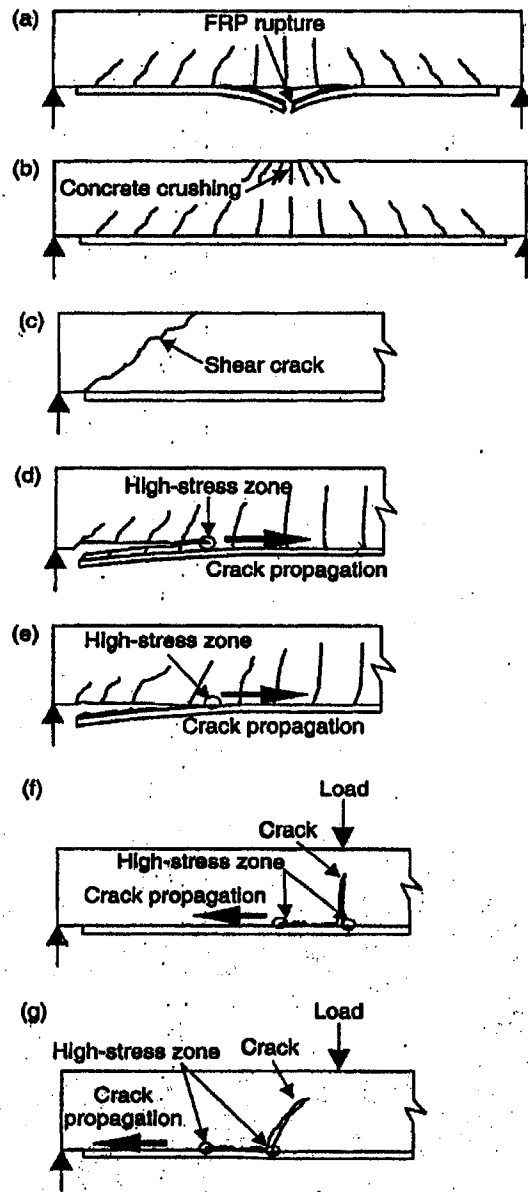
Fig. 2-25: Failure modes of FRP in RC beams

(a) FRP rupture; (b) crushing of compressive concrete; (c) tensile concrete failure;(d)

concrete cover separation;(e) plate end interfacial debonding;(f) intermediate flexural

crack-induced interfacial debonding;(g) intermediate flexural shear crack-induced

interfacial debonding.

66
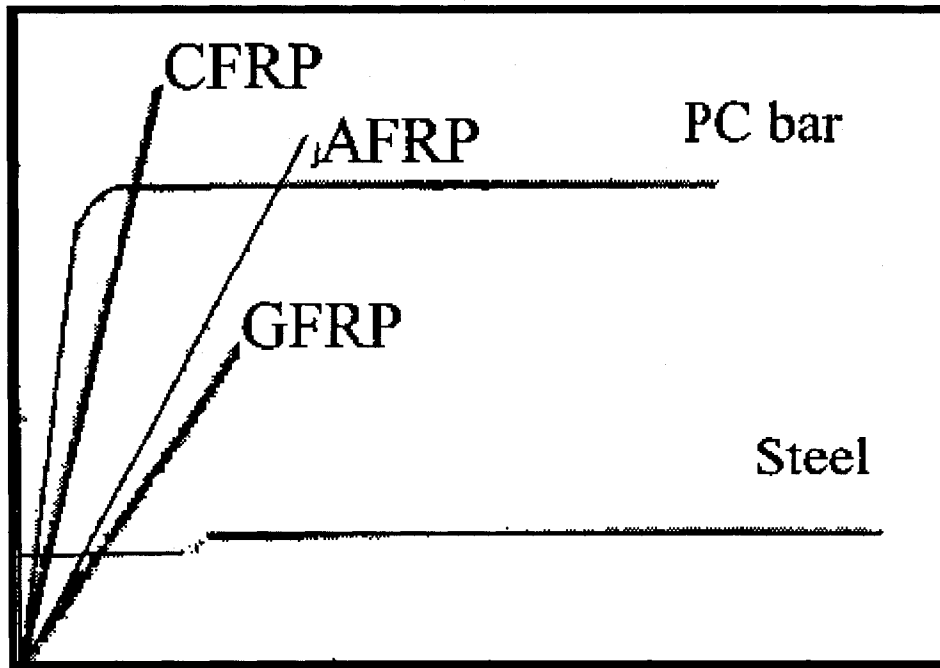
Fig. 2-26: Typical stress-strain curves for some fiber reinforced polymer composite

(Uomoto et al., 2002)

CHAPTER III

EXPERIMENTAL PROGRAM

3.1 Introduction

The objective of the experimental program was conducted to examine a rehabilitation technique of flexural cracked RC slab-column connections using CFRP sheets.

The experimental program consists of six RC slab-column connection specimens was conducted to evaluate the effectiveness of CFRP sheets used as external reinforcement for the rehabilitation and the strengthening of existing flexural damaged slab-column connection. This chapter describes the specimens (configuration, materials and fabrication), the instrumentation, the experimental setup, the procedure for flexural test, and the rehabilitation scheme using CFRP sheets.

3.2 Experimental Program

Six specimens consisting of a rectangular slab and a center column stub extending above and under the slab were built to model an interior RC slab-column connection representative of typical flat-slab structures.

All specimens were identical in design; to study the effect of eccentricity on the rehabilitation technique which is the major difference in geometry, the first three control specimens were tested to failure under a single monotonically increasing load using different eccentricity.

68

In order to demonstrate the rehabilitation application, three other specimens were cracked while they were being loaded at approximately 70% of the ultimate load recorded during testing of the control specimens. Then the cracked specimens were reinforced externally with carbon fiber reinforced polymer (CFRP) sheets on a tension (cracked) zone. The loading resumed to failure after curing, allowing the study of the efficiency of CFRP.

On the basis of the experimental results reported by Elstner and Hognestad, an unbalanced moment to gravity shear ratio (M/V) that was approximately equal to the length of the column side (250 mm) was found to successfully represent the actual demand in interior slab-column connections for high gravity load cases.

Three groups were formed according to the eccentricity of applied load (e), (0 , 0.25 , 0.35 m), as illustrated in Figures 3-1, 3-2, 3-3. The first specimen of each group is the control specimen which was tested to failure. The second specimen underwent two testing steps: in the first step the specimen was loaded up to 70% of the ultimate load of the control specimen of the same group was applied, creating cracks in the tension zone; in the second step the specimen was reinforced with CFRP sheets bonded on the concrete cracked surface then tested to failure.

The test specimens are referenced using specific identification labels. In this labelling scheme, CTRLe, CRAKe, and REHBe represent the control specimen (without CFRP), cracked specimen (before rehabilitation), and rehabilitated specimen using CFRP respectively, while e is variable taking one of the three values (0 mm, 250 mm, 350 mm) depending on the group (eccentricity of applied load).

3.3 Description of Test Specimen

The prototype for the experiment represents approximately the region of the slab around the column bounded by the lines of contra-flexure located in RC flat-plate structure. The specimens have a rectangular cross section of 1000 mm wide by 2000 mm length. The slab thickness was selected to be 150 mm which is sufficient to prevent the slab from a punching shear failure mode. The slab was connected with a 250 x 250 mm central column stub extending above the slab by 750 mm, and below the slab by 400 mm. The second and third groups of specimens have the same geometry as the first group; however, the upper loaded column stub was augmented by a cantilever projection of 450 mm from the face of the column with a 250 x 500 mm cross section as illustrated in Figure 3-4, this role of the cantilever is only to be able to impose an eccentric load.

3.4 Material Properties

The materials used in the tests include concrete, steel reinforcement, epoxy resin, and CFRP composite sheets.

3.4.1 Concrete

The concrete was ready mix ordered in three batches for each of the three groups. Thirty six (150 mm x 300 mm) concrete cylinders were cast, prepared and tested following the standard cylinder testing program to determine the average of compressive and tensile strength (modulus of rupture) of the concrete as shown in Figures 3-5 and 3-6. Based on testing cylinders an average result of the concrete at 28 days compressive strength (f'_c) was equal to 36, 47, and 53 MPa for group A, B and C, respectively. The 28

70

days tensile strength (f'_{ct}) obtained from testing cylinders was equal to 3.7, 4.5, and 4.8 MPa for group A, B, and C, respectively. Tables 3-1, 3-2, 3-3 summarizes the main characteristics of concrete mix for each group (batch). The compressive strength-time relationship for each group (batch) is illustrated in Figures 3-7, 3-8, 3-9.

The maximum aggregate size for second and third groups was 10 mm to enable the concrete to pass between the congested reinforcement bars in the cantilever projection according to ACI (Sections 7.6.3 and 3.3.2). Superplasticizing admixtures were added to the concrete mix to allow a reduction of the water content for a given workability and to reduce concrete shrinkage. This super workability only lasts for a limited period, generally about two to four hours. Slump test accordance with ASTM C 143 (Figure 3-10) was checked before casting to determine consistency or workability of the concrete mix, a slump of 25 mm was registered.

3.4.2 Steel Reinforcement

The RC specimens were fabricated using deformed bar reinforcement 10M and 20M. The properties of the steel reinforcement were assumed to have: yield strength of 400 MPa and elastic modulus of 200 GPa; as is typically used for purposes of design.

3.4.3 Electrical Strain gauges

Electrical strain gauges used in the test were manufactured by KYOWA Electronic Instruments Co. Steel strain gauges were Mode KFG-10-120-C1-11. This gauge mode has: 10 mm length, 119.8 Ω resistance, 11.70 PPM/°C adoptable thermal expansion, 0.20% transverse sensitivity, and 2.11% gauge factor. Concrete strain gauges

were Mode KFG-30-120-C1-11; this gauge mode has: 30 mm length, 120.20 Ω resistance, 11.70 PPM/°C adoptable thermal expansion, 0.20% transverse sensitivity, and 2.10%. The base of a strain gauge is made of a resin such as polyimide.

3.4.4 Carbon fiber reinforced polymers composite

Tyfo® SCH-11UP composite were used as external reinforcement to repair the cracked specimens in the tension zone (cracked zone). The Tyfo® SCH-11UP Composite is comprised of Tyfo® S and Tyfo® SCH-11UP reinforcing fabric. Tyfo® SCH-11UP is a custom, unidirectional carbon fabric. The Tyfo® S Epoxy is a two-component epoxy matrix material for bonding applications.

As reported by manufacturer (Table 3-4), the Composite gross laminate properties are: 903 MPa Ultimate tensile strength in primary fiber direction; 1.05% Elongation at break; 86.9 GPa Tensile Modulus, and 0.25 mm Laminate thickness.

3.4.5 Epoxy resin

Most of the FRPs use various kinds of resins, including epoxies. Although the resin does not carry any tensile load directly, it acts as a filler material and holds the fibers together. The resins also play a crucial role in transferring the load and protecting the fibers in much the same manner as the surrounding concrete protects the embedded reinforcing bars. It is important that the fracture strain of the resins and the compatibility with the fibers themselves are taken into consideration in an appropriate manner.

72

Tyfo® S Epoxy, a two-component epoxy matrix material, was used for bonding CFRP on the RC specimens. It is a high elongation material, which gives optimum properties and long working time for application, with no offensive odor. The materials properties for epoxy as reported by manufacturer (Table 3-4), are: Tensile strength of 72.4 MPa, Tensile Modulus of 3.18 GPa, and 5.0% Elongation.

3.5 Specimens Construction

The construction process was executed in three stages for the three groups. Each stage was carried out in the following sequence:

3.5.1 Formwork preparation

Plywood sheets of 19 mm ($\frac{3}{4}$ ") thickness were used as a mould of the slabs and column stubs. Details are shown in Figure 3-11. All parts of a set were nailed and fixed using steel angles. The slabs were supported on strong horses in addition to six wooden studs to control the deflection of the slab during the curing process. The cantilever parts were supported on the wooden studs as shown in Figure 3-19. The inner form surfaces of the formwork were brushed by oil in three layers.

3.5.2 Preparation of the reinforcement cages

Each specimen was reinforced as shown in Figure 3-12 by deformed steel bars having 25 mm (1") concrete cover. Figures 3-13 shows shop details of the reinforcement bars.

73

The position of the reinforcement bars were marked on the plywood before tying the reinforcement bars using tie wires as shown in Figure 3-14. The slabs had top and bottom layers of reinforcement running in both directions. The bottom (tension) layer consisted of 10M steel reinforcement bars at 100 mm equal spacing in both directions with a 25 mm concrete cover which was maintained using 25 mm (1″) high E-Z plastic chairs, while the top layer spacing is double as the bottom layer (Figure 3-15).

The columns were reinforced with six longitudinal bars of 20M. A stirrup arrangement using 10M was provided at 100 mm spacing along the column stubs with a 25 mm concrete cover in addition to the cross ties. Another longitudinal bar was added to the column stub in the third group with 0.35 m eccentricity to resist an expected unbalanced moment. Figure 3-16 shows the reinforcement works for the column stub and cantilever part during the preparation. The estimation of the total reinforcement weight for each specimen in the second and third group was 19 kg.

3.5.3 Casting of the specimens

The method of placing and vibrating the concrete is of the most importance as to keep it uniform and homogenous. Proper methods of placing and consolidating prevent segregation and porousness of honeycombed areas, secure a firm bond between layers, a close bond with reinforcement, minimize shrinkage cracking, and produce a structure of good appearance (ACI, 1967).

The slab and the column stubs reinforcement were positioned on the oiled wooden mould using a crane; the strain gauge wires were arranged; the position of the steel strain gauges was marked, and then the upper column stub form was positioned and supported.

74

Figures 3-17 and 3-18 show the last steps of preparation before closing the mould, while Figure 3-19 shows the steel cage in the formwork ready for casting.

The concrete was ordered and delivered in one batch for each group from a ready mix plant. Superplasticizer was added to the concrete mix in the truck, and then the concrete slump was checked before casting which was found to be 25 mm (1″). Concrete was placed in a metal bucket via the chute on the concrete truck; the crane was used to carry the bucket to the specimens. The concrete mix was cast monolithically in lower and upper column stubs. Concrete mix was consolidated using electrical vibrators. The vibrator was inserted vertically to the full depth of the layer being placed; vibration was continued until the concrete was thoroughly consolidated and the voids filled, as evidenced by the levelled appearance of the concrete at the exposed surface and the embedment of surface aggregate. The vibrator was inserted and withdrawn slowly, and operated continuously while being withdrawn so that no hole would be left in the concrete. To improve the appearance, the form was vibrated by hammering at a level of a few inches below the concrete surface. The top of a lift next to the forms had trimmed level to form a neat showing line. The casting process is illustrated in Figures 3-19 to 3-21.

3.5.4 Testing of concrete strength

Tests of concrete strength are not a necessary part of concrete construction; however, they are a valuable aid to inspection and they provide a record of the quality and uniformity of the concrete. Strength tests are made either to check on the potential

75

quality of concrete or to check on the probable development of strength in the actual structure at a given time.

Cylinders were made, cured, and tested in accordance with ASTM C31 and ASTM C 496 for compressive and tensile strength (split cylinder) tests respectively. The usual age of test to determine strength of concrete is 28 days. The tests, however, were conducted at the age of 7, 14, and 28 days. An additional test was made on the day of testing for each specimen.

3.5.5 Curing

The purpose of curing is to keep concrete moist so that hydration of the cement can continue. Curing improves greatly the surface condition and general quality of concrete. The cast specimens were flooded with water for seven days, which is recommended by the ACI for exposed surfaces of concrete containing normal cement. The concrete cylinders were flooded with water in room temperature up to the time of testing. Figures 3-22 shows the RC specimen and cylinders during curing.

3.6 Rehabilitation Scheme

Any successful rehabilitation measure demands proper preparation of the structural element. This includes surface preparation, storage of fiber, resin constituent materials as well as mixing of the resin system, and lastly applying CFRP.

76

3.6.1 Surface preparation

One of the most important steps in a successful rehabilitation of any project is the surface preparation of the repaired structural component. Therefore, special consideration was given to prepare the concrete surface before bonding CFRP sheets. To provide a smooth surface for bonding, any irregularities such as form lines or protruding aggregate were ground down. If a composite sheet was applied to concrete surfaces that contain high spots, the sheet would tend to form an air pocket. Surface preparation and application procedures had been followed closely to ensure proper interfacial bond strength.

The surface of the cracked slab to be wrapped with CFRP sheets was grinded, broomed, cleaned, and made free from fins, sharp edges, and protrusions or cavities that may cause voids between the CFRP sheets and the concrete surface. However, in certain cases, acid washing or other means of surface preparation may be acceptable. The column stub surface that received CFRP sheets only received a broom cleaning. The corners of all concrete edges in which CFRP sheets were applied were rounded to a 20 mm radius minimum. Final cleaning with pressurized air was also used to remove any dust or debris. Figure 3-70 illustrates the steps that were used to prepare the specimens' surface.

3.6.2 Prepare saturating resin

Correct proportioning and thorough mixing are imperative when using epoxy resin systems, as explained in chapter two, and debonding results in loss of composite strength in transverse tension, shear, and impact.

77

During mixing, several defects may be introduced to the system, and consequently, to the sheet itself. First, when using rotary mixers, air can be drawn into the resin and remain as small air bubbles, leading to sheet porosity. In some cases, this porosity may later result in the formation of air bubbles of much larger diameter. In contrast, a low degree of mixing can result in chemical inconsistency, meaning that some regions contain high percentages of reactant, while others may contain no reactant at all. The efficacy of the resin system depends on the appropriate use of mix ratio. Errors in mix ratio can result in under-cure. To prevent large-scale debonding, the most susceptible areas must be rolled repeatedly until resin tack can be confirmed. If the material sags there is no bond or intimate contact between the composite and the substrate; thus, the stress transfer capabilities are severely reduced. For two layers of fabric on top of each other, the air usually becomes entrapped between them. Rollers were used to eliminate most of the air. Consequently, the two components of epoxy resin were mixed with a rotary mixer. Attention was paid to the mix ratio and mixing was performed at a slow rate without drawing an excessive amount of air into the matrix. Extra care was taken during the application of epoxy mortar prior to the application of the sheets to ensure that it produces a continuous bond between CFRP and concrete surface and that full composite action is developed by transferring the stresses across the thickness of the adhesive layer.

3.6.3 Application of CFRP sheets

Fibers are the main contributors to the strength and the stiffness of CFRP; the matrix serves as a medium for transferring stresses between adjacent fibers. Thus, ideal unidirectional fiber reinforced composite material would have straight fibers running

78

exactly parallel to each other, with fibers completely embedded in a strongly adhering, uniform matrix material.

The CFRP sheets were cut to the required size. Once the epoxy was mixed properly, the CFRP sheets were constructed by saturation fabric sheets with epoxy (Figure 3-71). A primary layer of epoxy was applied to the bonded face with a paint roller, and the sheet was placed on and pressed into the epoxy using the same roller; the epoxy resin was applied again and squeezed onto the surface of the sheets. In the repair scheme, one layer of CFRP sheets was bonded to the tension zone where the slab exhibited flexural transverse cracks in the (E-W) direction as shown in Figures 3-72 to 3-75 for (CRAK0, CRAK25, CRAK35) specimens, respectively. CFRP sheets were bonded with the fibers oriented in the (N-S) longitudinal direction which is perpendicular to the cracks to reduce the crack's expansive forces, as mentioned in the previous chapter. The structural properties of the hardened CFRP sheet, such as strength and Young's modulus, rely upon the monolithic behaviour of all the CFRP layers. This can be ensured only if the resin completely impregnates the spaces between the fibers while it hardens. During application, the resin should have the required seal life and viscosity to hold the sheet in place. It may be pointed out that these properties are also related to the atmospheric temperature at the time of application, and therefore the resin should be carefully selected; this process was repeated for the second layer and for wrapping the column stub also. The second layer was wrapped with transverse sheets in the (S-W) direction where the fibers were oriented perpendicular to the fibers of the first layer to resist bond-splitting force, prevent a premature debonding failure of the first layer, to protect the system from any brittle failure if that might occur, and to avoid any punching shear

79

and/or flexural shear failure caused by an increase in the slab flexural capacity after the application of CFRP sheets. The end of each layer was extended to the free edge of the slab and then wrapped around the edge as shown in Figures 3-23 and 3-24 in an attempt to achieve effective anchorage of the free ends of the CFRP sheets, and to ensure that the sheets do not debond from the concrete surface due to differential deformation during loading. This protection provides an effect similar to that offered by the driving of anchors into the concrete. The wrapping also included the lower column stub to anchor the ends of the first and second layers of the sheets. Finally, an additional thin layer of well mixed epoxy was applied on the fabric. The CFRP sheets were then left for curing for at least 3 days before testing. During the hardening process, especially in outdoor applications, it is important that the resins are protected from the action of rain, sand and dirt, and any other physical element that might cut the fibers. The temperature of the atmosphere also needs to be carefully monitored to ensure proper and adequate strength development in the resins (JRTRI 1997).

After the resin has sufficiently hardened, the finishing coat may be applied with the objective of ensuring long-term durability, to improve its resistance to the environment and prevent degradation on account of sunlight, fire protection, and aesthetic appeal. Such painting must be done before a glossy film is formed on the surface; this film usually appears after 24 hours.

Kodur et al. (2004) reported their experiments on the fire resistance of FRP wrapped columns under sustained loading. The effectiveness of a two-component fire protection system, which is a combination of cementations plaster spray and an intumescent coating with low thermal conductivity, was investigated. A fire protection

system having a thickness of about 37 mm applied in their study was capable of achieving fire endurance ratings of 5 hours or more under full service loads. The CFRP repair scheme is shown schematically in Figures 3-23 and 3-24.

3.7 Instrumentation

This section discusses both Internal and External instrumentations. Internal instrumentation consists of steel strain gauges to measure reinforcing steel strain. External instruments are: concrete strain gauges to measure concrete strain, linear potentiometers to measure specimen deflection, a manual pump to be connected to the universal flat load cell of 444.8 kN (200 Kips) capacity; and four universal flat load cells of 111.2 kN (25 kips), and 222.4 kN (50 kips) capacity to monitor the reactions. Figures 3-25 to 3-28 illustrate the predetermined location of the internal and external instruments respectively.

3.7.1 Internal instruments

To assess the internal behaviour of the specimens, sixteen 10 mm long steel strain gauges were applied on the reinforcement deformed bars for both reinforcement directions longitudinal and short at different predetermined locations of each specimen (critical section), which were expected to exhibit maximum moment then maximum strain on the tension zone. Two strain gauges were also applied to the reinforcement bars in the compression zone for the third group.

The reinforcement steel bar surface was grinded using an air grinder, and then the surface was rubbed with "MCA-1 M" Prep. Conditioner A. After that the surface was

81

rubbed again using "MN5A-1" Neutralizer. M-Coat A air-drying polyurethane coating was applied to the back of the strain gauge to accelerate the bonding. The 10 mm strain gauge was attached to the surface "M-Bond 200" adhesive. A polyethylene sheet was applied over the strain gauge and was pressed for approximately 2 minutes. After making sure that the strain gauge was securely bonded and would not detach from the applied surface, the polyethylene sheet was removed. Lastly, the gauge terminal was soldered with the conductors of the lead wire cable and coated using "M–Bond adhesive (catalyst-c)". All strain gauges were tested and checked thoroughly before and after casting using a digital multimeter. Figure 3.29 and 3.30 show the steel strain gauges during and after installation.

3.7.2 External instruments

3.7.2.1 Concrete strain gauges

Twelve 30 mm long concrete strain gauges were applied at different predetermined locations on the compression zone (N-S) and (E-W) direction of the concrete surface for each specimen. The concrete strain gauges were placed on the surface of the concrete specimens as close as possible as the same position of the steel strain gauges (Figure 3-26).

In order to make a measuring area flat, an electrical grinder was used, and then the surface was cleaned by wiping the measuring area in one direction only with tissue slightly dampened with isopropanol. The gauge guidelines were marked another time using lead pencil. To fill up tiny holes on the surface, a mix of the two components of "PC-12" was applied on an area larger than the gauge base, using a brush. This undercoat

82

layer was cured for 24 hours then was made flat using sand paper. A mix of the two components A and B of the same adhesive was mixed at a prescribed mixing ratio depending on the time that we expected the process to be done. Using toothpicks the mix was applied to the back of the gauge and also to the measuring area. The gauge was put in place, covered with a polyethylene sheet, with pressure applied via a rubber pad and suitable load (30 to 50 kPa). After removing the load, the polyethylene sheet was removed. Lastly, the gauge terminal was soldered with the conductors of the lead wire cable and coated using the same mix as a protection while moving the specimens before and after the rehabilitation process. All strain gauges were tested and checked thoroughly using a digital multimeter. Figures 3-31 and 3-33 show the concrete strain gauges during and after installation.

3.7.2.2 Linear Potentiometers (LP)

Deflections at four points on the top of the slab and one under the lower column stub were continuously monitored using linear potentiometers (LP) as shown in Figure 3-27 for the first group and Figure 3-28 for the second and third group. All the LPs have length of 150 mm; they were calibrated in order to find the gauge factor.

3.7.2.3 Universal Flat load cells

Load measurements were taken through a universal flat load cell of 444.8 kN (200 Kips) capacity connected to the manual pump. The load was transferred monotonically to the bearing plate through a hemispherical bearing assembly at the top of the upper column stub as was marked before (Figure 3-34). The position of the applied load was

variable for each group depending on the required eccentricity. Figure 3-35 shows the location of the load cell for each group during loading.

The specimen was supported on four hemispherical bearing assemblies at the four point hinged support, to be able to rotate with the specimen movement throughout the loading time. All seats were installed on a universal flat load cell of 222.4 kN (50 kips) and 111.2 kN (25 kips) capacity to monitor the reactions at each support at the bottom of the slab. The load cells were installed on two stiff wide beams as shown in Figure 3-34. All load cells were calibrated using a Universal Testing Machine. Figures 3-36 to 3-40 show the calibration curve for each load cell.

3.7.2.4 Data Acquisition system

A total 38, 40, and 43 data channels were required to collect the data for each specimen for the first, second, and third group, respectively. Data collection was facilitated using Dalite software, recording all readings electronically into a computer file (Figure 3-42).

3.8 Test Set-up and Loading

The location of the support, loading point, and Linear Potentiometers (LP) were marked. Then the specimen was placed on the four hinged point according to the specified eccentricity of each specimen in the test frame. The distance between the center line of the hinges was 1700 mm in the long (N-S) direction and 700 mm in the short (E-W) direction. Figures 3-43 to 3-45 preset a close-up view of the loading assembly and instrumentation set-up for each group.

84

Steel angles were connected to the frame to support the LPs, which were adjusted and placed at their marked positions.

All instruments (steel strain gauges, concrete strain gauges, linear potentiometers, reactions load cells, and the main load cell) were checked and connected to the data acquisition panel which was connected to the computer to record all readings.

The control specimen (CTRL0) in the first group, while the load was applied with zero eccentricity, was tested to failure under a single monotonically increasing load. Initially, all cracked slabs (CRAK0) were loaded to 80% of the ultimate load capacity as recorded from the control specimen test of the same group (CTRL0). The load at that stage led to the appearance of cracks within the tension zone of the specimen. Subsequently, the load had been kept for one day; furthermore all instruments were removed. Afterward, the specimen was moved by the crane. The resulting cracks in a RC concrete slab specimen were repaired using the techniques scheme mentioned before. This specimen labelled (REHB0) was then replaced in the same original position in the frame. All instruments were reconnected. Lastly the specimen was re-tested to failure after a suitable curing period for at least three days, allowing for the study of the efficiency of CFRP. The same process was repeated for all of the second and third group's specimens. Figures 3-46 to 3-69 illustrate the testing process for all groups.

3.9 Carbon Fiber Reinforced Polymer Tensile Test

Five samples of the CFRP sheet were tested according to ASTM D3039/D 3039M – 00 specifications in order to compare its behaviour in tension with the theoretically predicted loading behaviour (Figure 3-77). Tabs were used and applied at 45° to the

85

loading direction to provide a soft interface using a high-elongation adhesive system. INSTRON test frame and Model 8500+ with controller was used with INSTRON's series IX software (Figure 3-76). Figure 3-78 shows the coupons test before and after failure. Figures 3-79 and 3-80 show the tensile load-displacement curve for five samples.

The average of the ultimate load from the five samples was calculated to be 3.5 kN and the average of displacement at maximum applied load (peak point) was 1.6 mm and the percentage of elongation was 1.6%, while the percentage of elongation reported by the manufacturer was 1.7% as shown in Table 3-5.

86

Table 3-1: Compression and Splitting test result for group I (first batch)

Testing day	Type of test	Test result (MPa)	Test result average (MPa)
7 days	Compression	24.7	24.8
	Compression	25.0	
14 days	Compression	29.6	32.4
	Compression	35.1	
28 days	Compression	36.0	36.1
	Compression	36.2	
28 days	Splitting	3.7	3.7
	Splitting	3.6	
	Splitting	3.8	
108 days (CTRL0)	Compression	37.6	37.6
122 days (REHB0)	Compression	38.4	38.4

Table 3-2: Compression and Splitting test result for group II (second batch)

Testing day	Type of test	Test result (MPa)	Test result average (MPa)
7 days	Compression	34.0	33.8
	Compression	33.5	
14 days	Compression	40.9	40.6
	Compression	40.3	
28 days	Compression	45.0	46.6
	Compression	47.8	
	Compression	46.9	
28 days	Splitting	4.3	4.5
	Splitting	4.8	
78 days (CTRL25)	Compression	50.1	50.1
111 days (REHB25)	Compression	51.3	51.3

Table 3-3: Compression and Splitting test result for group III (third batch)

Testing day	Type of test	Test result (MPa)	Test result average (MPa)
7 days	Compression	31.0	32.8
	Compression	33.5	
	Compression	33.8	
14 days	Compression	42.5	41.9
	Compression	41.2	
	Compression	47.8	
28 days	Compression	50.8	53.2
	Compression	52.7	
	Compression	56.0	
28 days	Splitting	5.1	4.8
	Splitting	4.5	
25 days (CTRL35)	Compression	49.1	49.1
38 days (REHB35)	Compression	51.7	51.7

| 47.8 | This value is ignored. |

88

Table 3-4: Material properties for composite system as reported by Manufacturer

Material	Commercial name	Description	Tensile Strength (MPa)	Tensile Modulus (GPa)	Ultimate Elongation %	Flexural Strength (MPa)	Flexural Modulus (GPa)
Dry fiber	Tyfo® SCH_11UP Fabric	Reinforcing fabric	3790	230	1.70	N/A	N/A
Epoxy	Tyfo® S	Two component matrix	72.4	3.18	5.00	123.4	3.12
Composite system	Tyfo® SCH_11UP Composite	Composite Unidirectional CF @ 0°	903*	86.9	1.05	N/A	N/A

* The ultimate tensile strength in primary fiber direction

Table 3-5: Tensile test result for CFRP sheet

Sample No.	Type of test	Ultimate Tensile load (kN)	Elongation %
I		3.3	1.6
II		3.1	2.0
III	Tensile	4.3	1.7
IV		3.3	1.2
V		3.4	1.6
Average of the result		3.5	1.6

90
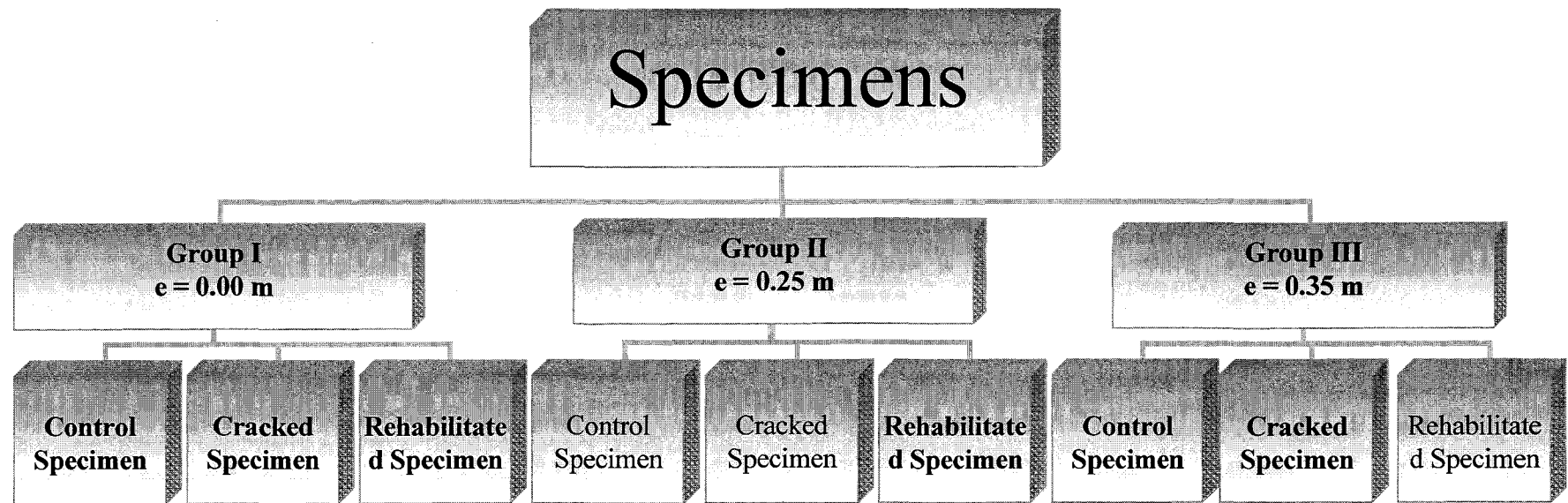
Fig. 3-1: Organization of the three groups' specimens

91
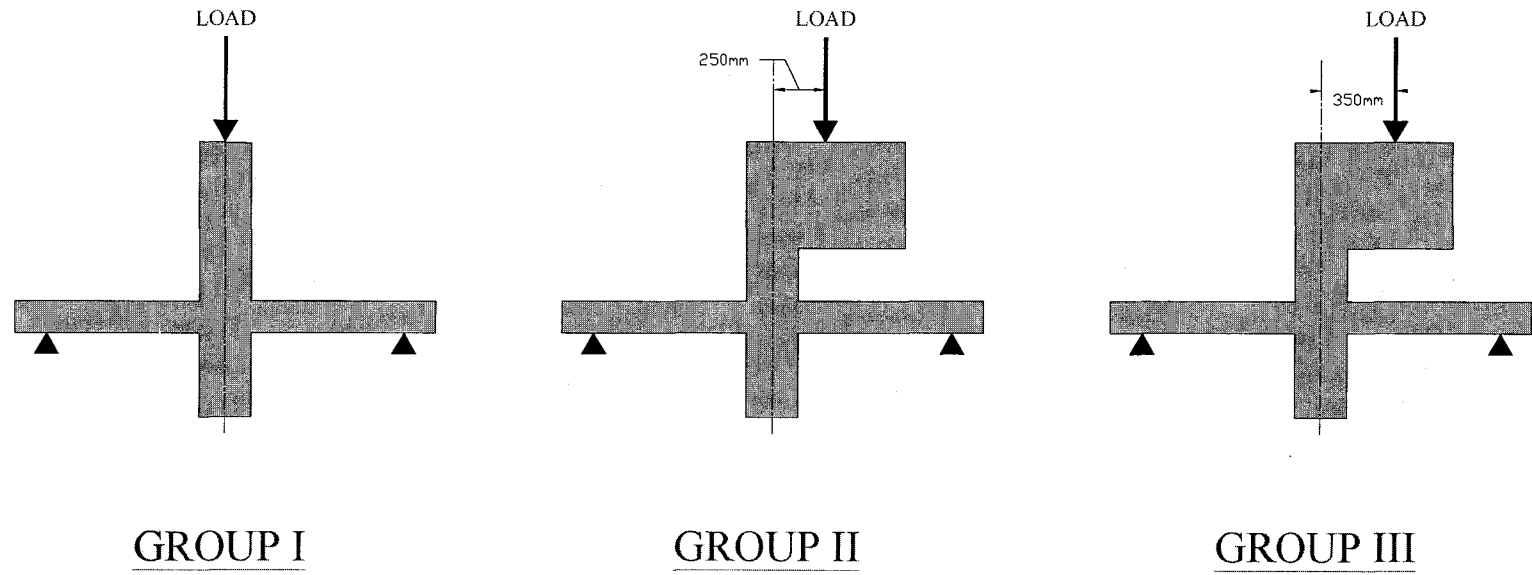
Fig. 3-2: The three groups of laboratory works
Group I (zero eccentricity), Group II (eccentricity = 250 mm),
Group III (eccentricity = 350 mm)

92

(a)

(b)
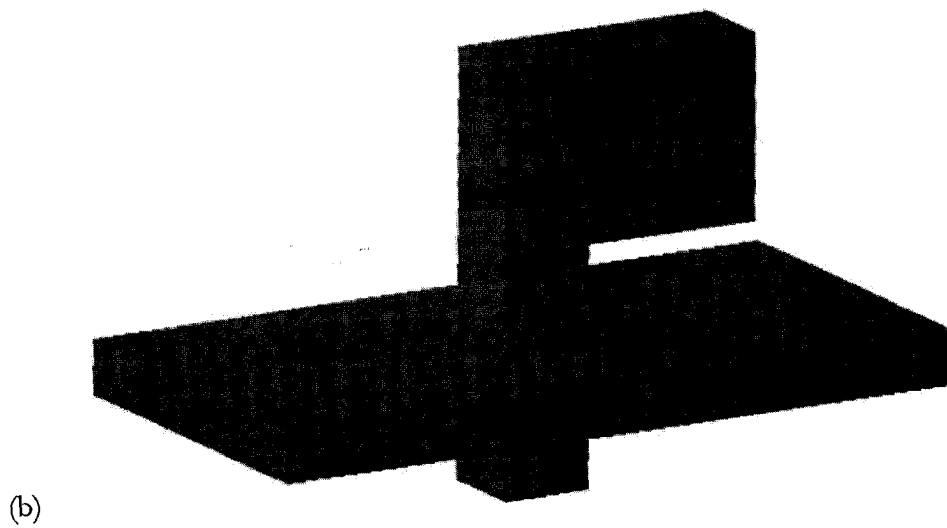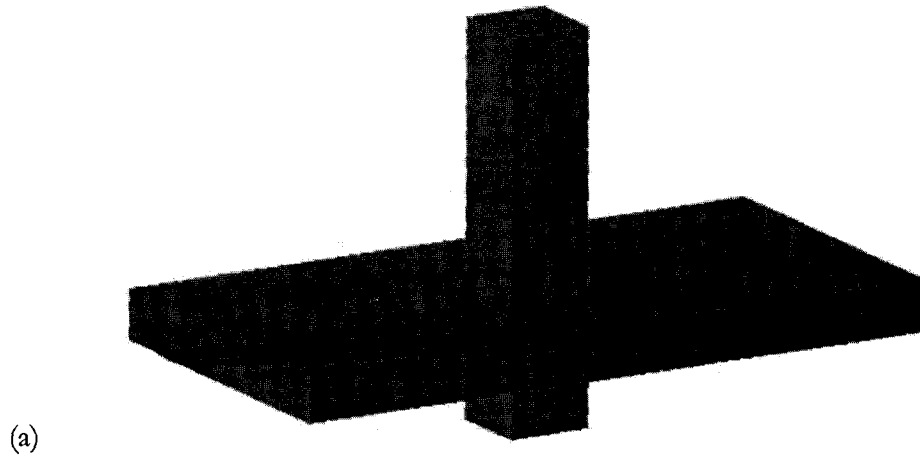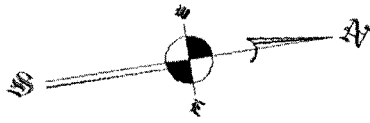
Fig.3-3: Specimen orientation
(a) Specimen used for group I, (b) Specimen used for group II and III

93
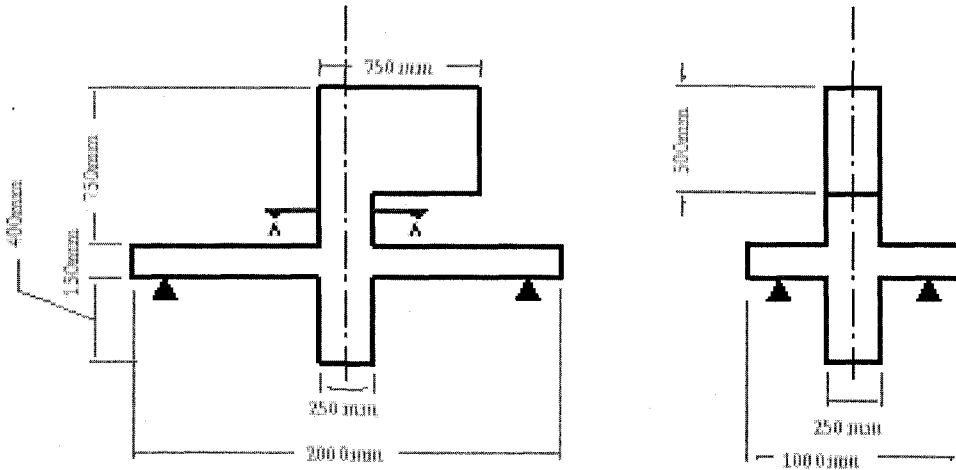
ELEVATION   SIDE VIEW
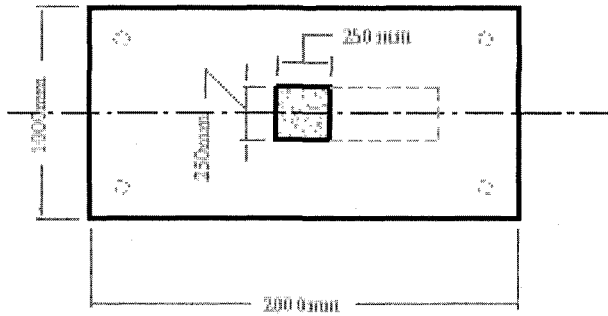
SECTION A-A

Fig. 3-4: Geometry of the specimens

94
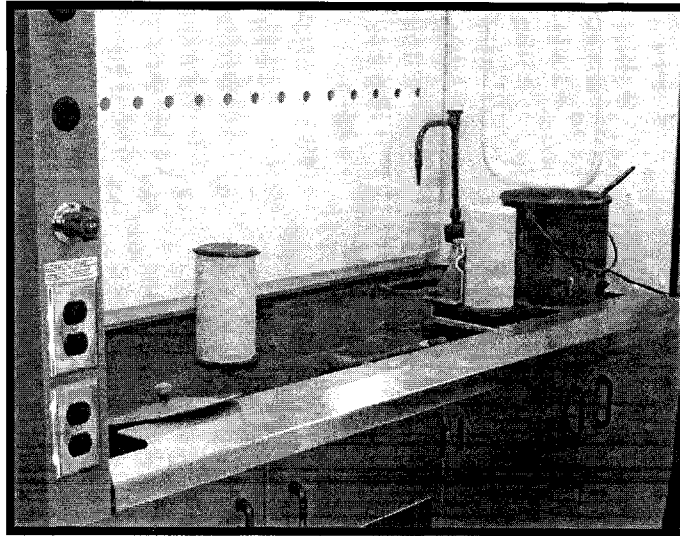
Cylinder capping
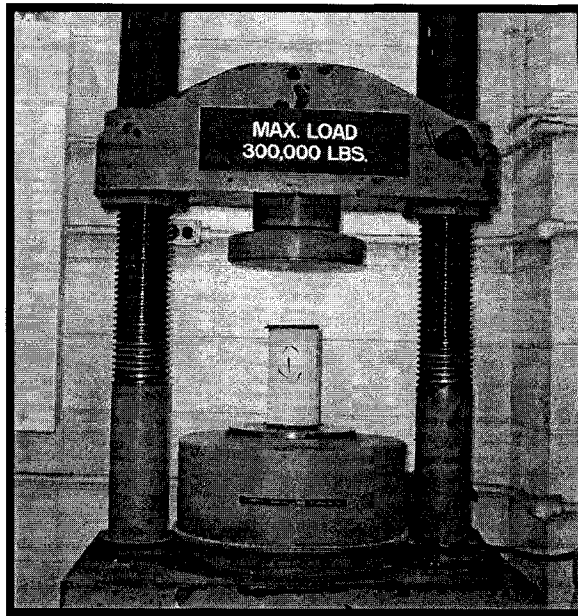
Cylinder test machine

Fig. 3-5: Compression test of the concrete cylinder

95
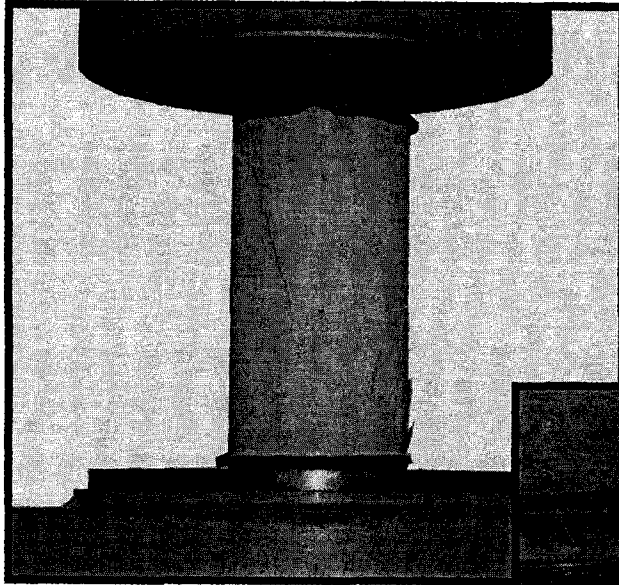
Compressive strength test
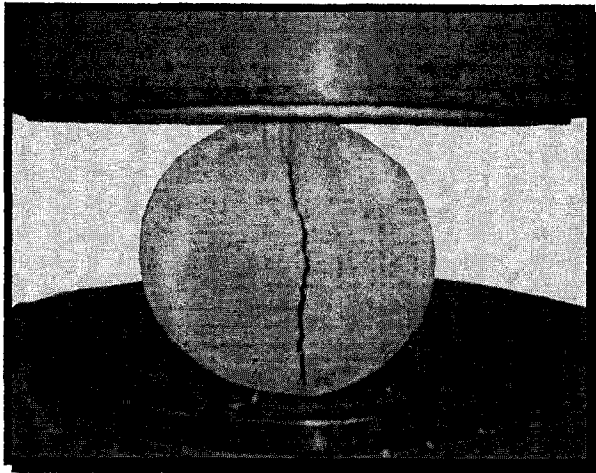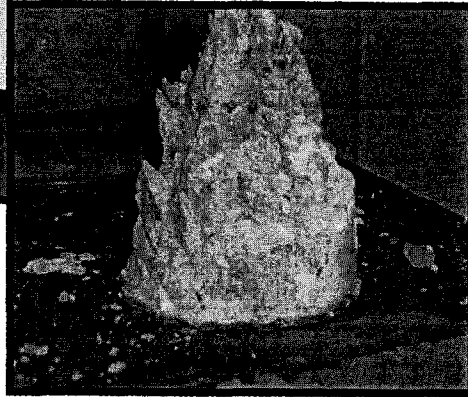
Splitting test
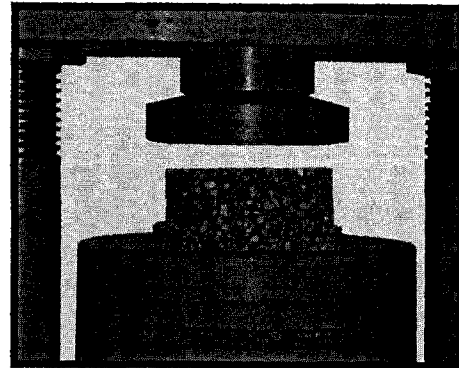
Fig. 3-6: Compressive and splitting test of concrete cylinders

96
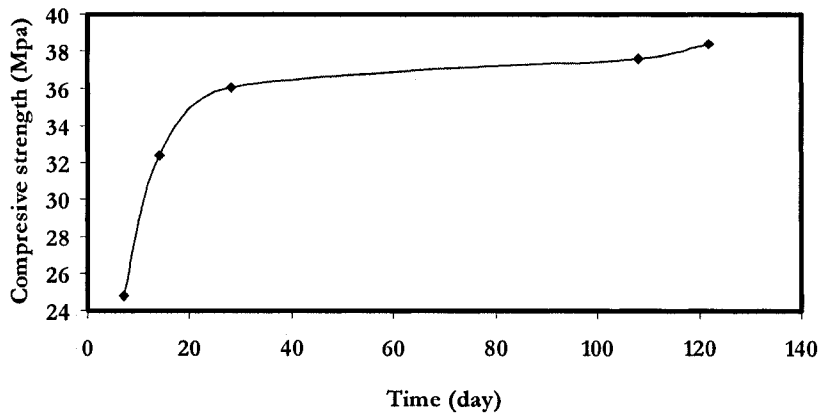
Fig. 3-7: Compressive strength of concrete cylinder for group I (first batch)
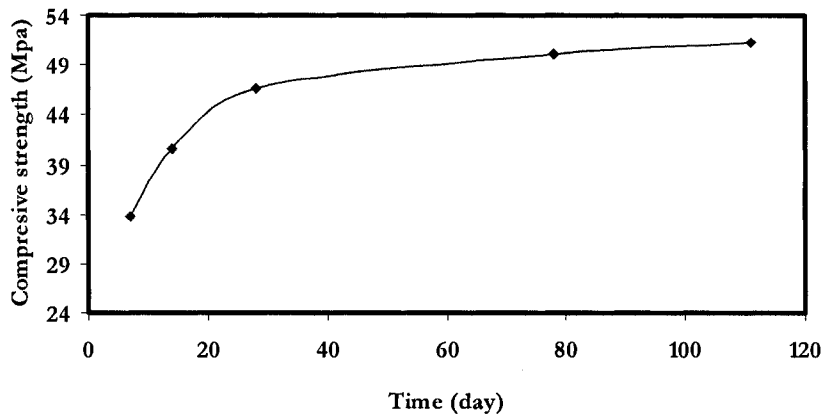
Fig. 3-8: Compressive strength of concrete cylinder for group II
(second batch)
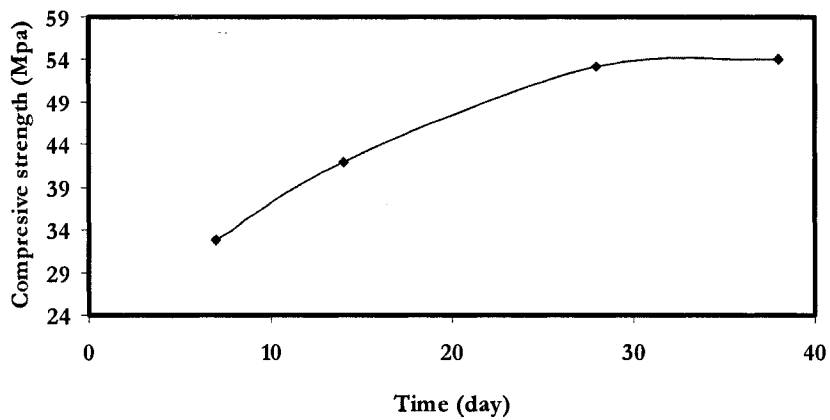
Fig. 3-9: Compressive strength of concrete cylinder for group III
(third batch)

97
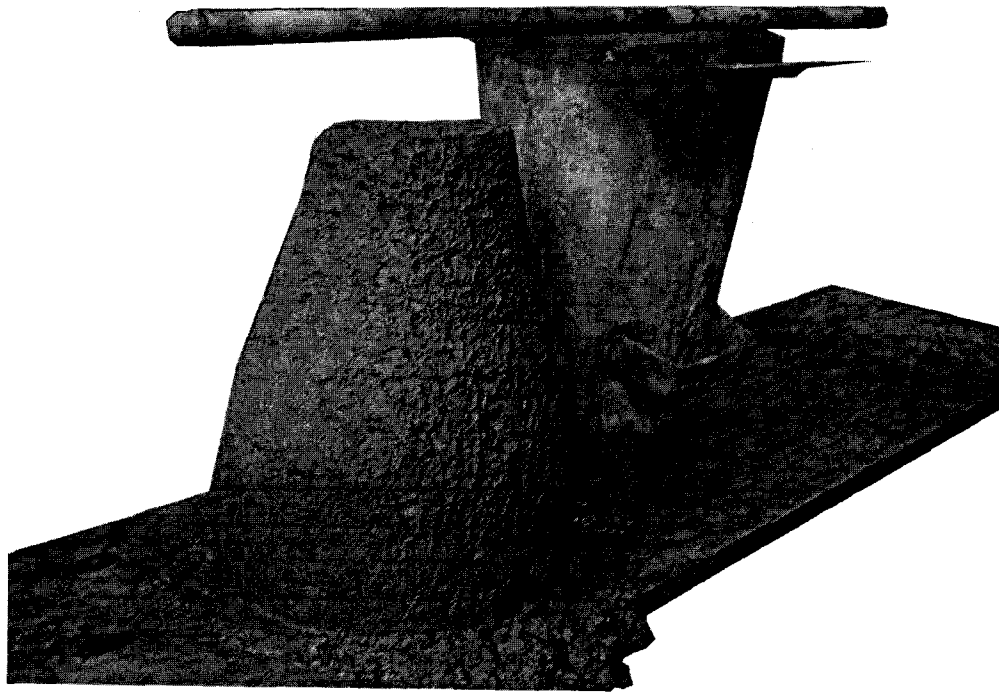
Fig. 3-10: Slump test of concrete

98

Fig. 3-11 Form work

10#10 vertical stirrups
(68 clear distance)

3#10 horizontal stirrups
@130mm c/c

#10 @ 200mm

#10 @ 100mm

12#10 @ 100mm

Section elevatiion

6#20

12#10 @100mm c/c
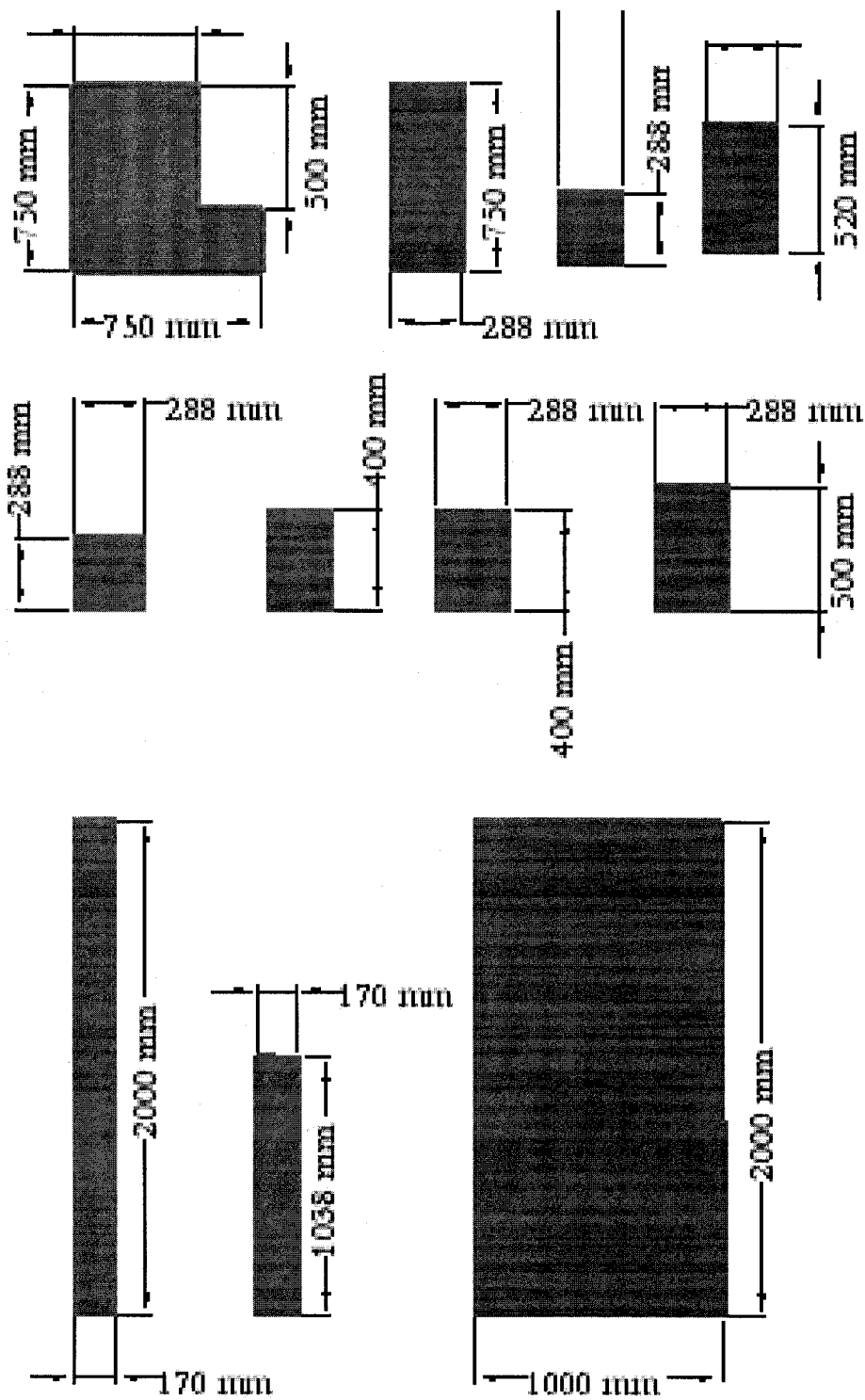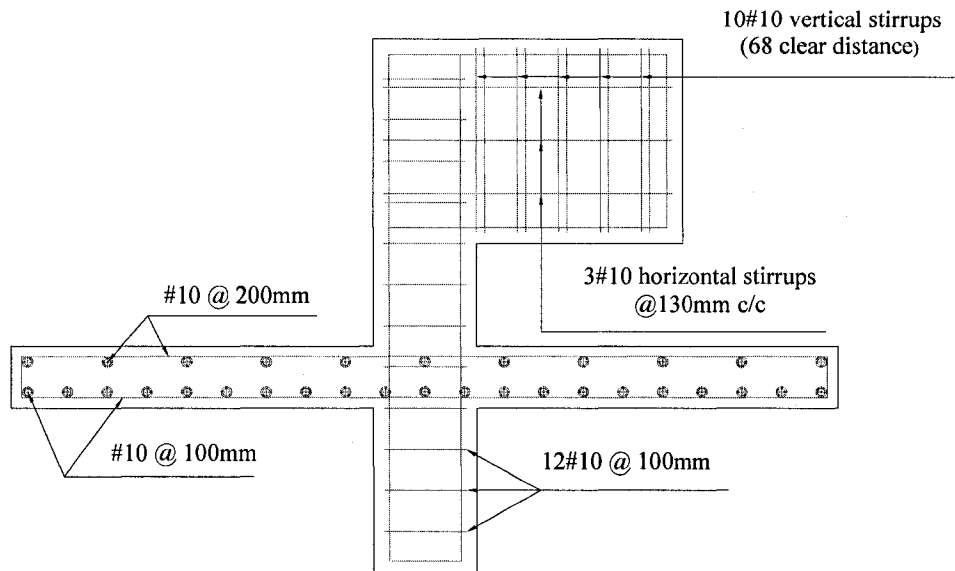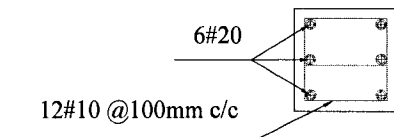
Column section

Fig. 3-12: Reinforcement details

100
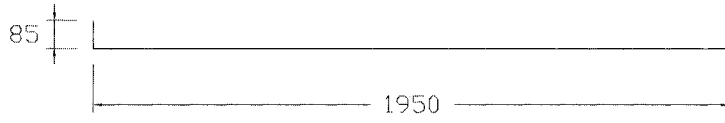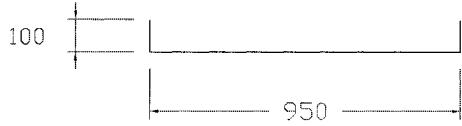
SLAB REINFORCEMENT
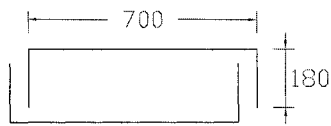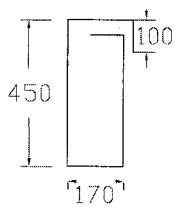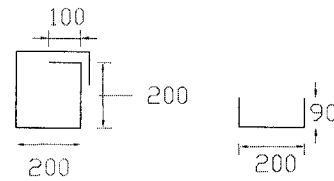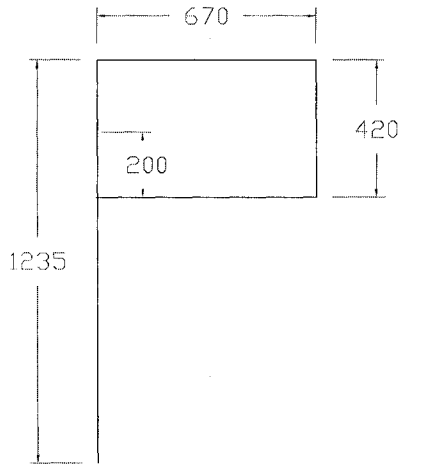
COLUMN STUB AND CANTILEVER PART REINFORCEMENT

Fig. 3-13: Reinforcement work shop

101
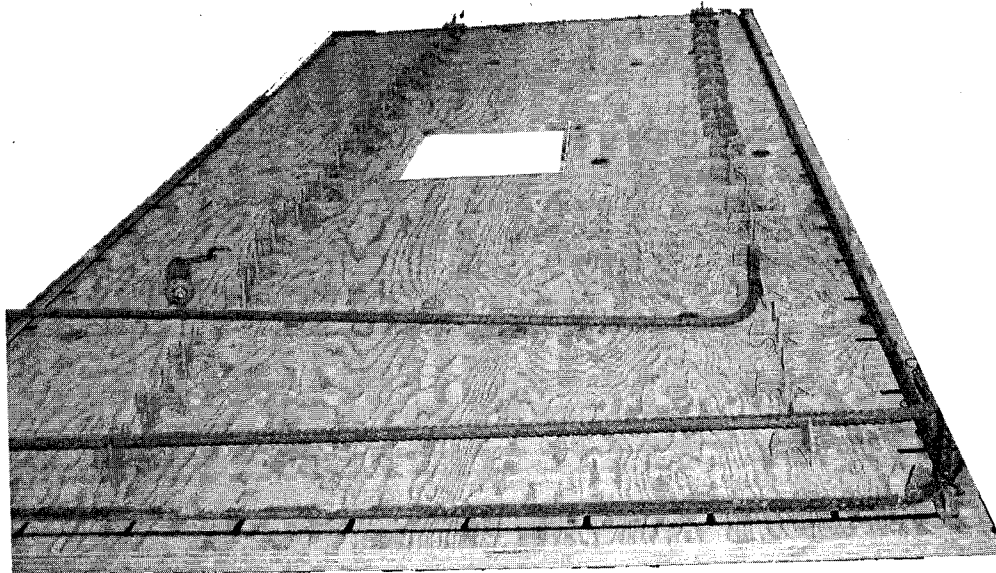
Fig. 3-14: Preparation of reinforcement cage
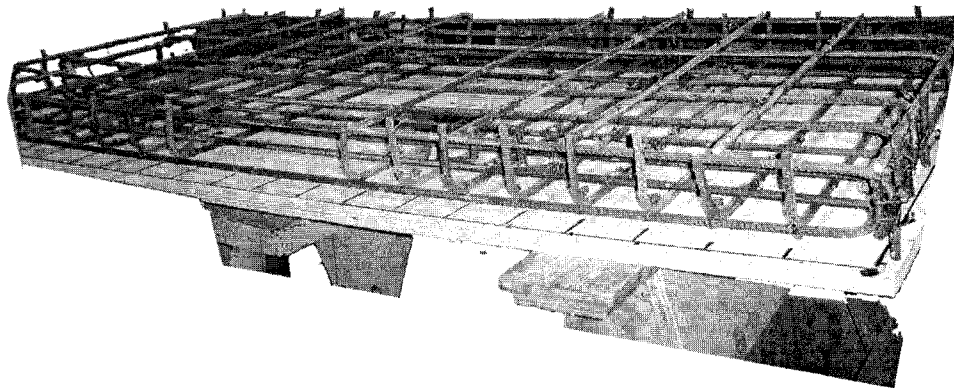
Fig. 3-15: Slab reinforcement

102

Fig. 3-16: Preparation of reinforcement
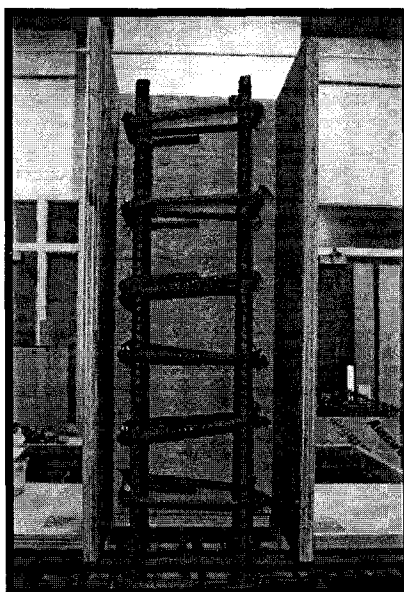
Fig. 3-17: Column reinforcement of group I specimen

103
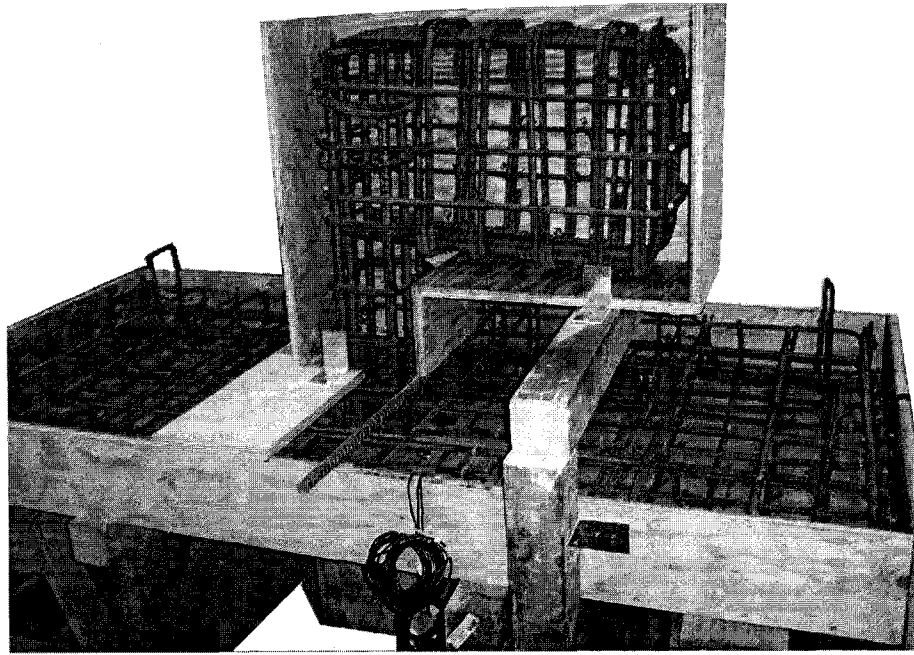
Fig. 3-18: Column reinforcement of group II and group III specimens
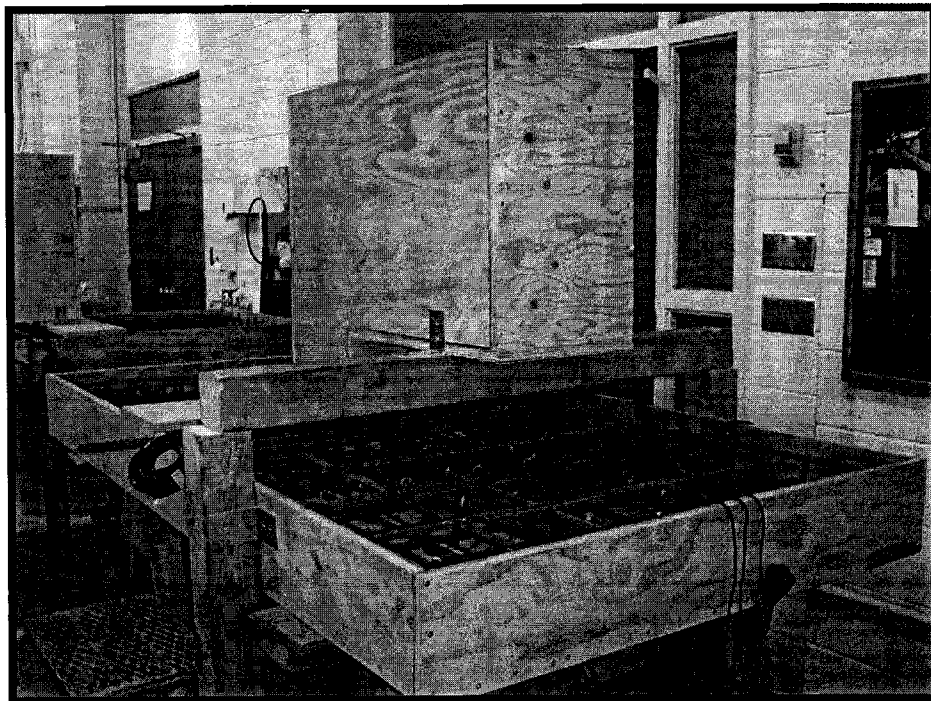
Fig. 3-19: The specimen ready for casting

104
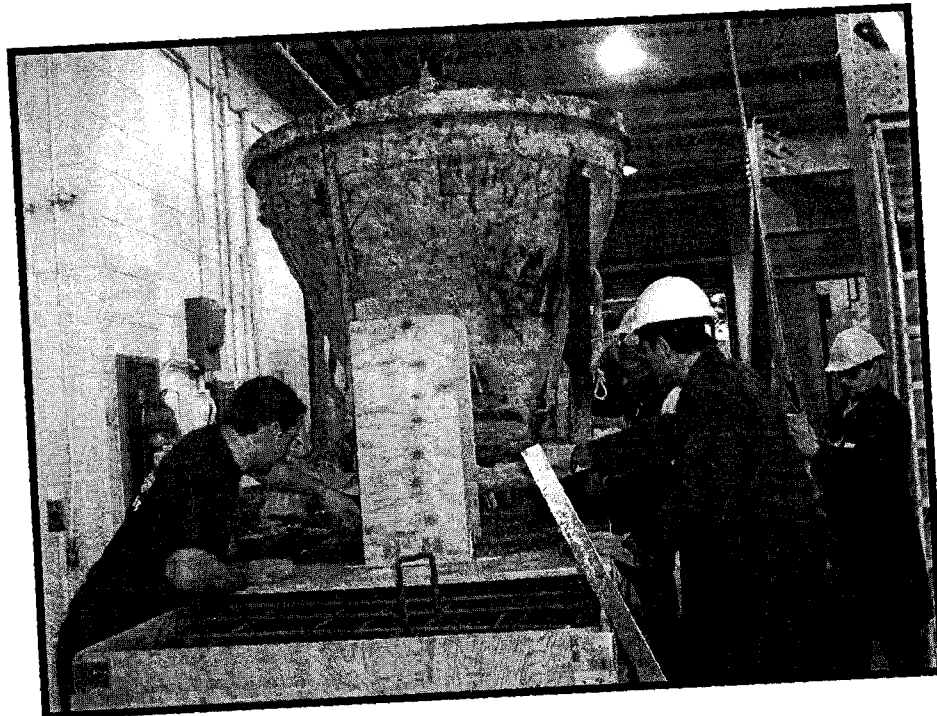
Fig. 3-20: casting works

105
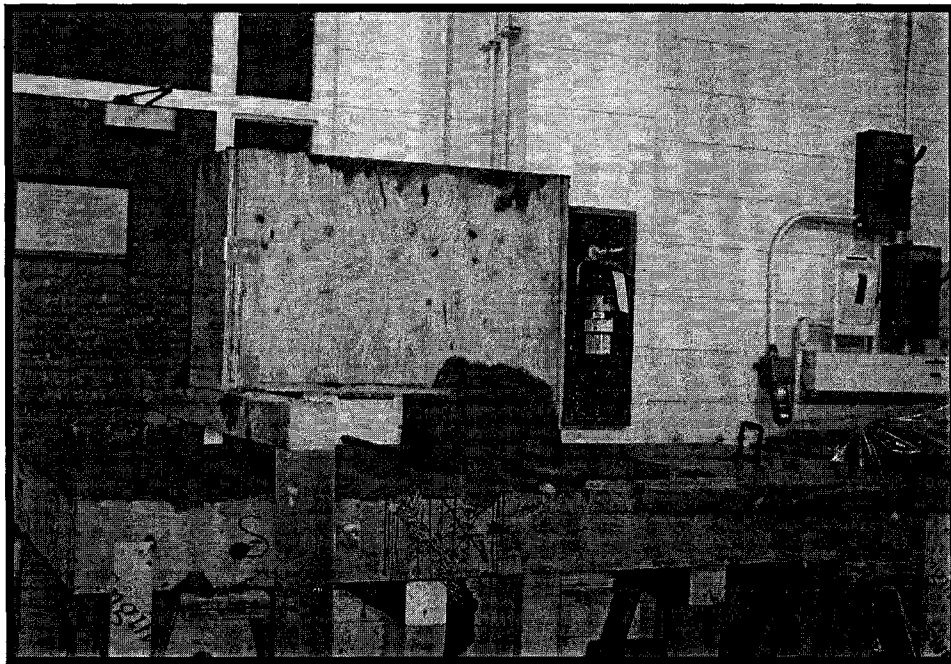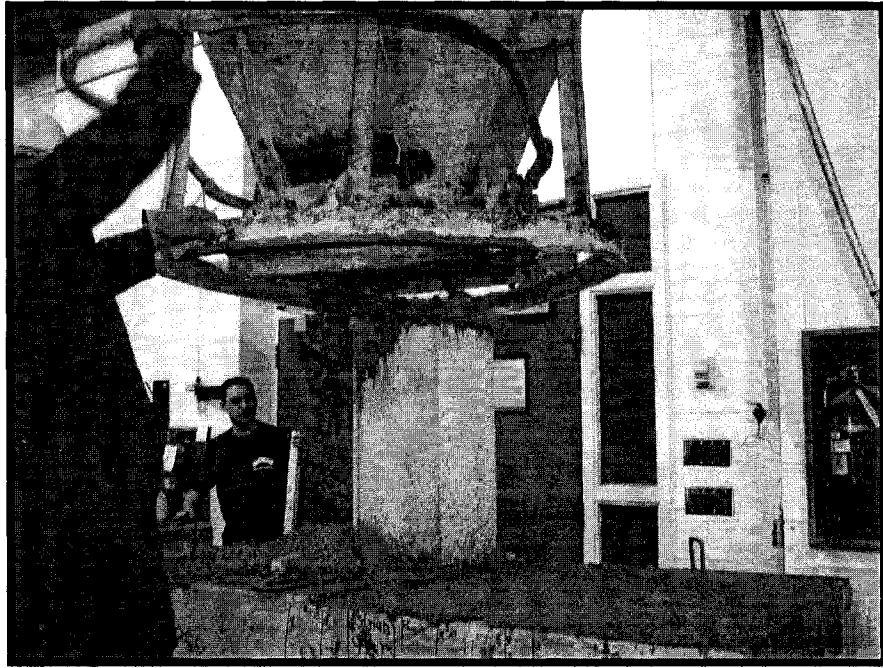
Fig. 3-21: casting works

106
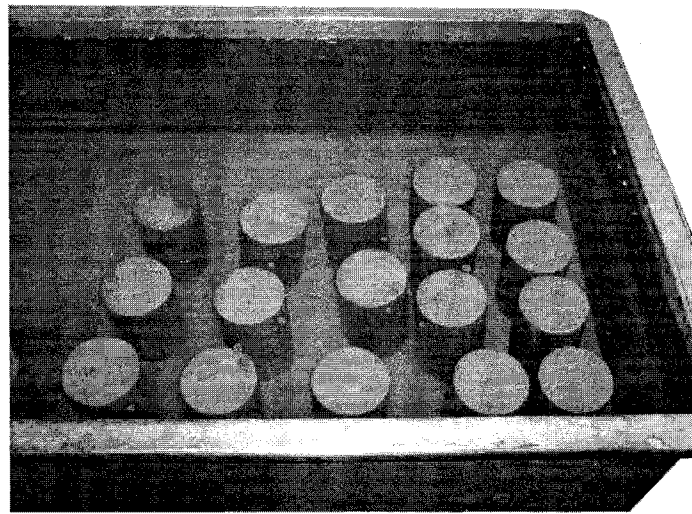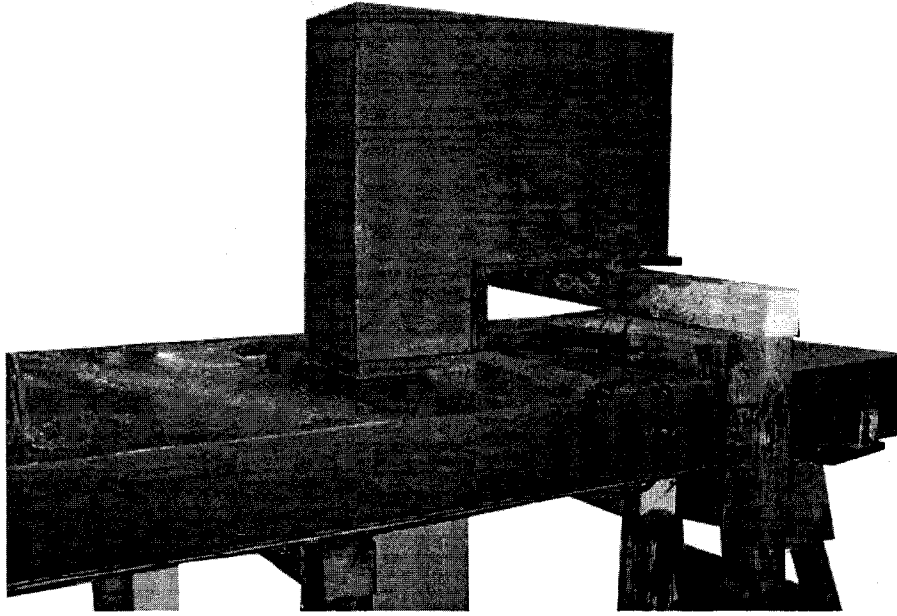
Fig. 3-22: curing works

107
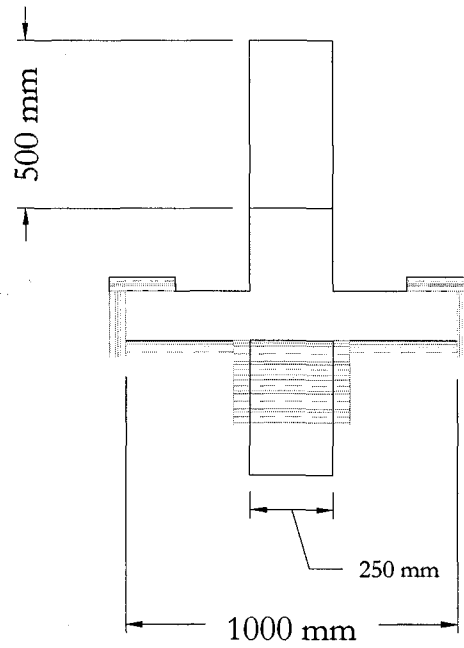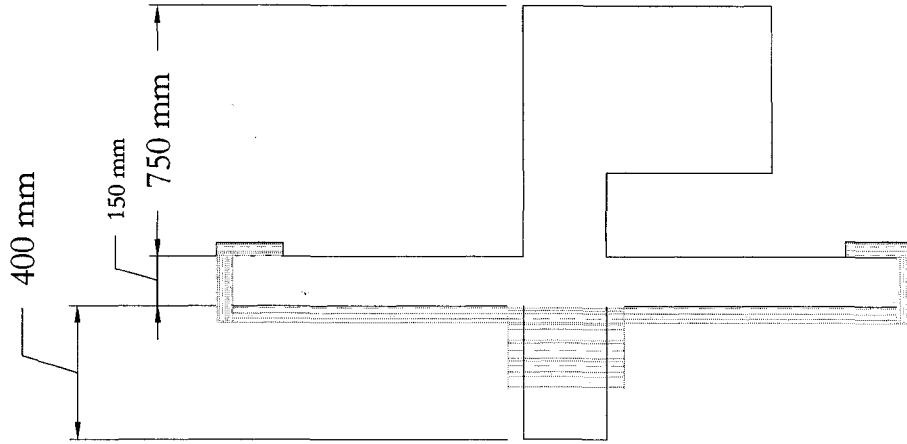
Fig. 3-23: Geometry of the rehabilitated specimen (REHBe) with CFRP application

108
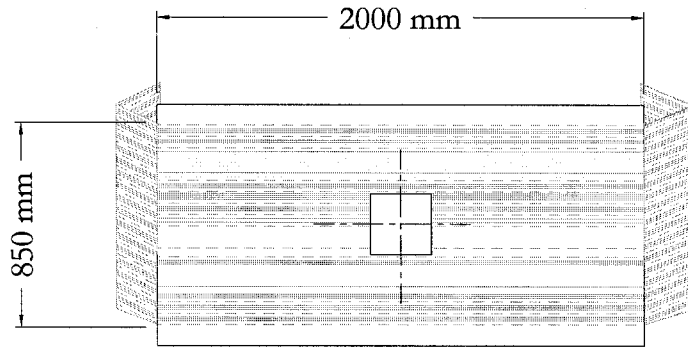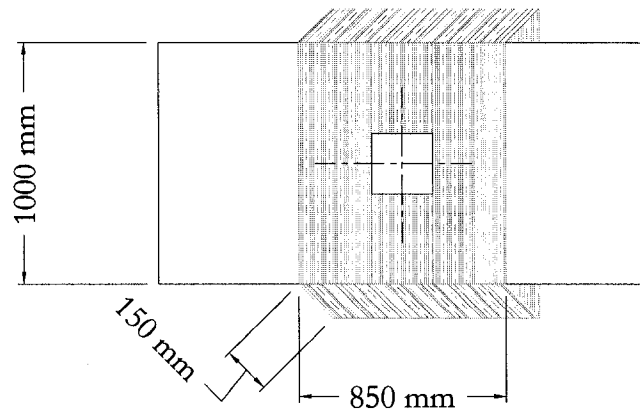
FIRST LAYER OF CFRP

SECOND LAYER OF CFRP
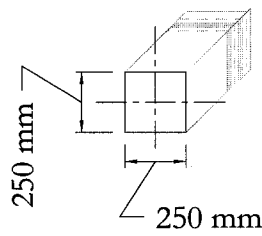
COLUMN WRAPPED
WITH CFRP

Fig. 3-24: Schematic of CFRP installation

109

7 Steel srain gauges@100 mm

Ch. 5
Ch. 6
Ch. 7
Ch. 8
Ch. 13
Ch. 14
Ch. 15

Ch. 16
Ch. 21
Ch. 22
Ch. 23
Ch. 24
Ch. 29
Ch. 30
Ch. 31
Ch. 32

9 Steel strain gauges @ ˙100 mm

2000
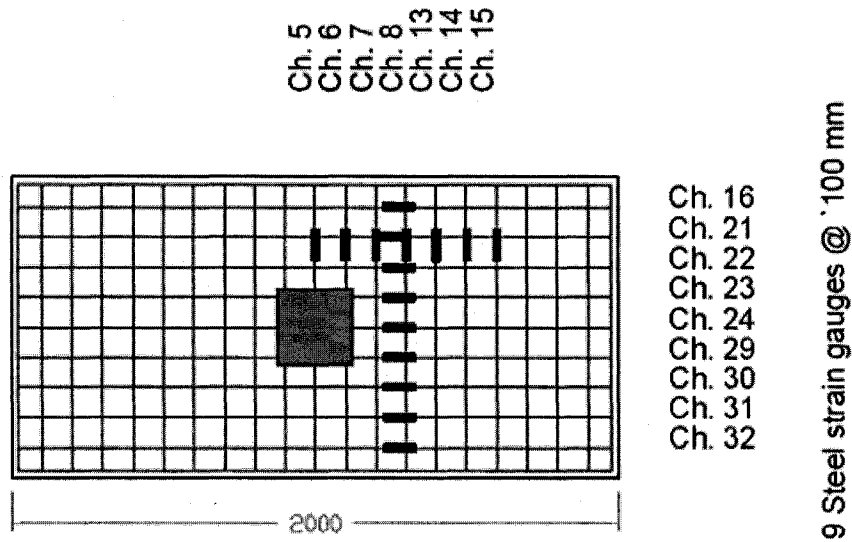
Fig. 3-25: Internal instruments (Steel strain gauges)

5 concrete srain gauges@100 mm

Ch.1
Ch.2
Ch.3
Ch.4
Ch.9

Ch. 20
Ch. 19
Ch. 18
Ch. 17
Ch. 12
Ch. 11
Ch. 10

7 Concrete strain gauges @ ˙100 mm

2000
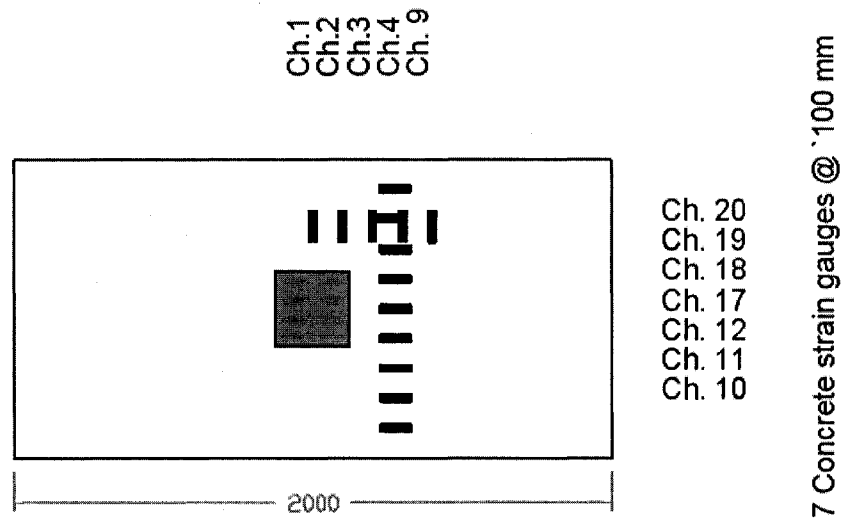
Fig. 3-26: External instruments (Concrete strain gauges)

110
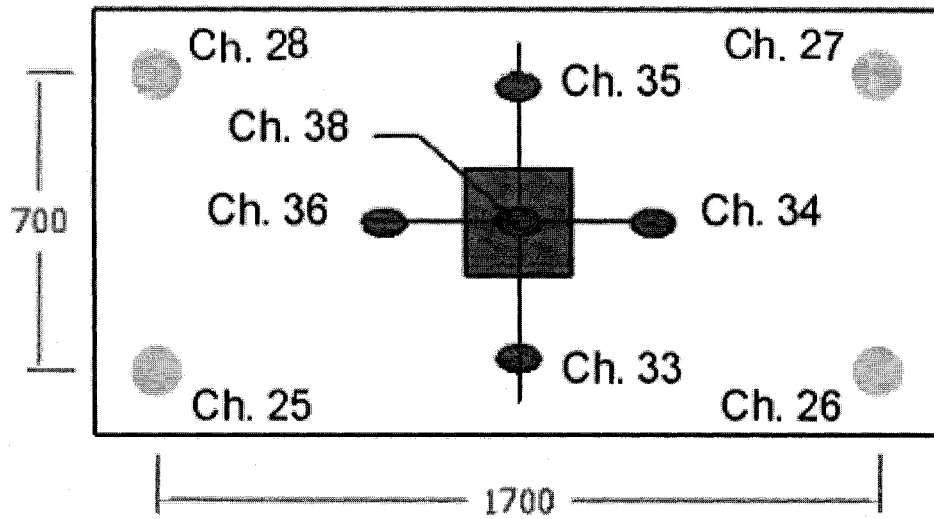
Fig. 3-27: External instruments (Group I)
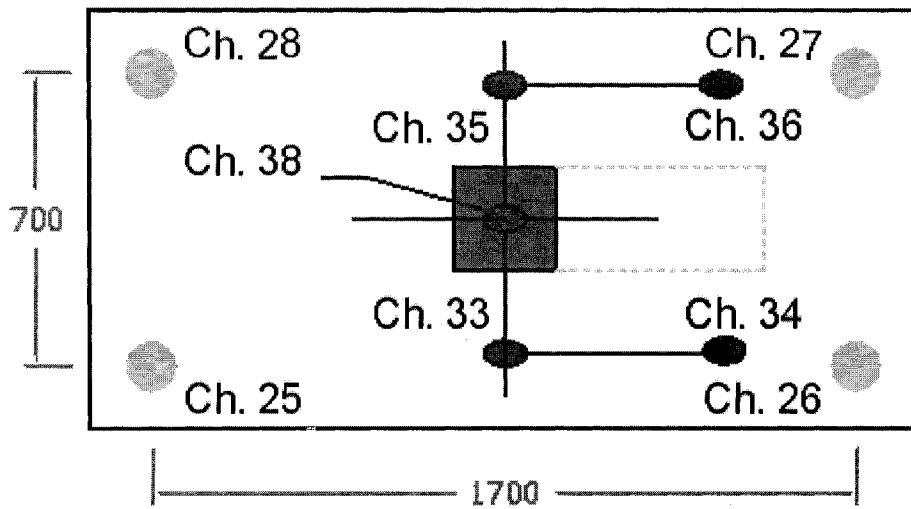
●   Linear Potentiometers (LP)

○   Hinged support

Fig. 3-28: External instruments (Group II and group III)

111
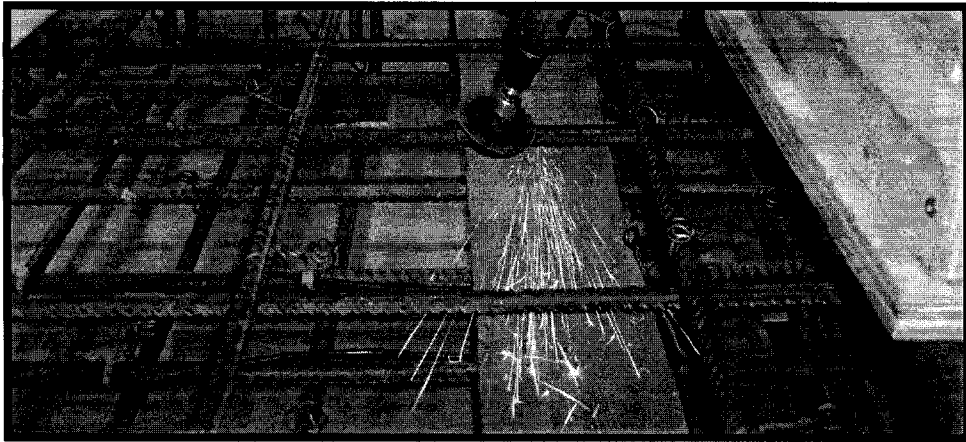
Grinding the reinforcement bars

The instrument used for installation

Fig. 3-29: Steel strain gauges preparations

112
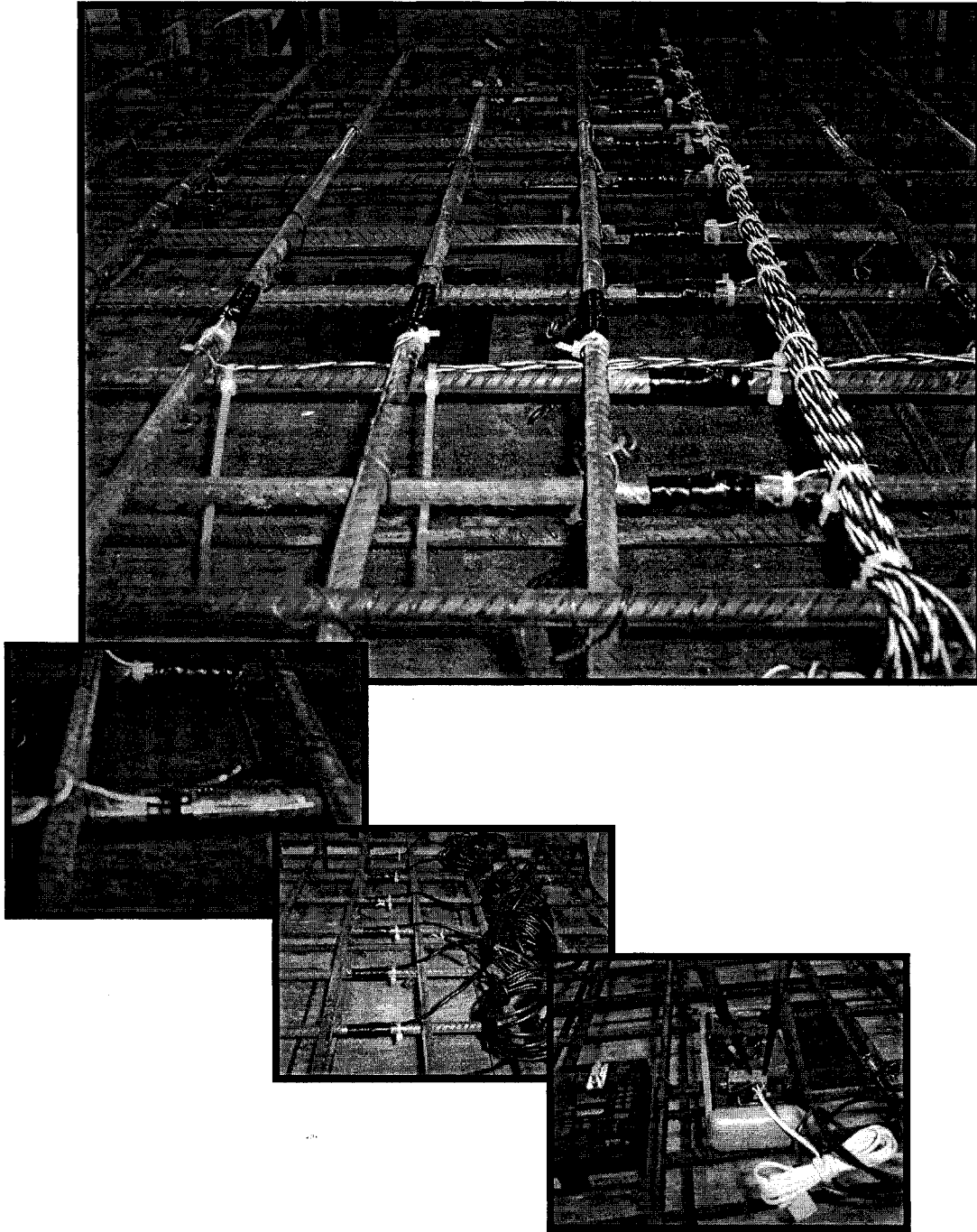
Fig. 3-30: Steel strain gauges preparations

113
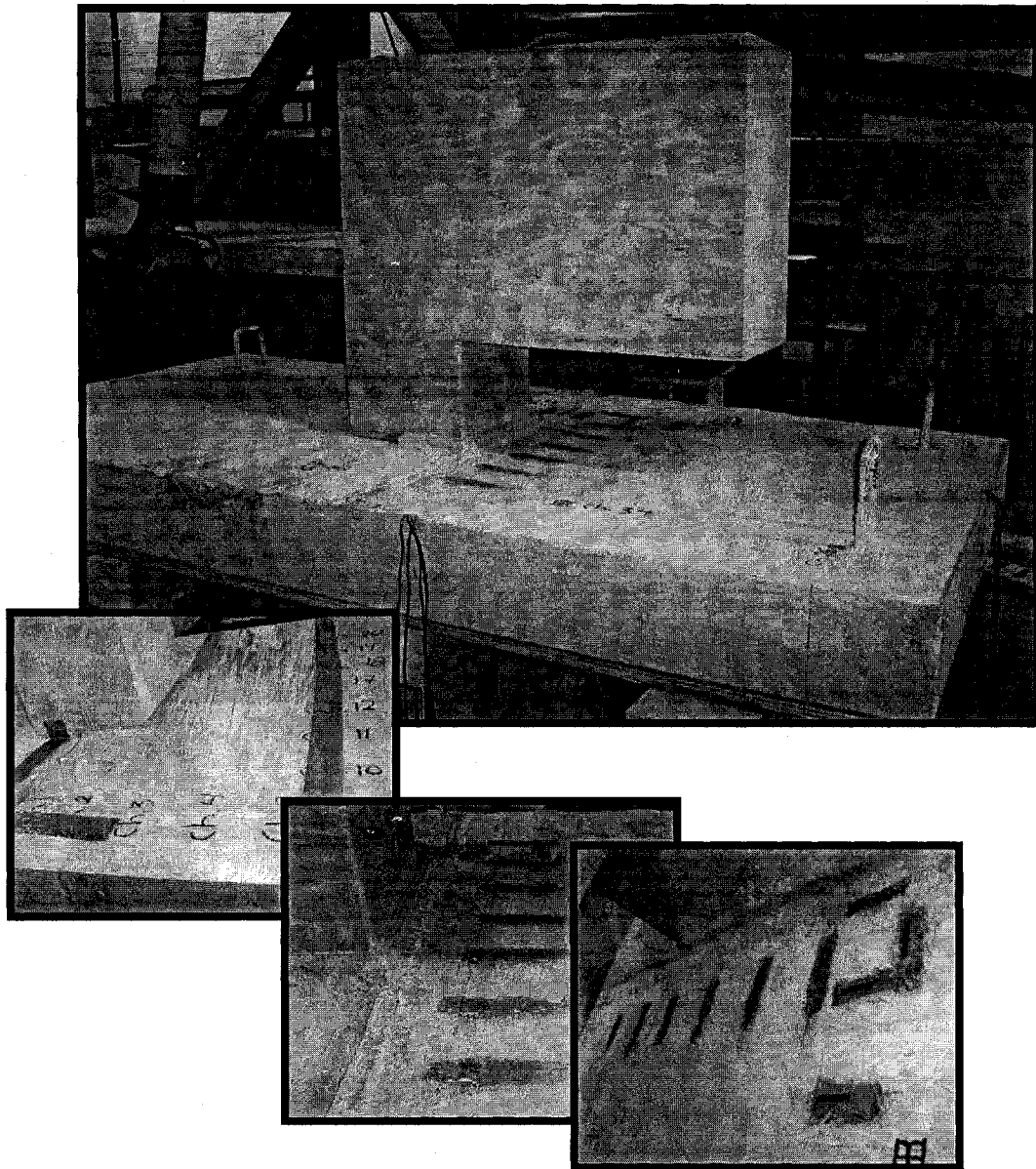
Fig. 3-31: Concrete strain gauges during installation

114
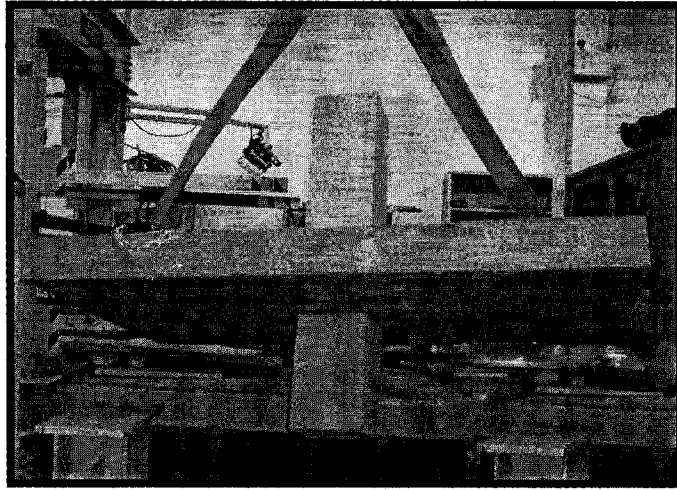
Fig. 3-32: The control specimen (CTRL0) during positioning
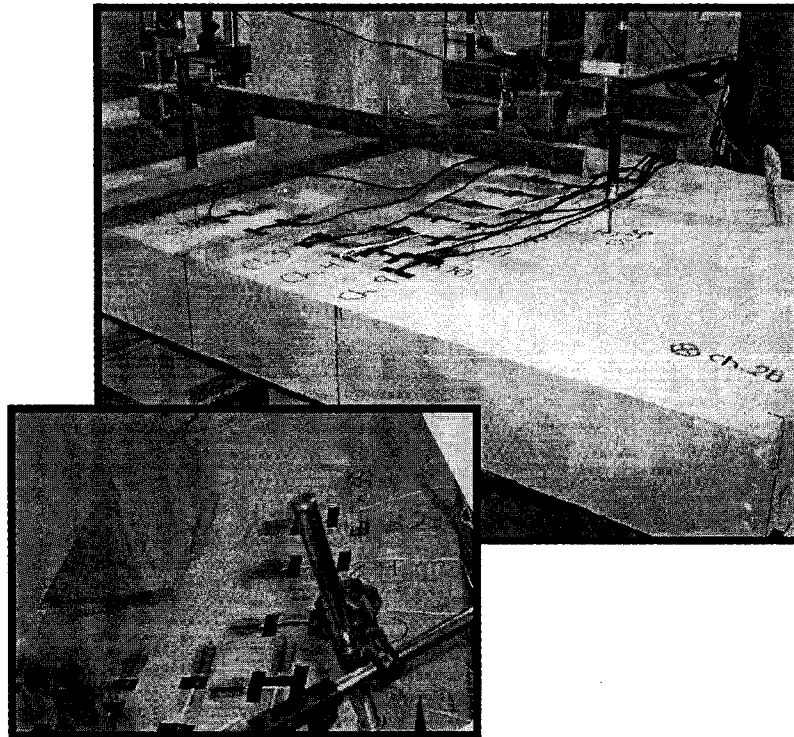
Fig. 3-33: Concrete strain gauges after installation

115
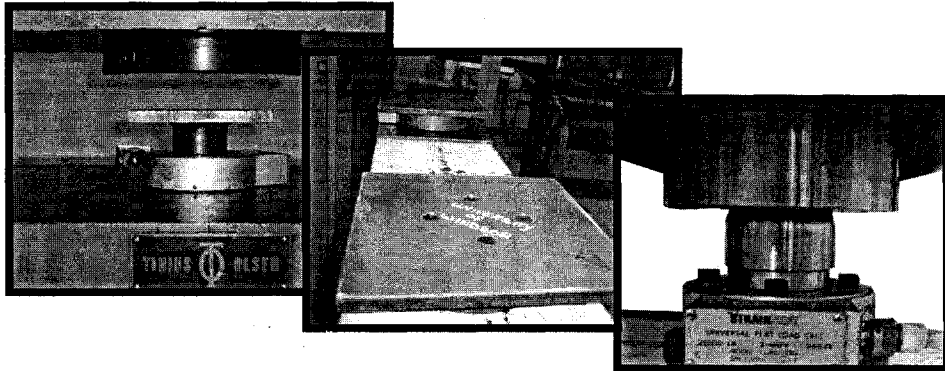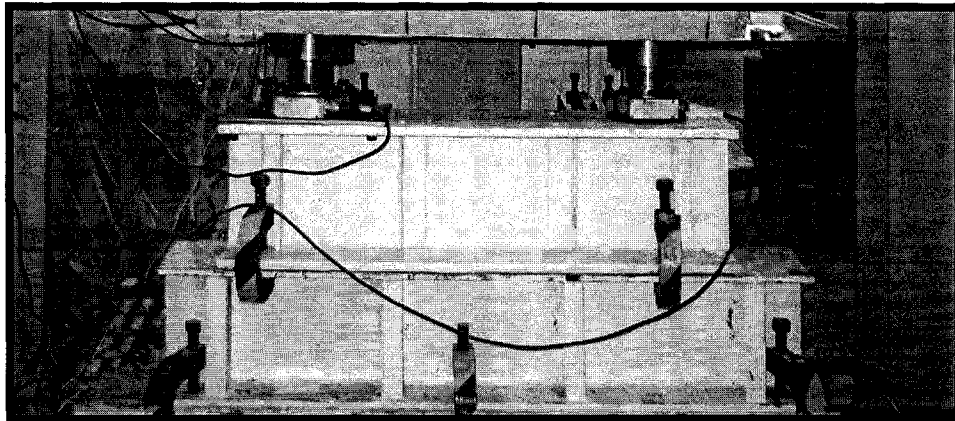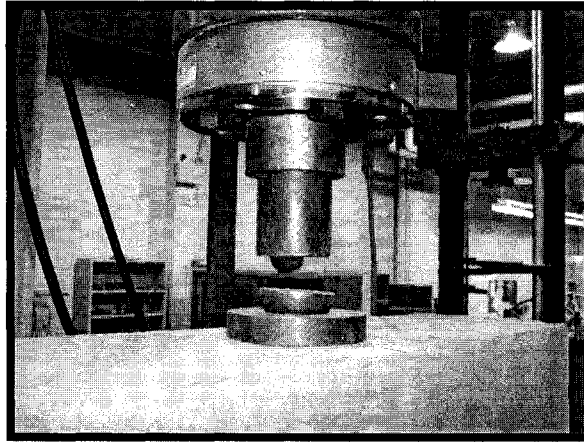
Fig. 3-34: Load cells
(Calibration, preparations and positions)

116
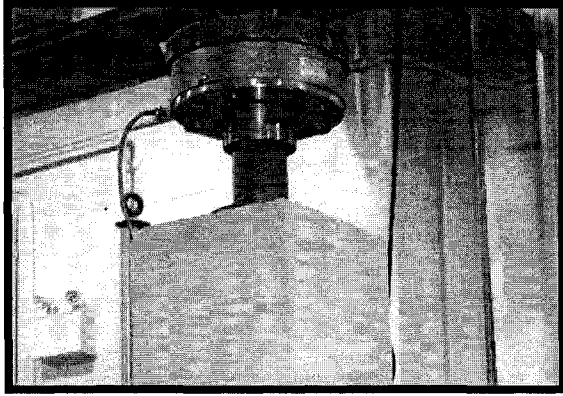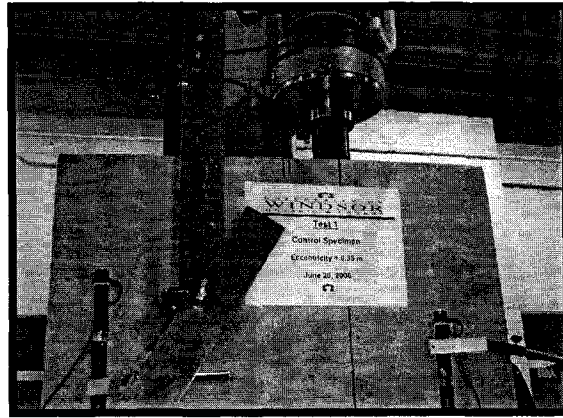
Group I
(e=0.00 mm)

Group II
(e=250 mm)
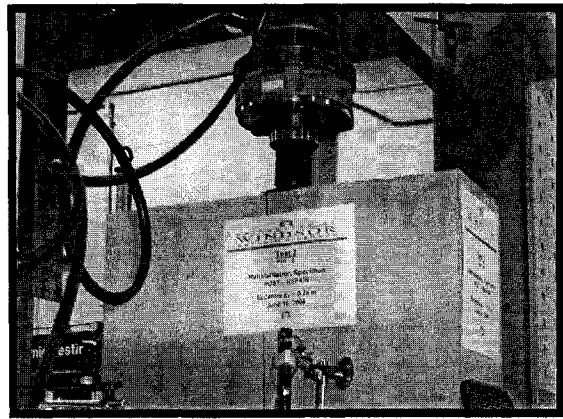
Group III
(e=350 mm)

Fig. 3-35: Location of the load cell for each group during loading

117
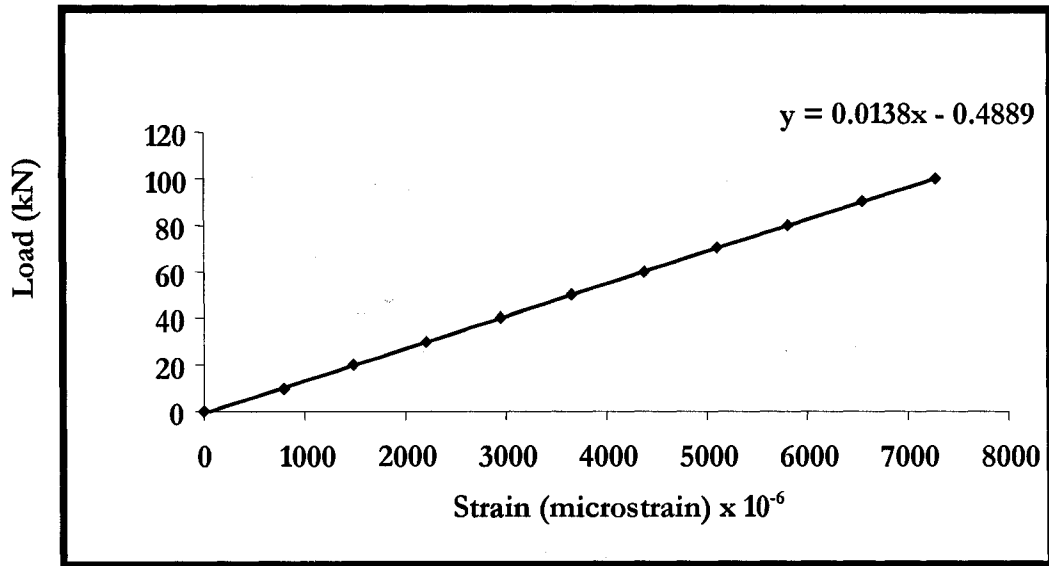
Fig. 3-36: Channel 25 calibration curve
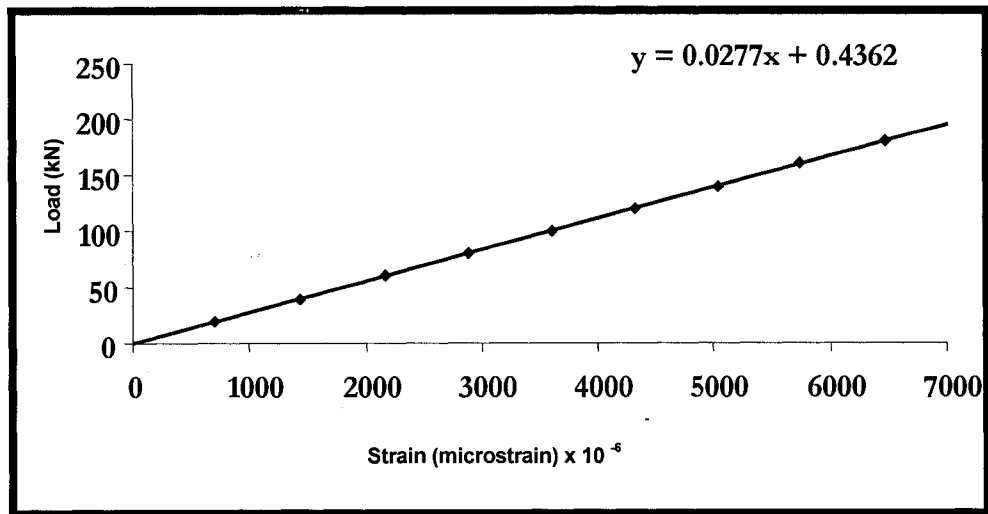
Fig. 3-37: Channel 26 calibration curve

118

$$y = 0.0136x - 0.9514$$
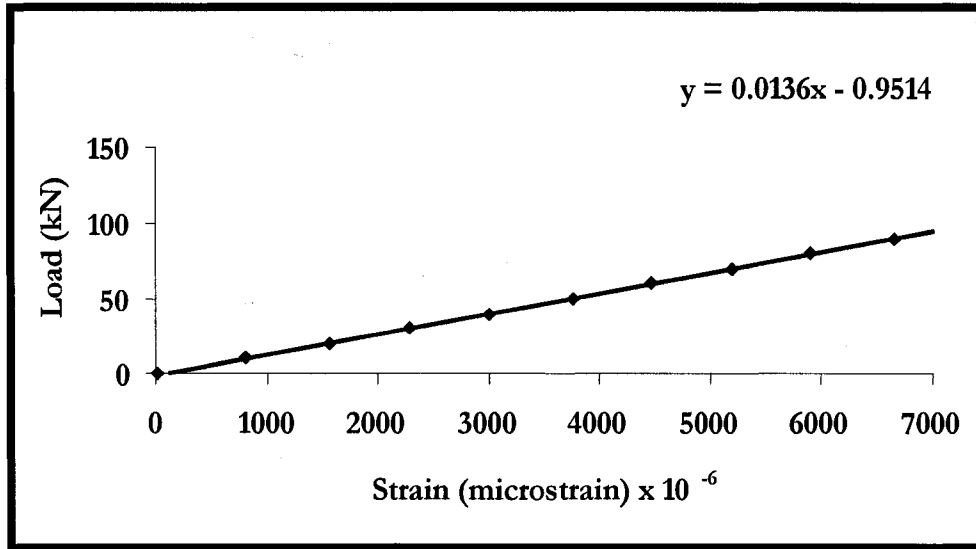
Fig. 3-38: Channel 27 calibration curve

$$y = 0.027x + 0.0158$$
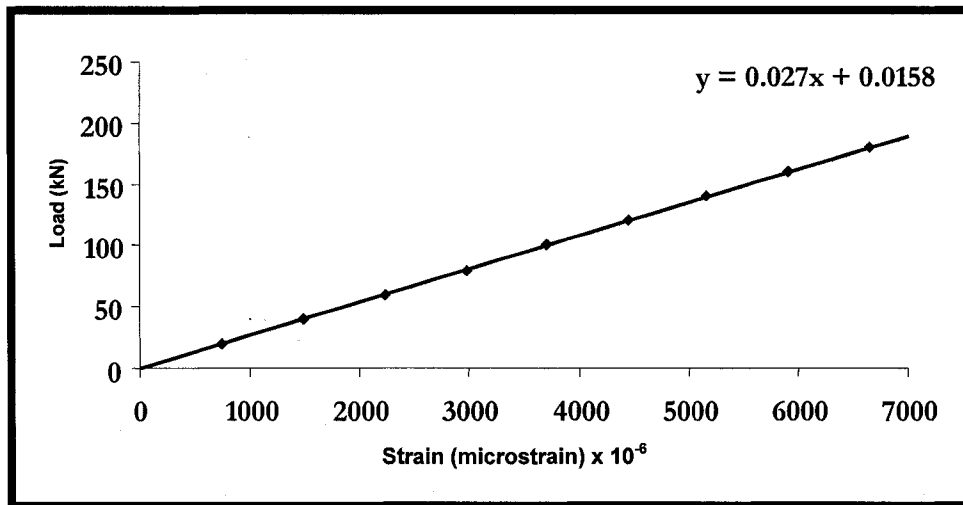
Fig. 3-39: Channel 28 calibration curve

119

$y = 0.0558x + 8.3571$

Strain (microstrain) x 10⁻⁶
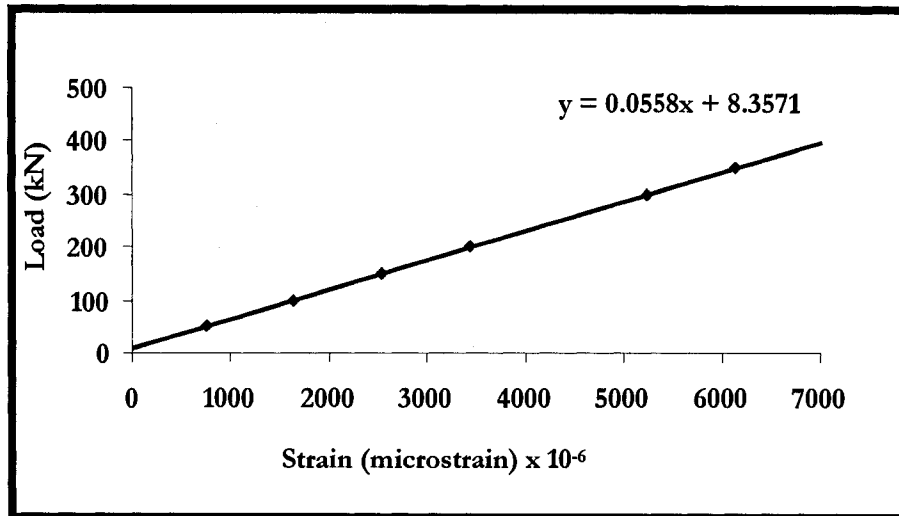
Fig. 3-40: Channel 37 calibration curve

120
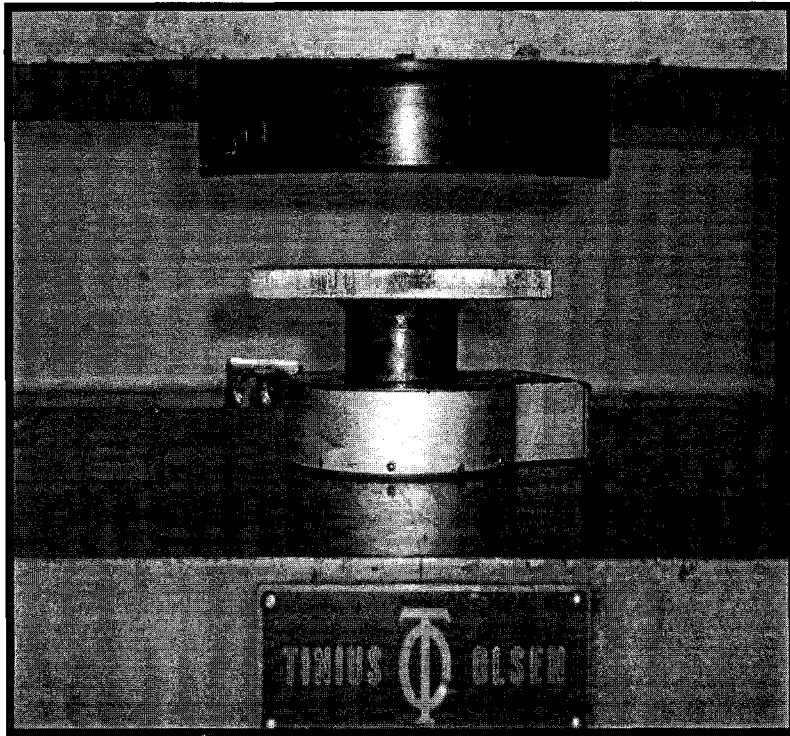
Fig. 3-41: Load cell calibration
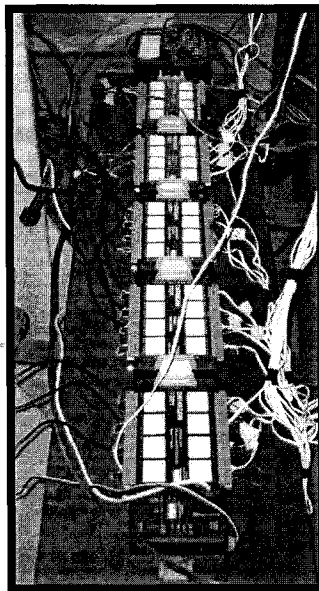
Data scan

Fig. 3-42: Data acquisition system

121
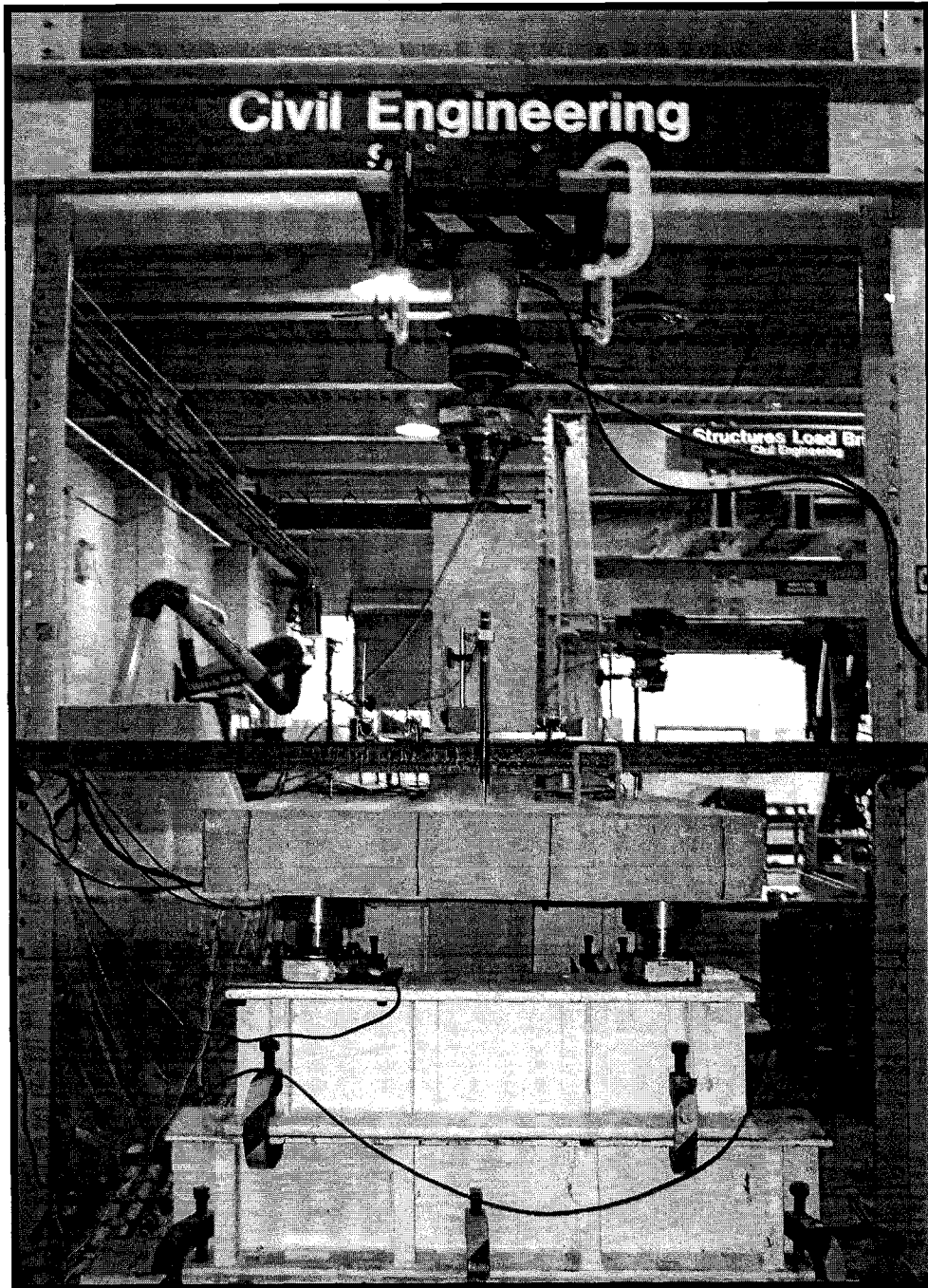
Fig. 3-43: View of the control specimen (CTRL0) during testing

122
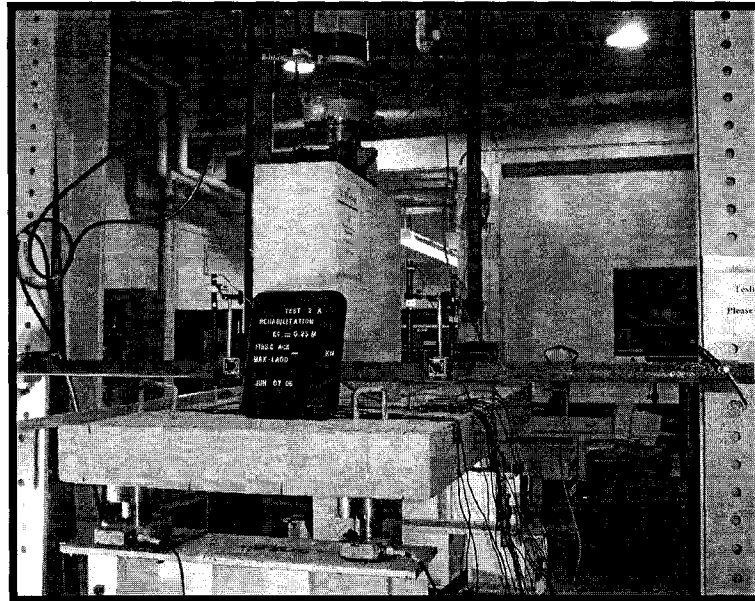
Fig. 3-44: View of the cracked specimen (CRAK25) during testing
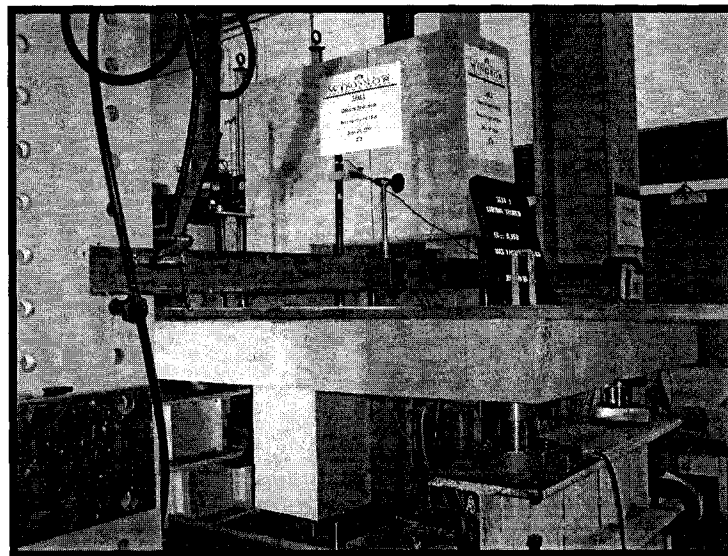
Fig. 3-45: View of the control specimen (CTRL35) during testing

123
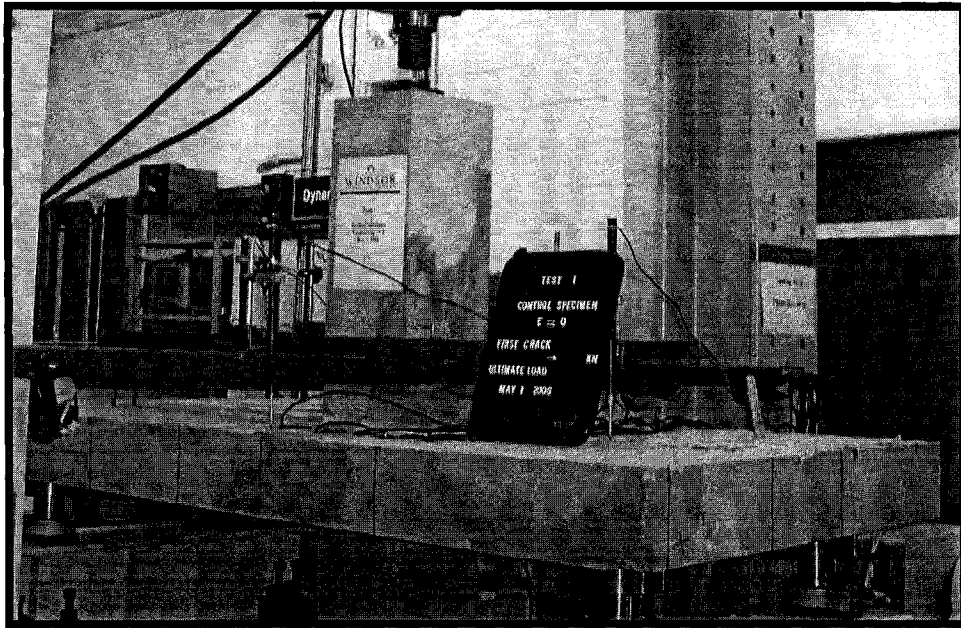
Fig. 3-46: The control specimen (CTRL0) before testing

174 kN
Ult. Load

1ˢᵗ crack
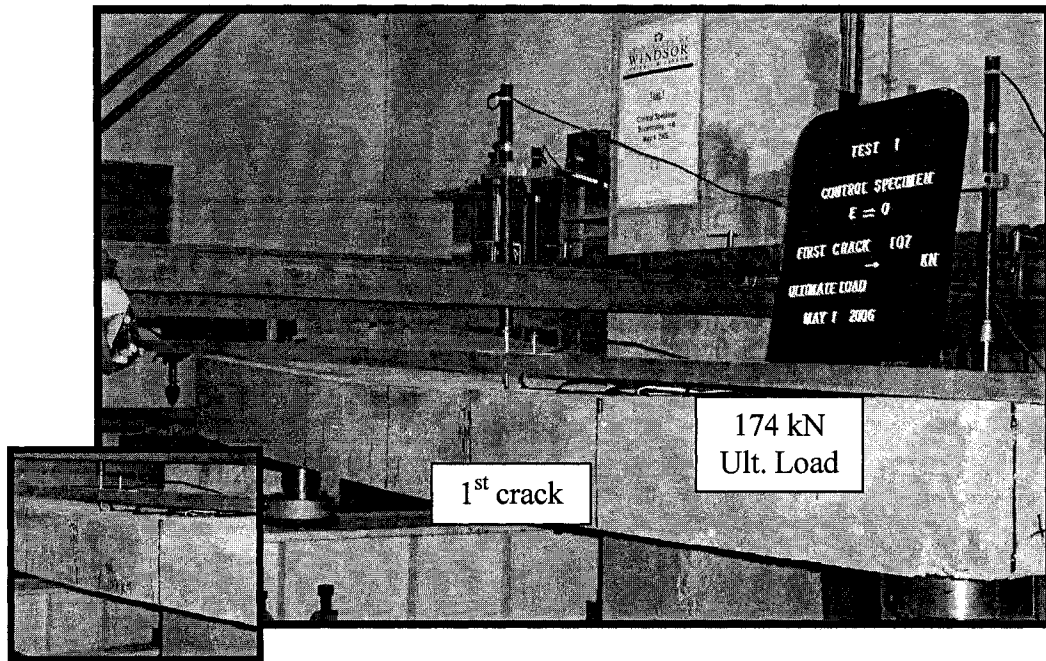
Fig. 3-47: The control specimen (CTRL0) after failure

124
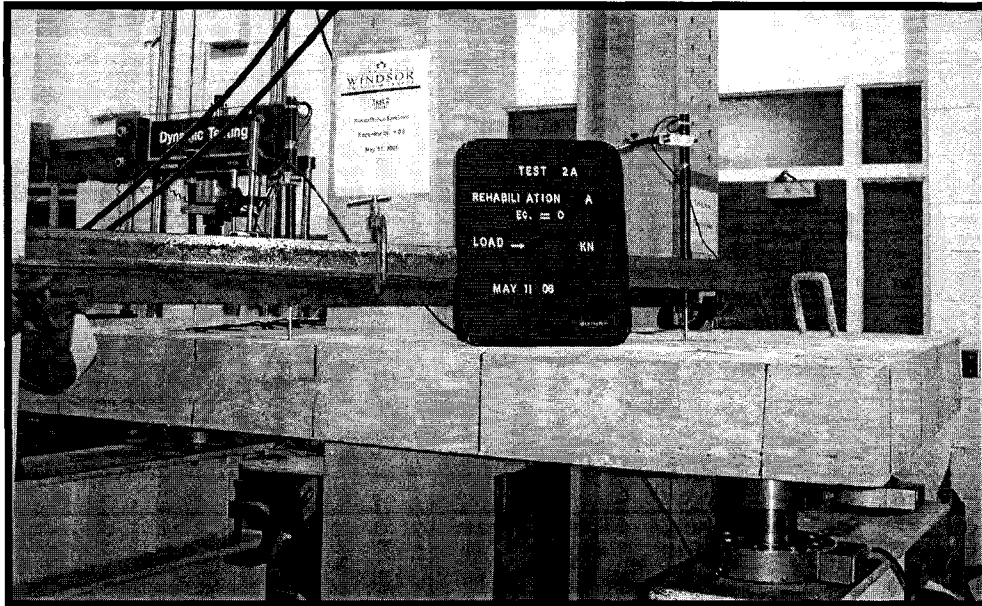
Fig. 3-48: The cracked specimen (CRAK0) before test
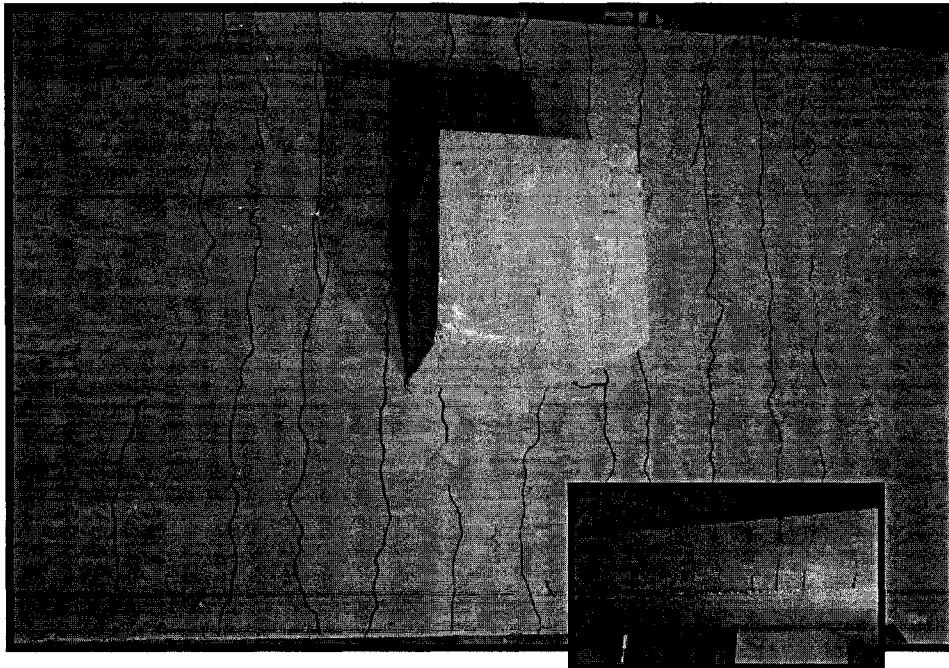
Fig. 3-49: The cracked specimen (CRAK0) after failure

125
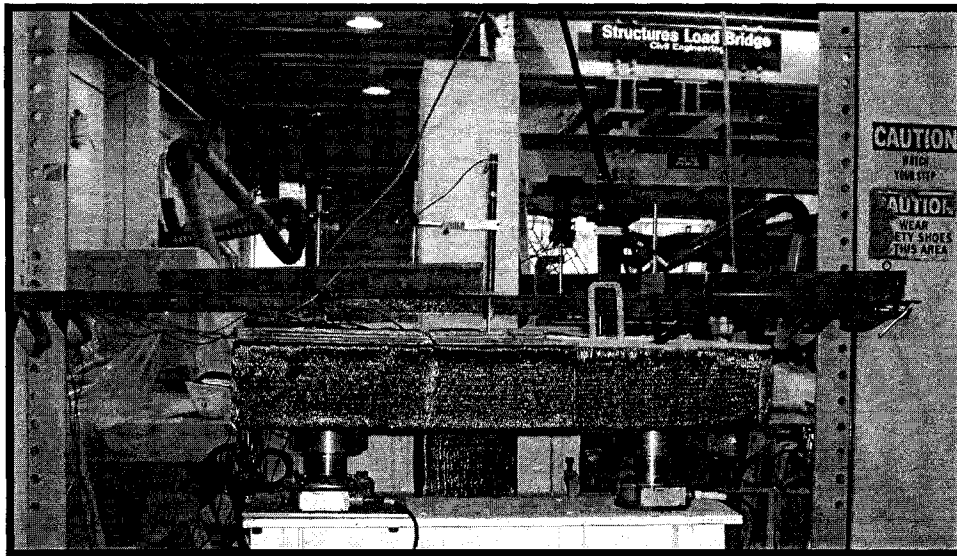
Fig. 3-50: The rehabilitated specimen (REHB0) before testing
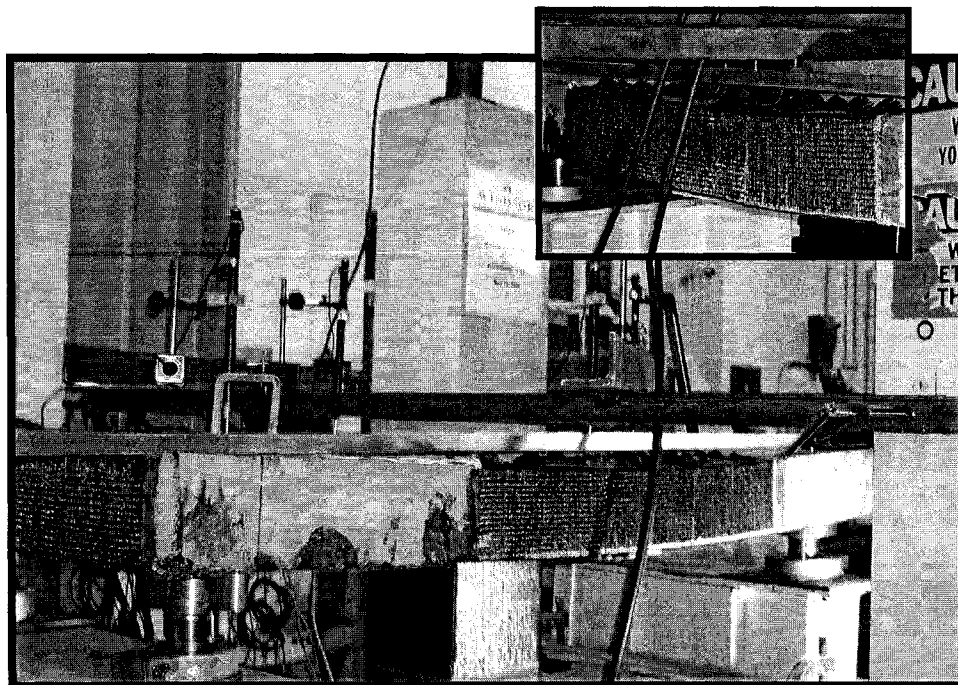
Fig. 3-51: The rehabilitated specimen (REHB0) after failure

126
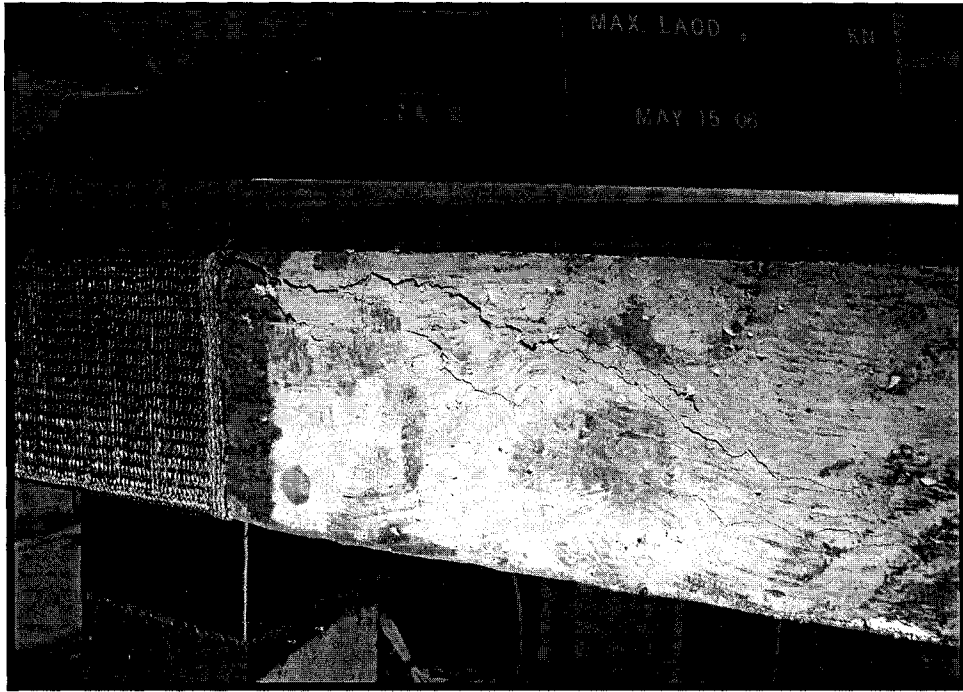
Side view
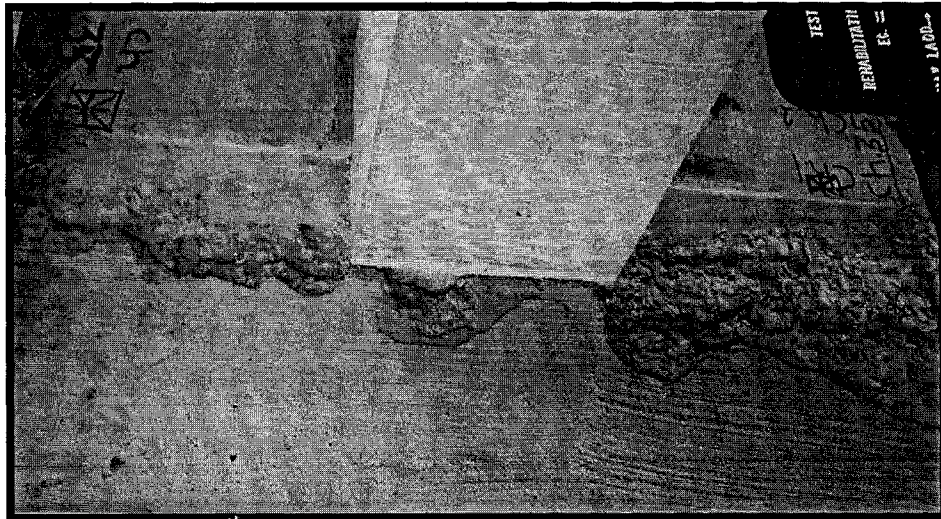
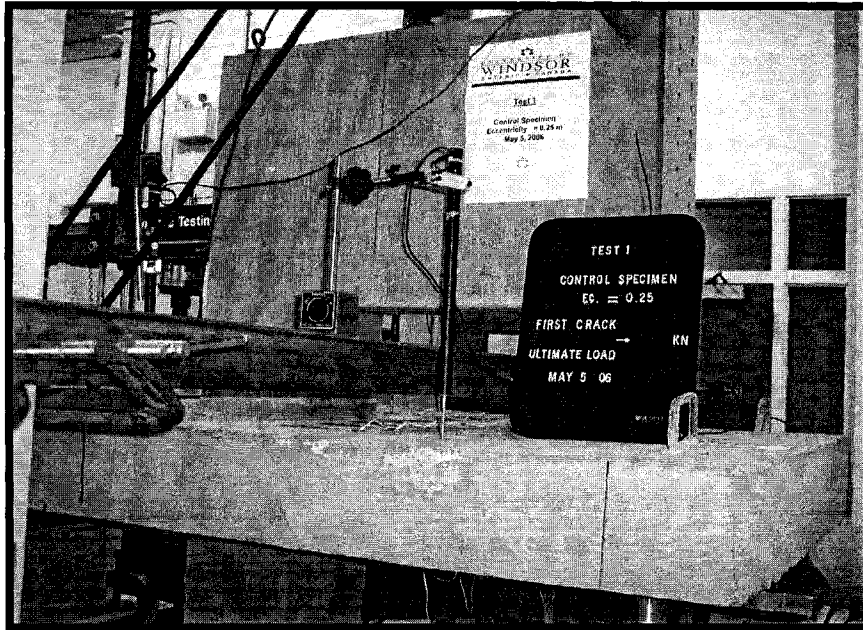Fig. 3-52: The rehabilitated specimen (REHB0) after failure

127

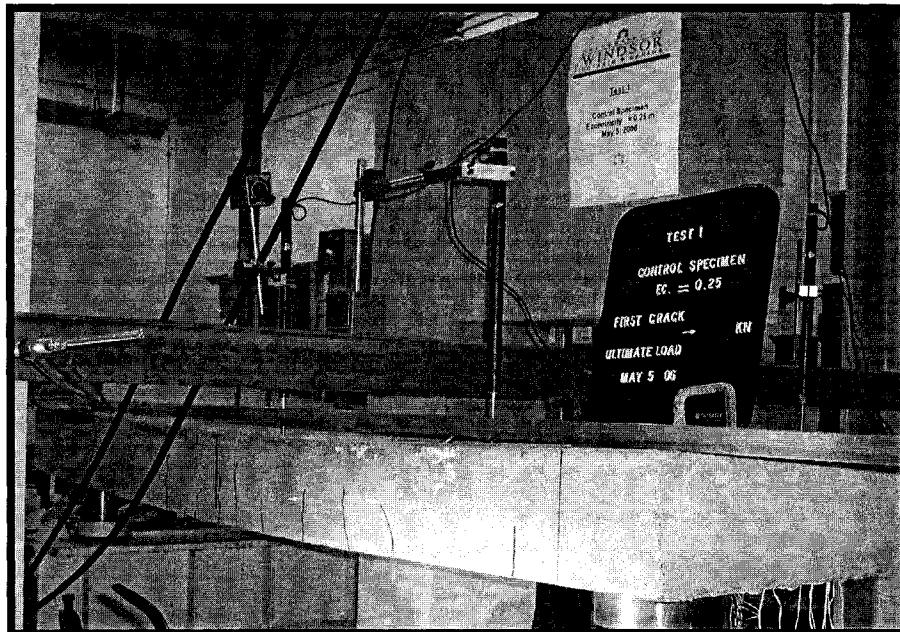Fig. 3-53: The control specimen (CTRL25) before testing

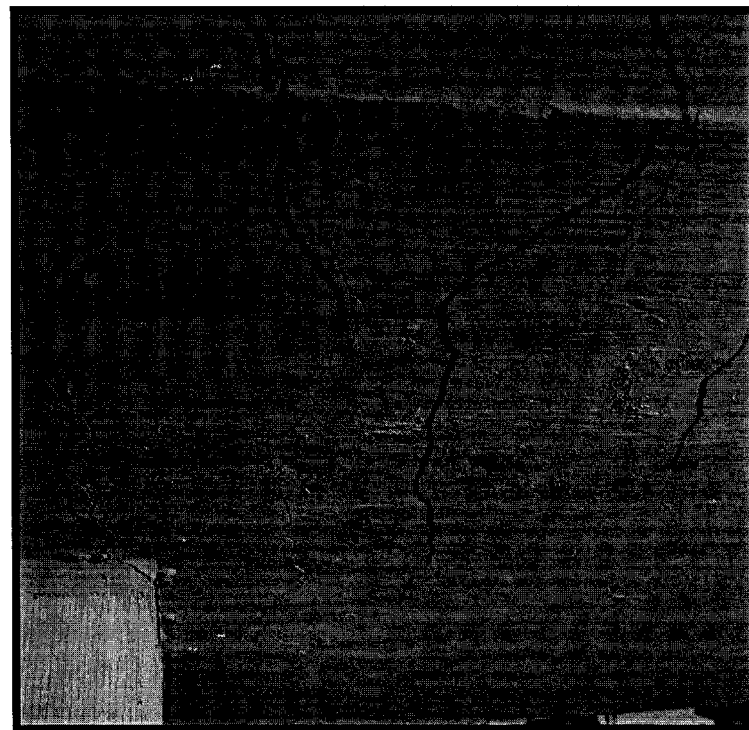Fig. 3-54: The control specimen (CTRL25) during testing
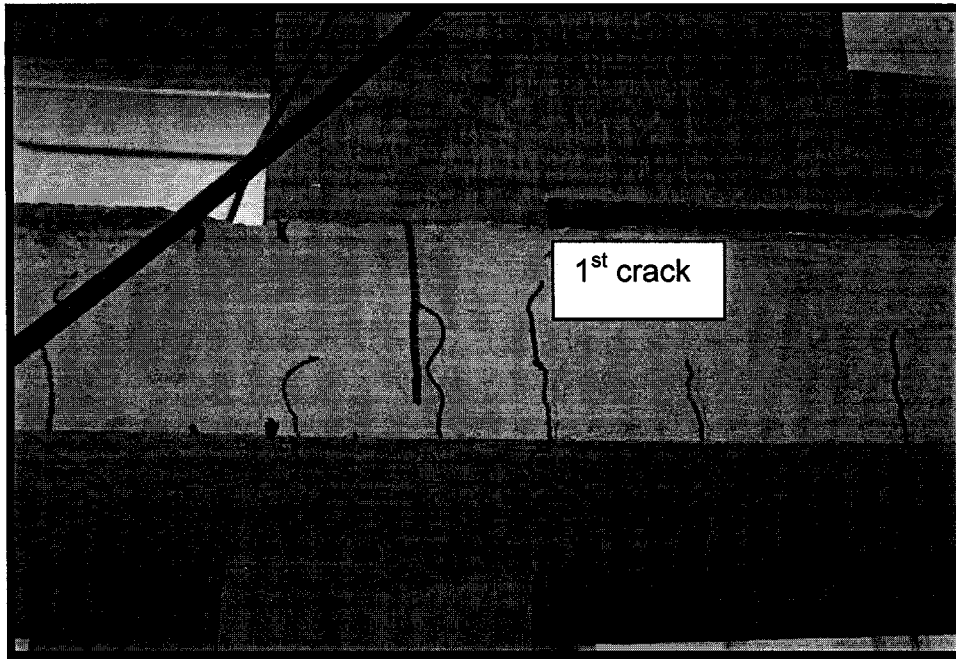
128

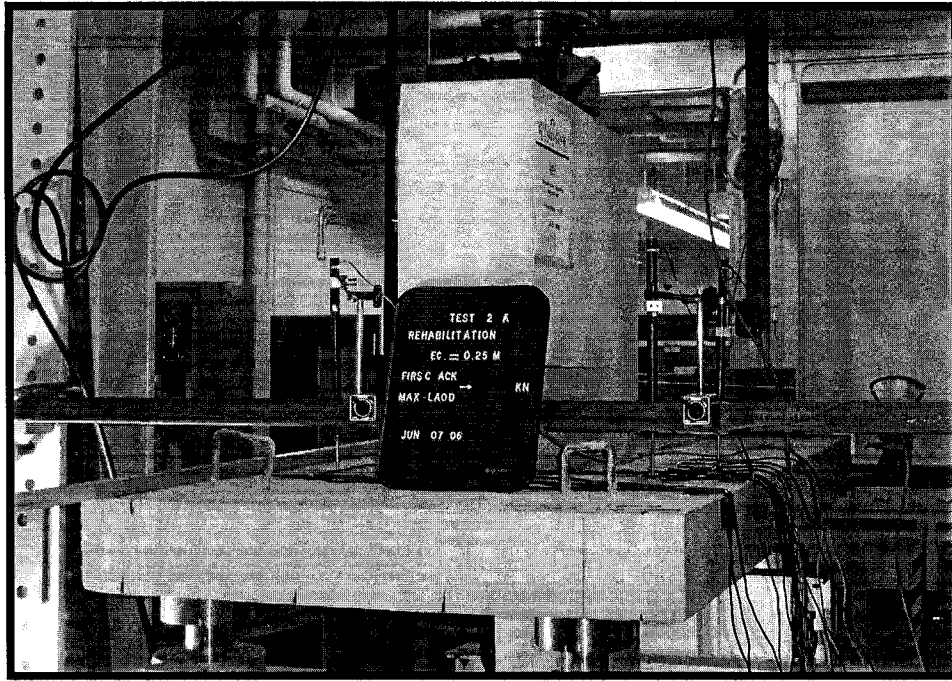Fig. 3-55: The control specimen (CTRL25) after failure

129

Fig. 3-56: The cracked specimen (CRAK25) before testing

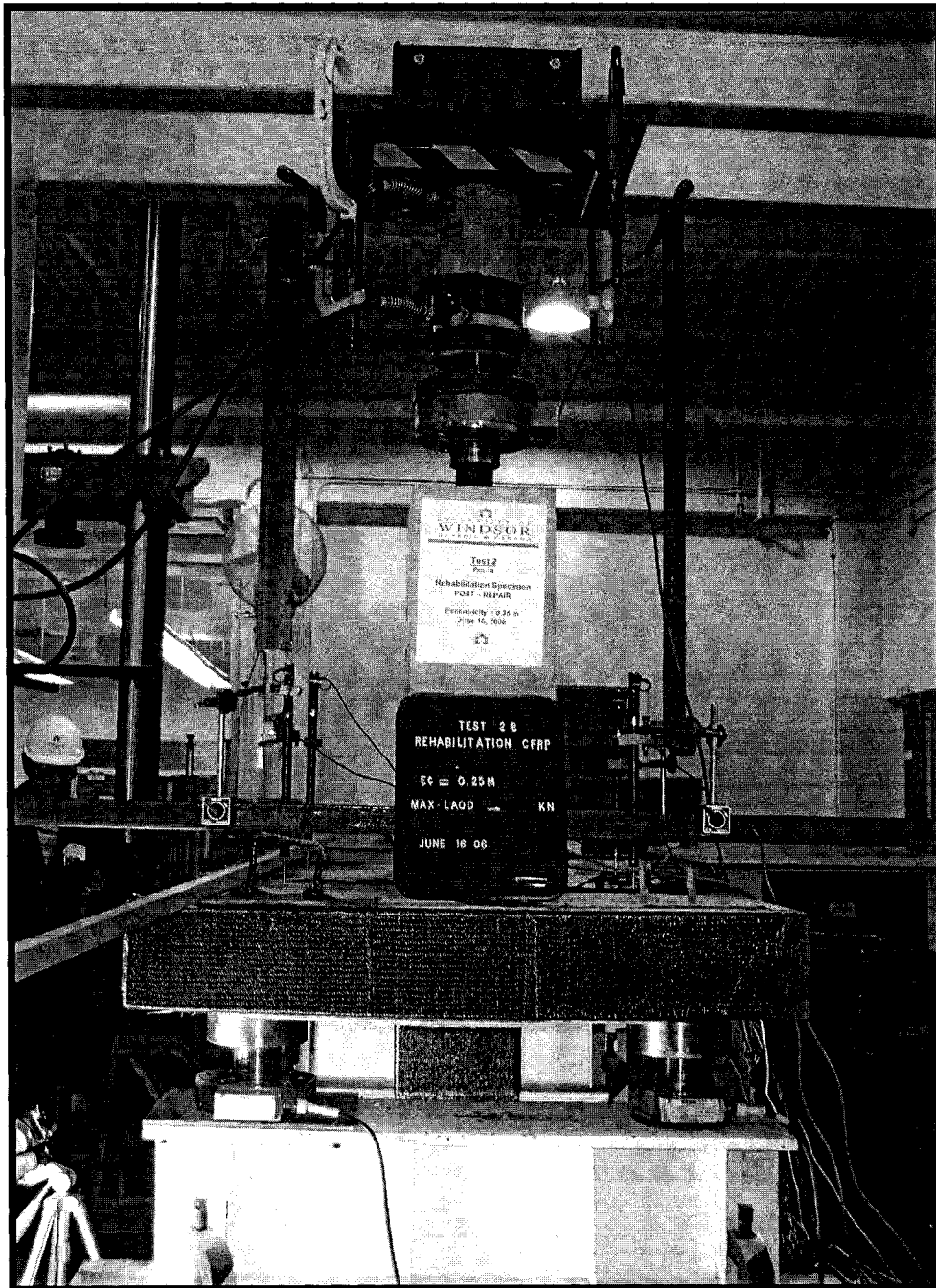Fig. 3-57: The cracked specimen (CRAK25) after failure

130

Fig. 3-58: View of the rehabilitated specimen (REHAB25) during testing
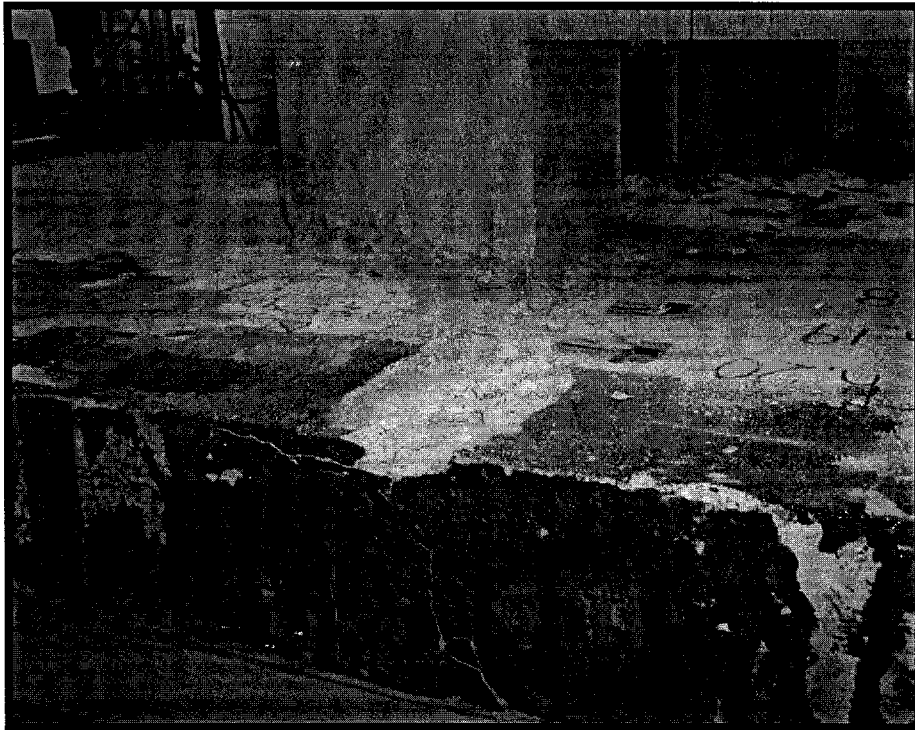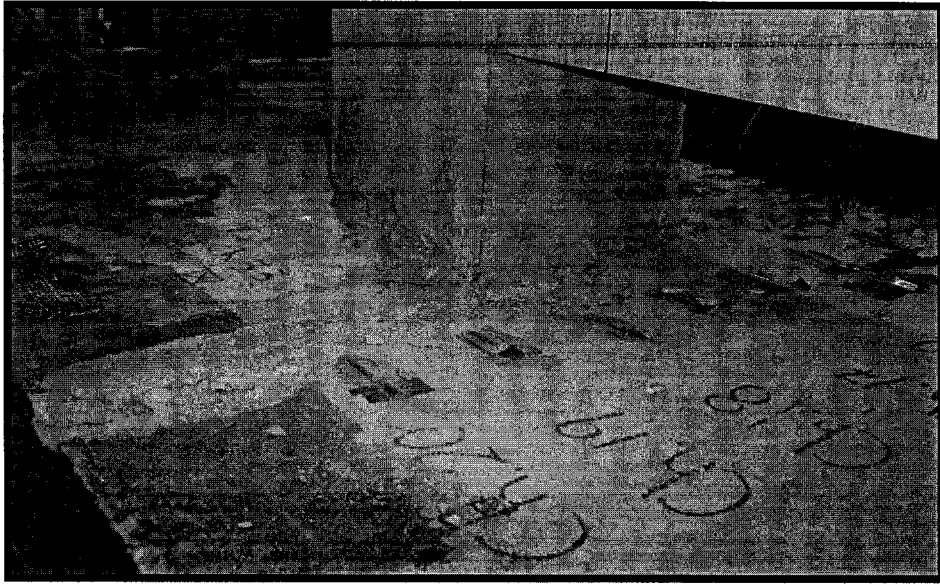
131

Fig. 3-59: The rehabilitated specimen (REHAB25) after failure
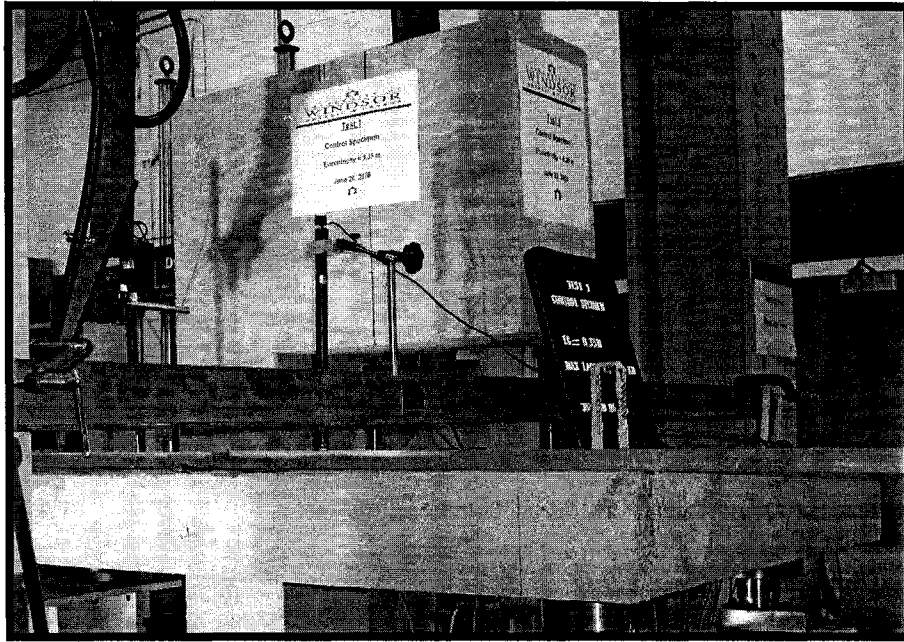(after removing CFRP from the side)

132

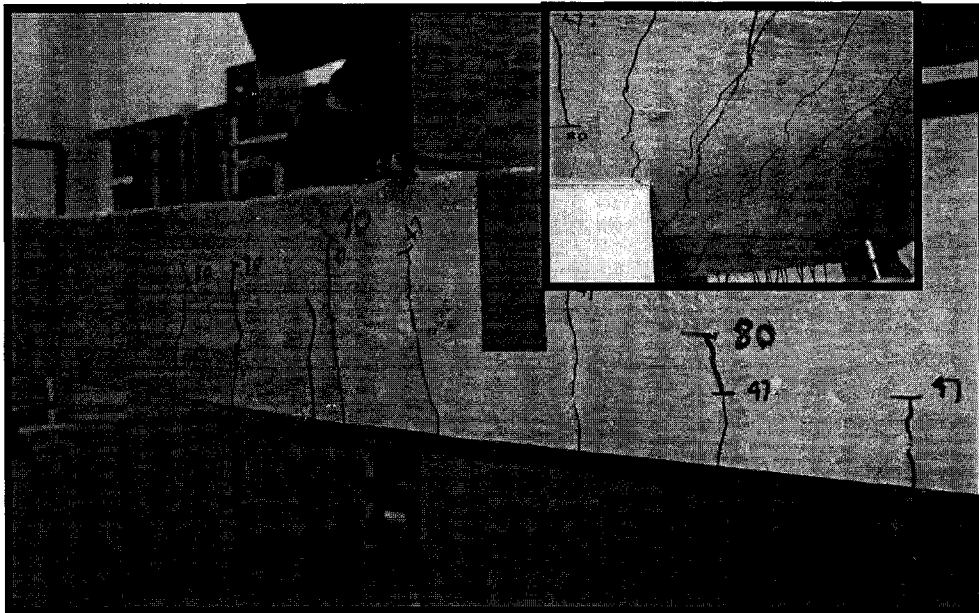Fig. 3-60: The control specimen (CTRL35) before testing

Fig. 3-61: The control specimen (CTRL35) after failure

133

Fig. 3-62: The cracked specimen (CRAK35) before test

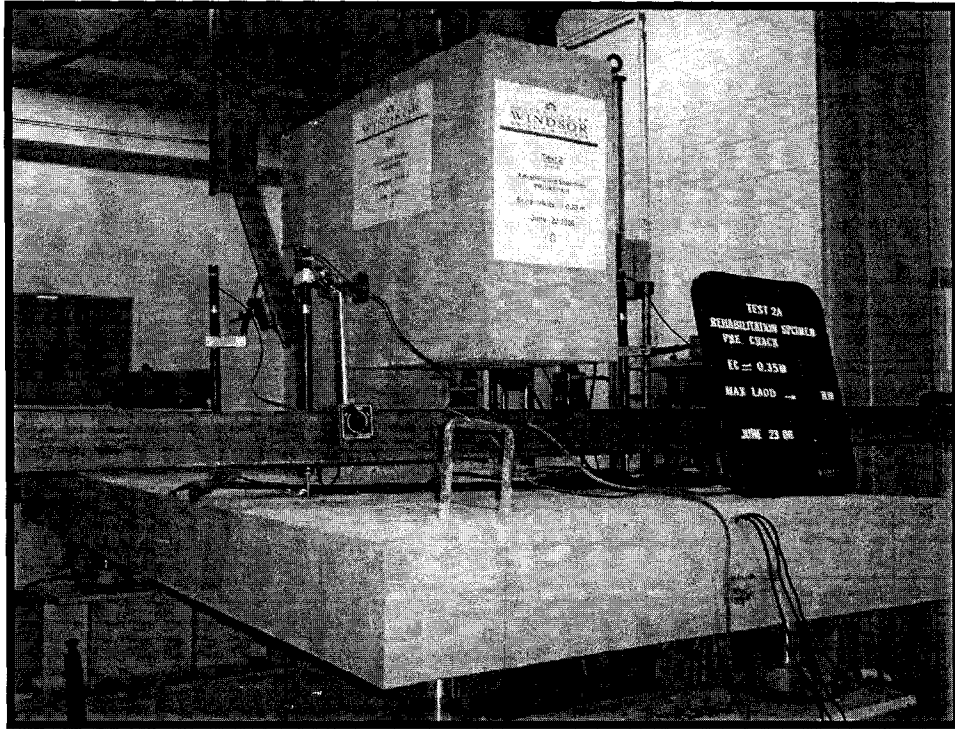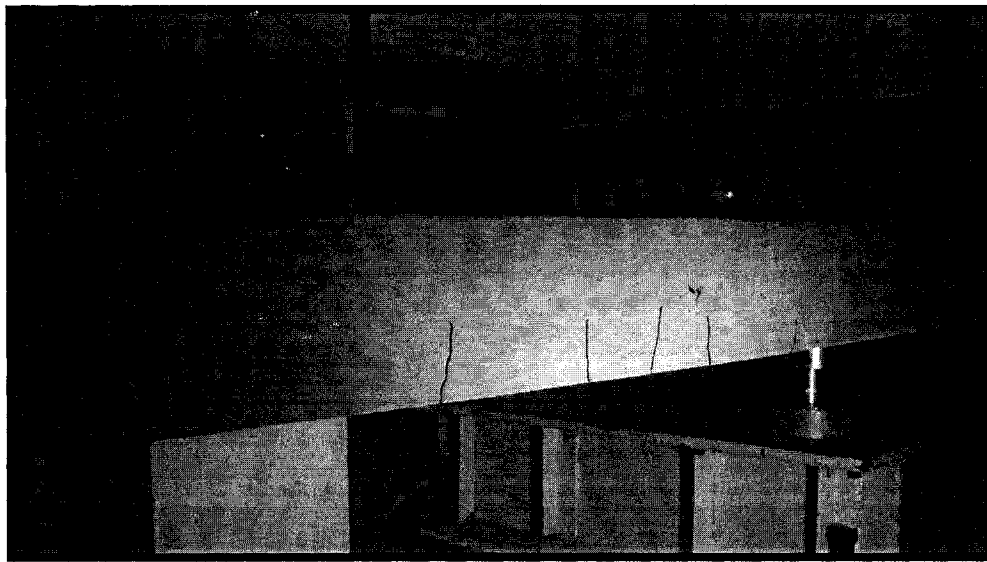Fig. 3-63: The cracked specimen (CRAK35) after failure

134
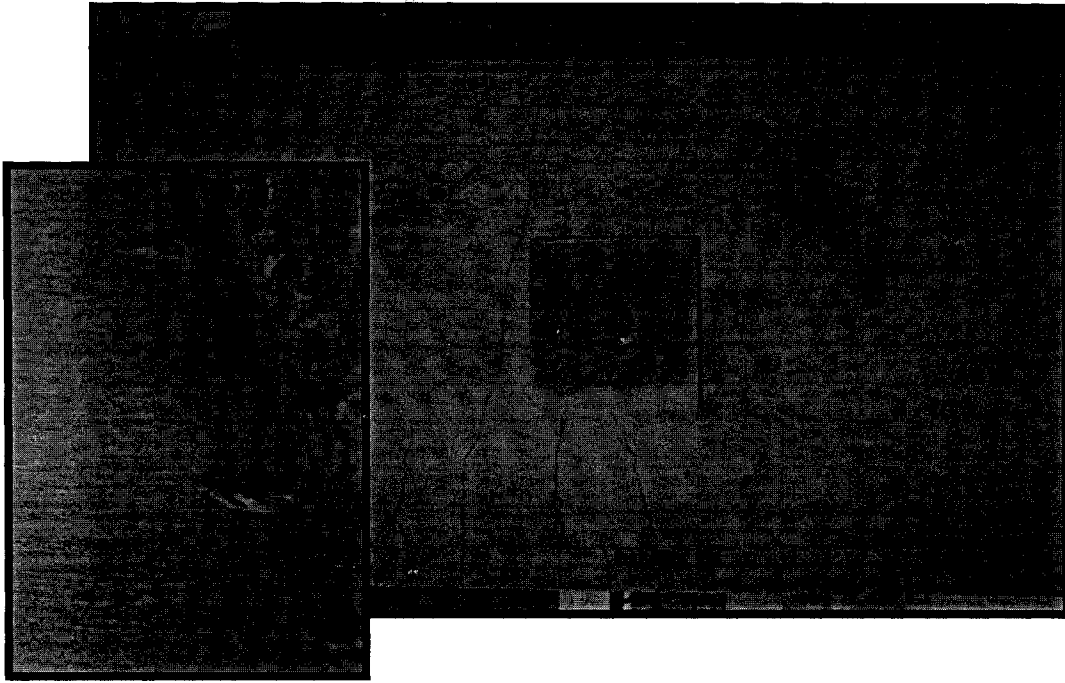
Fig. 3-64: The cracked specimen (CRAK35) after failure
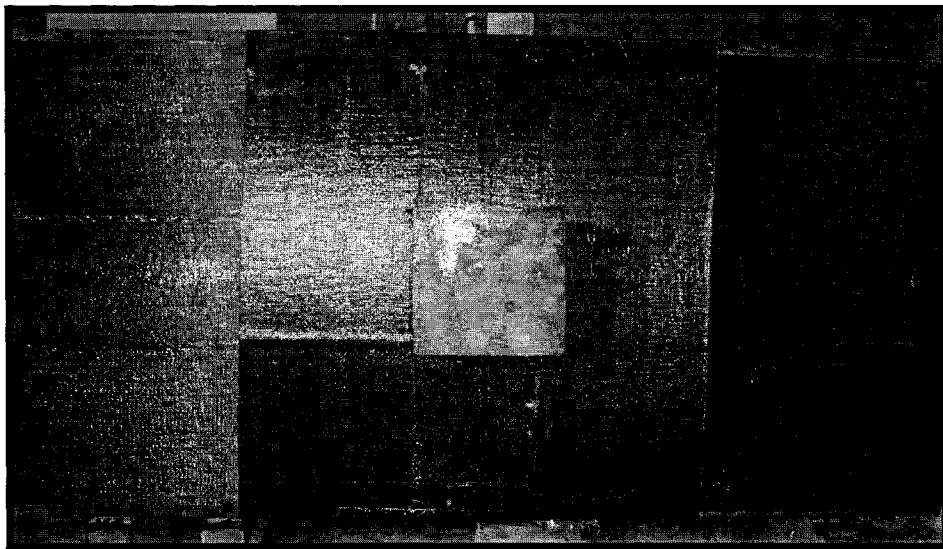
Fig. 3-65: The cracked specimen (CRAK35) after rehabilitation
Rehabilitated specimen (REHB35)

135
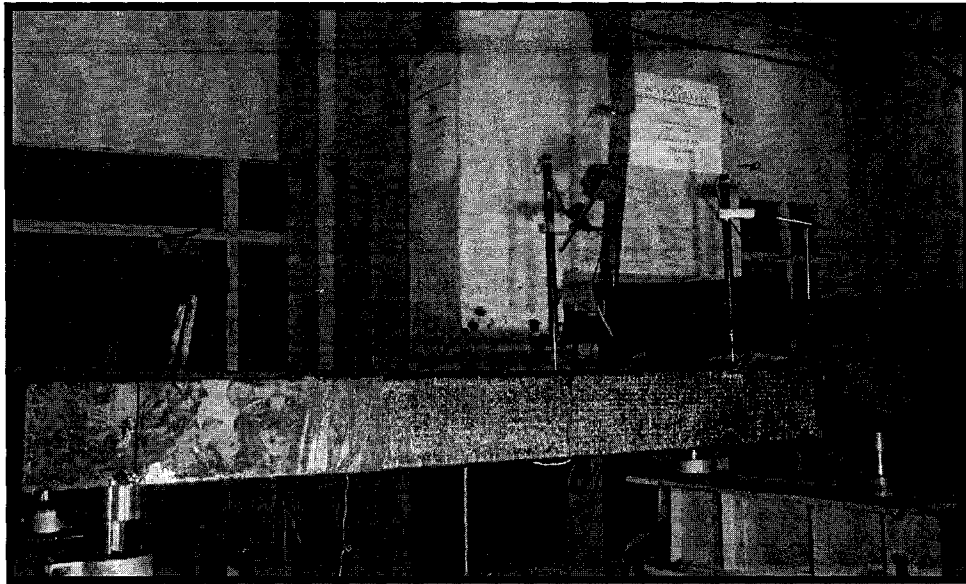
Fig. 3-66: The rehabilitated specimen (REHAB35) before test
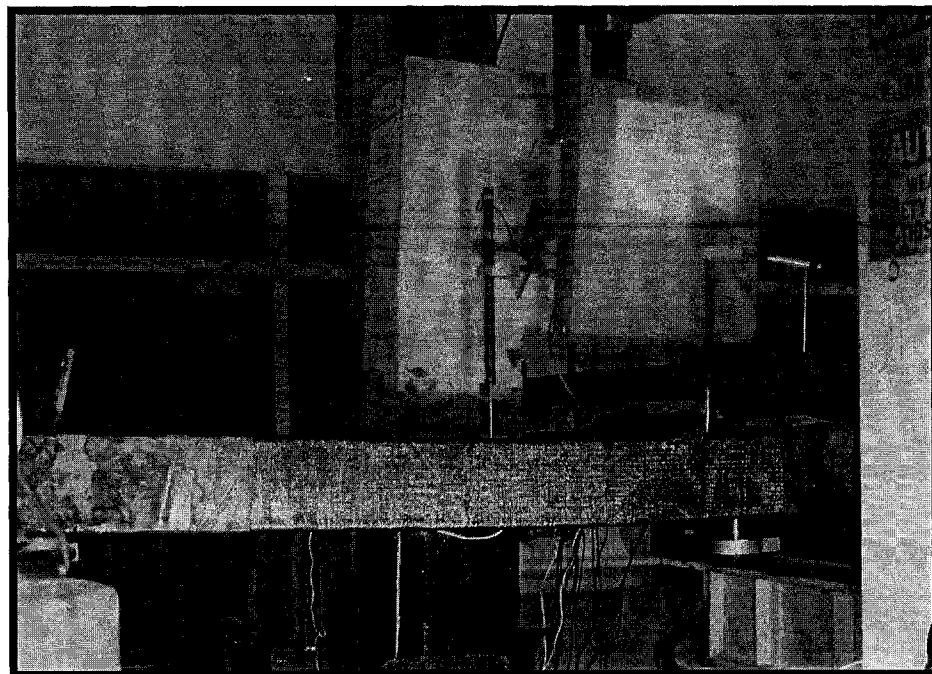
Fig. 3-67: The rehabilitated specimen (REHAB35) after failure

136
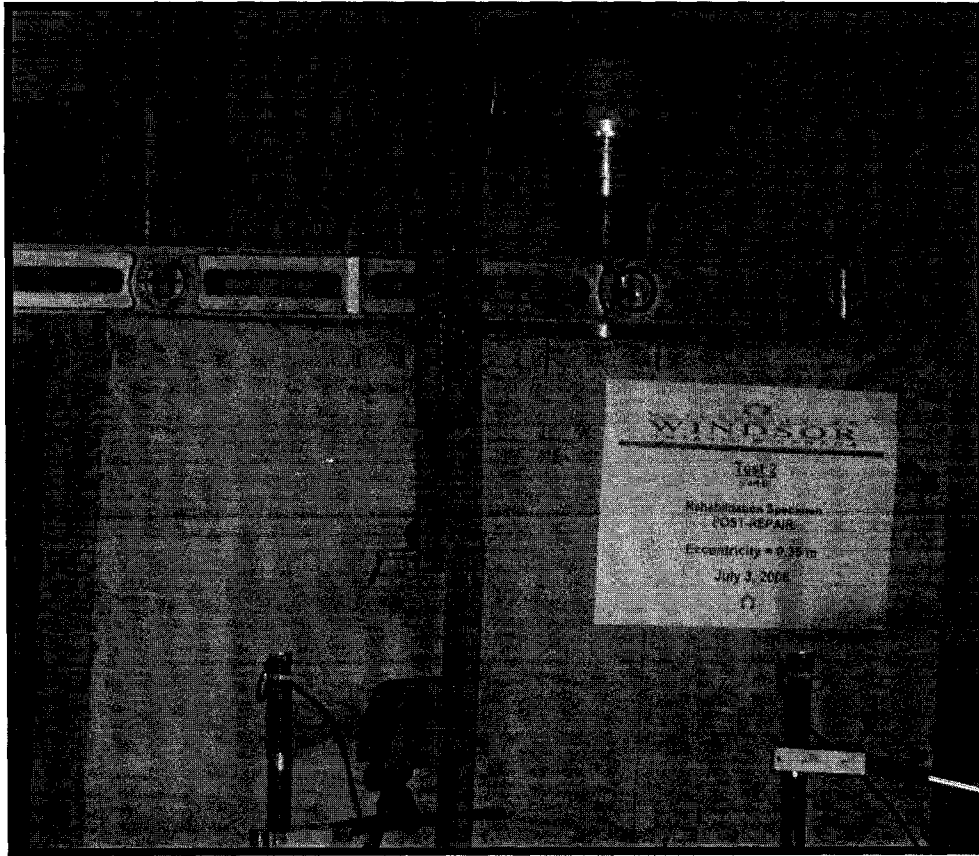
Fig. 3-68: The rehabilitated specimen (REHAB35) after failure

137
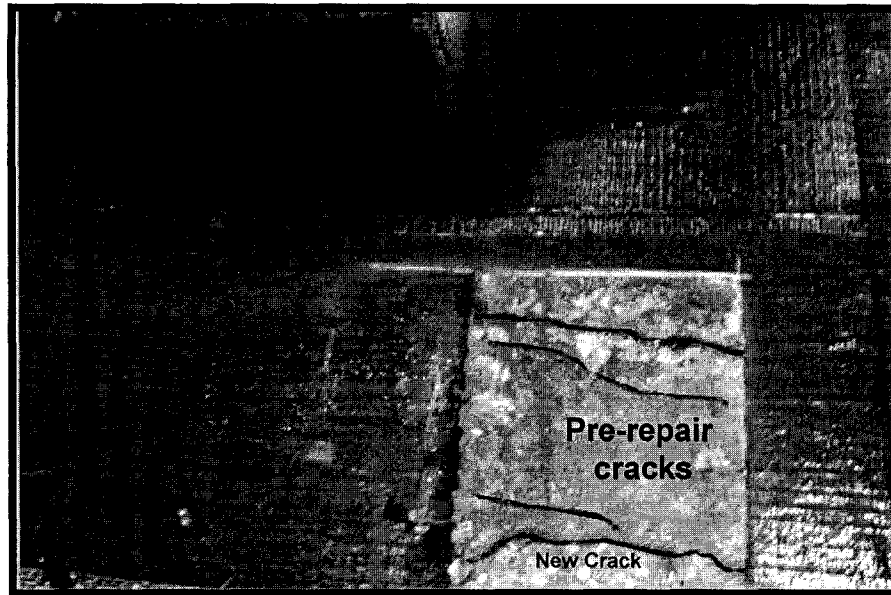
Fig. 3-69: The rehabilitated specimen (REHAB35) after failure
(after removing CFRP from the bottom side, tension zone, of the slab)

138
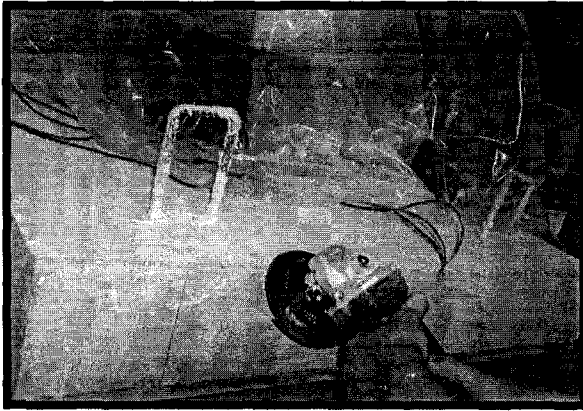
Edge grinding

Surface grinding
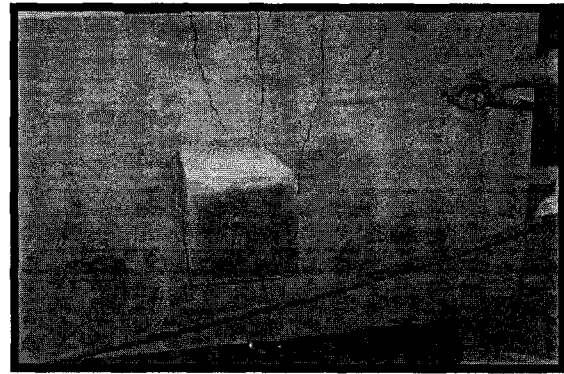
Blowing

Fig. 3-70: CFRP works (Surface preparation)

139
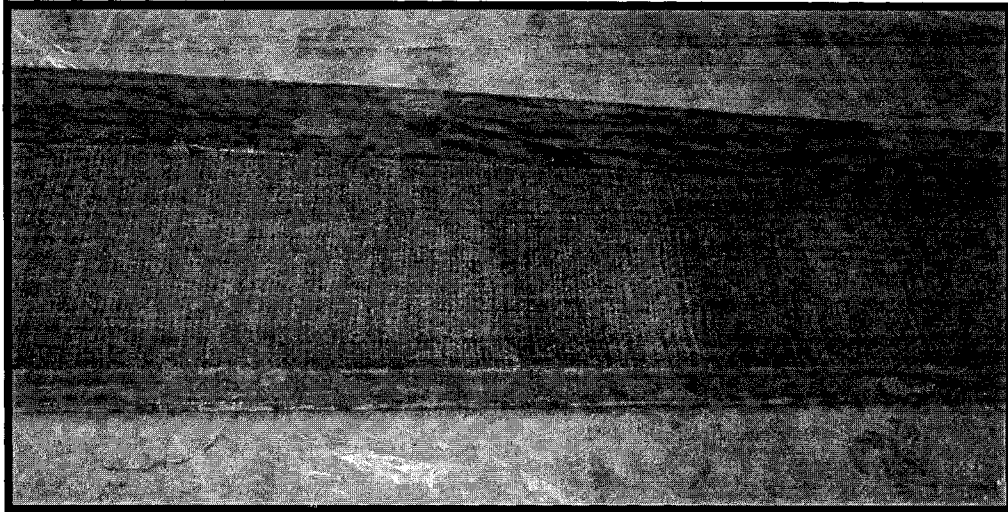
Fig. 3-71: Saturation of CFRP sheets with epoxy
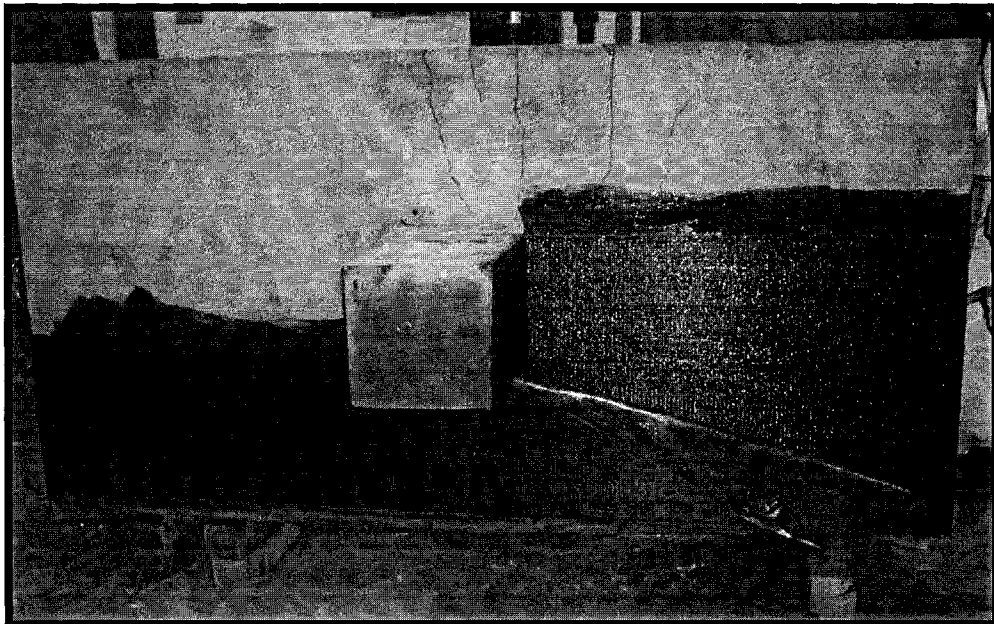
Fig. 3-72: Installation of the first layer of CFRP sheets

140

Fig. 3-73: Applying primary layer of epoxy to the bonded face
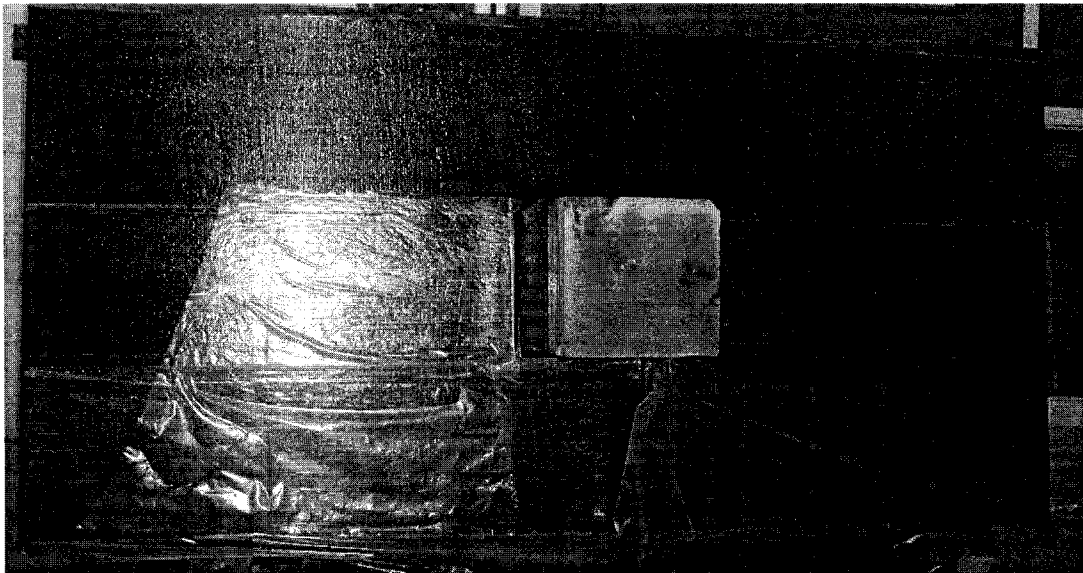
Fig. 3-74: First layer of CFRP sheets

141
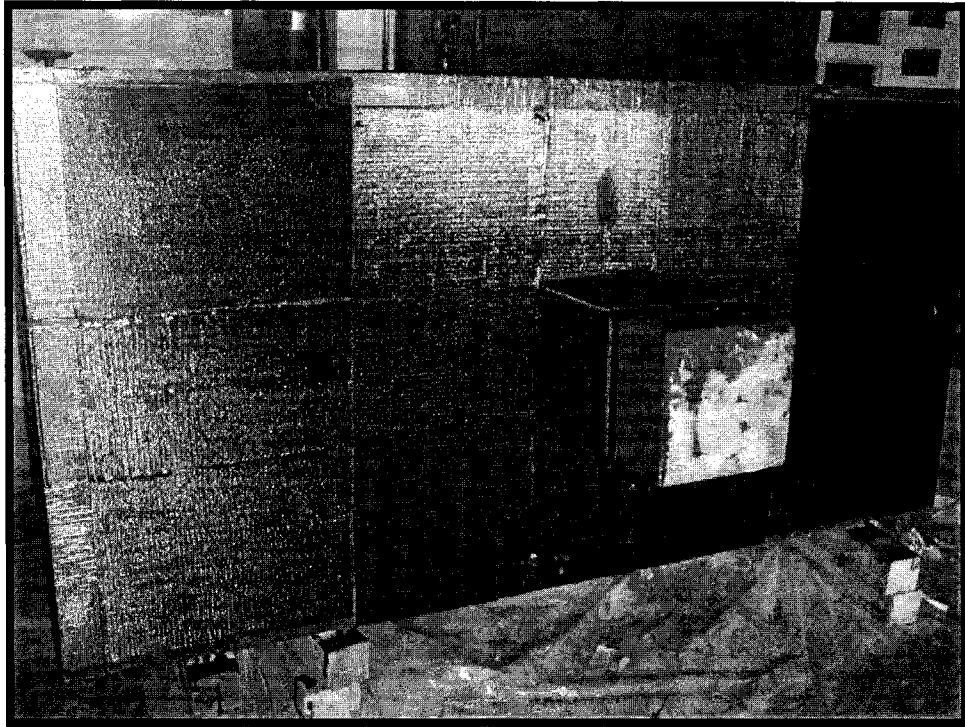
Fig. 3-75: Second layer of CFRP sheets

142
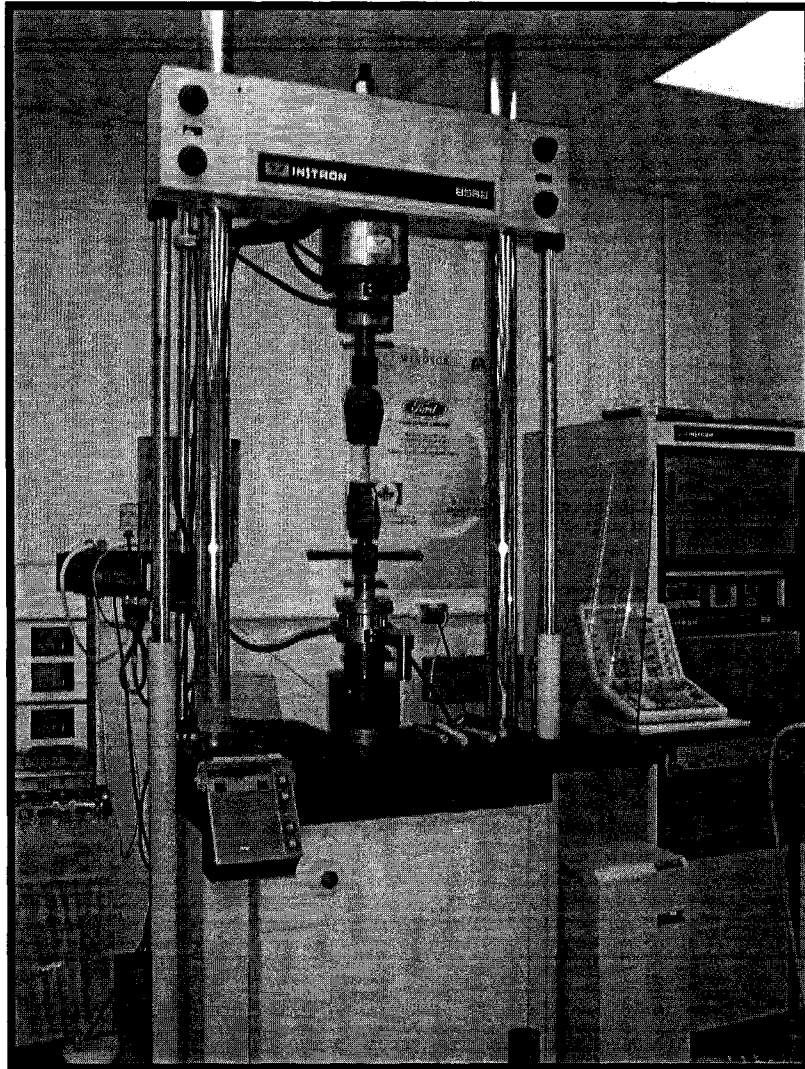
Fig. 3-76: INSTRON test frame
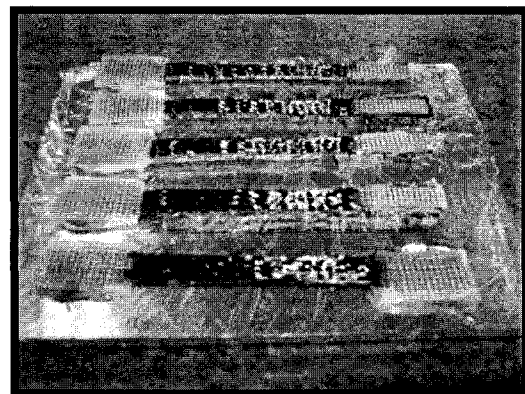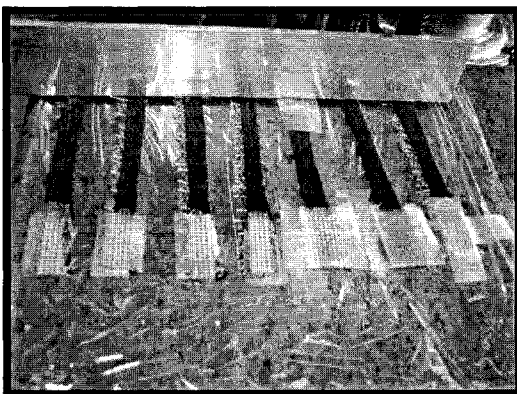
Fig. 3-77: CFRP samples during preparation

143

Decreasing
of the width
after failure
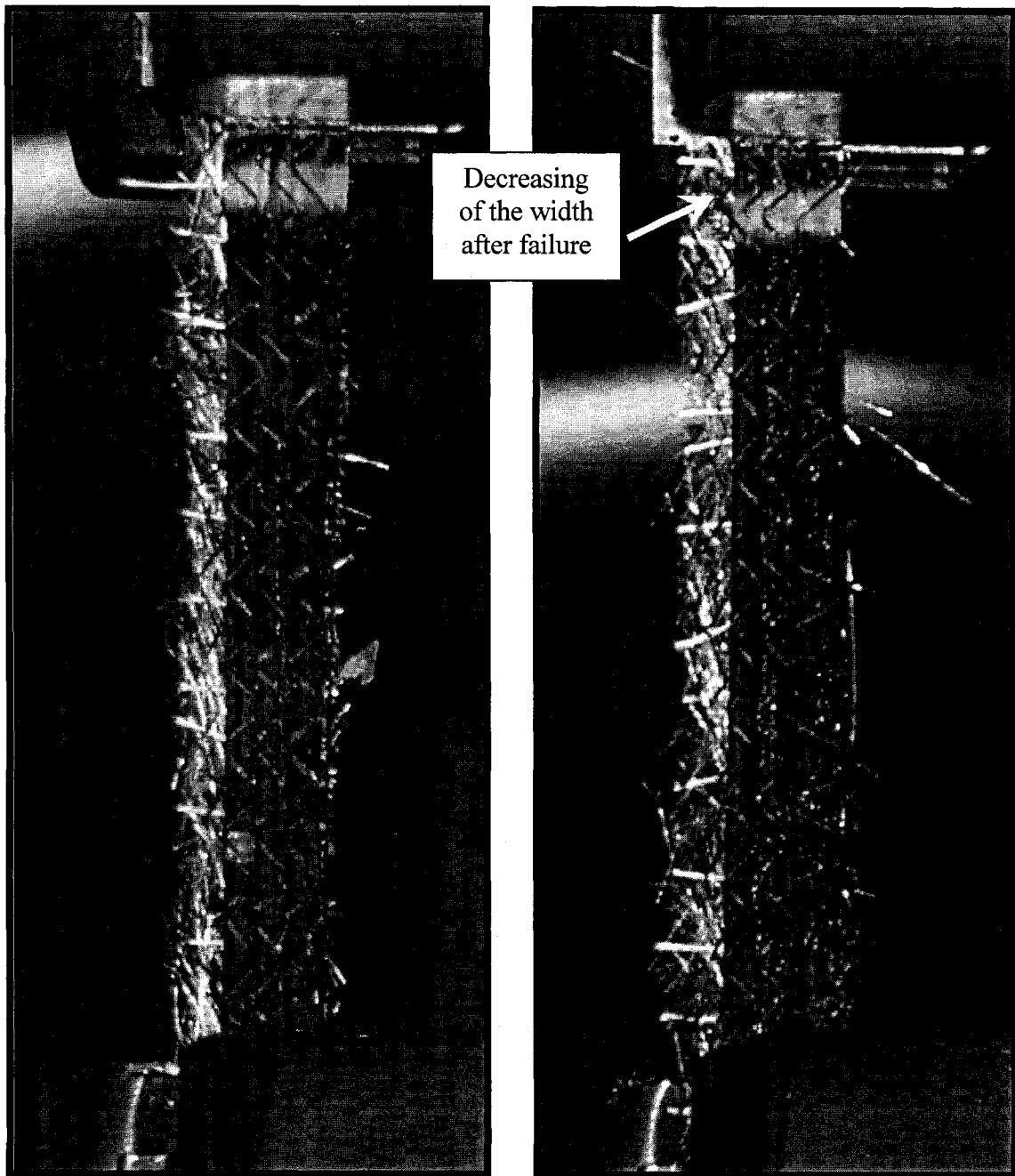
During the test   After failure

Fig. 3-78: Tensile test of CFRP sheets

144
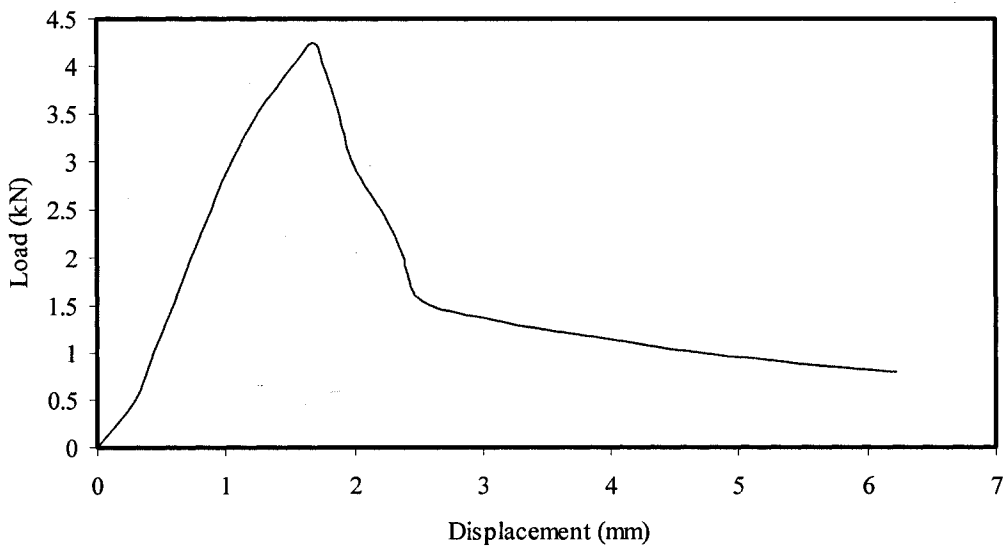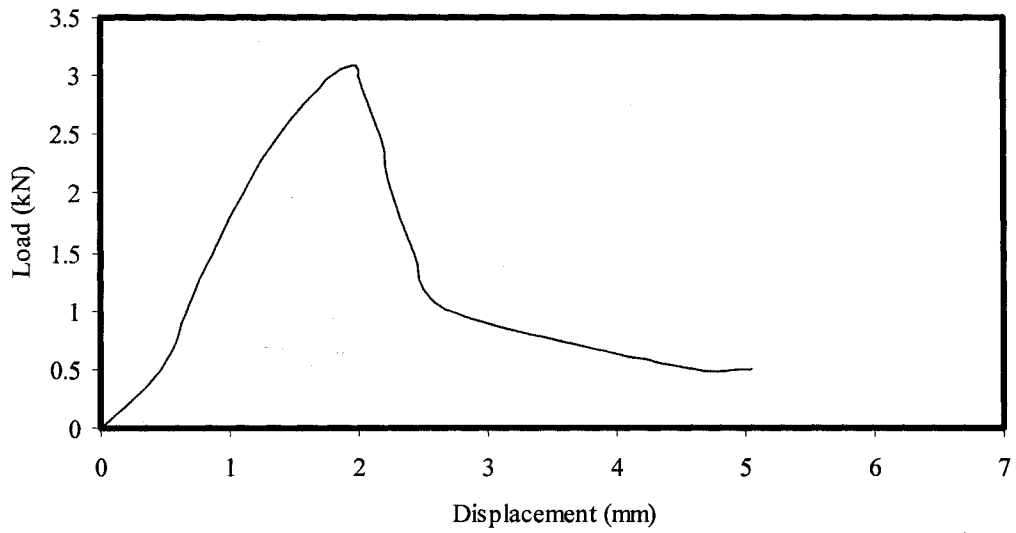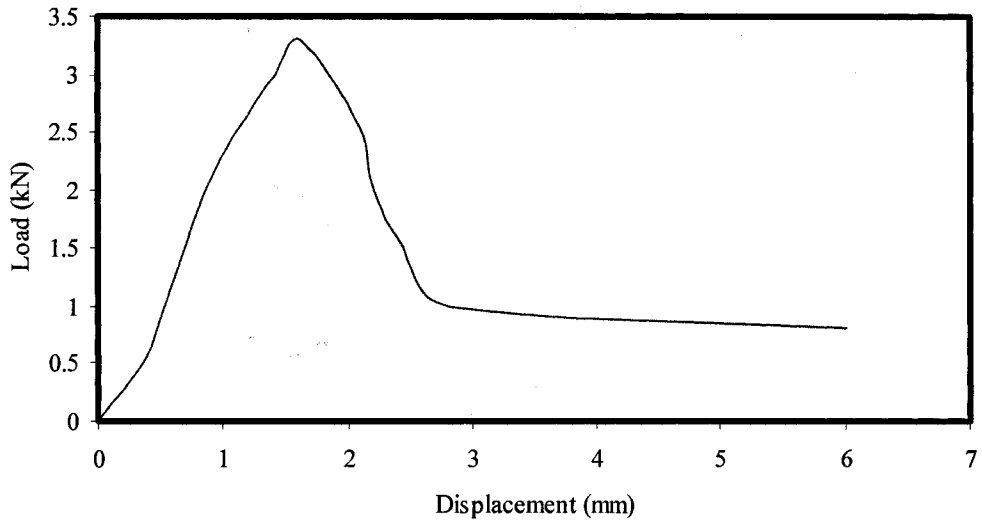
Fig. 3-79: CFRP sheets tensile strength test (Load-Displacement relationship)

145
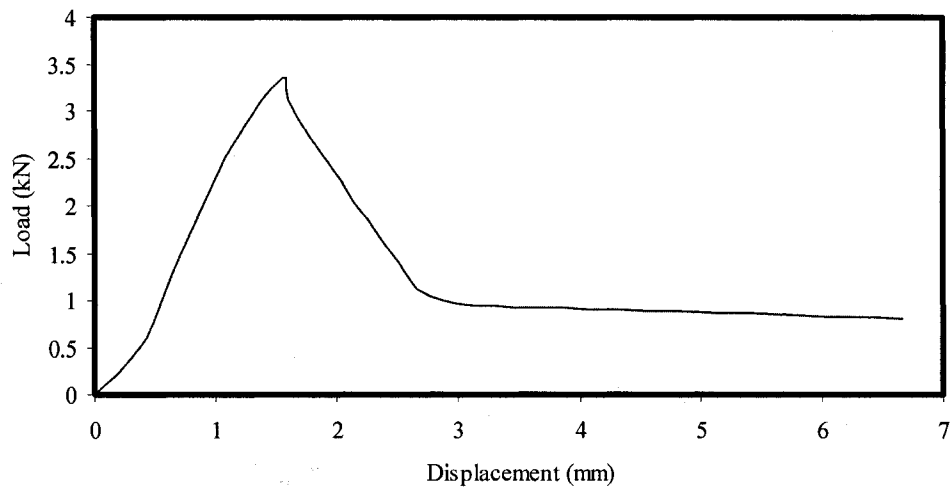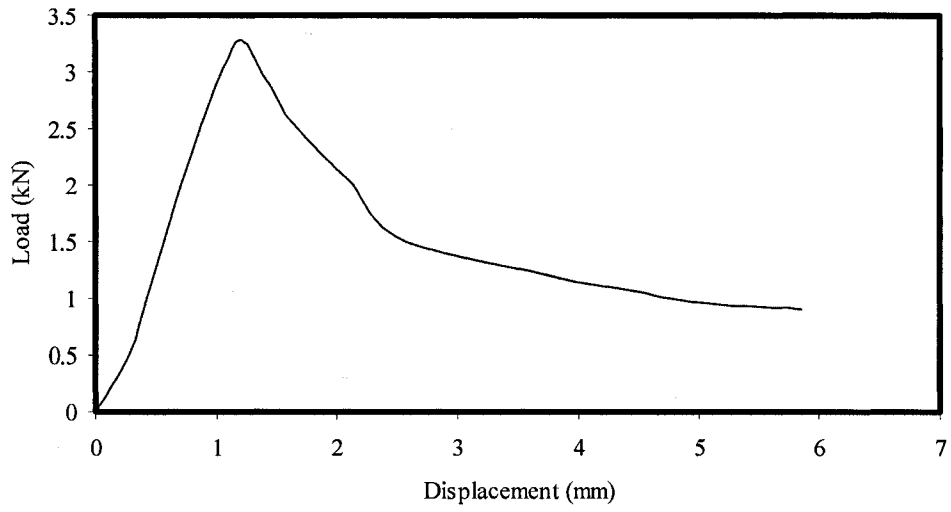
Fig. 3-80: CFRP sheets tensile strength test (Load-Displacement relationship)

146

CHAPTER IV

EXPERIMENTAL RESULTS AND ANALYSIS

4.1 General

The results, observations, and discussion of this series of tests describe the behaviour of flat-slab-column system. The response of each specimen in terms of steel strain, concrete strain, deflection, ultimate load, and failure mechanism obtained from the collected data from a wide range of instrumentation which is described and analyzed in this chapter. Focus is on the effect and evaluation of CFRP on rehabilitation of a cracked slab-column system. Furthermore, the observations of cracking propagation are described with particular emphasis on the cracking behaviour at working load of the control specimen with eccentric load of 250 mm (CTRL25) as an example of the cracking phenomenon of this system. The summary of the test results is presented in Tables 4-1 to 4-5.

As mentioned in the previous chapter, the control specimen of each group was first tested to failure to study and compare the behaviour of each group. For the pre-cracked specimen (used in repair evaluations), the load was kept at approximately 70% of ultimate load of the control specimen for one day, the specimen is then repaired using CFRP, cured, and lastly tested to failure.

4.2 Behaviour of Group I Specimens

As mentioned in chapter III, a single monolithically increasing concentrated load was applied on the center of the top column stub of the specimens in this group as

147

illustrated in Figure 3-35. Two specimens were tested: CTRL0 is the control specimen loaded up to failure, and specimen CRAK0 was loaded up to 72% of the ultimate load recorded from the control specimen (CTRL0); REHB0 specimen is CRAK0 specimen repaired using external reinforcing with CFRP sheets on the tension cracked (bottom) surface followed by curing, and tested up to failure.

4.2.1 Control specimen (CTRL0)

The load was applied up to 169 kN on this specimen. Under this load, the maximum concrete strain on the long direction compression zone was found to be -1774E-6, while all longitudinal direction tension steel yielded. Moreover, the maximum recorded deflection was 33 mm on the east central point. Figure 4-159 shows the CTRL0 specimen during different stages of loading.

4.2.1 (a) Crack propagation

The first theoretical invisible crack was calculated to be occurred at 38 kN as shown in Table 4-5. Moreover, the steel stress in this stage was 87 MPa (434E-6); yet before cracking, and at 30 kN, the steel stress was only 35 MPa (173E-6) as shown in Table 4-2.

The first visible crack was observed at the jacking load of 89 kN. This crack of 0.3 mm width started on the north sides of the specimen from the tension (bottom) zone and penetrated the slab thickness vertically toward the compression (top) zone in the position parallel to the north face of the column stub. The second crack appeared in the same manner on the other side of the specimen parallel to the south face of the column

148

stub. With an increase to the applied load, more "live" tension cracks were observed away from the loading axis toward both north and south free edges on both east and west sides. While these cracks penetrated the slab thickness towards the loading axis, some of them spread to the tension surface on the short direction (east-west). By continuing to increase the load, more cracks expanded from both sides along the short direction on the slab's tension (bottom) zone; the width of a larger crack in this stage was measured at 130 kN to be 0.4 mm and at 155 kN to be 0.5 mm.

The last stage of cracking started when no new cracks was observed, while, the width of the existing "live" cracks was increased, especially in the area beside the column stub. The tension cracks continued to widen and penetrate more into the slab thickness. Also, the tension cracks on the bottom surface continued to widen till no more load could be resisted by the specimen. Flexural failure occurred at 169 kN with 1 mm crack width. Figure 4-159 shows the tension cracks concentrated around the column stub on the tension zone.

4.2.1 (b) Strain gauge reading analysis

This section will focus on presentation of the result of the strain measurement. The analysis will begin with a study of the strain measured in the longitudinal direction (ε_x) as illustrated in Figures 4-14 to 4-16 for longitudinal steel strain in tension zone and 4-19 to 4-20 for longitudinal direction of concrete strain in compression (top face) zone.

The longitudinal strain readings before the cracking load increased gradually within a small range; however, after cracking took place in the tension zone, the strain readings started to increase rapidly (Figure 4-52). The stiffness of the slab decreased as a

consequence of cracking. This behaviour is expected under service load. As an explanation of this phenomenon: the stresses at the bottom face of the slab (tension zone) reached the tensile strength of the concrete, and cracking took place. Then, the tensile force in the concrete was transferred to the steel. As a result, less concrete in the cross section was contributing in the resisting moments. Crack occurrence is obvious from the change of the curve's slope in the same Figures remarked (4-14 to 4-16). As mentioned earlier, the steel stress before cracking was calculated to be only 35 MPa, while immediately after cracking it was 87 MPa (Table 4-2). The readings of the strain gauge at channel 23 for a longitudinal tension steel bar, and the readings of strain gauge at channel 12 for a longitudinal concrete strain gauge on the compression zone (directly above channel 23) were recorded as an example to illustrate the behaviour of this specimen at different stages of loading. At 140 kN (83% of ultimate load) all tension reinforcement steel yielded while the specimen was still resisting the load, this is a confirmation of flexural failure (under reinforcement design). After the yielding point, another change occurred to the curve's slope as an indication of starting the new stage of deformation (plastic deformation); the strain was increasing rapidly with a slight increasing of load.

Figures 4-19 and 4-20 show the response of concrete strain in the compression longitudinal direction, the maximum recorded concrete strain at channel 12 was -949E-6 at ultimate load. This is another indication of the ductile flexural failure. Figures 4-40, 4-49 and 4-46, 4-52 show concrete and steel strain gauge readings for each channel on the longitudinal direction during different stages of loading, respectively. The steel strain till yielding was increasing by the same average at all strain gauges as an indication of the tendency of a one-way dominant effect while the average of concrete strain increase

150

changed after cracking load. Furthermore, Figure 4-54 shows the strain reading for all steel and concrete channels together on the longitudinal direction.

Figures 4-11 to 4-13 show load versus tension steel strain gauge reading along the short direction (ε_y). As illustrated, the steel strain was increasing slightly with continuous loading; the maximum recorded strain at ultimate load was 1773E-6 with a stress of 355 MPa. Therefore, we can conclude that all short direction reinforcement bars did not yield.

The concrete strain gauge along the short direction recorded a small strain of 310E-6 only as a maximum strain recorded at ultimate load. Figures 4-17 and 4-18 show the concrete strain readings (ε_y) at different positions on the compression zone of the slab. Finally, Figures 4-37and 4-43 show the concrete and the steel strain reading, respectively, at all strain gauges in the short direction.

4.2.1 (c) Response of Linear Potentiometers (LP)

The flexural stiffness behaviour of a concrete slab (one-way slab) can be divided into three stages: an un-cracked stage, a cracked stage, and a plastic stage. Figure 4-162 shows a schematic idealized load-deflection curve of the flexural load-deflection behaviour of a reinforced concrete beam where these three stages are illustrated.

As the load increases, the tensile stress in the extreme tension fibers increases causing flexural cracks in the specimen corresponding to the stress in the tension fiber exceeding the tensile strength of concrete. Up to this load level, the specimen remains un-cracked. Beyond the cracking load, the flexural stiffness decreases. The slab continues to

151

resist the load with a higher increase in deflection per unit load than in the un-cracked stage. This is referred to as the cracked stage.

When the load reaches a level at which the reinforcing steel yields, the elastic (cracked) stage ends and the plastic stage begins. This stage continues until complete failure of the specimen as shown in Figures 4-1 and 4-2. The slope of each stage defines the flexural stiffness, K_u, K_{cr}, K_p for the un-cracked, cracked, and plastic stages, respectively.

The deflection was recorded to examine the behaviour of the tested specimen. For example, the deflection at 160 kN at channels 33, 38 and 35, shown in Figure 4-1 (on the central short direction line), was 19.3 mm, 19.75 mm and 12.2 mm, respectively. The deflection at channels 34 and 36 on the central longitudinal direction (the center line of the slab in the plane of moment) was 9.1 mm and 8 mm, respectively, under the same load level (Figures 4-2). This is attributed to the one-way behaviour of the slab as represented in Figures 4-3 and 4-6. Figure 4-9 illustrates the deflection readings on both directions longitudinal and transverse together for this specimen. All load versus deflection curves are taking shapes similar of Figures 2-3 and 4-158 as an indication of a flexural controlled design of the specimen.

4.2.1 (d) Support reactions

As indicated in chapter III, the slab was simply supported on four edges where four load cells were used to record the load reaction readings. Figure 4-21 shows the load readings on each support at different loading stages. Under self weight (0 kN applied force) we have a reading of a total of 8 kN for all load cells representing the weight of the

152

specimen. With increased load, readings on those load cells increased at about the same rate; however, at high level loading, the difference of load reading started indicating the redistribution of the load after cracking. Moreover, after unloading, all the load cell readings returned to the original reading before loading. Also, Figures 4-26 to 4-30 illustrate the percentage of the load on each load cell during different stages of loading. Lastly, Figure 4-24 illustrates the reaction distribution curve for each load cell. The resultant of reaction forces which is the sum of the load cell reading is found to be very close to the applied load and the self weight of the specimen.

4.2.2 Cracked specimen (CRAK0)

The general behaviour of this specimen was similar to the control specimen (CTRL0). This specimen was loaded up to 121 kN which represents 71% of the ultimate load recorded for the control specimen (CTRL0). At this stage of loading, none of any reinforcement bars yielded. The maximum recorded steel stress was 393 MPa (Figures 4-11 to 4-20). The maximum deflection was found to be 8.1 mm at the west center side of the specimen (ch. 35). Figures 4-1 and 4-2 show the deflection response of the specimen represented by the dark line which took approximately the profile of the control specimen CTRL0 with some differences that can be attributed to: the casting process, vibration works, positions of the instruments, and the heterogeneity of concrete material. The load of 121 kN was kept on the specimen for one day.

It can be seen from Figures 4-1 and 4-2 that this specimen which represented by the dark line had the same behaviour of the previous one (CTRL0). The first visible crack was observed at 89 kN on the east side parallel to the south face of column stub. The

second crack was observed on the east side also but at the north of the specimen; then the cracks propagated and expanded in the same manner as in CTRL0. The first tension crack on the bottom surface was observed at the north face of the column stub, while the second crack at the other side (south) was observed at the face of the column stub at 99 kN. The maximum crack width was found to be 0.7 mm.

Figures 4-160 shows CRAK0 specimen during loading, while Figure 4-167 shows the cracks concentrated around the column stub on the tension zone of the specimen after transferring, preparing for the rehabilitation process.

4.2.3 Rehabilitated specimen (REHB0)

The rehabilitated specimen is obviously different from the control specimen since CFRP sheets act as an external reinforcement added to the tension zone where the cracks were pre-exist. The failure was characterized by shearing of the concrete-CFRP interface associated with less warning compared to control specimen (CTRL0) however, the failure was still ductile.

The REHB0 specimen failed at an ultimate load of 358 kN. Under this load, the maximum concrete strain in the long direction compression zone was found to be -2471E-6, while all the steel reinforcement in the tension zone of the slab yielded at 260 kN. Moreover, the maximum recorded deflection was only 26 mm on the east central point (ch. 33).

4.2.3. (a) Crack propagation

Since the tension surface was covered with the CFRP sheets, it was difficult to observe the crack propagation on that zone. However, a small crushing of the concrete

154

was seen on the north-west side of the slab near the north-west support corner at channel 27, which was expanded as an inclined shear crack as shown in Figure 4-162. The failure was characterized by debonding of the concrete-CFRP interface at the north side of the specimen as shown in Figure 4-162. The width of the observed cracks on the sides of the specimen at failure was smaller compared to the control specimen (CTRL0), associated with less warning compared to the CTRL0 specimen; but still with some ductility. Figure 4-164 shows the crack on the compression zone after failure, releasing the load, and moving the specimen.

4.2.3 (b) Strain gauge reading analysis

The analysis will begin with a study of the strain measured in the longitudinal direction (ε_x) as illustrated in Figures 4-14 to 4-16 for longitudinal steel strain in tension zone and 4-19 to 4-20 for longitudinal direction of concrete strain in compression (top face) zone.

The longitudinal steel strain readings before the cracking load calculated for REHB0 (38 kN) increased gradually; however, after cracking, the readings started to increase rapidly from 111E-6 to 180E-6, but this jump was less than the one of CTRL0 and CRAK0 specimen which increased from 173E-6 to 434E-6 as shown in Table 4-2 for channel 23 and Figure 4-53 because of the presence of CFRP sheets on the tension zone which confined the widening of the cracks then helped in the tension stiffening of concrete. The steel stress before cracking was calculated to be only 22 MPa, while immediately after cracking it reached 36 MPa. The second stage started with a change in the curve's slope as shown in Figures 4-14 to 4-16. However, the slope increase was also

155

less than the one of the CTRL0 and CRAK0 as an indication that the CFRP sheets increased the slab strength and stiffness and resulted in an even distribution of the cracks. At 260 kN (72% of ultimate load) all tension reinforcement steel yielded, while the specimen was still resisting the load. After yielding, rapid change occurred to the curve's slope, indicating the start a new stage where the CFRP sheets start to carry the increasing of the load which caused a slight increase of concrete and steel strain.

Figures 4-19 and 4-20 show the response of concrete strain in the compression longitudinal direction (ε_x); the maximum recorded strain at channel 12 was -1650E-6 at ultimate load. This is another indication of the strengthening of the tension zone caused by the use CFRP sheets

Figures 4-41, 4-50 and 4-47, 4-53 show concrete and steel strain gauge readings for each channel along the longitudinal direction during different stages of loading, respectively. From Figure 4-50, the rapid increase in concrete strain after steel yielding is clear, especially for channel 10 where the shear crack starts at this location. Furthermore, Figure 4-55 shows the strain reading for all steel and concrete channels together on the longitudinal direction; the sudden increasing of concrete strain occurred after steel yielding at 260 kN.

Figures 4-11 to 4-13 show a load versus tension steel strain gauge reading on the short direction (ε_y). As illustrated, the steel strain was increasing slowly with continuing loading; the maximum recorded strain at ultimate load was 1265E-6. Therefore, all short direction reinforcement bars did not yield.

The concrete strain in the short direction was very small (86E-6) only as a maximum strain recorded at the ultimate load. Figures 4-17 and 4-18 show the concrete

156

strain readings (ε_y) at different positions on the compression zone of the slab. Finally, Figures 4-38 and 4-44 show the concrete and the steel strain readings, respectively, of all strain gauges in the short direction.

4.2.3 (c) Response of Linear Potentiometers (LP)

The stiffness behaviour of this specimen can also be divided into the three stages from the experimental data results. However, it shows from Figures 4-1 and 4-2 that the transfer from one stage to another is not easily recognized as for the CTRL0 specimen. This is an indication of reduction of the flexural dominant behaviour after adding the CFRP sheets to the tension zone as external tension reinforcement. Figure 4-171 is an expansion of Figure 4-1, allowing for a more detail depiction of the changes to be analyzed. As shown, the curve of the first stage (un-cracked stage) is a rough profile of the curve of the same stage for the control and cracked specimens, and all three curves end at approximately the same point of deflection. That is a sign that the CFRP sheets have a minor effect on the specimen global behaviour at this stage. Beyond the cracking load, the flexural stiffness decreases. However, the slab continues to resist the load with less increase of the deflection per unit load comparing with cracked stage for CTRL0 and CRAK0 specimens. This stage of the curve (cracked-stage) ended when tension steel yielded at 260 kN with 12.3 mm deflection, as an indication that this specimen had higher stiffness than CTRL0; the difference in stiffness between the two specimens increased with loading. The third stage starts after yielding of the tension reinforcement bars; a recognized change in stiffness is shown in the same figure. This stage continues until failure of the specimen at load level of 358 kN.

157

Deflection was also recorded to examine the behaviour of the tested specimen. For example, the deflection at 160 kN recorded by channels 33, 38 and 35, shown in Figure 4-1 (on the central short direction line), was 6.9 mm, 6.8 mm and 6.7 mm, respectively; the deflection recorded by channels 34 and 36, on the central longitudinal direction, (the center line of the slab in the plane of moment) was 3.3 mm and 3.4 mm, respectively, under the same load (Figures 4-2). This is attributed to the dominance of the one-way behaviour of REHB0 specimen as represented in Figures 4-4 and 4-7. Figure 4-10 illustrates the deflection readings on both directions together for this specimen.

4.2.3 (d) Support reactions

Figure 4-22 shows the load reading on each reaction at different stages of loading. As shown at 0 kN, we have a reading of 7.4 kN for the sum of load cells readings together which represents the weight of the specimen. With increased load, the reading of each load cell increased with about the same rate; however, for high loading and after cracking onset, the difference of load increase started as an indication of the redistribution of load after cracking. Channel 27 is a good example for the load redistribution where the cracks were observed; as shown in the Figure remarked earlier (4-22), the reading of this channel is less than others while the summation of all reactions was approximately the same as the applied load at failure which was 358 kN, added to the specimen weight. Moreover, after unloading, all the load cell readings returned to the original reading before loading. Furthermore, Figures 4-31 to 4-36 illustrate the percentage of the load on each load cell during different stages of loading. Those figures show that the percentage of load on channel 27 was less than others for the same reason

158

mentioned earlier. Figure 4-25 illustrates the reaction distribution on each load cell, which if we add them together with the specimen weight gives us the total applied load roughly with an acceptable difference. It is interesting to notice that the curve of channel 27 exhibited less increase in loading than the other channels, particularly before failure of the specimen when the loading approached the limit load.

4.3 Behaviour of Group II Specimens

The objective is to study the behaviour of the slab-column system subjected to a combination of shear-moment forces. As was explained in chapter three; in order to apply a shear and a moment forces, an eccentric load was applied at a distance of 250 mm from the center of the top column stub on the cantilever part (Figures 3-35). Two specimens were tested: CTRL35 is the control specimen loaded up to failure, and specimen CRAK25 was loaded up to 72% of the ultimate load recorded from the control specimen (CTRL25); REHB25 specimen is CRAK25 specimen repaired using external reinforcing with CFRP sheets on the tension cracked (bottom) surface followed by curing, and tested up to failure.

4.3.1 Control specimen (CTRL25)

A total load of 138 kN was applied progressively; Figure 4-166 shows the CTRL25 specimen during different loading stages. Under this load, the maximum concrete strain in the long direction compression zone was found to be -2487E-6, while all tension steel bars yielded. Moreover, the maximum recorded deflection was 23 mm on the east central point.

159

4.3.1 (a) Crack propagation

The first theoretical invisible crack was calculated to occurred at 30 kN load. Moreover, the steel strain in this stage was 431E-6 as shown in Table 4-2. These processes represent the first stage of cracking as was explained in chapter (2.2.4).

The first visible crack was observed at the jacking load of 66 kN. This crack of 0.5 mm width started on the east and west sides of the specimen from the tension (bottom face) zone and penetrated the slab thickness vertically toward the compression (top) zone in the position parallel to the face of the column stub. The second crack appeared in the same manner on both sides in position parallel to the loading axis. After increasing the applied load, more "live" tension cracks were observed away from the loading axis toward the north free edge on both east and west sides. While these cracks penetrated the slab thickness towards the loading axis, some of them spread to the tension surface in the short direction. With continuous increase of the load, more cracks expanded crossing the short direction on the slab's tension (bottom face) zone which is higher in width and length from east to west until crossing the side's crack; the width of this crack was measured at 96 kN to be 0.8 mm. There after, a secondary crack appeared in between the first and the second primary cracks on the tension surface.

The last stage of cracking started when no appearance of new cracks was observed, while, the width of the existing "live" cracks increased especially in the area beside the column stub at the loading side; at 100 kN all longitudinal reinforcement bars were yielded. The concrete strain readings were still far from yielding strain for concrete, an indication of flexural dominant failure.

160

The width of the cracks beside the column stub was recorded to be 1 mm at a load of 127 kN. The tension cracks on the east and west sides of the specimen continued to widen and penetrate into the slab thickness. Also, the tension cracks on the bottom surface continued to widen till the flexural ductile failure occurred at 138 kN; at this stage the width of the crack was 1.3 mm.

4.3.1 (b) Strain gauge reading analysis

The analysis will begin with a study of the strain measured in the longitudinal direction (ε_x) as illustrated in Figures 4-65 to 4-67 for the longitudinal steel strain in the tension zone and Figures 4-69 to 4-71 for longitudinal direction of concrete strain in the compression (top face) zone.

The longitudinal strain readings before the cracking load increased with a small rate; however, after cracking, that occurred on the tension zone, the strain readings increased rapidly (Figure 4-93), and the stiffness of the beam decreased. Cracks are noticeable from the change of the curve's slope in all the mentioned figures. As mentioned before, the steel stress before cracking was calculated to be only 24.8 MPa (124 E-6), while immediately after cracking it was 86 MPa (431E-6) as shown in Table 4-2. The readings of the strain gauge at channel 23 for a longitudinal tension steel bar, and the readings of strain gauge at channel 12 for a longitudinal concrete strain gauge on the compression zone were recorded as an example to illustrate the behaviour of this specimen at different stages of loading. At 100 kN (73% of ultimate load) all tension reinforcement steel yielded while the specimen was still resisting the load as an indication of a flexural failure (under reinforcement design). After the yielding point,

161

another change occurred to the curve's slope as an indication of the onset of a new stage of deformation (plastic deformation); where the strain was increasing with a slight increasing of load.

Figures 4-69 to 4-71 show the response of concrete strain in the compression longitudinal direction; the maximum recorded strain at channel 12 was -2250E-6 which is far from concrete crushing strain. This is another indication of ductile flexural failure.

Figures 4-88, 4-92, and 4-89, 4-93 show concrete and steel strain gauge readings for each channel on the longitudinal direction during different stages of loading, respectively. The steel strain before yielding was increasing by the same rate at all channels. Also, the rapid change in the strain after cracking load is very clear in these Figures. The tendency of a dominant one-way behaviour is obvious. It is also apparent that all the readings of concrete strain gauges were less than the crushing strain of concrete (Figure 4-88 and 4-93). Furthermore, Figures 4-90 and 4-94 show the strain readings for all steel and concrete channels together on the longitudinal direction; the flexural control design (ductile) is clear in these two figures where all steel reinforcement bars yielded, while concrete did not reaching crushing stage.

Figures 4-63, and 4-64 show load versus strain for the tension steel in the short direction (ε_y). As illustrated, the steel strain was increasing slightly with continuous loading; the maximum recorded strain at ultimate load was 1653E-6. It can be concluded that, all short direction reinforcement bars did not reach yielding point.

In the short direction, concrete exhibited a small strain of only 785E-6 recorded at the ultimate load. Figures 4-67 and 4-68 show the concrete strain readings (ε_y) at different positions on the compression zone of the slab. It is interesting to see that the

162

concrete strain starts to increase rapidly after yielding of the longitudinal steel at the first three channels. Finally, Figures 4-87 and 4-91 show the concrete and the steel strain readings, respectively, at all strain gauges in the short direction.

4.3.1 (c) Response of Linear Potentiometers (LP)

Figure 4-56 to 4-58 show that as the load increased, the tensile stress in the extreme tension fibers increased within a small rate until the cracking load (30 kN). Up to this load level, the specimen was un-cracked. Beyond the cracking load, the flexural stiffness decreased. The slab continued to resist the load with a higher increase in deflection per unit load than in the un-cracked stage. This is referred to as the cracked stage. When the load reaches a level imposing yielding of the reinforcing steel, the elastic (cracked) stage ends and the plastic stage begins. This stage continues up to failure of the specimen, (Figures 4-56 to 4-58). The slope of the load deflection curve of each stage defines the flexural stiffness, K_u, K_{cr}, K_p for the un-cracked, cracked, and plastic stages, respectively.

The deflection was recorded to examine the behaviour of the tested specimen. For example, the deflection at 130 kN at channels 33, 38 and 35, shown in Figure 4-56 (on the central short direction line), was 17.5 mm, 17.3 mm and 17.2 mm, respectively. The deflection at channels 34 and 36 positioned on the line parallel to the central short direction line (at a distance of 450 mm in the loading part-north) was 9.1 mm and 9.2 mm, respectively under the same load (Figures 4-57 and 4-58). This is another indication to the dominance of the one-way behaviour of the slab, as represented in Figures 4-59 to 4-62, we should remained here that the slab aspect ratio was 2. All load versus deflection

163

curves take the shape similar to Figures 2-3 and 4-158, indicating of a flexural dominant behaviour of the specimen.

4.3.1 (d) Support reactions

Figure 4-72 shows the load reading on each reaction at different stages of loading. As shown, the load is not equally distributed on all load cells because of the of the cantilever part in the north portion in this group; it logical that channels 26 and 27 in the north part of the specimen register more load than channels 25 and 28 on the south part; the variation of carrying load is obvious in Figures 4-76 to 4-80 for which the percentage of load on each load cell was illustrated. From the same Figure (4-72), it can be noted that at 0 kN we have a total reading of 9.4 kN for all load cells which represents the weight of the specimen. With the increased load, the readings on those load cells increased; however, with more loading, the difference of the readings increase started, especially on channels 26 and 27. Moreover, after unloading, all the load cell readings returned to the original reading before loading. Finally, Figure 4-74 illustrates the reaction distribution curve for each load cell, which added them together at the same applied load with the specimen weight, gives us around the same applied load value with an acceptable difference.

4.3.2 Cracked specimen (CRAK25)

This specimen was loaded up to 99 kN with an eccentricity of 250 mm from the center of the top column stub cantilever part, this load represents 72% of the ultimate load recorded from the control specimen (CTRL25).

164

The specimen had the same behaviour as the previous one (CTRL25). The first visible crack was observed at 66 kN on the east side with 0.3 mm width; then the cracks propagated and expanded in the same manner of CTRL25. The first tension crack on the bottom surface was observed at the face of the column stub and the second one at 74 kN parallel to the first one at the loading side (north portion). The first crack at the other side (south portion) was observed at the face of the column stub at 98 kN. At 99 kN the maximum crack width was recorded to be approximately 0.8 mm. In this stage, most of the longitudinal reinforcement bars yielded and the maximum deflection recorded was 7.3 mm at the east side center of the specimen. This load was kept on the specimen for one day. Figures 4-168 to 4-170 show CRAK25 specimen during different stages of loading, while figure 4-171 shows the cracks on the surface of the specimen after transferring, preparing for the rehabilitation process. Figures 4-56 to 4-71 illustrate the behaviour of this specimen represented by a dark line which took the same profile as for the control specimen CTRL25.

4.3.3 Rehabilitation specimen (REHB25)

As mentioned before, this specimen is CRAK25 specimen repaired using external reinforcing with CFRP sheets on the tension cracked (bottom) surface followed by curing. The load was applied in the same manner at an eccentricity of 250 mm from the center of the top cantilever part column stub.

The failure was characterized by a combination of concrete crushing in the east side of the compression zone and flexural shear after debonding of CFRP sheets at the east side of the specimen as shown in Figure 4-173 associated with less warning

165

compared to the control specimen (CTRL25). However, the failure remained ductile. The REHB25 specimen failed with an ultimate load of 255 kN. Under this load, the maximum concrete strain on the long direction compression zone was found to be -2446E-6, while all the steel reinforcement in the tension zone of the slab yielded at 200 kN. Moreover, the maximum recorded deflection was 16.1 mm only on the east central point (ch. 33).

4.3.3. (a) Crack propagation

The situation is the same as a previous rehabilitated specimen with CFRP (REHB0); deflection increase serves as a warning. It was observed that the warning regain is less than for the corresponding control specimen (CTRL25). While cracking in tension zone of the slab was difficult to be observed since the tension surface was covered with the CFRP sheets; furthermore the cracking in compression zone was obvious before failure. It was observed that debonding of CFRP sheets on the east side of the specimen was followed by concrete crushing on the top zone at the east-north side of the north face of the top column stub. Figure 4-173, (represented by the bold black line). On the other hand, after the test termination and by removing the debonded CFRP sheet from the east side, an inclined crack was observed as shown in the same figure. The width of the observed side's cracks of the specimen after failure was smaller than the CTRL25 cracks, associated with less warning; the failure, though, was remained ductile.

4.3.3 (b) Strain gauge reading analysis

The analysis will begin with a study of the strain measured in the longitudinal direction (ε_x) as illustrated in Figures 4-65 to 4-67 for longitudinal steel strain in tension

166

zone and 4-69 to 4-71 for longitudinal direction of concrete strain in compression (top face) zone.

The longitudinal steel strain readings before the calculated cracking load for CTRL25 (30 kN) increased gradually; however, after cracking, these readings started to increase rapidly from 74E-6 to 105E-6, but on average with lower rate than for specimens CTRL25 and CRAK25 which increased from 124E-6 to 431E-6 and from 94E-6 to 237E-6, respectively. Table 4-2 shows the strain readings for channel 23 and Figure 4-93 because of the presence of CFRP sheets on the tension zone which confined the widening of the cracks and then decreased the reduction of the tension zone concrete resistance (effective cross-section). The steel stress before cracking was calculated to be only 14.8 MPa, while immediately after cracking it was 17.3 MPa. The second stage started with a change in the load displacement curve's slope as shown in Figures 4-65 to 4-67. However, the increase of the slope was also less than for the CTRL25 and CRAK25 specimens as an indication that the CFRP sheets increased the slab strength and stiffness and resulted in an even distribution of the cracks. At 200 kN (78% of ultimate load) all tension reinforcement steel yielded, while the specimen was still resisting the load. After the yielding point, rapid change occurred to the curve's slope as an indication of starting the new stage where the CFRP sheets start to carry the load increase which caused a lower increase in strain with load increase, (Figure 3-66, ch.24 and ch. 29).

Figures 4-69 to 4-71 show the response of the concrete strain in the compression longitudinal direction (ε_x); the maximum recorded strain at channel 12 was -1439E-6. This is another indication of the strengthening effect in the tension zone due to the CFRP use. The curves of the load-strain relationship in all mentioned figures (4-56 to 4-58) also

167

show the increasing of the specimen's stiffness. Figures 4-88, 4-92 and 4-89, 4-93 show concrete and steel strain gauge readings for each channel on the longitudinal direction during different stages of loading respectively. Figure 4-92 shows a rapid increase in concrete strain after steel yielding, especially for channels 10 and 11 where the concrete crushing onset can be observed. Furthermore, Figure 4-95 shows the strain reading for all steel and concrete channels along the longitudinal direction; the sudden increase of concrete strain occurred after steel yielding at 200 kN.

Figures 4-63 and 4-64 show a load versus tension steel strain gauge reading on the short direction (ε_y). As illustrated, the steel strain increased slightly with continuous loading; the maximum recorded strain at ultimate load was 1016E-6 on the center-line of the slab. It can be concluded that all reinforcement bars in the short direction did not yielded.

The short direction concrete exhibited a small strain of 317E-6 only as a maximum strain recorded at ultimate load. Figures 4-67 and 4-68 show the concrete strain readings (ε_y) at different positions on the compression zone of the slab. Finally, Figures 4-87 and 4-88 show the concrete and the steel strain readings, respectively, at all strain gauges in the short direction.

4.3.3 (c) Response of Linear Potentiometers (LP)

The behaviour of this specimen can also be divided into the three described stages from the data of the experimental result; however, Figures 4-56 and 4-57 show that transferring from one stage to another is not as easily recognized as for the CTRL25 specimen. The fact that there is no clear transition between the different stages can be

168

attributed to the additional effect of the CFRP sheets to the tension zone as an external tension reinforcement. Figure 4-180 is an expanded representation of Figure 4-56 (channel 38), allowing for a more detailed depiction of the changes to be analyzed. As shown, the curve of the first stage (un-cracked stage) is a rough profile of the curve of the same stage for the control and cracked specimens, and all three curves end at approximately the same point of deflection. That is a sign that the CFRP sheets have a minor effect on the specimen at this stage. Beyond the cracking load, the flexural stiffness decreased. However, the slab continued to resist the load with less increasing in deflection per unit load compared to the cracked stage for the CTRL25 and CRAK25 specimens. This stage of the curve (cracked-stage) ended when tension steel yielded at 200 kN with 7.9 mm of deflection. These results are an indication that this specimen had higher stiffness than CTRL25 specimen. However, the difference in stiffness between the two specimens increased with loading. The third stage starts after tension steel yielding; change in stiffness is easily recognized in the same figure. This stage continues until complete failure of the specimen at 255 kN.

Deflection was also recorded to examine the behaviour of the tested specimen. For example, the deflection at 140 kN at channels 33, 38 and 35, shown in figure 4-62 (on the central short direction line), was 5.9 mm, 4.9 mm and 6.5 mm respectively; the deflection at channels 34 and 36 on the side short direction of loading portion (on the line parallel to the short center line by 350 mm) was 4.1 mm and 3.6 mm, respectively, under the same load (Figures 4-58). This is attributed to the dominance of the one-way behaviour of REHB25 specimen as represented in figures 4-59 to 4-62.

169

Figure 4-73 shows the load readings on each reaction load cells at different stages of loading. As shown at 0 kN, we have a reading of 10.5 kN for all load cells together which represents the specimen's own weight. With increased applied load, the load on each load cell increased with about the same rate; however, for high loading and after cracking onset, the difference of load increasing for each support started and it indicates redistribution of load after cracking. The sum of all reactions added to the self weight is in equilibrium with the applied load. Moreover, after unloading, all the load cell readings returned approximately to the original reading before loading. Figures 4-81 to 4-86 illustrate the percentage of the load on each load cell during different stages of loading. Finally, Figure 4-75 illustrates the reaction distribution on each load cell. It is interesting to see that the load is not equally distributed on all load cells because of the existence of the cantilever part in the north portion in this group; it is therefore natural that channels 26 and 27 in the north part of the specimen registered more load than channels 25 and 28 on the south part; the variation of carrying load is obvious also in Figures 4-82 to 4-86 where the percentage of load on each load cell was illustrated.

4.4 Behaviour of Group III Specimens

In order to study the feasibility of increasing the eccentricity, the single increasing eccentric load was applied at 350 mm from the center of the top column stub on the cantilever part as illustrated in Figure 3-35. Two specimens were tested: CTRL35 is the control specimen loaded up to failure, and specimen CRAK35 was loaded up to 70% of the ultimate load recorded from the control specimen (CTRL35); REHB35 specimen is

170

CRAK35 specimen repaired using external reinforcing with CFRP sheets on the tension cracked (bottom) surface followed by curing, and tested up to failure.

4.4.1 Control specimen (CTRL35)

Figure 4-175 and 4-176 show the CTRL35 specimen during different stages of loading. A total load of 133 kN was applied progressively. Under this load, the maximum concrete strain in the long direction compression zone reached the value of -2977E-6, while all tension steel bars yielded. Moreover, the maximum recorded deflection was 21 mm on the west central point.

4.4.1 (a) Crack propagation

The first theoretical invisible crack was calculated to be at 27 kN load. Moreover, the steel strain in this stage was 639E-6 as shown in Table 4-2. These processes represent the first stage of cracking as was explained in chapter (2.2.4).

The first visible cracks were observed at the load of 47 kN. These cracks started on the east and west sides of the specimen from the tension (bottom face) zone and penetrated the slab thickness vertically toward the compression (top face) zone as shown in Figure 4-175. Those cracks started from the position parallel to the north face of the column stub increasing towards the north free edge (loading portion). Furthermore, some of these cracks ran underneath the tension surface, the first one was beside the column stub as shown in Figure 4-176. Additional cracks appeared at 80 kN in the same manner on both sides of the first group of cracks (north and south); moreover, at this load some of the first cracks expanded on the tension surface and penetrated more towards the

171

compression zone as shown in Figures 4-181 and 4-182. At a load level of 100 kN the existing cracks propagated upwards and on the tension surface; in addition, a new crack was observed at the intersection between the tension surface and the lower-north face of the column stub; all tension steel yielded. Following these, only two more new small cracks were observed at 120 kN far in the south portion of the slab, while all existing cracks penetrated the slab thickness with continued loading (Figure 4-183). The deflection increase was clear in this stage of loading. In the later loading stage, the only change observed was that the widening of the cracks, especially beside the column stub in the loading portion as shown in Figure 4-184, were followed by the flexural failure of the specimen at 133 kN.

4.4.1 (b) Strain gauge reading analysis

The analysis will begin with a study of the strain measured in the longitudinal direction (ε_x) as illustrated in Figures 4-106 to 4-108 for the longitudinal steel strain in the tension zone, Figure 4-109 for the longitudinal steel strain in the compression zone, and Figures 4-112 to 4-114 for the longitudinal direction of concrete strain in the compression (top face) zone.

The longitudinal strain readings before the cracking load (27 kN) increased within a very small rate; however, after cracking took place in the tension zone, the strain readings increased rapidly (Figure 4-138), and the stiffness of the slab decreased; thus, the slope of the curve as shown in Figures 4-106 to 4-108 decreased as well. The appearance of the crack is noticeable from the change of the curve's slope in the same figures remarked earlier. The steel strain before cracking was 232E-6, while immediately

172

after cracking it jumped to 639E-6 corresponding to a stress of 128 MPa as shown in Table 4-2, where the readings of the strain gauge at channel 23 for a longitudinal tension steel bar, at channel 39 for a longitudinal compression steel bar, and the readings of strain gauge at channel 12 for a longitudinal concrete strain gauge on the compression zone were recorded as an example to illustrate the behaviour of this specimen at different stages of loading. For further illustration, Figure 4-147 demonstrates the load-strain relationship between those channels. As shown after cracking, the slope of the curve for channel 23 (tension reinforcement) changes rapidly because of a decrease in the effective concrete cross-section, the tension reinforcement started to carry most of the load; at the same time, the slope of channel 12 curve changed also, but slowly as an indication that the first crack did not have a noticeable effect on the concrete in the compression zone. The steel behaviour in the compression zone (channel 39), did not change indicating that the first crack did not have that effect on the compression reinforcement. It should be seen that the slope of channel 23 in Figure 4-147 was roughly constant until yielding which indicates that the new stage of deformation starts (plastic deformation); the strain increased rapidly with a slight increasing of the load. Meanwhile, no strain is recognized on channel 39 until all tension zone reinforcement bars yielded at 100 kN, as the specimen acted as one composite unit; then the slope of this channel changes rapidly as an indication that the compression reinforcement starts to carry the load at approximately 103 kN. The curve's slope in channel 12 started to change, as an indicating the start of a new loading stage (plastic) started on the concrete compression zone at approximately 120 kN. The specimen was continuing to resist this load until the flexural failure at 133 kN.

173

Figures 4-134, 4-136 and 4-137, 4-138 show concrete and steel strain gauge readings for each channel on the longitudinal direction during different stages of loading, respectively. The steel strain increased by the same rate for all channels. The rapid change in the strain after cracking load is clear in these Figures. The dominance of the one-way slab behaviour is obvious. It is apparent that all the readings of concrete strain gauges were less than the crushing strain of concrete (Figures 4-134 and 4-136). Furthermore, Figure 4-139 shows the strain readings for all steel and concrete channels together on the longitudinal direction; the flexural controlled design (ductile) is clear in this figure where all steel reinforcement bars yielded, while concrete did not reach crushing stage.

Figures 4-103 to 4-105 show the load versus the readings of tension steel strain gauges in the short direction (ε_y). As illustrated, the steel strain was increasing slightly with continuous loading; the maximum recorded strain at the ultimate load was 1207E-6. Therefore, we can conclude that all short direction reinforcement bars did not reach yielding point.

The concrete strain gauges in the short direction recorded a small strain; the maximum registered value was 419E-6 as a maximum strain recorded at the ultimate load. Figures 4-110 and 4-111 show the concrete strain readings (ε_y) at different positions on the compression zone of the slab. Lastly, Figures 4-133 show all short direction concrete strain gauge readings together.

174

<u>4.4.1 (c) Response of Linear Potentiometers (LP)</u>

Figures 4-96 to 4-98 show that as the load increase, the tensile stress in the extreme tension fiber increase at a small rate until the cracking load (27 kN). Up to this load level, the specimen is assumed un-cracked. Beyond the cracking load, the flexural stiffness decreases. The slab continues to resist the load with a higher increase in deflection per unit load than in the un-cracked stage. This is referred to as the cracked stage.

When the reinforcing steel yields, the elastic (cracked) stage ends and the plastic stage begins. This stage continues until failure of the specimen as shown in figures 4-96 to 4-98. The slope of each stage defines the flexural stiffness, K_u, K_{cr}, K_p for the un-cracked, cracked, and plastic stages respectively.

The deflection was recorded to examine the behaviour of the tested specimen. For example, the deflection at 133 kN at channels 33, 38 and 35, shown in Figures 4-96 and 4-99 (on the central short direction line), was 20 mm, 21 mm and 14 mm, respectively. The deflection at channels 34 and 36 positioned on the line parallel to the central short direction line (at a distance of 450 mm in the loading part-north) was 15 mm and 13 mm, respectively, under the same load level (133 kN) (Figures 4-97 and 4-98). This is another attribution to the dominance of the one-way behaviour of the slab as illustrated in Figures 4-99 to 4-102. All load versus deflection curves take the shape similar to Figures 2-3 and 4-162 as an indication of a flexural control design of the specimen.

175

<u>4.4.1 (d) Support reactions</u>

Figure 4-117 shows the load readings on each reaction at different stages of loading. As shown, the load is not equally distributed on all load cells because of the existence of the cantilever part in the north portion in this group of specimen; it is reasonable that channels 26 and 27 in the north part of the specimen register more load than channels 25 and 28 on the south part. The variation in carrying load is obvious in Figures 4-122 to 4-127 for which the percentage of load on each load cell was illustrated. From the same Figure (4-117) it can be noted that under self weight (0 kN applied force), a total reading of 10.8 kN for all load cells representing the weight of the specimen. With the increased load, load cells readings increased also; however, with more loading, channels 26 and 27 (in the north side) recorded higher loads than channels 25 and 28. Moreover, after unloading, all the load cell readings returned to the original reading before loading for each portion. Finally, Figure 4-120 illustrates the reaction distribution curve for each load cell. If the reactions are summed up with the specimen weight, the result is a load close to the applied load with an acceptable difference.

<u>4.4.2 Cracked specimen (CRAK35)</u>

This specimen was loaded up to 90 kN at 350 mm eccentricity from the center of the top column stub, this load represents 70% of the ultimate load recorded from the control specimen (CTRL35).

The first visible crack was observed at 59 kN on both sides of the specimen parallel to the north edge of the column stub; then the cracks expanded toward the north free edge. The first tension crack on the bottom surface was observed beside and parallel

176

to the face of the column stub and the second one was observed at the face of the column stub. At 90 kN, the maximum deflection recorded was 6.3 mm at the east side center of the specimen. Figures 4-180 show specimen CRAK35 during different loading stages, while Figure 4-181 shows the cracks on the surface of the specimen after transfer, and preparation for the rehabilitation process. Figures 4-103 to 4-114 illustrate the behaviour of this specimen represented by a dark black line.

4.4.3 Rehabilitation specimen (REHB35)

As mentioned before, this specimen represents the specimen CRAK35 after application of external reinforcement with CFRP sheets on the tension cracked (bottom) surface followed by curing. The load was applied in the same manner with an eccentricity of 350 mm from the center of the column stub.

The failure was characterized by a flexural shear after debonding of CFRP sheets on the tension zone near the north face of column stub of the specimen followed by concrete crushing on the compression zone as shown in Figures 4-184 to 4-186; the failure, although still ductile, was associated with less warning compared to the control specimen (CTRL35).

The REHB35 specimen failed at an ultimate load of 224 kN. Under this load, the maximum concrete strain on the long direction compression zone was -1725E-6, while most of the steel reinforcement in the tension zone of the slab yielded at 190 kN. Moreover, the maximum recorded deflection was 16.9 mm only on the east central point (channel 33).

177

4.4.3. (a) Crack propagation

The situation is the same as previous rehabilitated specimens with CFRP (REHB0 and REHB25), where deflection serves as a warning indicator, but less than for the control specimen (CTRL35). However, cracking in the tension zone of the slab was difficult to observe since the tension surface was covered with CFRP sheets. Concrete crushing on the top zone at the north face of the column stub was seen in addition to debonding of CFRP sheets on the top east side of the specimen as shown in Figures 4-184 to 4-186. After releasing the load and removing the debonded CFRP sheet from the east side, an inclined crack was observed as shown in Figure 4-187. The width of the observed side's cracks of the specimen after failure was smaller than the CTRL35 cracks. Moreover, the debonding of CFRP sheets from the tension surface near the column stub was recognized, in order to get more information, part of the CFRP sheet was removed as shown in Figure 4-188. At this position, the tension reinforcement yielded, and compression reinforcement carried part of the load with 837E-6, while the strain reading of the CFRP sheet was recorded to be 2074E-6. It was interesting to find that new cracks appeared on this part of the surface, as those cracks were wider than the cracks observed in the cracked specimen CRAK35 (pre-rehabilitated specimen) as shown in Figure 4-188. Furthermore, to classify the new cracks, the weak concrete was removed from this area as shown in Figure 4-189. It was interesting to see a large crack with a roughly 45 degree inclination which was expanded to the north face of the column stub along the short direction on the compression zone, exactly where the crack in the compression zone was observed as an indication of flexural shear failure, especially since all compression strain gauge readings were far from yielding. This phenomenon is not easily explained without additional data which is necessary to better understand the deterioration mechanism more

178

precisely. However, with the limited available data the following explanation is given: From Figure 4-188 the main cracks that existed before the rehabilitation process affected the bond properties between the CFRP sheets and tension concrete surface; then diagonal cracks induced by the bond of CFRP sheets near the main cracks affected the stiffness of the CFRP sheet; peak average bond strain occurred as shown in Figure 4-115 after debonding of the CFRP sheet which later on affected the stiffness of tension steel reinforcement in the longitudinal direction as shown in Figures 4-144 and 4-148.

4.4.3 (b) Strain gauge reading analysis

The analysis will begin with a study of the strain measured in the longitudinal direction (ε_x) as illustrated in Figures 4-106 to 4-109 for longitudinal steel strain in the tension zone and Figures 4-112 to 4-114 for longitudinal direction of concrete strain in the compression (top face) zone.

The longitudinal steel strain readings after the cracking load, calculated for CTRL35 (27 kN) increased rapidly, although on average less than for the CRAK35 specimen after cracking. The strain reading increased from 37E-6 to 102E-6 as shown in Table 4-2 for channel 23 and Figure 4-138 because of the presence of CFRP sheets on the tension zone which confined the widening of the cracks and then decreased of the tension zone concrete resistance (effective cross-section). The steel stress before cracking was calculated to be only 7.4 MPa, while immediately after cracking it was 20.4 MPa. The second loading stage started with a change in the curve's slope as shown in Figures 4-106 to 4-108. However, the increase of the slope was also less than for the CTRL35 and CRAK35 specimens as an indication that the CFRP sheets increased the slab strength and

179

stiffness and resulted in an even distribution of the cracks. At 150 kN, the reading of the strain gauges at channel 40 (the compression zone reinforcement) started to increase as an indication that the steel at that zone started to carry the load, while at channel 39 of the same zone started at 160 kN as shown in Figure 4-109. At 190 kN (84% of ultimate load) most of the tension reinforcement steel yielded, while the specimen was still resisting the load. After the yielding point, rapid change occurred to the curve's slope. A high stiffness is an indication of beginning the new stage where the CFRP sheets start to carry the increasing load which caused a slight increase in strain. Figure 4-115 shows the strain gauge readings of the CFRP sheet (Channel 42) on the longitudinal direction. It is obvious from the curve that there is a rapid increase in the strain at a cracking load of 27 kN; tension steel yielded for the control specimen CTRL35 at 100 kN, while for the REHB35 yielding occurred at 190 kN. This is an indication that the CFRP sheets responsive to any change occurring at the tension zone which gives a reason for the stiffness increase of rehabilitated specimens.

Figures 4-112 and 4-114 show the response of concrete strain in the compression longitudinal direction (ε_x); the maximum recorded strain at channel 12 was -815E-6. This is another indication of the effect of the strengthening using CFRP sheets. The curves of the load-strain relationship in all mentioned figures also show the increasing of the stiffness of this specimen. Figures 4-134, 4-136 and Figures 4-137, 4-138 show concrete and steel strain gauge readings for each channel on the longitudinal direction during different stages of loading, respectively. From Figure 4-136 the rapid increase in concrete strain after steel yielding was clear, especially at edges channels where the crushing of concrete starts; it is obvious also in Figure 4-134 that the channels on the east and west

180

edge of the specimen exhibited more strain than the central channels after yielding of the tension steel. Furthermore, Figure 4-140 shows the strain reading for all steel and concrete channels together on the longitudinal direction.

Figures 4-103 and 4-105 show a load versus tension steel strain gauge reading on the short direction (ε_y). The maximum recorded strain at ultimate load was 971E-6 at the face of the column stub. All short direction reinforcement bars did not yield.

Figure 4-144 shows concrete, steel and CFRP strain readings in the long direction for the same cross-section; from this figure it is obvious that the CFRP sheet did not sustain any strain until the cracking load even though it affected the tension reinforcement. At 140 kN the stiffness of the CFRP sheet changed while the tension reinforcement still hading roughly the same stiffness. Finally, Figure 4-146 shows the long direction strain response for concrete, steel in tension and compression zone, and CFRP of the same cross-section during different stage of loading; at this section, after cracking load there is a strain on the tension steel and CFRP sheets only, while at 151 kN (51% of the ultimate load), there was no responsive sign of strain on the compression steel whose reading was only -78 microstrain; the average of strain increasing on the CFRP sheets was more than the tension steel where the strain changed from 115, 96 to 1500, 1242 microstrain for CFRP sheets and steel, respectively, and the strain on the concrete compression zone increased also from -78E-6 to -553E-6. At 190 kN (84% ultimate load) when most of the tension steel yielded, all channels exhibited the same average of strain increasing while the CFRP sheet verified more strain. Finally, at the ultimate load 224 kN, tension and compression steel show an increase in strain (1908 and 638 microstrain), while there was no sign of strain increase of concrete in the

181

compression zone (-643E-6), and a slight increase was shown on CFRP sheet strain (2073E-6). These experiences give us an explanation about the effect of CFRP sheets in increasing the strength and stiffness of the specimen when it was carrying most of the load, and then was exposed to more strain than the specimen's other components (concrete and steel).

Figure 4-146 shows the strain in concrete in the long direction, steel in tension and compression zone, and CFRP at the same longitudinal cross-section along the west face of column-slab connection during different stages of loading; at this section, after cracking load there is a strain on the tension steel and CFRP sheets only, while at 151 kN (51% of the ultimate load), there was very little of strain in the compression steel; the reading was only -78E-6, and the average of strain increase in the CFRP sheets was more than tension steel where the strain changed from 115E-6, 96E-6 to 1500E-6, 1242E-6 for CFRP sheets and steel, respectively, and the strain on the concrete compression zone was increased also from -78E-6 to -553E-6. At load level of 190 kN, 84% of the ultimate load, when most of the tension steel yielded, all channels exhibited the same rate of strain increase while the CFRP sheet sustained more strain. Finally, at the ultimate load 224 kN, both tension and compression steel show significant of increase in strain (1908E-6 and 638E-6), while there was no sign of strain increase on concrete in the compression zone (-643E-6), and a slight increase of strain was detected in the CFRP sheet (2073E-6). These findings illustrate the effect of CFRP sheets in increasing the strength and stiffness of the specimen when it was carrying most of the load, and as a result, was exposed to more strain.

182

Concrete in the short direction exhibited a small strain of only 63E-6 at the ultimate load. Figures 4-110 and 4-111 show the concrete strain readings (ε_y) at different positions on the compression zone of the slab. Figure 4-133 and 4-135 show the concrete strain readings (ε_y) at all the concrete strain gauges in the short direction.

Finally, Figure 4-148 illustrates the concrete, steel and CFRP strain readings in the long direction for the same longitudinal cross-section along the east face of column-slab connection; from this Figure it is obvious that the CFRP sheet and the tension reinforcement exhibited the same strain up to the cracking load, while there is no noticeable sign of strain on the compression steel and concrete. After the cracking load, the rate strain started to increase more on the tension steel and the CFRP sheet as an indication of elastic modulus decreasing from E_u to E_{cr}; CFRP exhibited more strain for the same rate up to a load level of 210 kN. At 140 kN the strain of the CFRP sheet increased rapidly followed by an increase in tension steel reinforcement stiffness at 150 kN, while the compression reinforcement started to carry significant stress. When most of the tension steel yielded at 190 kN, the slope of the compression reinforcement curve increased rapidly as an indication that the compression steel starts to carry more load after yielding of tension steel. It is interesting to note from this curve that at 210 kN, the CFRP sheet stopped carrying additional stress, while another rapid increase in strain recorded on tension and compression reinforcement could be an indication of debonding of the CFRP sheet at this position of tension surface where the new large crack was observed.

An attempt to explain the complex failure mode is given below:

With increasing the load, debonding was observed at existing flexural cracks near the region of maximum moment. A critical diagonal (flexural-shear) cracks opened and propagated through the slab thickness towards the compression zone. Accordingly, the condition of the change in the mode of failure depends largely on bond conditions, surface preparation, the percentage of CFRP being used, availability of anchorage, and the presence of shear reinforcement in the existing system specially that the concrete in compression zone did not yield.

4.4.3 (c) Response Linear Potentiometers (LP)

Experimental results show that the stiffness behaviour of this specimen can be divided into the three stages. However, Figures 4-96 and 4-98 show that transfer from one stage to another is not easily recognized as of the specimen CTRL35. This is an indication that the flexural behaviour is no longer dominant after adding the CFRP sheets to the tension zone. Figure 4-180 is an expanded representation of Figure 4-96 (channel 38), allowing for a more detailed depiction of the changes to be analyzed. As shown, the curve of the first stage (un-cracked stage) is a rough profile of the curve of the same stage for the control specimens, and both curves end at approximately the same point of deflection. This finding suggests that the CFRP sheets have a minor effect on the specimen at this stage. Beyond the cracking load, the flexural stiffness decreased. However, the slab continues to resist the load with less increase in deflection per unit load compared to the cracked stage for the CTRL35 specimen. This loading stage (cracked-stage) ended when tension steel yielded at 190 kN with 8 mm deflection. It is also observed that the rehabilitated specimen has higher stiffness than CTRL35; the

184

difference in this stiffness between the two specimens increased with the loading. The third loading stage starts after yielding of tension steel; a recognized change in the stiffness is shown in the same figure. This stage continues until failure of the specimen at 224 kN.

Deflection was also recorded to examine the behaviour of the tested specimen. For example, the deflection at 224 kN recorded by channels 33, 38 and 35, shown in Figure 4-99 (on the central short direction line), was 16.9 mm, 13.2 mm and 16.4 mm, respectively. Under the same load, the deflection recorded by channels 34 and 36 on the side short direction of loading portion (on the line parallel to the short center line by 350 mm) was 13 mm and 10.4 mm, respectively, (Figures 4-102). This is attributed illustrates the dominant of the one-way behaviour of specimen REHB35, (Figures 4-99 to 4-102).

4.4.3 (d) Support reactions

Figure 4-119 shows the load readings on each reaction load cells at different loading stages. As shown at 0 kN, the sum of all readings is 10.2 kN which represents the weight of the specimen. With the increased load, the recorded load on each load cell increased with about the same rate; however, for advanced loading stage, the difference of load increase for each support started to be significant, as an indication of the redistribution of the load after cracking. At failure, the sum of all reactions added to the self weight was approximately the same as the applied load which was 224 kN. Moreover, after unloading, all the load cell readings returned roughly to the original reading before loading. Figures 4-128 to 4-132 illustrate the percentage of the load on each load cell during different loading stages. Finally, Figure 4-121 illustrates the

185

reaction distribution on each load cell, which if added together with the specimen self weight results into a load comparable to the total applied load, with an acceptable difference. It is interesting to see that the load is not equally distributed on all load cells because of the eccentric load applied on the cantilever part in the north portion in this group. Therefore, logical to have readings of channels 26 and 27 in the north part of the specimen higher than those of channels 25 and 28 on the south part. The variation of the load distribution is obvious also in Figures 4-130 to 4-131 where the percentage of load on each load cell is illustrated.

4.5 Summary of the Result

As expected, all control and cracked specimens exhibited a pure flexural mode failure. Both the control and cracked specimens failure started by yielding of the tensile steel reinforcement. The rehabilitated specimens exhibited different behaviour than the control specimens, because of CFRP sheets. The results of the rehabilitation technique did not only succeed in restoring the strength of the cracked reinforced concrete slab, but also upgraded their capacities compared to the control specimens.

4.5.1 Cracking load

From the load-deflection Figures in this chapter, the profile of the curves in most Figures did not change before the cracking load. We can conclude that the presence of CFRP sheets did not have a significant effect on the behaviour of the specimens before the onset cracking.

4.5.2 Yielding load

Yielding load is associated with tension steel strain; Table 4-2 illustrates a sample of the test results during different loading stages for steel in the tension zone strain and concrete in the compression zone strain. Since the CFRP sheets were installed on the outside surface of the slab that sustains more strain than the inner tension steel reinforcement. The yielding load was affected by using CFRP sheets. Table 4-4 illustrates the measured yield loads before and after rehabilitation, a percentage increase of 86%, 100%, and 90% between the control and rehabilitated specimens was obtained for groups I, II, and III respectively.

4.5.3 Ultimate load

Table 4-4 summarizes the ultimate load carrying capacity for each group. The rehabilitation technique upgraded the capacity of the system by 112%, 85%, and 68% for groups I, II, and III, respectively. From this result it should be noted that the unbalanced moment affected the efficiency of the rehabilitation technique, as the moment increased, the percentage of the ultimate load carrying capacity decreased. Nevertheless, rehabilitation technique was effective for all groups.

4.5.4 Flexural stiffness

As explained earlier, the flexural stiffness behaviour can be divided into three stages (the un-cracked, cracked, and plastic stages). Within the un-cracked stage the flexural stiffness was not affected by the presence of CFRP sheets for all groups. After the cracking load, the flexural stiffness did not change significantly for all rehabilitated

187

specimens until their yielding load is reached. Then the stiffness started to degrade in the plastic stage; however, this decrease was smaller compared to the control specimens. The three stages for the rehabilitated specimen were not clearly separated as for the control specimens. Table 4-3 illustrates the decrease in deflection at yielding and ultimate load for the control specimen of each group at that position. As shown, the difference of the percentage of deflection decrease was more significant for high load levels.

4.5.5 Ductility

Ductility, the ability of a structure to undergo large deformations before failure, is an important requirement in the design of any structural element. Ductile structures can exhibit large deformation before failure and thus provide visual indicators that give the opportunity for remedial actions prior to complete collapse.

Ductility index is defined as the ratio of the deflection at the maximum load to the deflection at yield which is presented in Table 4-4 for all groups. As expected, control specimens exhibited the most ductile behaviour. Since many retrofit applications result in an extra reinforcement, the behaviour of concrete in compression is critical to the response of the member. Ductility is often the only characteristic that is reduced after rehabilitation. The Ductility Index changed from 3.1 to 2.1 (32% reduction) for group I after rehabilitation; this change is from 2.6 to 1.7 (34% reduction) for group II, and from 2.6 to 1.5 (42% reduction) for group III. The increase of the eccentricity resulted in a reduction of the ductility index. The change in ductility Index depends mainly on the quantity of CFRP sheets used in tension zone.

188

4.5.6 Failure mode

Although the failure mode was ductile for both the control and rehabilitated specimens, the later exhibited relatively less ductility. Debonding of the CFRP sheets from the tension concrete surface near the face of the column stub occurred for the rehabilitated specimens. The debonding was accompanied by distinctly audible sounds. The failure mode of the rehabilitated specimen was a flexural-shear failure followed by crushing of concrete in the compression zone.

4.5.7 Plastic deformation

From load-deflection relationships, it is observed that the plastic deformation for all rehabilitated specimens is less than the control specimens, as an indication that although the ultimate load was increased using CFRP sheets, the elastic range increased too, to be larger than the corresponding the elastic range for the control specimens.

4.6 General Behaviour of the Three Groups

As additional information, this article summarizes the behaviour of the three groups together, (Figures 4-150 to 4-158).

Concerning the control and rehabilitated specimens for all three groups, the deflection of the first group which experienced shear only (group I) is relatively different than the others which have a combination of shear and unbalanced moment.

The ductility index for the first group is more than the last two groups which are relatively closer, as shown in figurer 4-162. Finally, results show that the ultimate load

189

capacity of the rehabilitated specimens increased by 112, 85, and 68% corresponding to zero, 250, and 350 mm eccentricity respectively.

As conclusion, the changes in the behaviour of specimens after exhibiting unbalanced moment is more comparing to the changes in the behaviour of specimens exhibited increasing of the existence unbalanced moment (group II and group III).

For fire resistance of FRP strengthened concrete members, The protection systems of a two-component fire protection system, which is a combination of cementations plaster spray and an intumescent coating with low thermal conductivity, was investigated by Kodur et al 2004 and can be applied conveniently on the surface of CFRP sheets described in this research. According to their study, a 37 mm thickness was capable of achieving fire endurance ratings of 5 hours or more under full service loads. Moreover, Kaiser (1989) studied the temperature effect over 100 freeze-thaw cycles from +20 °C to -25 °C on concrete beams strengthened with CFRP and found no negative influence on the flexural capacity. In addition, Creep experiments were performed to determine the effect of CFRP on the behaviour of strengthened beams. It was concluded that the composite sheet can be modeled as a creep-free element perfectly bonded to the concrete [ACI committee 440, 1996].

4.7 Assessment of Experimental Result Quality

Bernoulli hypothesis (the strain at any point within the section, is proportional to its distance from the neutral axis) was applied on REHB35 specimen to evaluate the results as follows:

190

From the calculation, 10% error was found at the cracking load stage, while a 13% error was found at the yielding load stage. This error could be attributed to many factors: the accurate position of strain gauges; the position of the reinforcement bars where the strain gauges had been installed; and the effect of concrete on reinforcement strain gauges, in particular, coarse aggregate, especially after cracking and so forth. In addition, this hypothesis represents an ideal situation for the purpose of design and analysis. As seen, the error increased at yielding which could be attributed to the debonding of the CFRP sheets from the tension surface of concrete and/or increasing propagation of the cracks.

Curvature (φ) also was calculated to be (26.4, 48, and 80) 1/mm before cracking, at cracking and at yielding respectively.

At the end, the performance of all specimens reviewed in this chapter provided results that were agreeable with the laboratory observation and the main principles of RC structure.

191

Table 4-1: Specimen definition and characteristic

Group	Specimen	e (M/V) mm	Degree of loading	Rehabilitation material
I	CTRL0	0	until failure	N/A
	CRAK0		71% (CTRL0 P_{ult})	N/A
	REHB0		until failure	CFRP
II	CTRL25	250	until failure	N/A
	CRAK25		72% (CTRL25 P_{ult})	N/A
	REHB25		until failure	CFRP
III	CTRL35	350	until failure	N/A
	CRAK35		70% (CTRL35 P_{ult})	N/A
	REHB35		until failure	CFRP

192

Table 4-2: Sample of the test results (steel and concrete strain)

Slab Group	Specimen	Steel strain ε (microstrain)			Concrete strain (microstrain)	
		ε before P_{cr}	ε P_{cr}	ε P_y	ε P_y	ε P_{ult}
I	CTRL0	173	434	2148	-778	-949
	CRAK0	72	157	1965	.....	-741
	REHB0	111	180	2335	-1114	-1650
II	CTRL25	124	431	2382	-1030	-1545
	CRAK25	94	237	2100	.....	-739
	REHB25	74	105	2076	-1102	-1439
III	CTRL35	232	639	2846	-1153	-2250
	CRAK35	9	242	N/A	.....	-576
	REHB35	37	102	2060	-739	-815

*The readings represent: Ch. 23 (longitudinal tension reinforcement strain),

Ch.12 (longitudinal concrete strain in compression zone)

193

Table 4-3: Summary of the test results (Central deflection)

Slab Group	Specimen	Δ_y* mm	Δ_{ult}** mm	%Δ_y* Decreasing	%Δ_{ult}** Decreasing
I	CTRL0	10.6	32.5	43	77
	REHB0	6	7.3		
II	CTRL25	9.1	23.7	57	75
	REHB25	3.9	5.9		
III	CTRL35	7.7	20.1	42	67
	REHB35	4.5	6.6		

* The values represent the deflection at yielding and ultimate load of control specimens
  for each group respectively

194

Table 4-4: Summary of the test results (load and deflection)

Slab Group	Specimen	Py kN	Pult kN	% Py Increasing	% Pult Increasing	Δy* mm	Δult** mm	Ductility Index
I	CTRL0	140	169	86	112	10.6	32.5	3.1
I	REHB0	260	358	86	112	12.4	26.5	2.1
II	CTRL25	100	138	100	85	9.1	23.7	2.6
II	REHB25	200	255	100	85	9.7	16.1	1.7
III	CTRL35	100	133	90	68	7.7	20.1	2.6
III	REHB35	190	224	90	68	11.2	16.9	1.5

*   These values represent the deflection at yielding load of each specimen

**   These values represent the deflection at ultimate load of each specimen

***   All deflection were measured at Ch. 33 on the east central side channel

195

Table 4-5: Summary of the test results

Slab Group	Specimen	P_{cr} (Theoretical) kN	P_{cr} (visible) kN	P_y kN	P_{ult} kN	Type of failure	% P_{ult} increasing
I	CTRL0	38	89	140	169	Steel yield followed by tension failure	112
	CRAK0		89	just one rebar	121 (71% CTRL0$_{ult}$)	N/A	
	REHB0	… N/A..	N/A	260	358	Steel yield followed by Flexural shear and concrete crushing	
II	CTRL25	30	67	100	138	Steel yield followed by tension failure	85
	CRAK25		66	99	99 (72%CTRL25ult)	N/A	
	REHB25	… N/A..	N/A	200	255	Steel yield followed by Flexural shear and concrete crushing	
III	CTRL35	27	47	100	133	Steel yield followed by tension failure	68
	CRAK35		59	99	90 (70% CTRL35$_{ult}$)	N/A	
	REHB35	… N/A..	N/A	190	224	Steel yield followed by Flexural shear and concrete crushing	

196

GROUP I FIGURES

(Specimens with zero eccentricity)
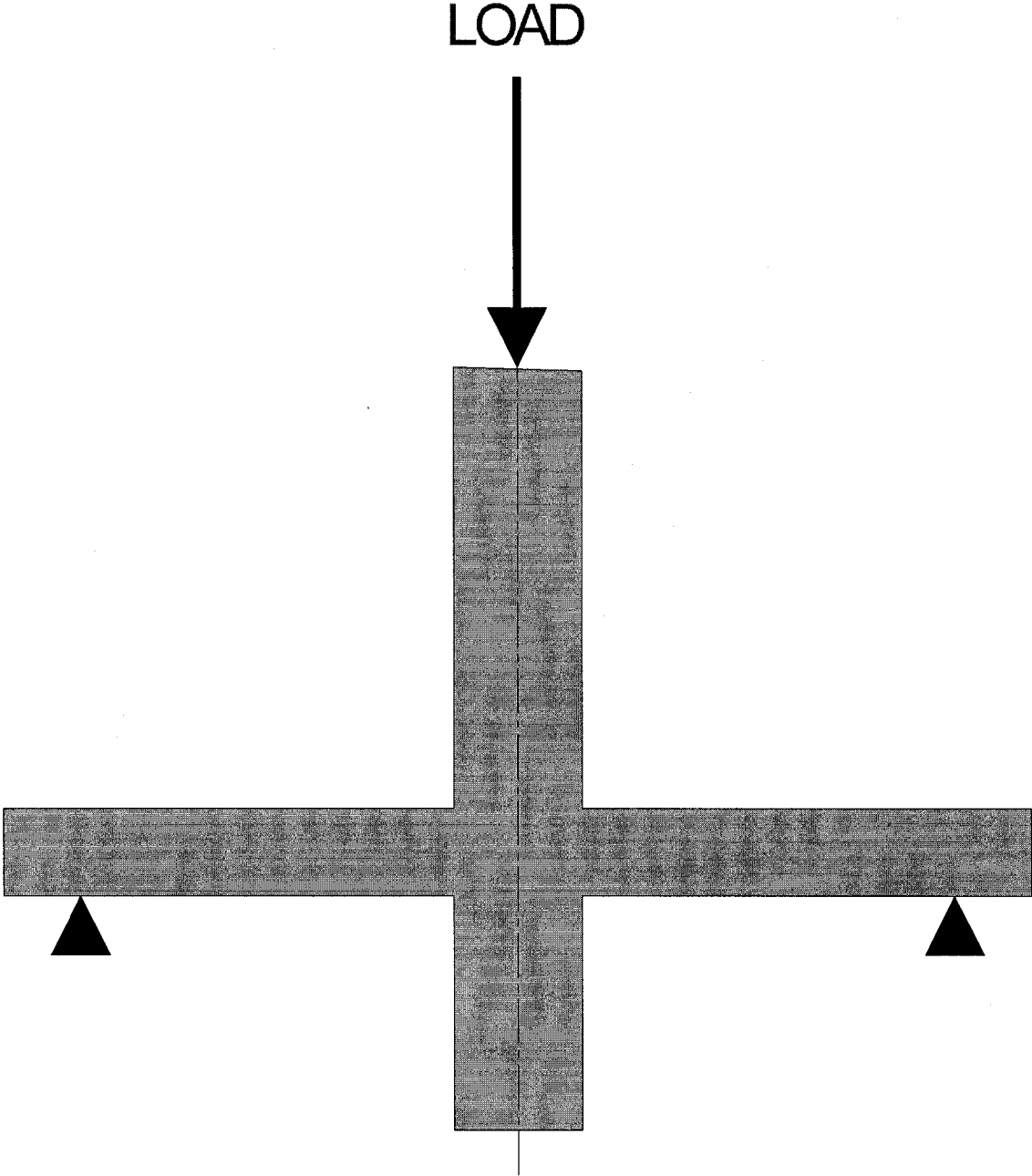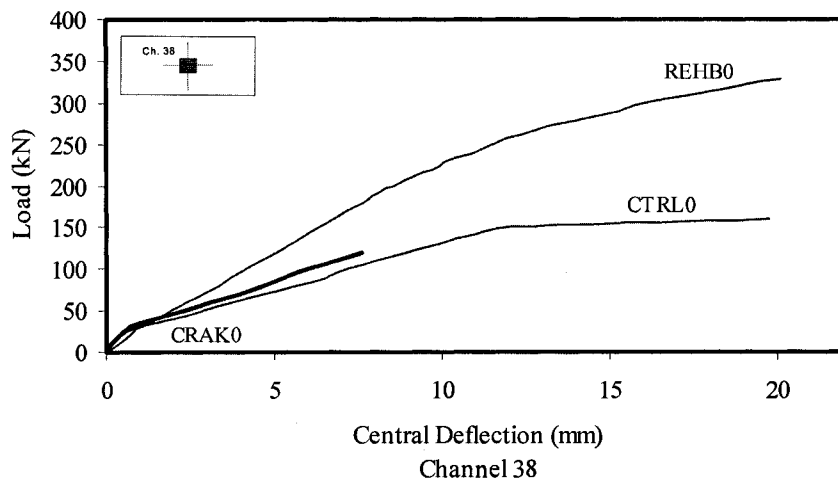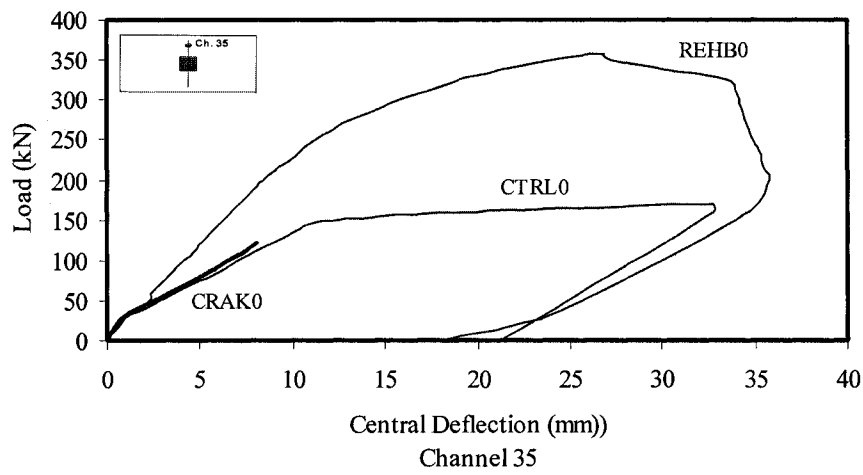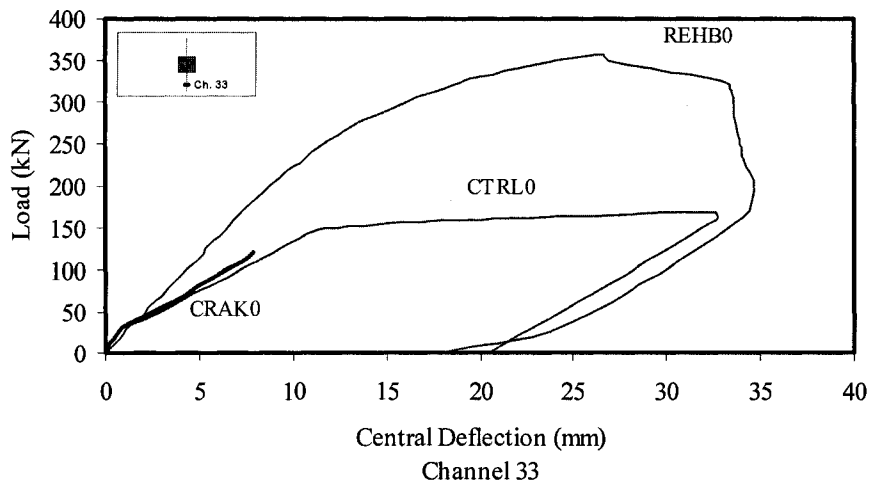
LOAD

Fig. 4-1: Load versus central short direction deflection

198
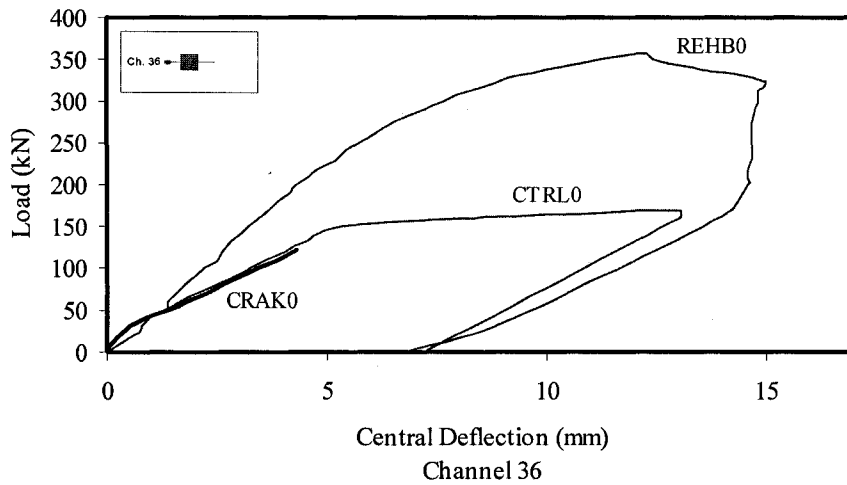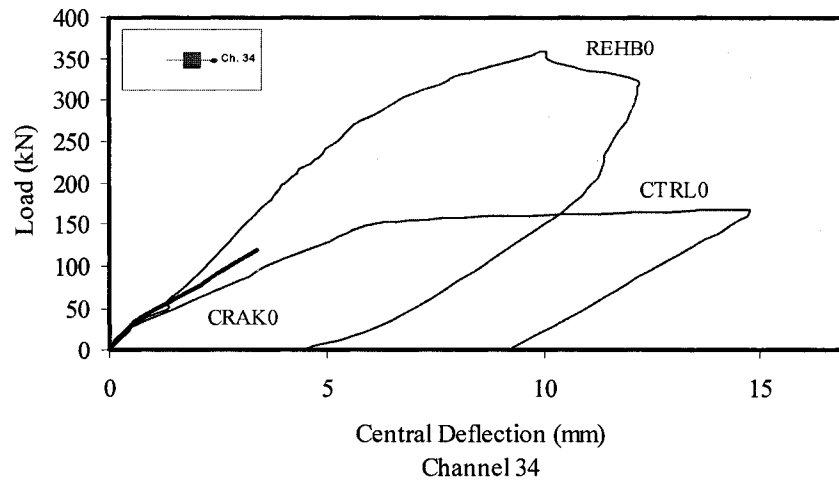
Fig. 4-2: Load versus central long direction deflection

199
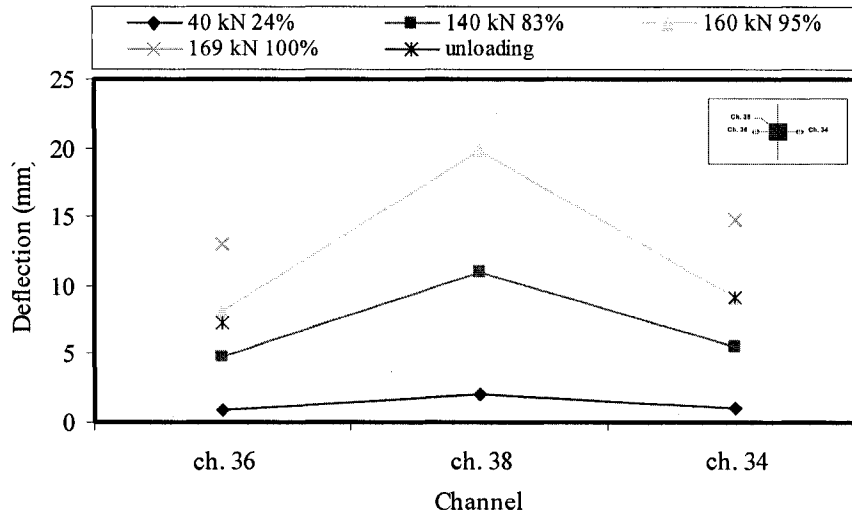
Fig. 4-3: Deflection response on the central long direction (CTRL0)
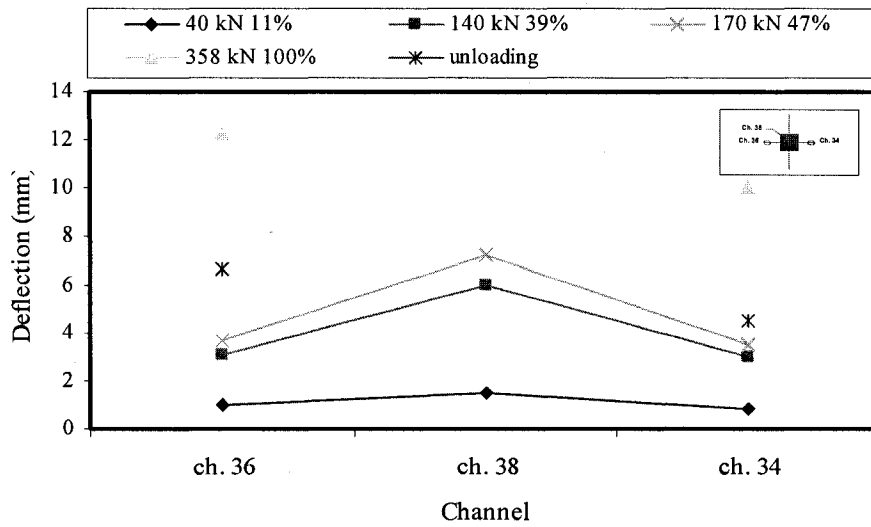
Fig. 4-4: Deflection response on the central long direction (REHB0)

200
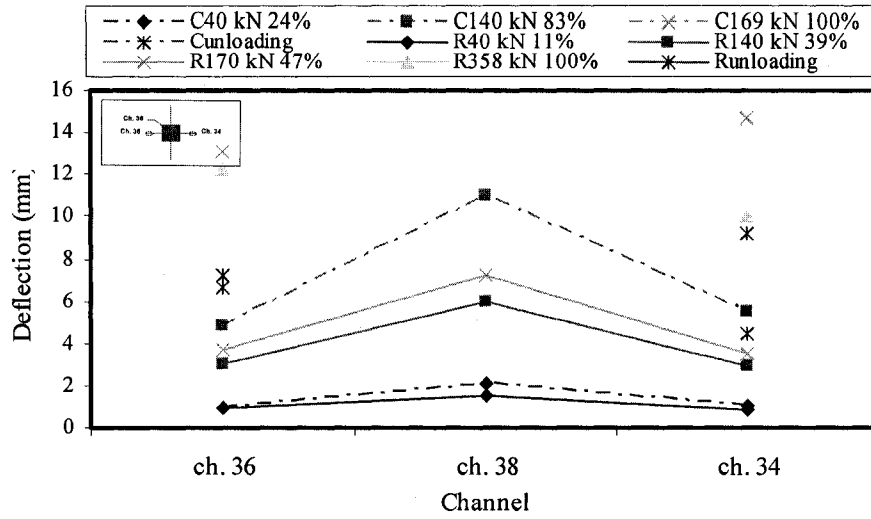
Fig. 4-5: Deflection response on the central long direction for

the control (CTRL0) and rehabilitated specimen (REHB0)
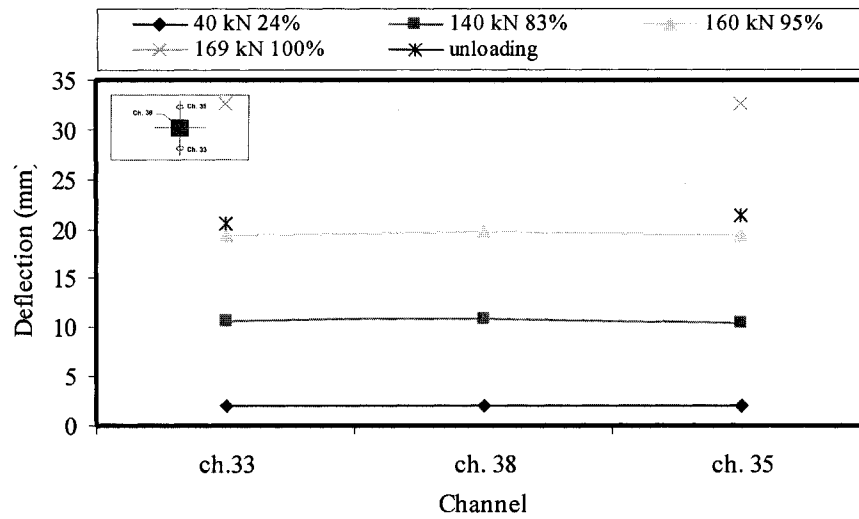
Fig. 4-6: Deflection response on the central short direction for

the control specimen (CTRL0)

201
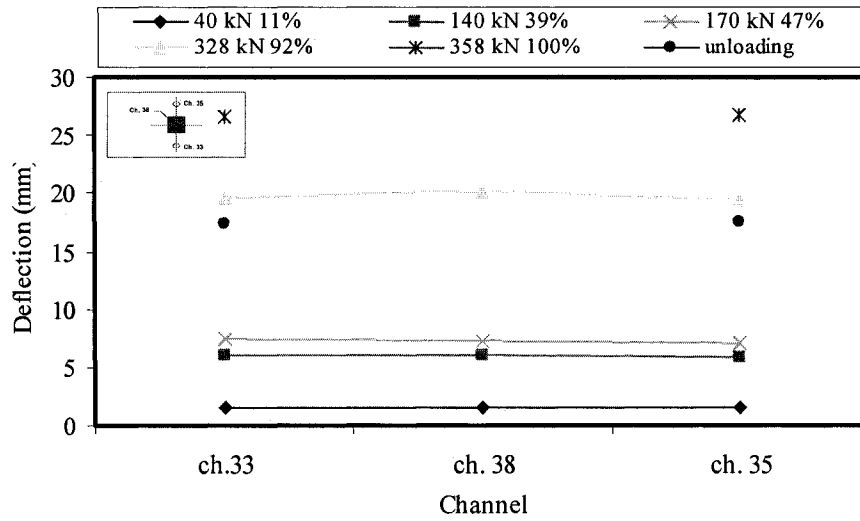
Fig. 4-7: Deflection response on the central short direction for

the rehabilitated specimen (REHB0)
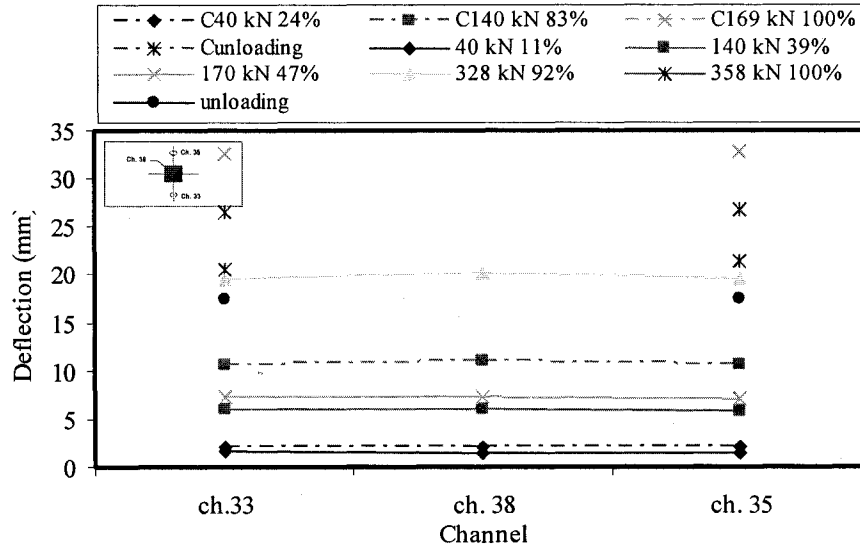
Fig. 4-8: Deflection response on the central short direction for

the control (CTRL0) and rehabilitated (REHB0)

202
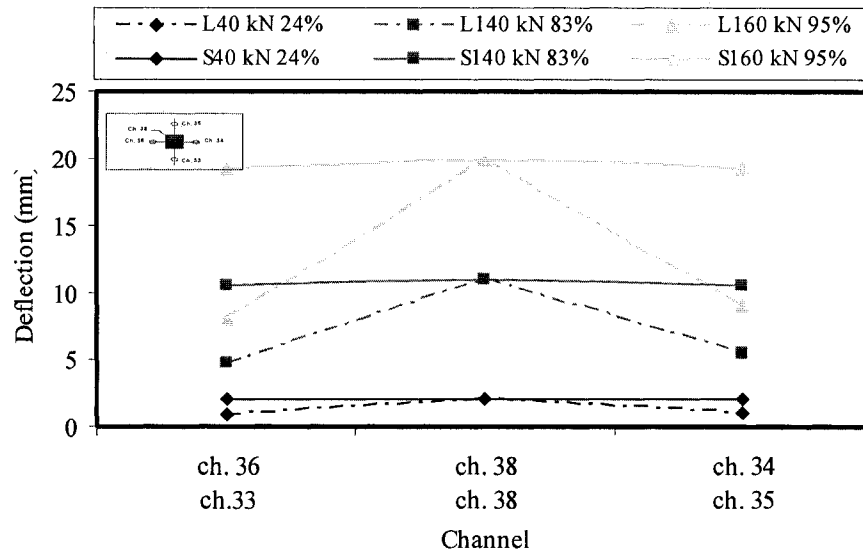
Fig. 4-9: Deflection response on the central long (L) and short (S) direction for

the control specimen (CTRL0)
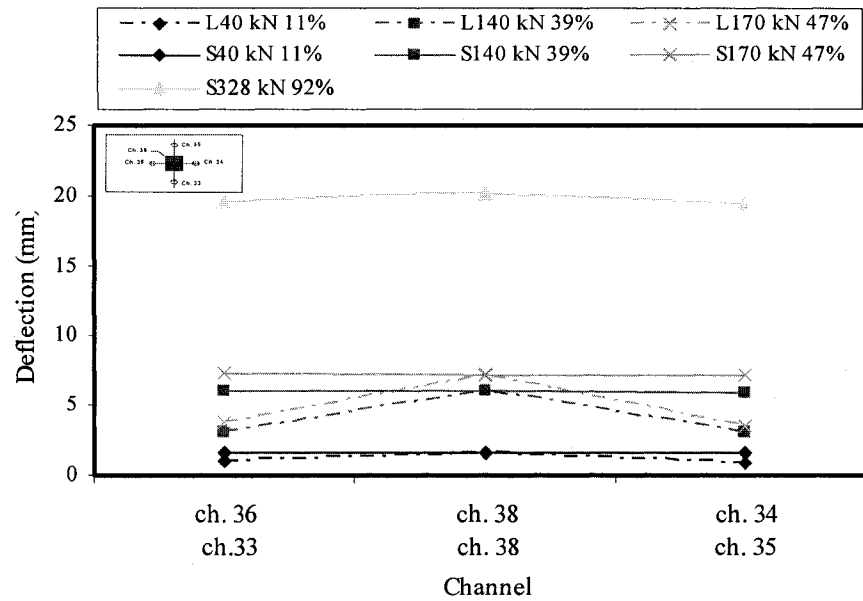
4-10: Deflection response on the central long (L) and short (S) direction for

the rehabilitated specimen (REHB0)

(The dominance of one-way slab)

203
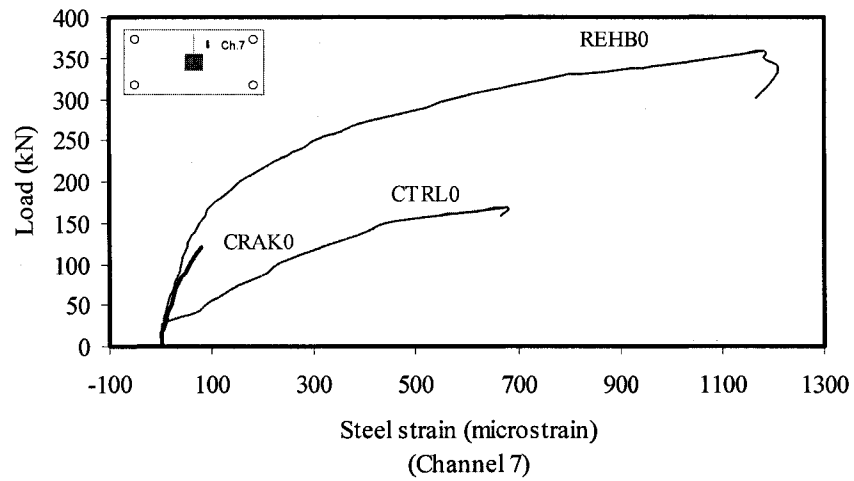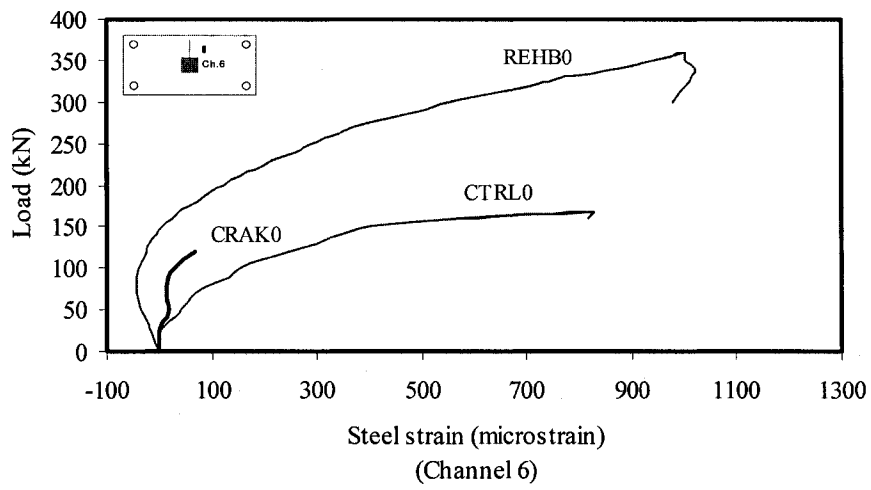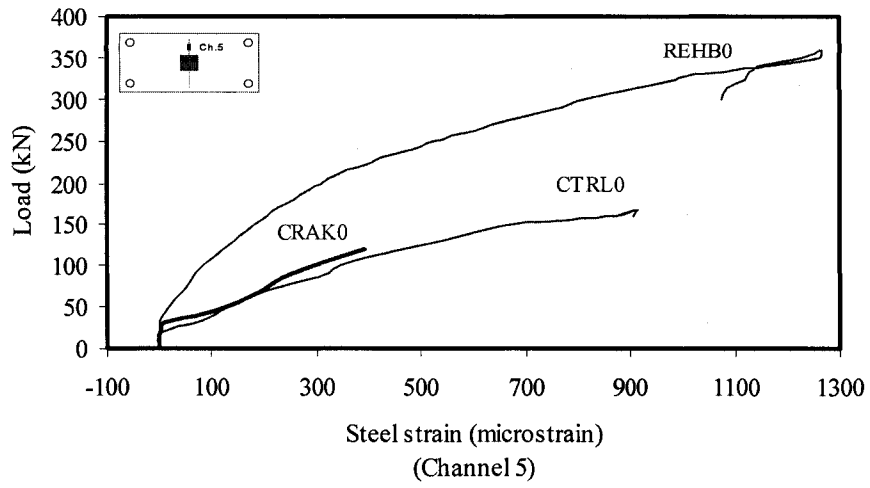
Fig. 4-11: Load versus tension short direction steel strain

204
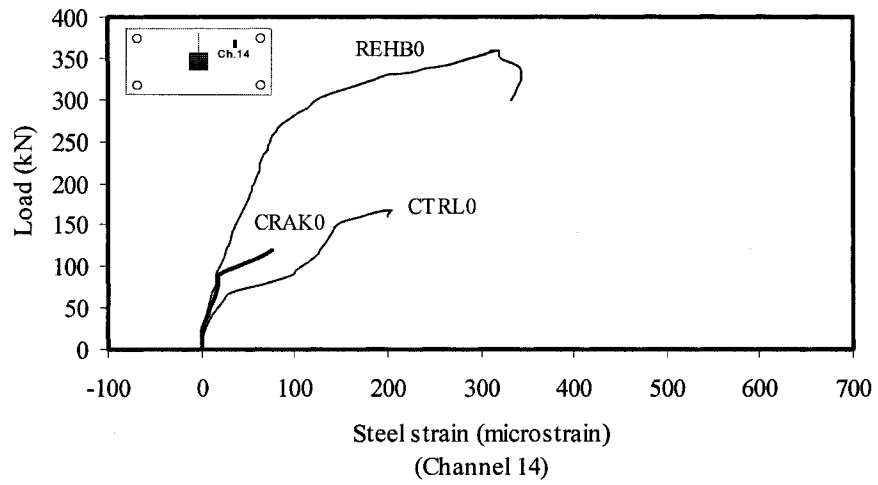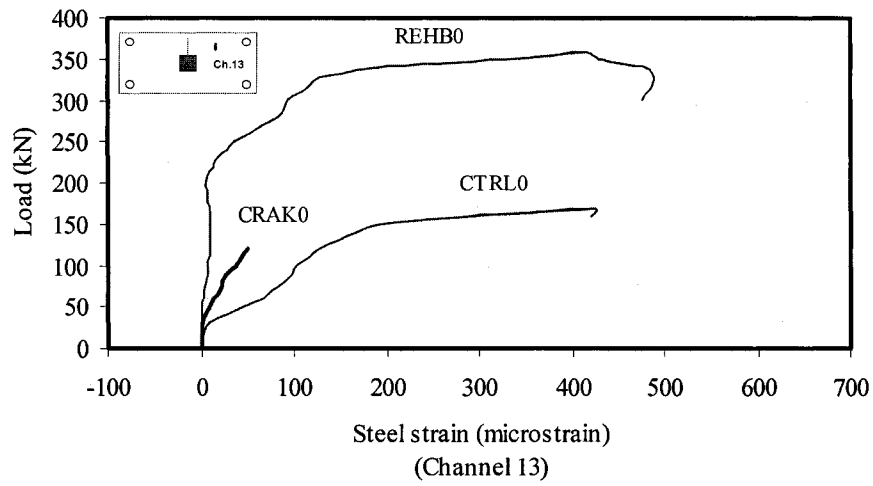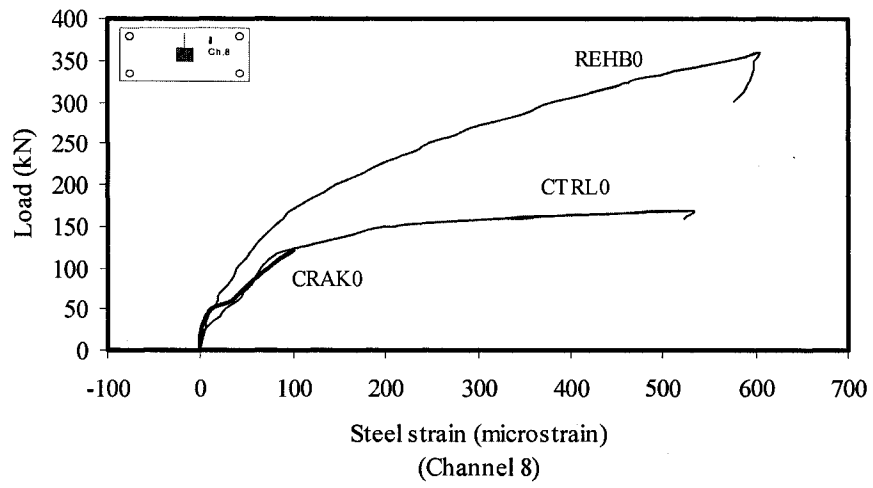
Fig. 4-12: Load versus tension short direction steel strain

205
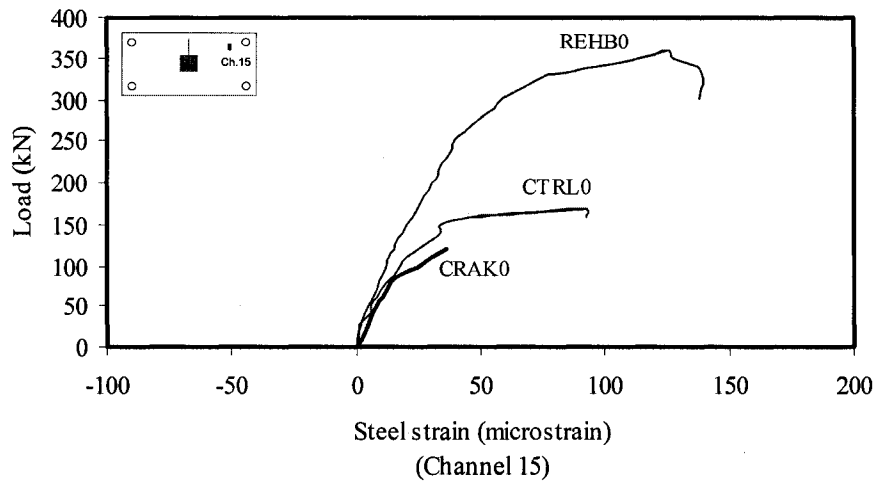
Fig. 4-13: Load versus tension short direction steel strain

206
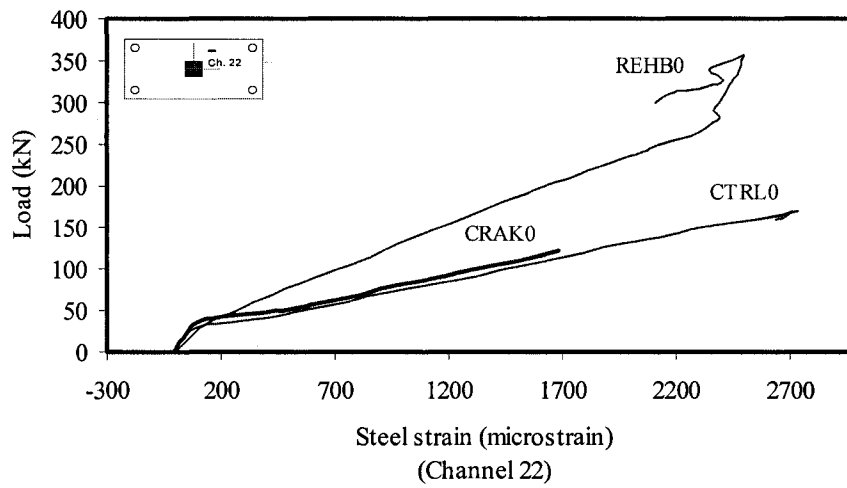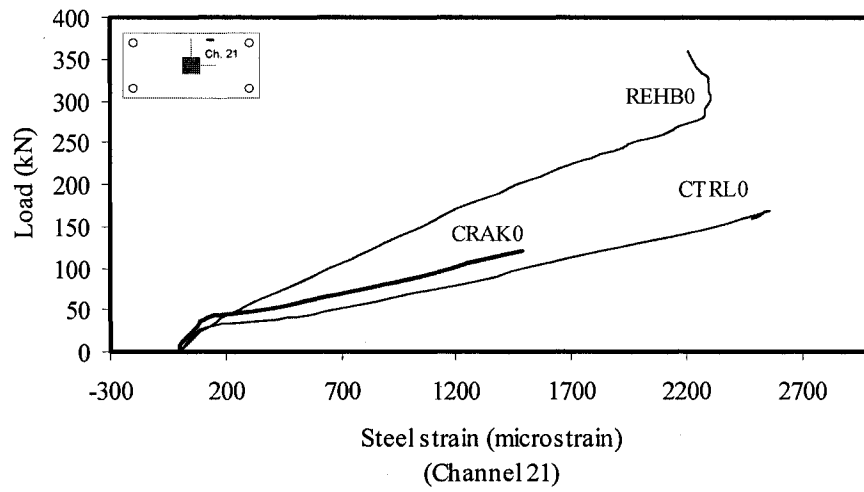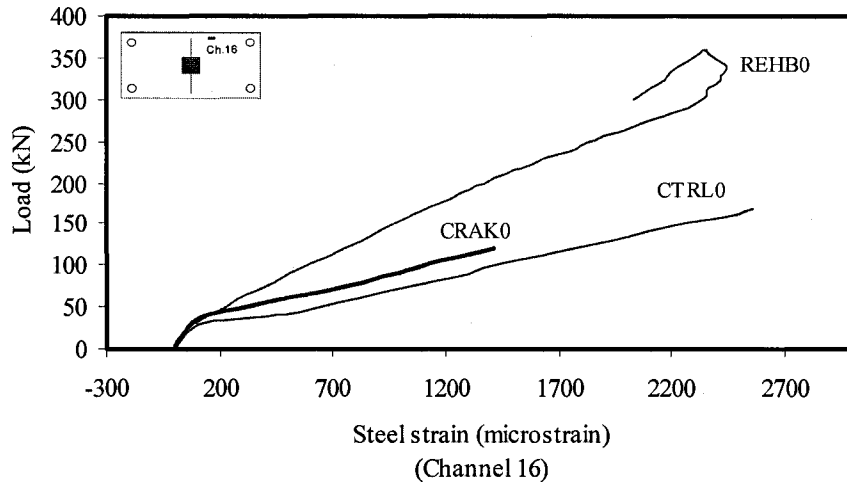
Fig. 4-14: Load versus tension long direction steel strain

207
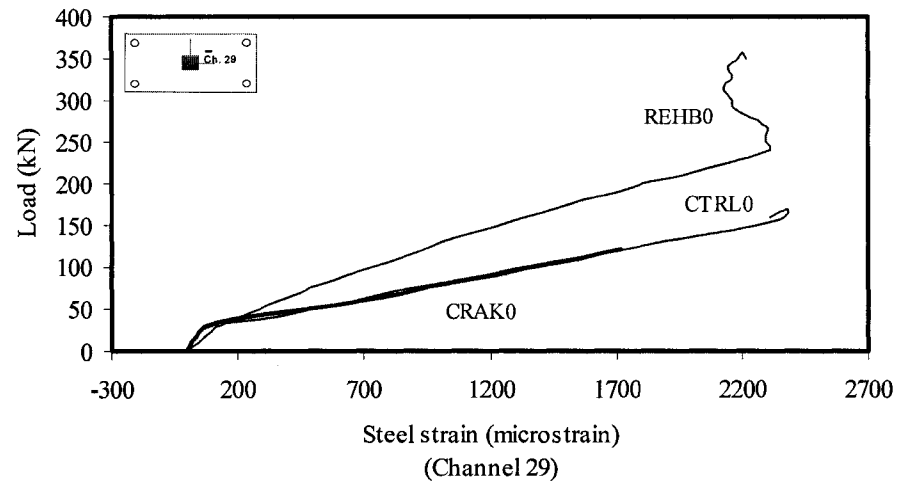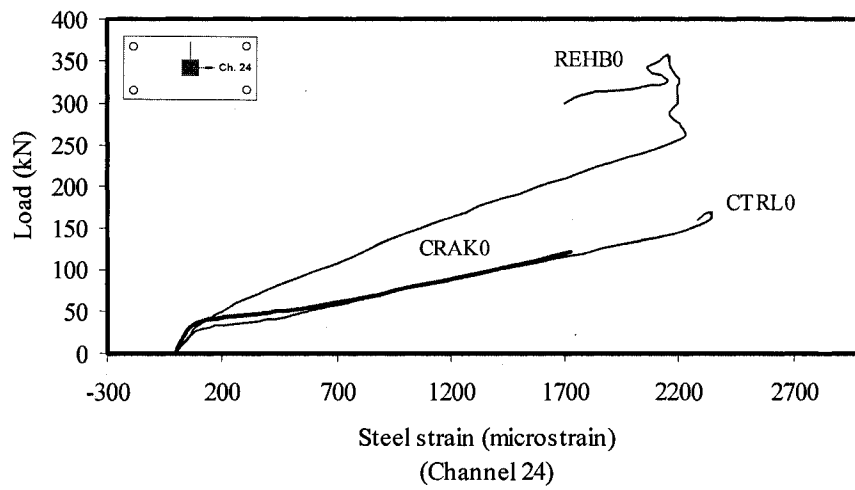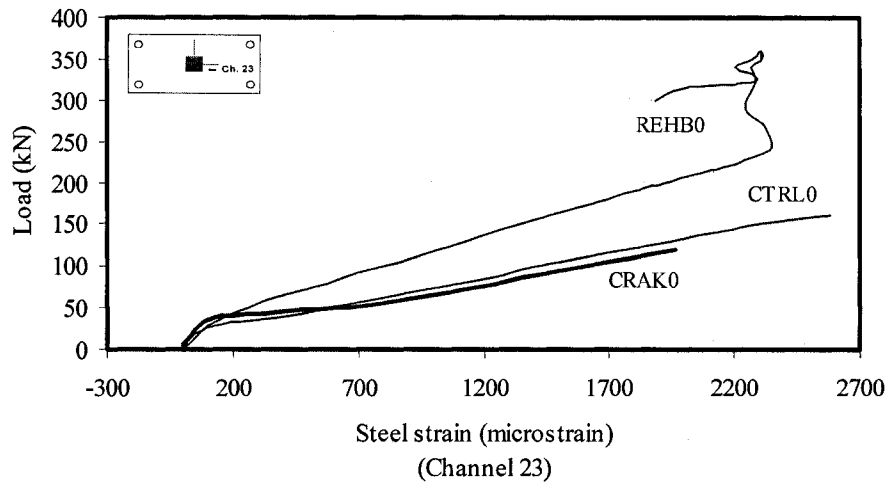
Fig. 4-15: Load versus tension long direction steel strain

208
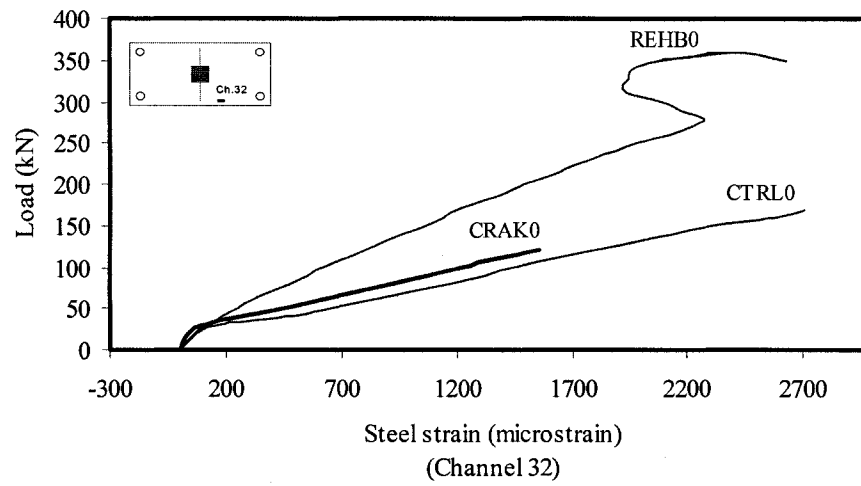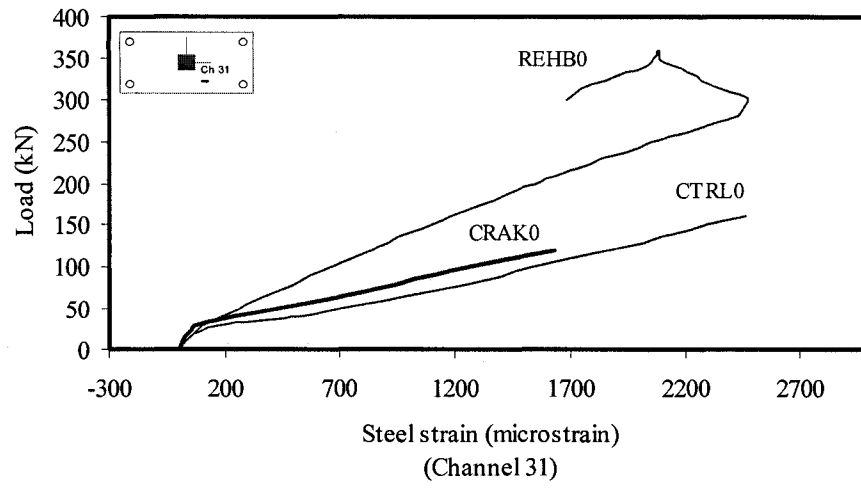
Fig. 4-16: Load versus tension long direction steel strain

209
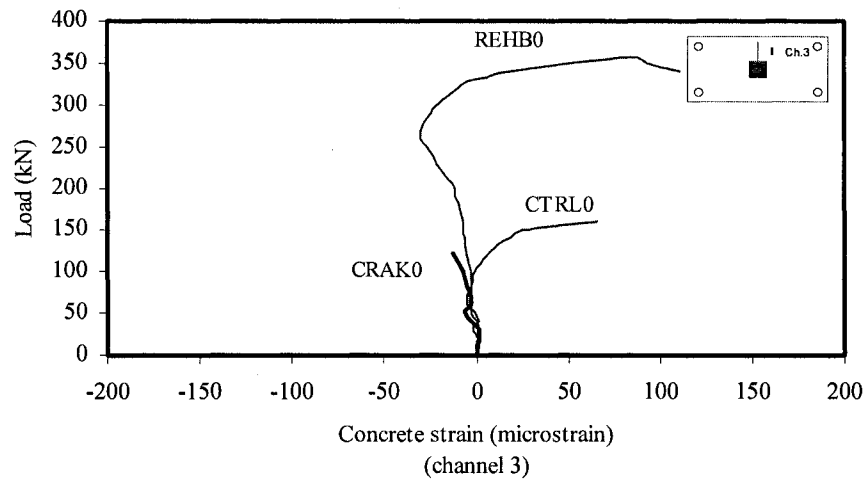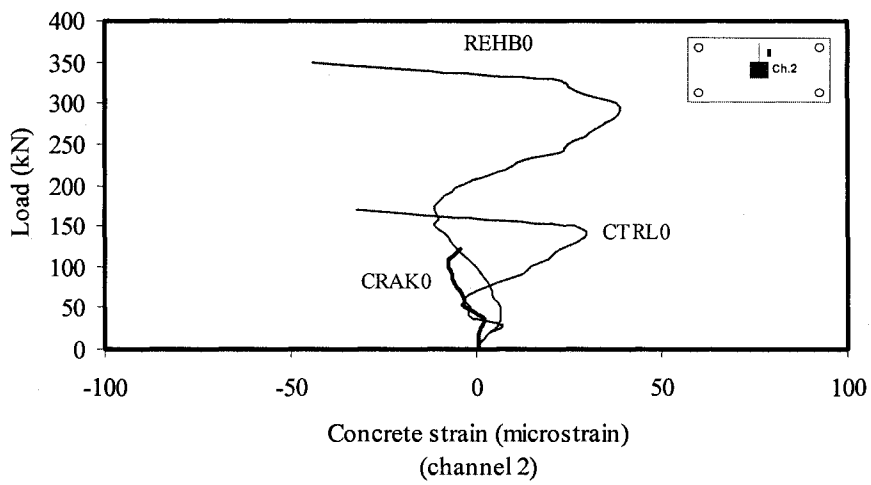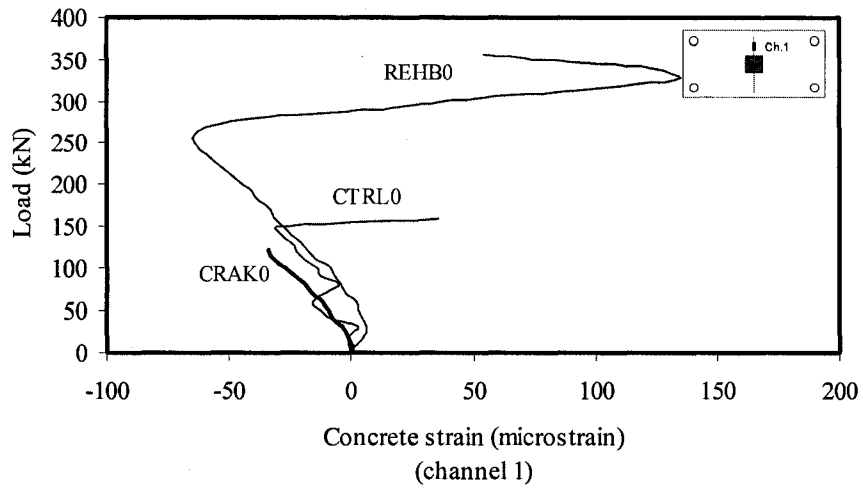
Fig. 4-17: Load versus short direction concrete strain

210
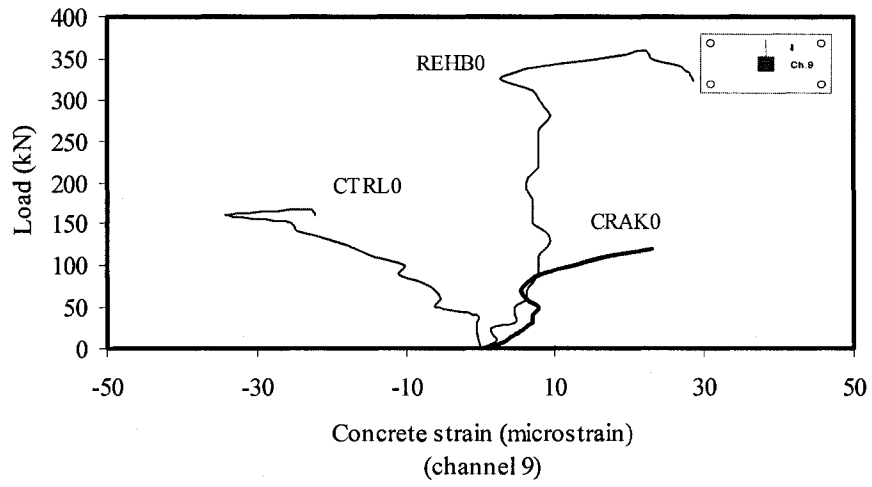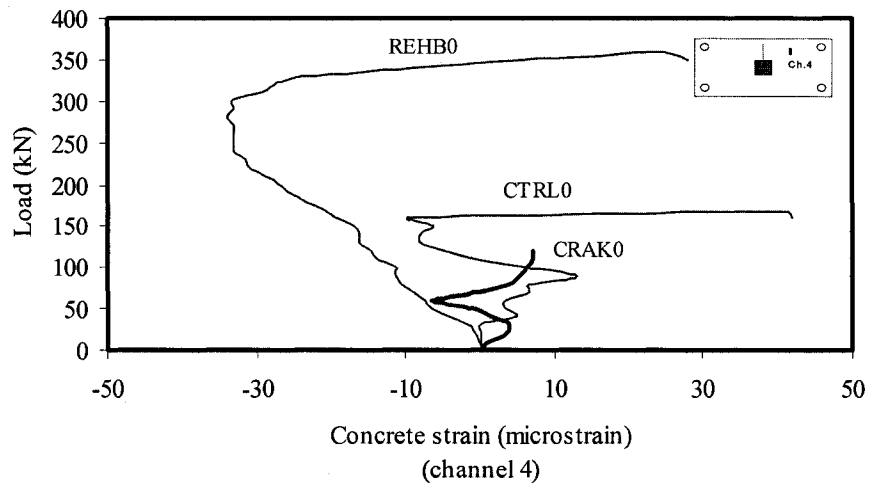
Fig. 4-18: Load versus short direction concrete strain

211
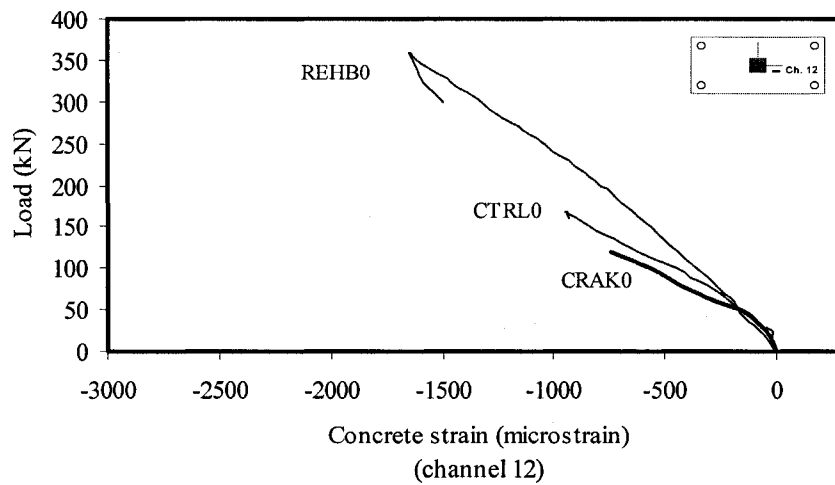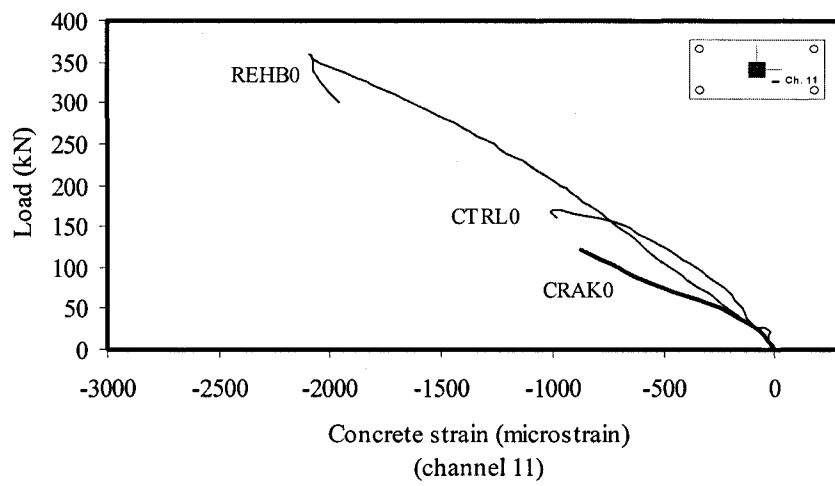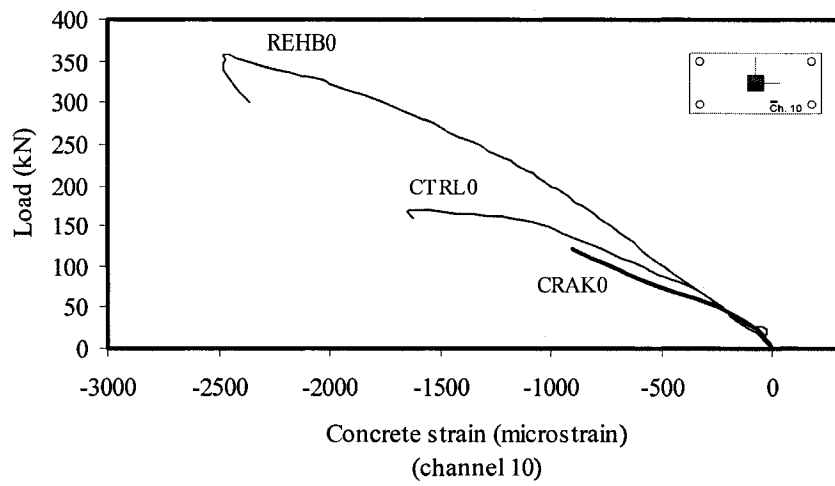
Fig. 4-19: Load versus compression long direction concrete strain

212
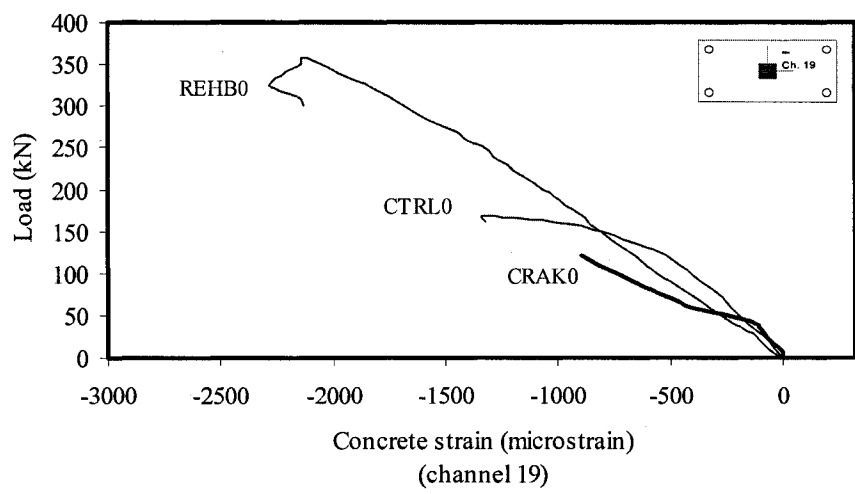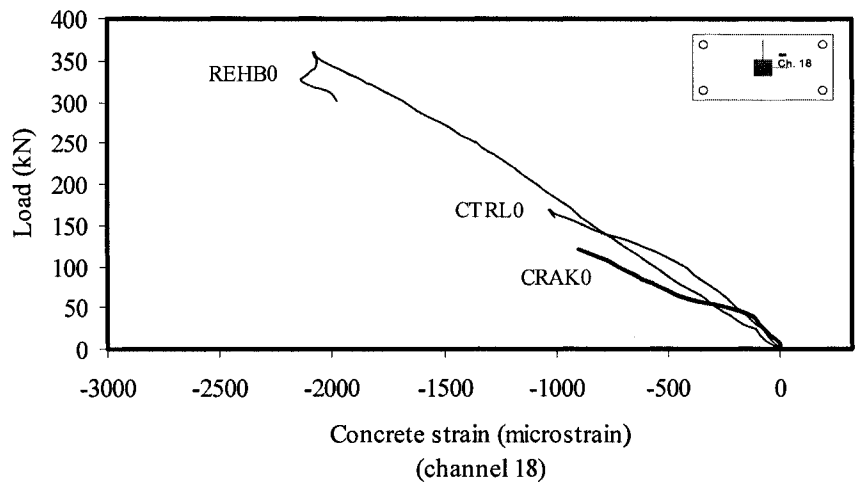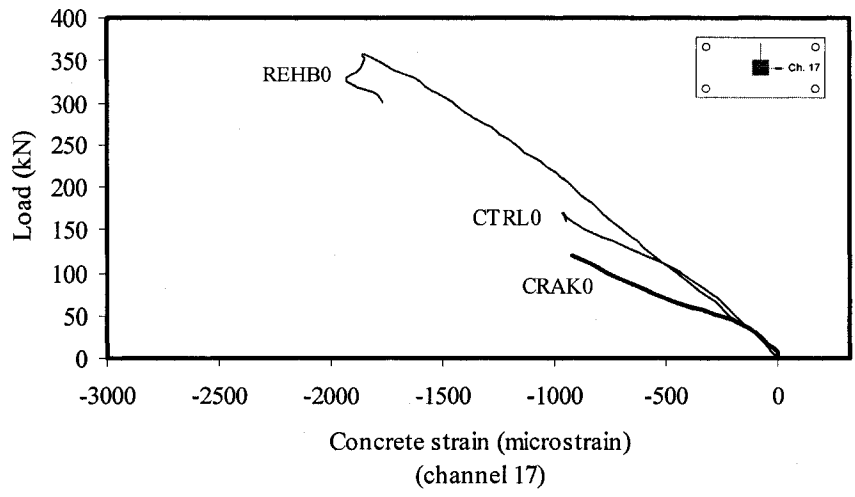
Fig. 4-20: Load versus compression long direction concrete strain

213
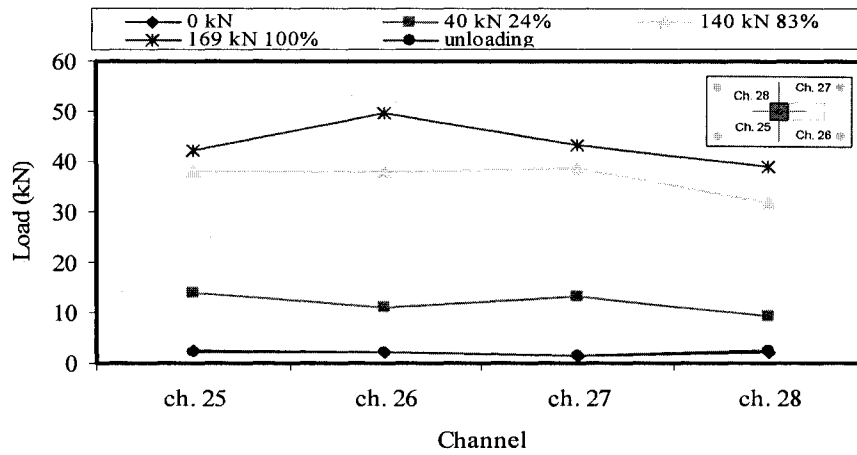
Fig. 4-21: Load distribution on each reaction (CTRL0)
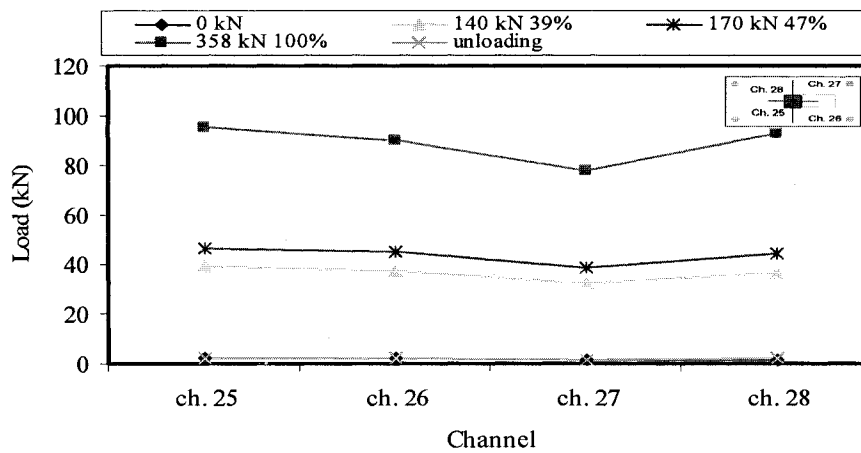
Fig. 4-22: Load distribution on each reaction (REHB0)
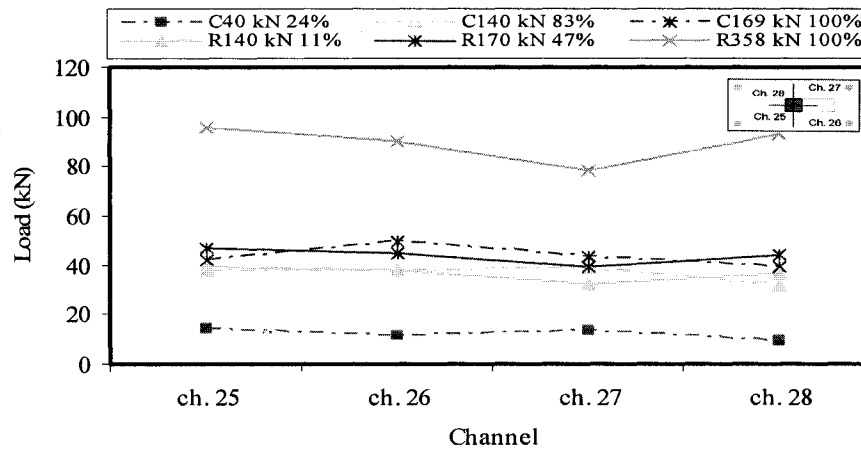
Fig. 4-23: Load distribution on each reaction for (CTRL0) and (REHB0)

214
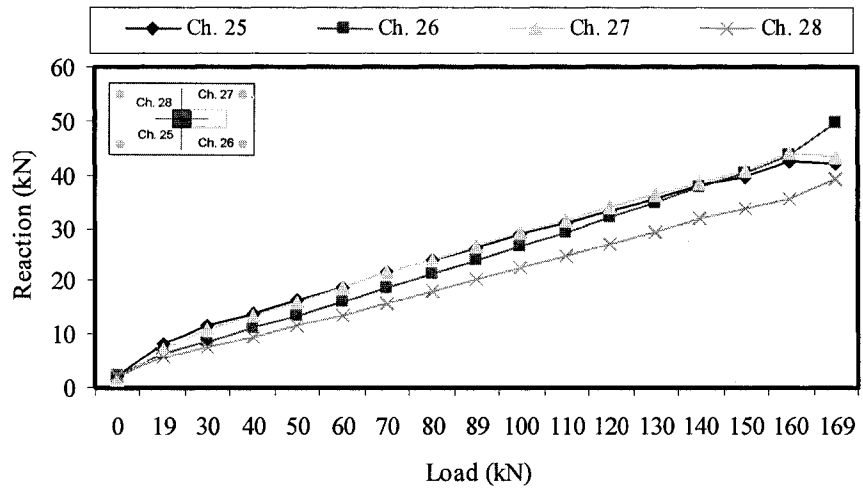
Fig. 4-24: Reaction distribution for the control specimen (CTRL0)
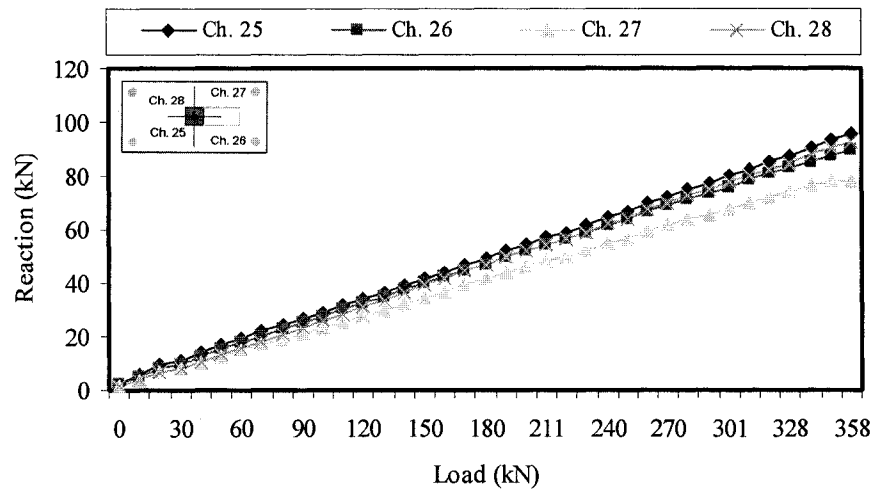
Fig. 4-25: Reaction distribution for the rehabilitated specimen (REHB0)

215
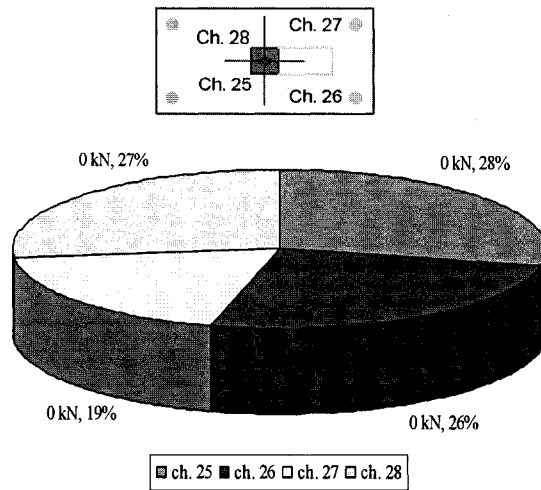
Fig. 4-26: Percentage of load on the four reactions before loading (CTRL0)
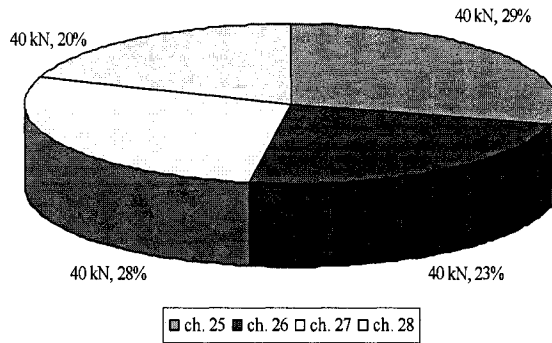
Fig. 4-27: Percentage of load on the four reactions at cracking load (CTRL0)
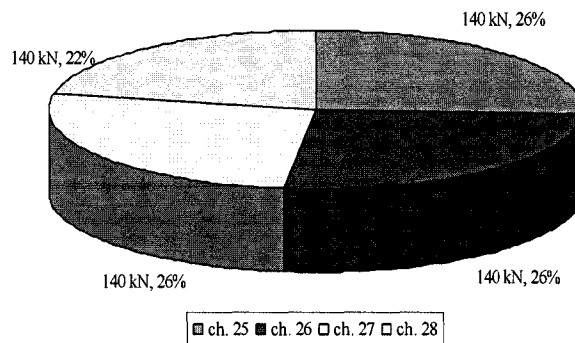
Fig. 4-28: Percentage of load on the four reactions at steel yielding (CTRL0)

Control specimen

216
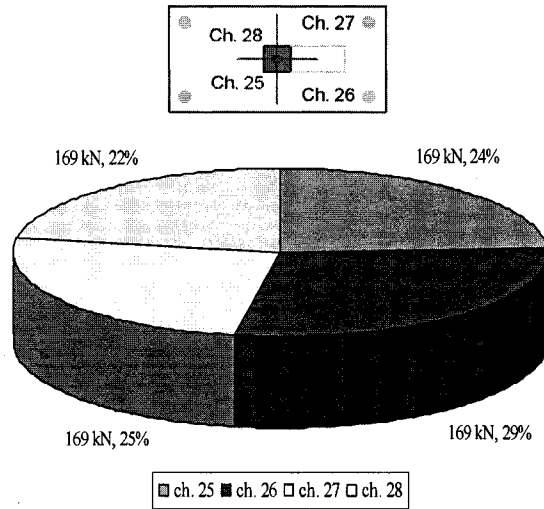
Fig. 4-29: Percentage of load on the four reactions at ultimate load (CTRL0)
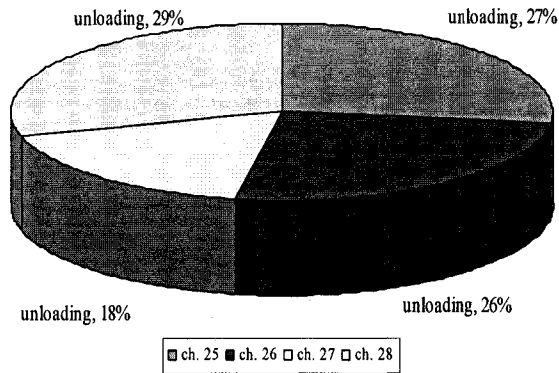
Fig. 4-30: Percentage of load on the four reactions after unloading (CTRL0)
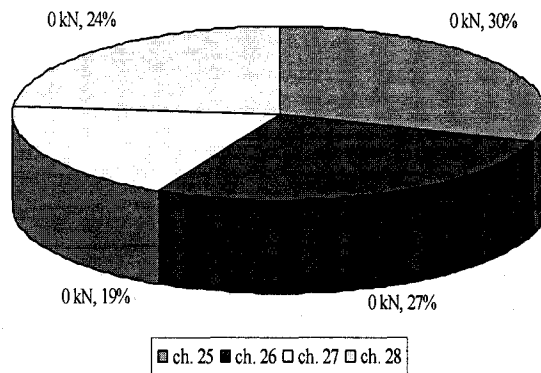
Fig. 4-31: Percentage of load on the four reactions before loading (REHB0)

Rehabilitated specimen

217
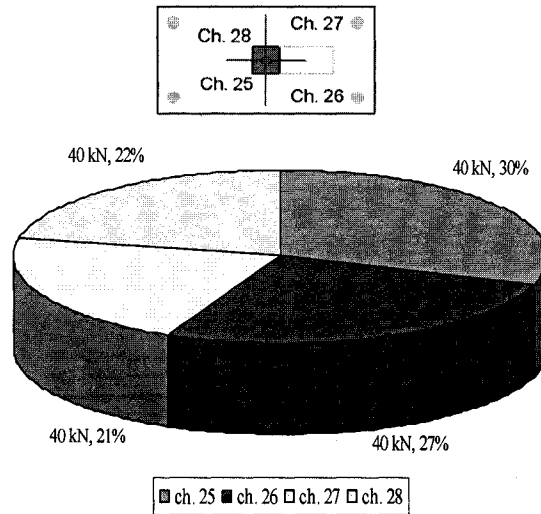
Fig. 4-32: Percentage of load on the four reactions at cracking load (REHB0)
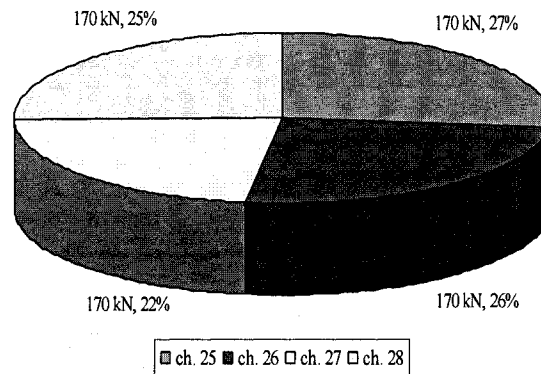
Fig. 4-33: Percentage of load on the four reactions at ultimate load (REHB0)
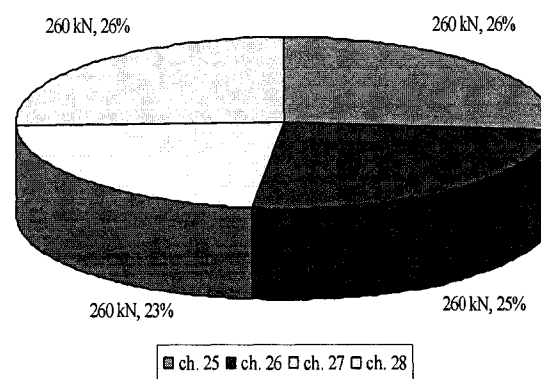
Fig. 4-34: Percentage of load on the four reactions at steel yielding (REHB0)

Rehabilitated specimen

218
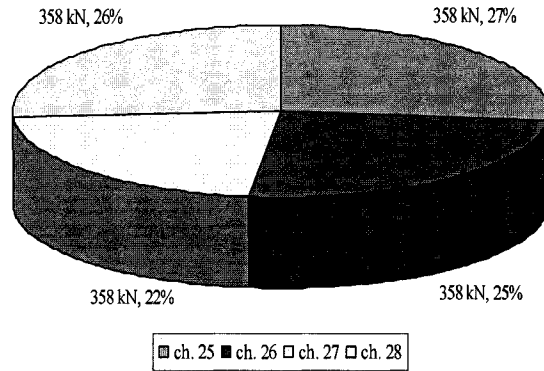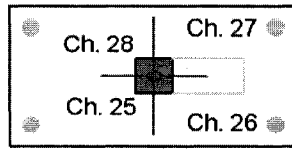
Fig. 4-35: Percentage of load on the four reactions at ultimate load for the

rehabilitated specimen (REHB0)
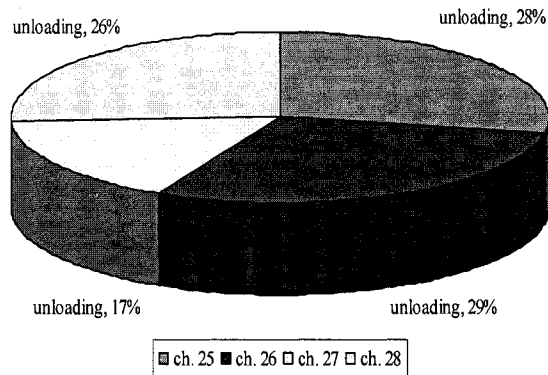
Fig. 4-36: Percentage of load on the four reactions after unloading for

the rehabilitated specimen (REHB0)

219
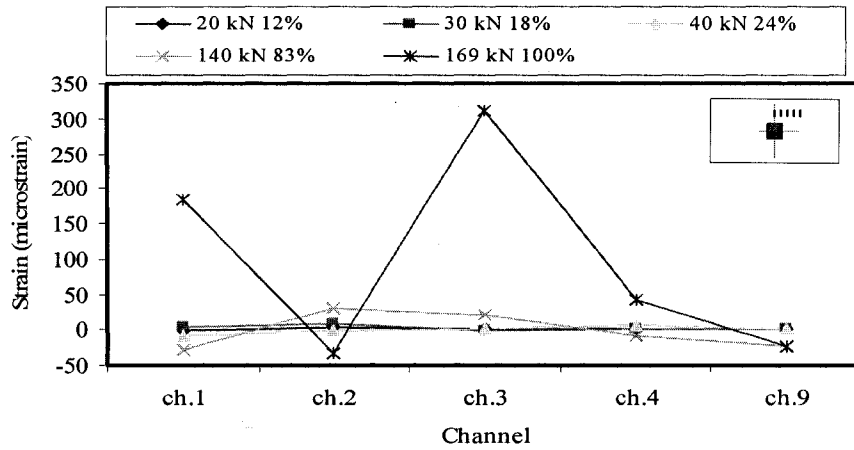
Fig. 4-37: Load versus short direction concrete strain (CTRL0)
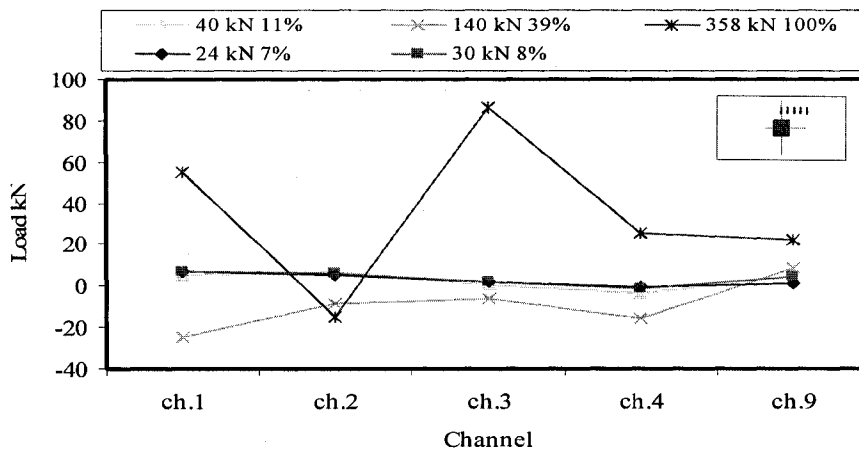
Fig. 4-38: Load versus short direction concrete strain (REHB0)
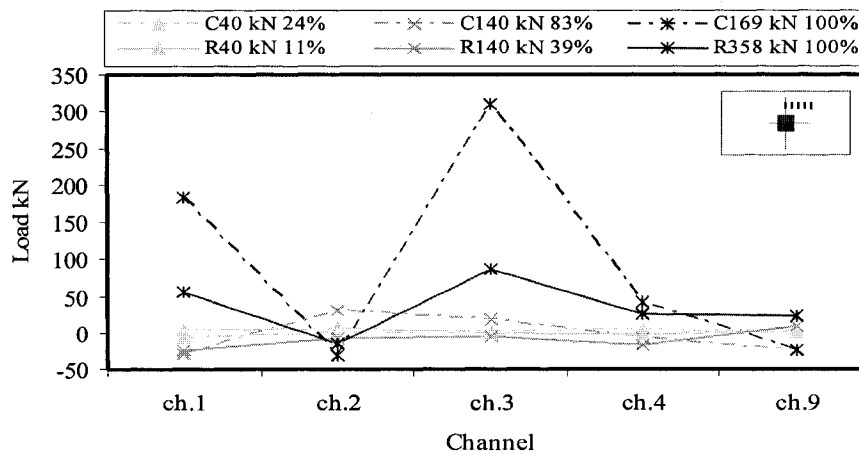
Fig. 4-39: Load versus short direction concrete strain (CTRL0) and (REHB)

220
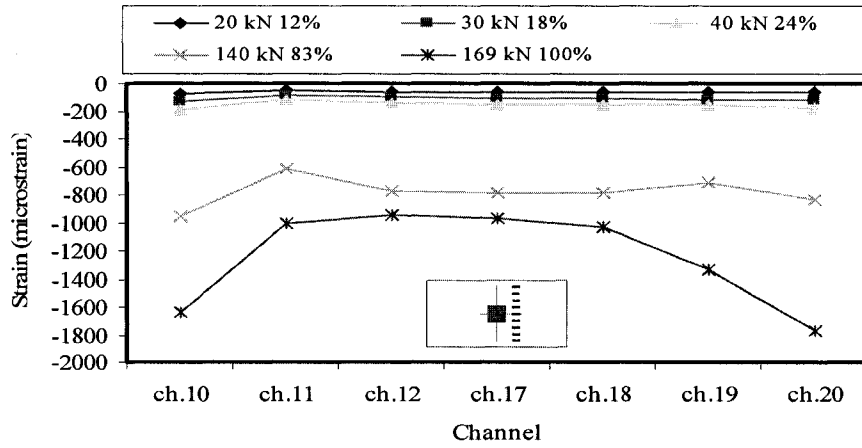
Fig. 4-40: Load versus long direction concrete strain (CTRL0)
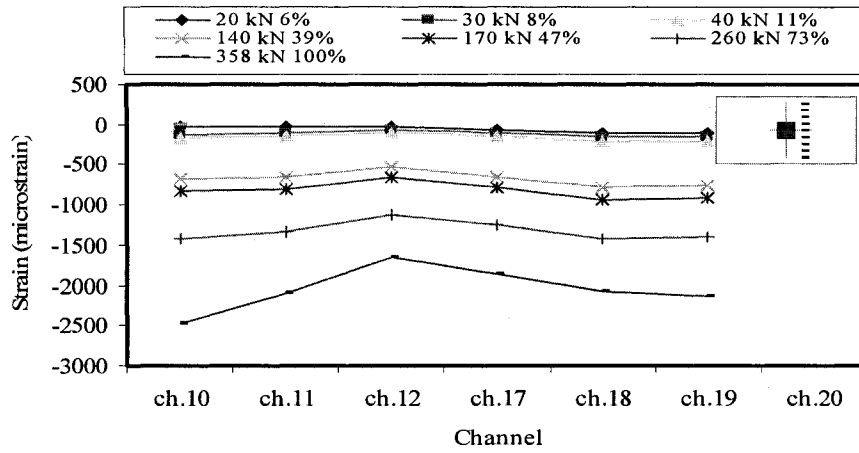
Fig. 4-41: Load versus long direction concrete strain (REHB0)
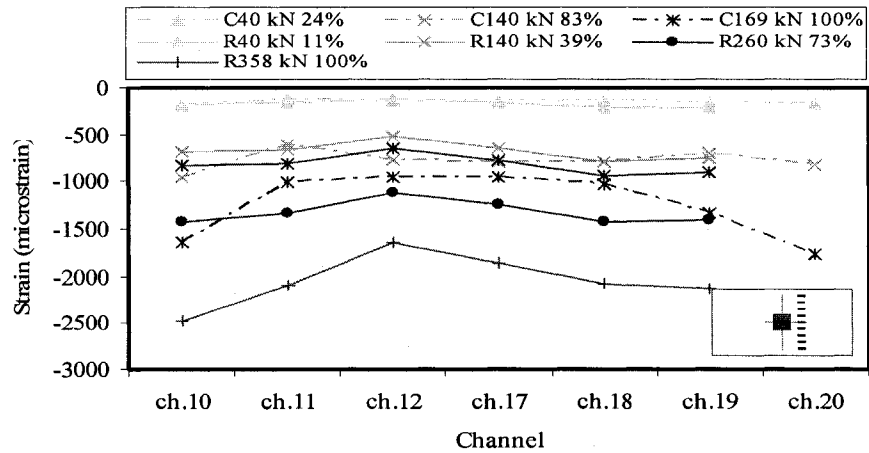
Fig. 4-42: Load versus long direction concrete strain (CTRL0) and (REHB0)

221
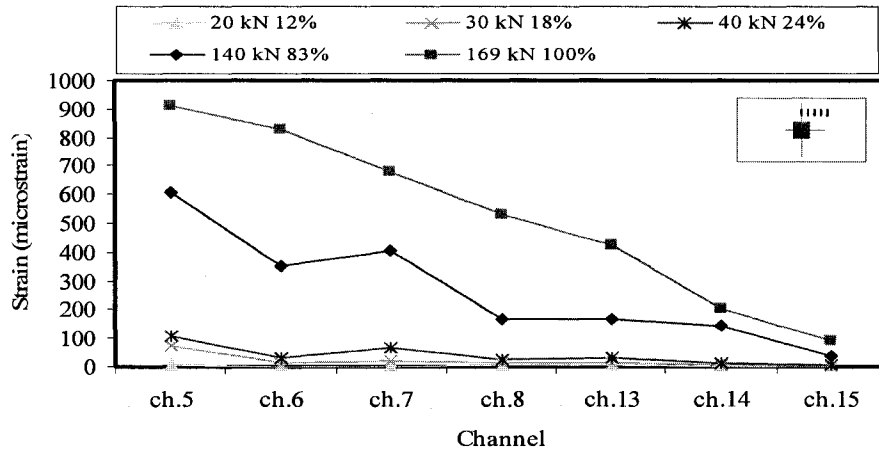
Fig. 4-43: Load versus short direction concrete strain (CTRL0)
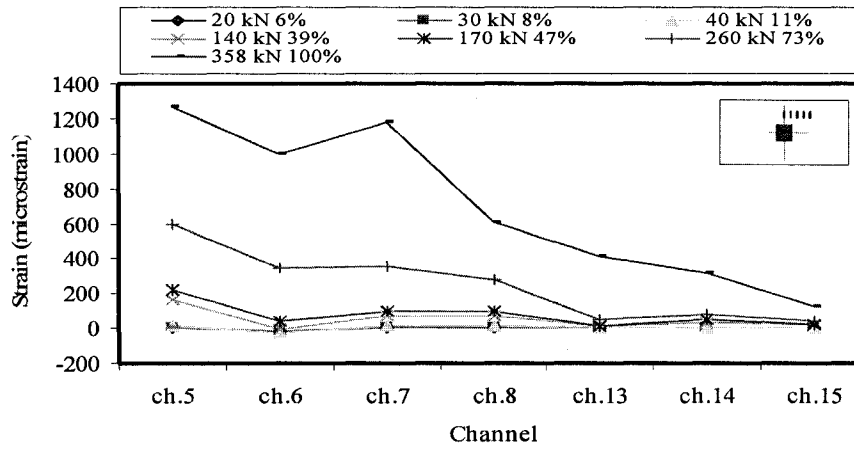
Fig. 4-44: Load versus short direction concrete strain (REHB0)
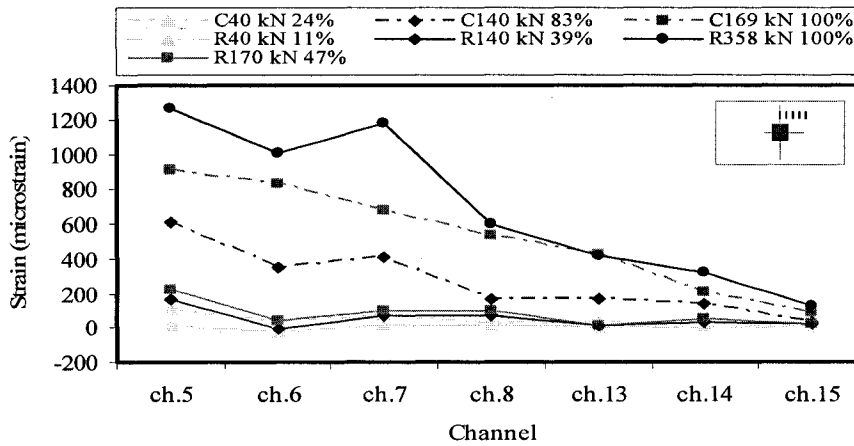
Fig. 4-45: Load versus short direction steel strain (CTRL0) and (REHB)

222
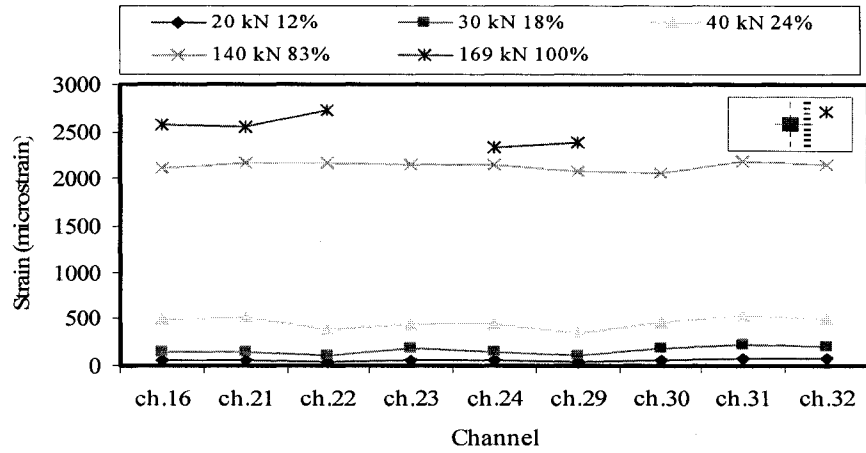
Fig. 4-46: Load versus long direction steel strain (CTRL0)
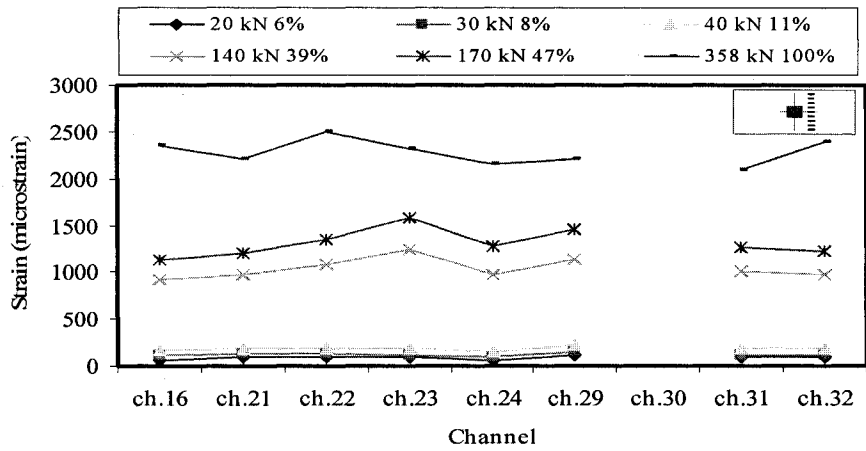
Fig. 4-47: Load versus long direction steel strain (REHB0)
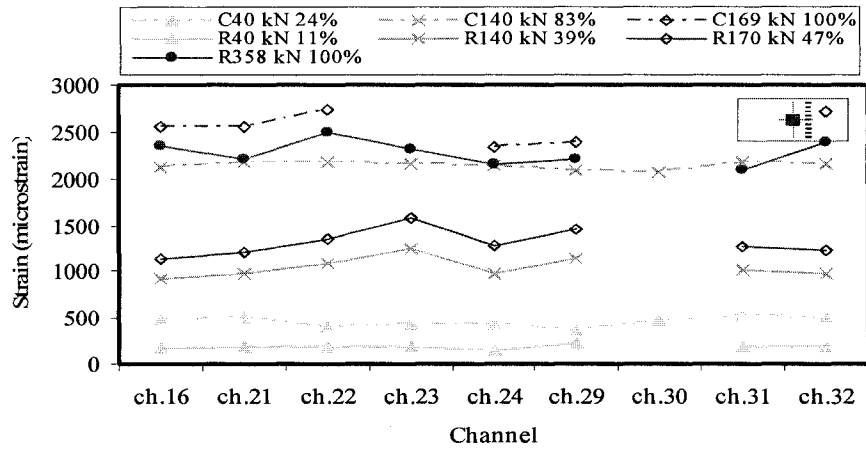
Fig. 4-48: Load versus long direction steel strain (CTRL0) and (REHB)

223
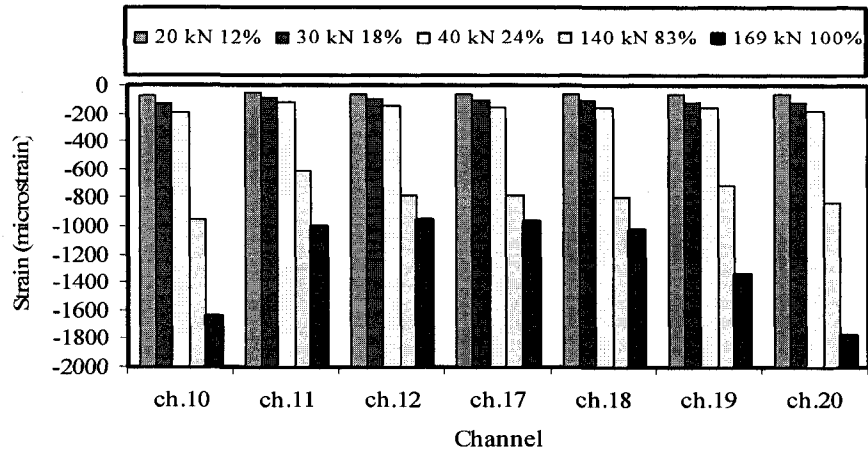
Fig. 4-49: Load versus long direction concrete strain (CTRL0)
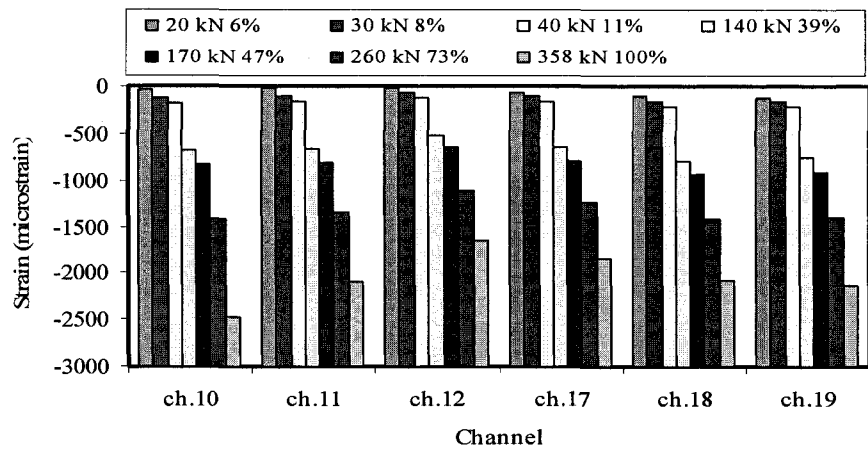
Fig. 4-50: Load versus long direction concrete strain (REHB0)
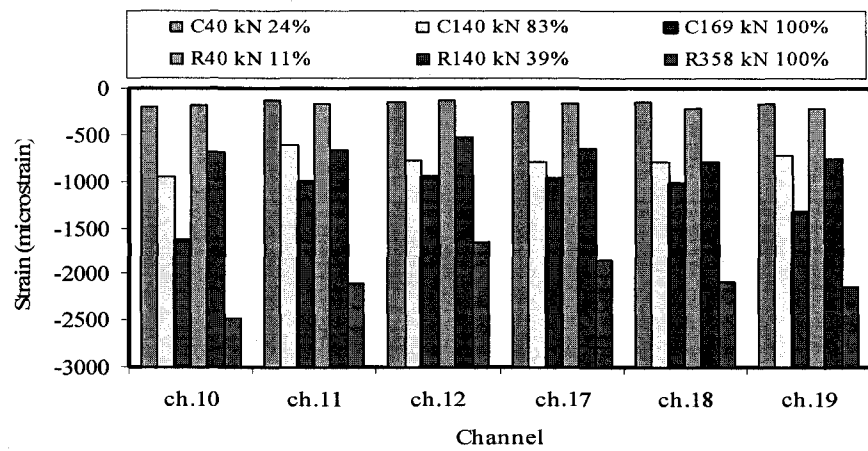
Fig. 4-51: Load versus long direction concrete strain (CTRL0) and (REHB0)

224
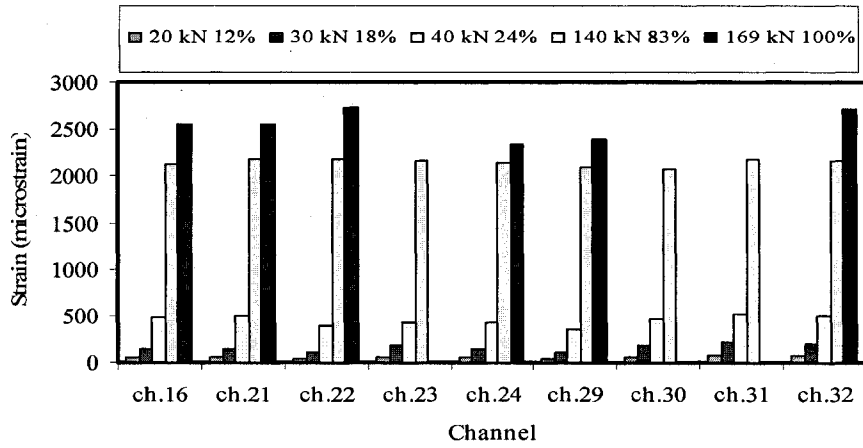
Fig. 4-52: Load versus long direction steel strain for
the control specimen (CTRL0)
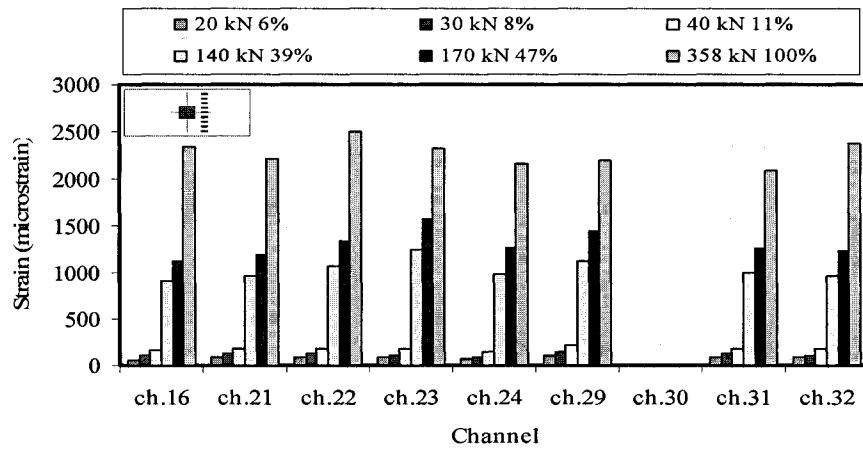
Fig. 4-53: Load versus long direction steel strain for

the rehabilitated specimen (REHB0)

225
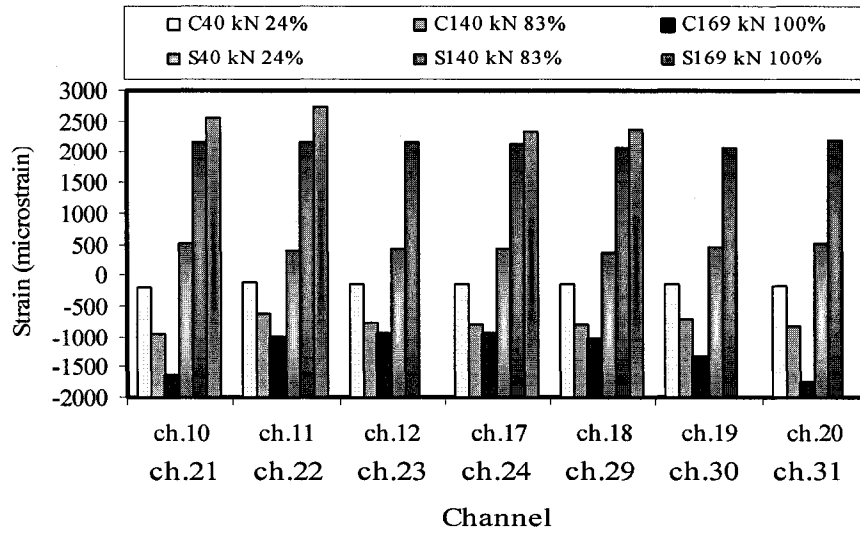
Fig. 4-54: Load versus long direction concrete and steel strain for

the control specimen (CTRL0)
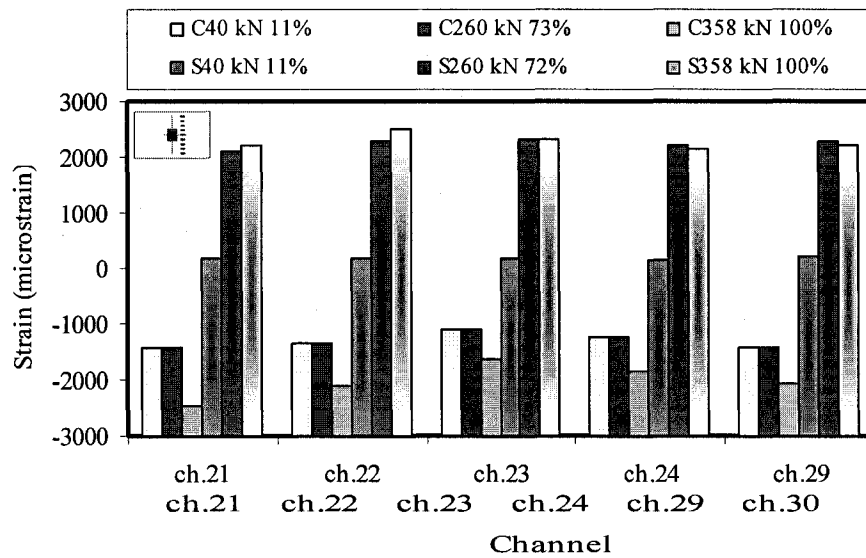
Fig. 4-55: Load versus long direction concrete and steel strain for

the rehabilitated specimen (REHB0)

226

GROUP II FIGURES

(Specimens with 250 mm eccentricity)

227
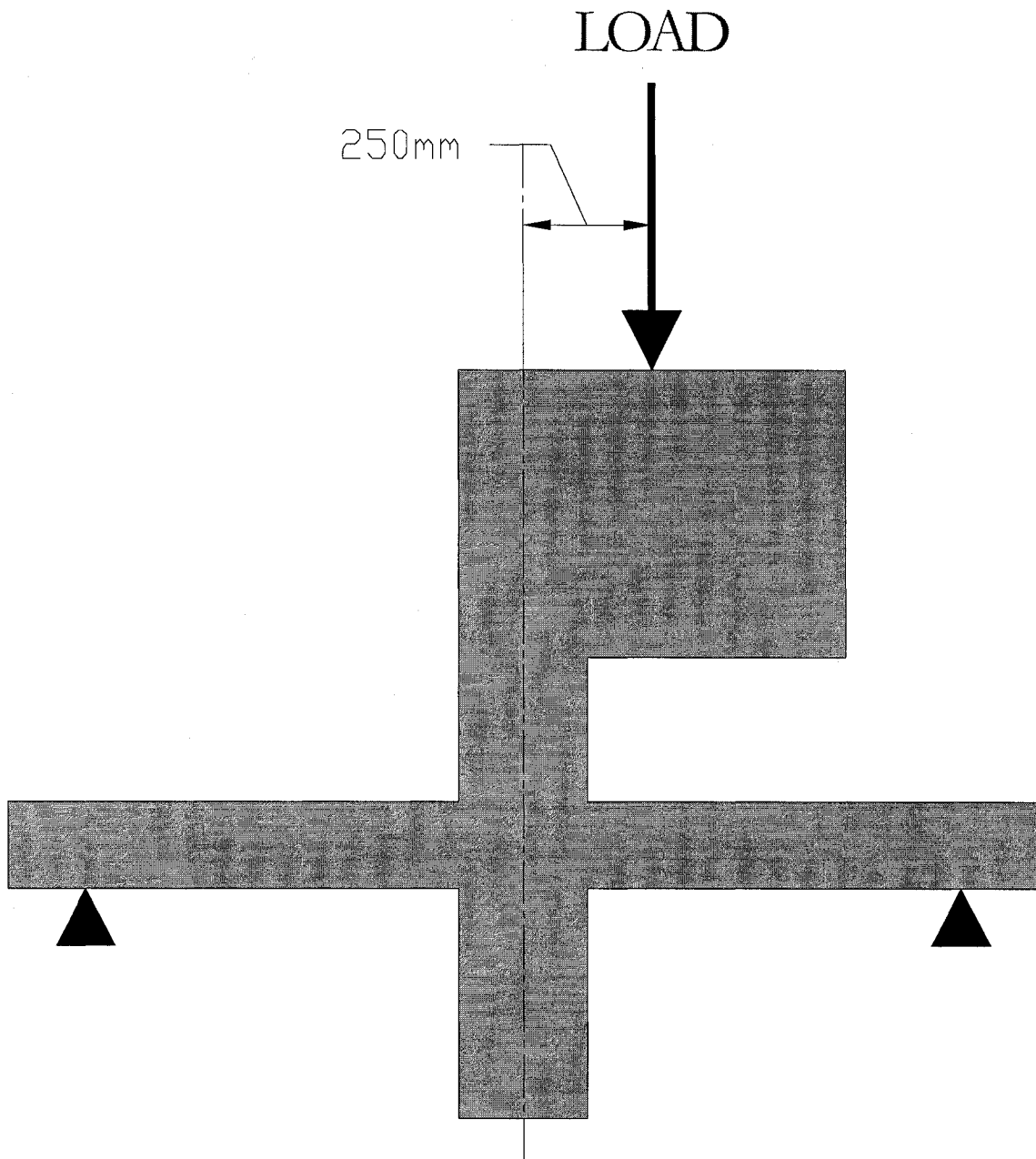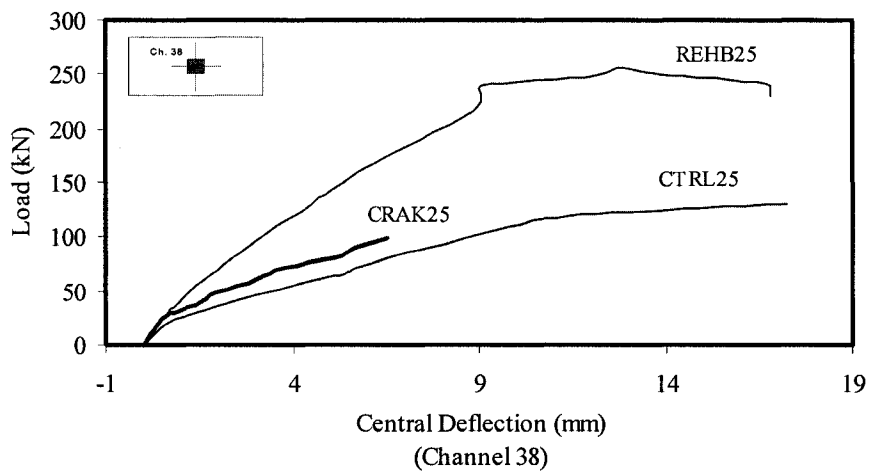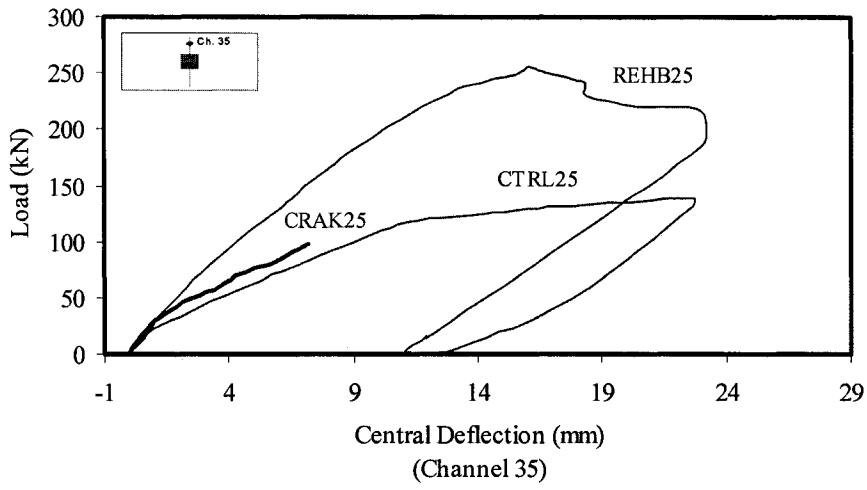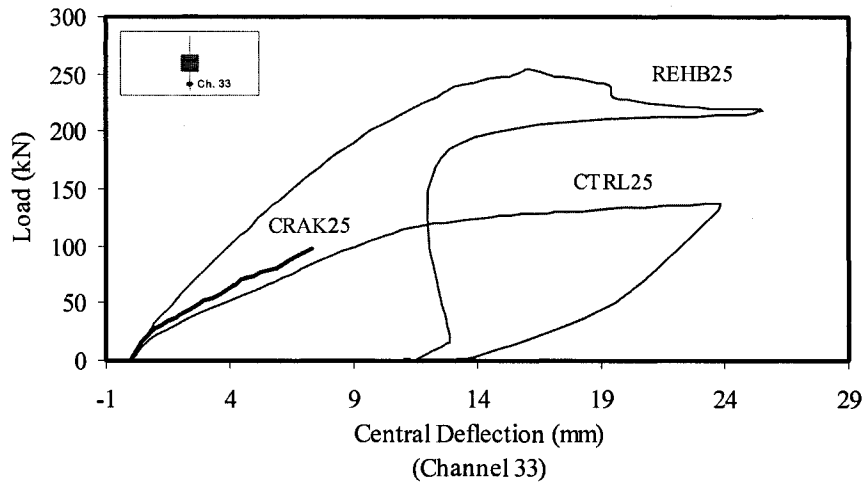
Fig. 4-56: Load versus central short direction deflection

228
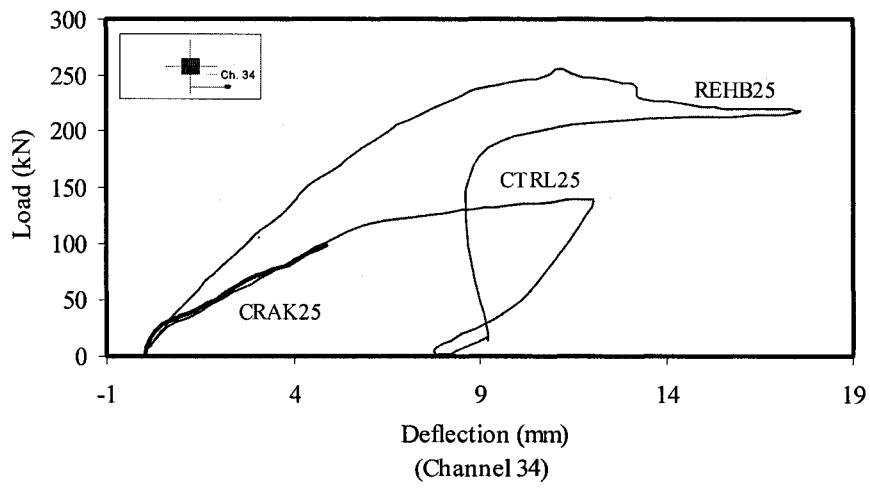
Fig. 4-57: Load versus east long direction deflection
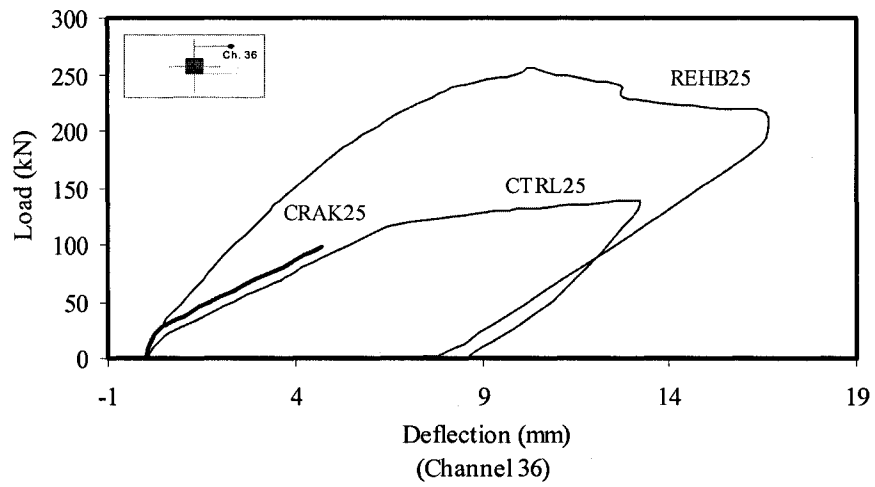
Fig. 4-58: Load versus west long direction deflection

229
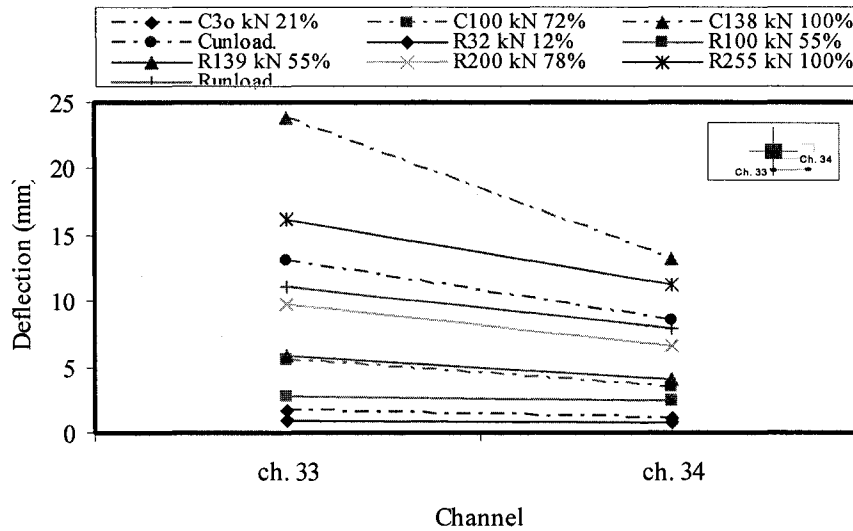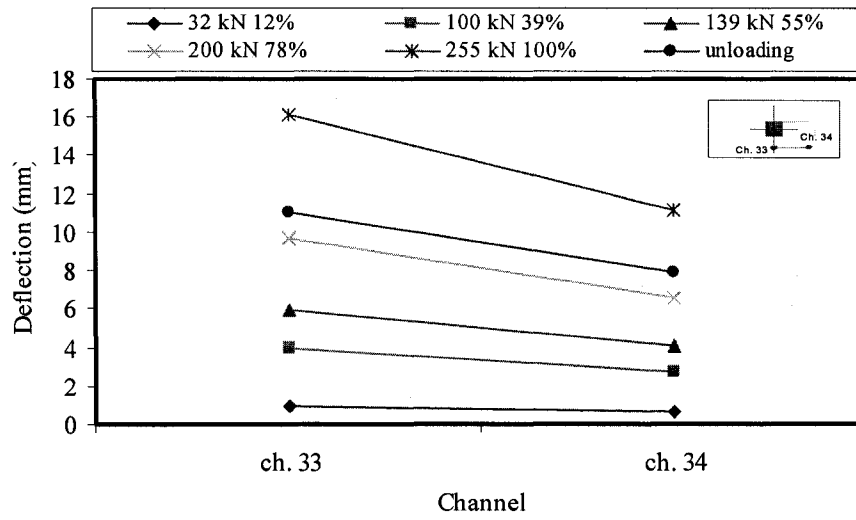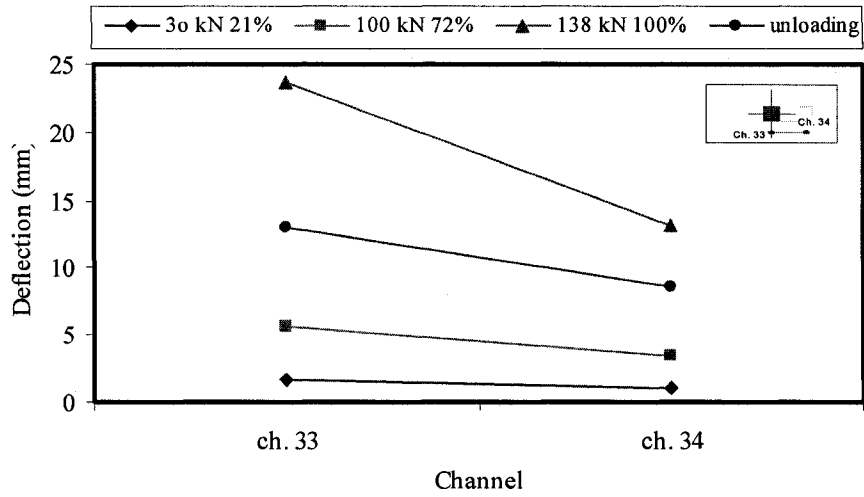
Fig. 4-59: Deflection on the east long direction for CTRL25(C), REHB25(R) and C & R

230
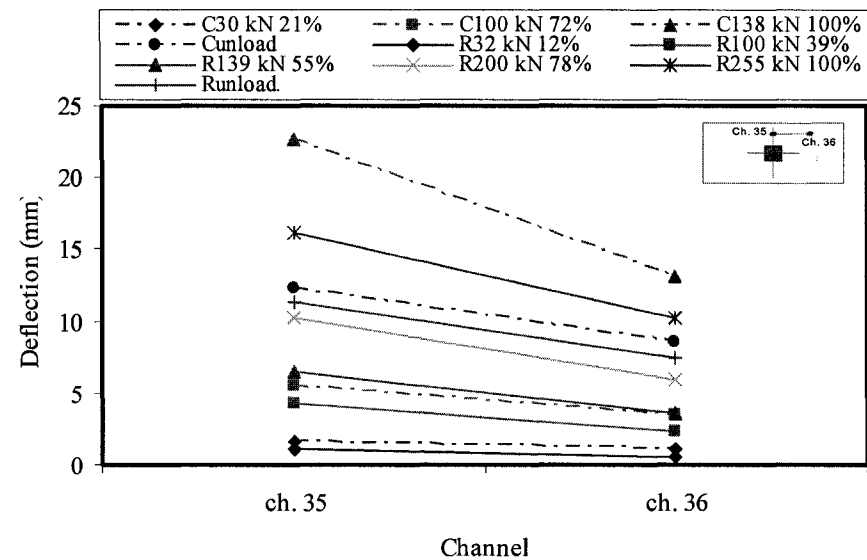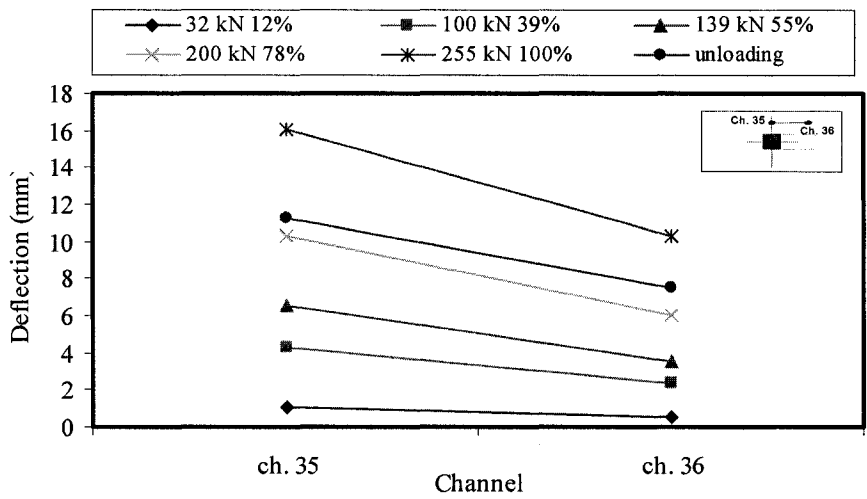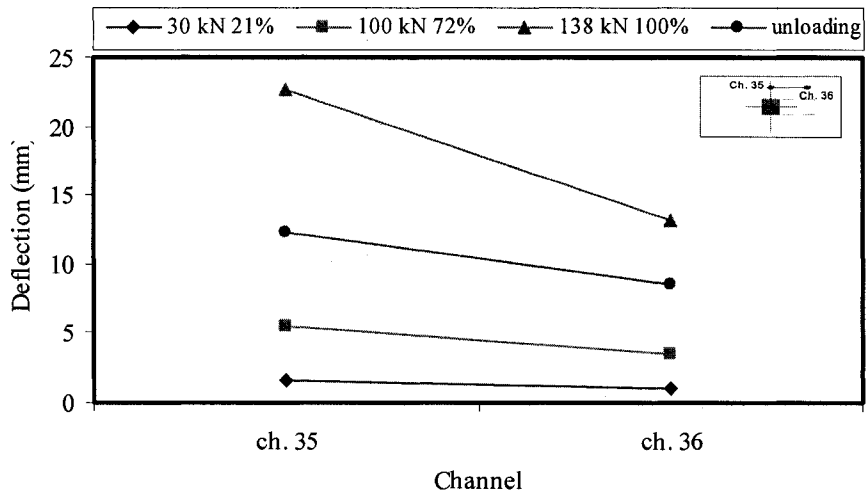
Fig. 4-60 Deflection on the west long direction for CTRL25(C), REHB25(R) and C&R

231
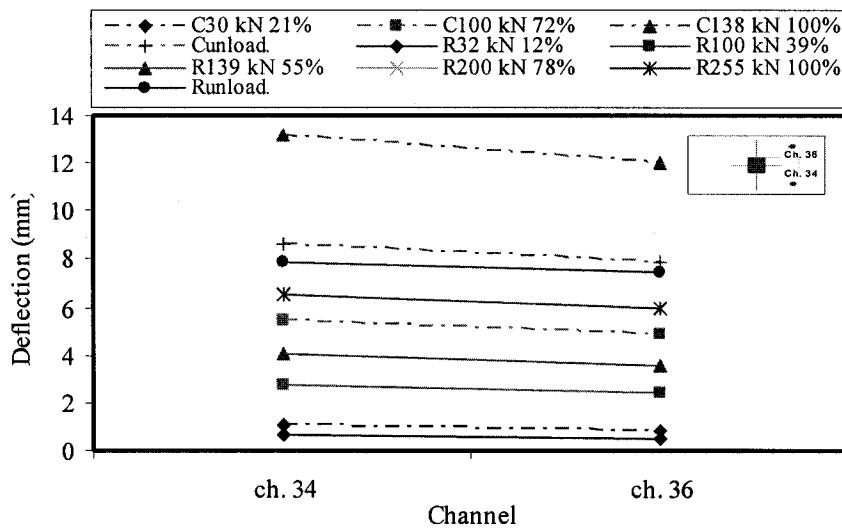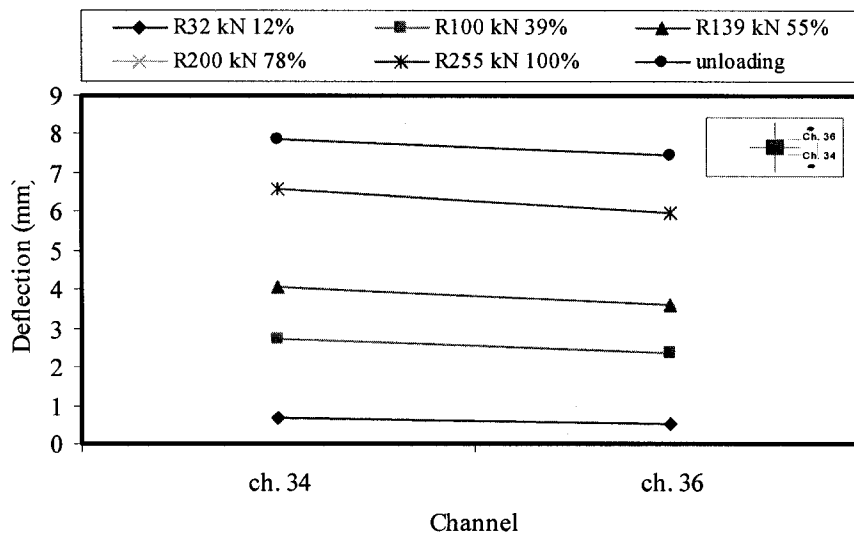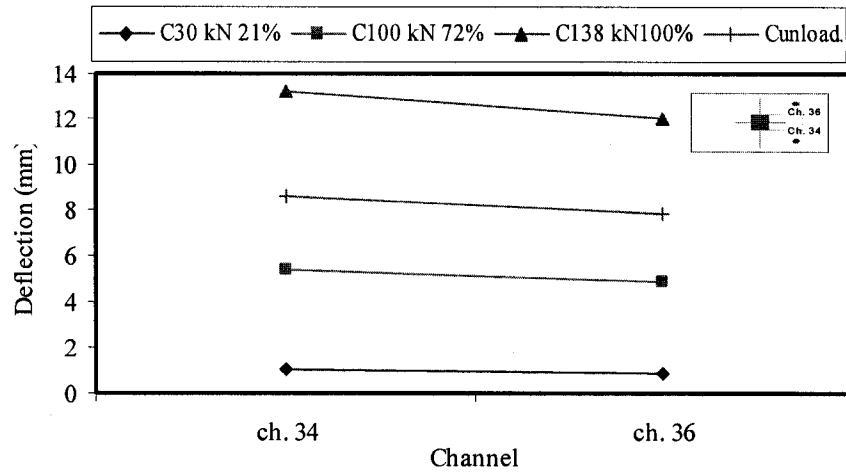
Fig. 4-61: Deflection on the north short direction for CTRL25(C), REHB25(R) and C&R

232
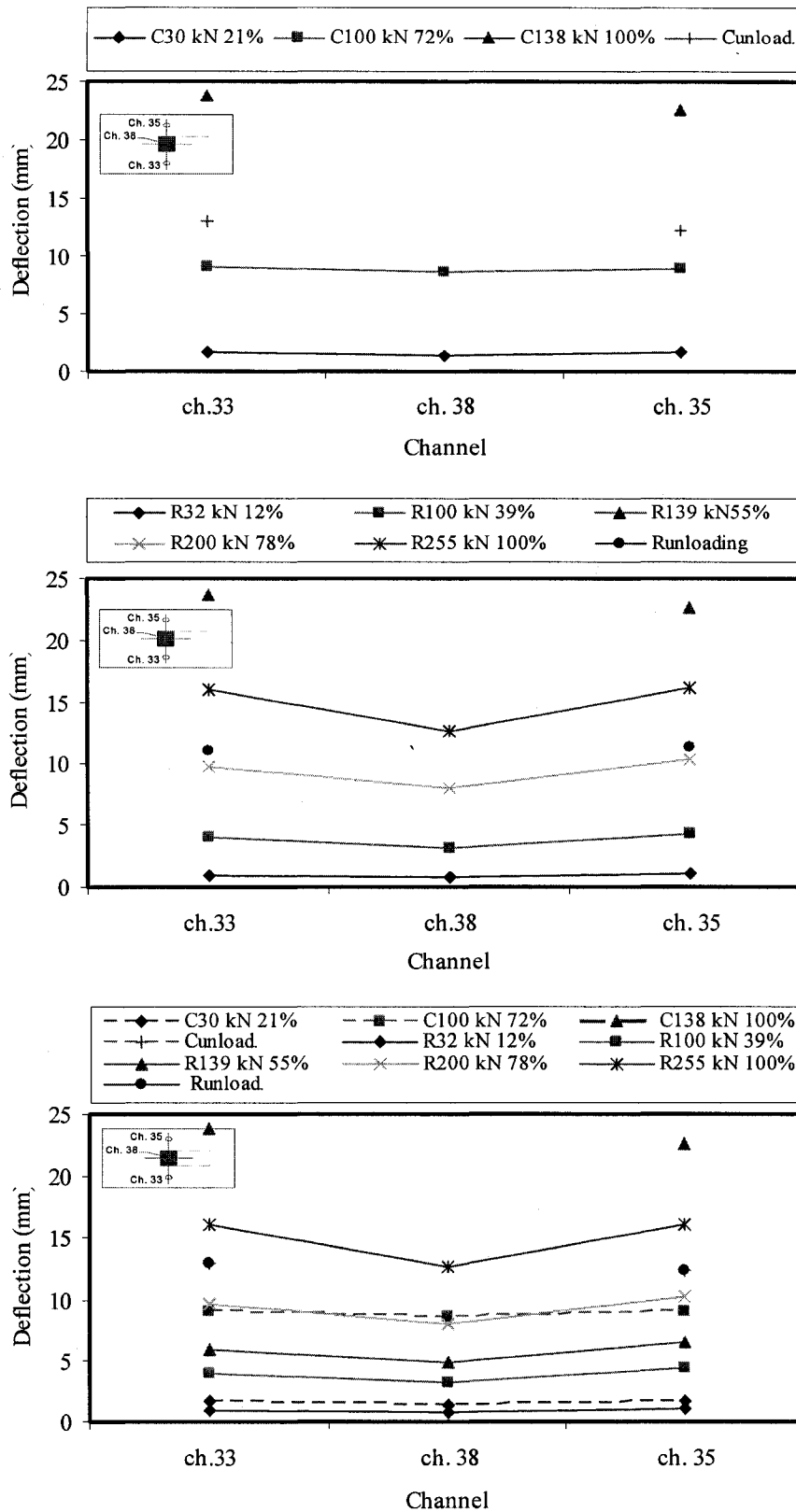
Fig. 4-62: Deflection on the central short direction for CTRL25 (C) REHB25 (R)

233
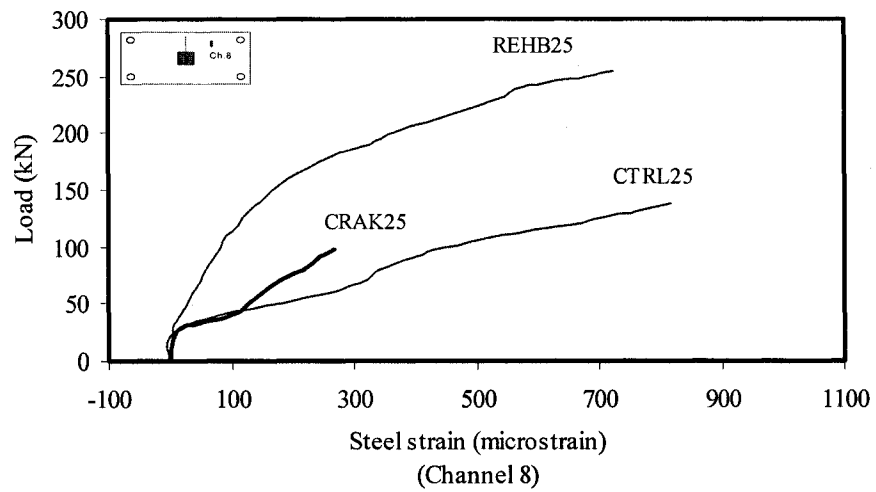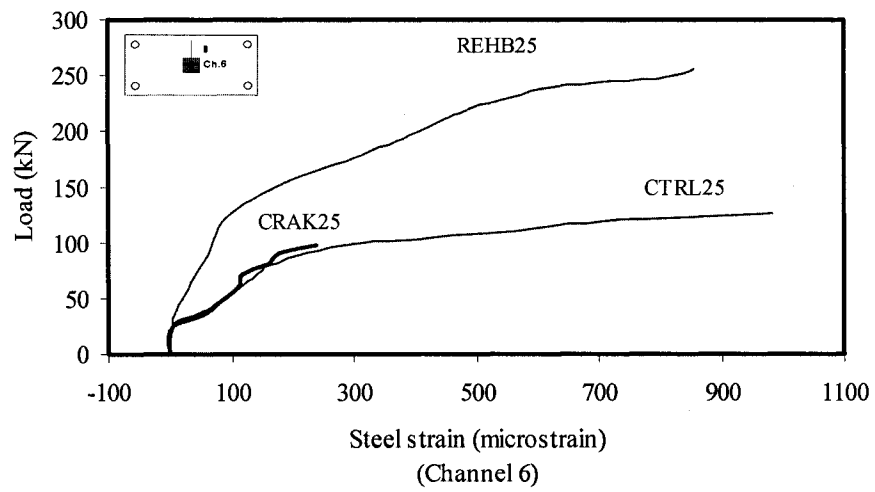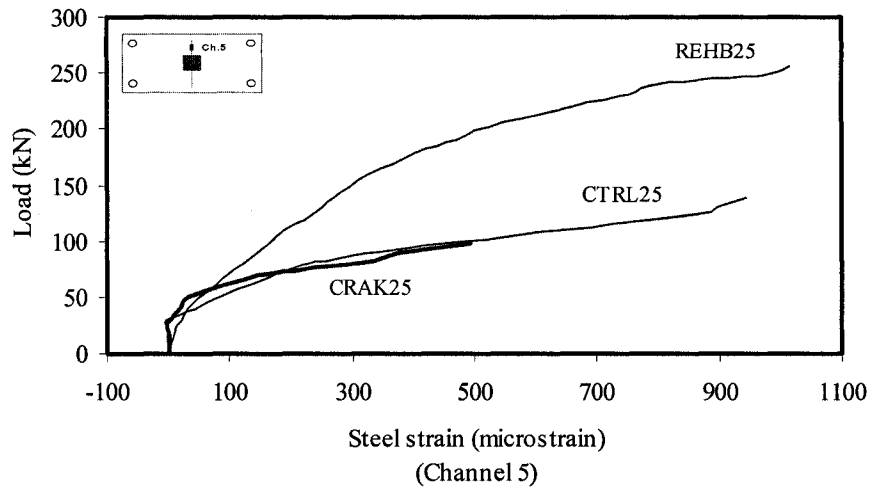
Fig. 4-63: Load versus tension short direction steel strain

234
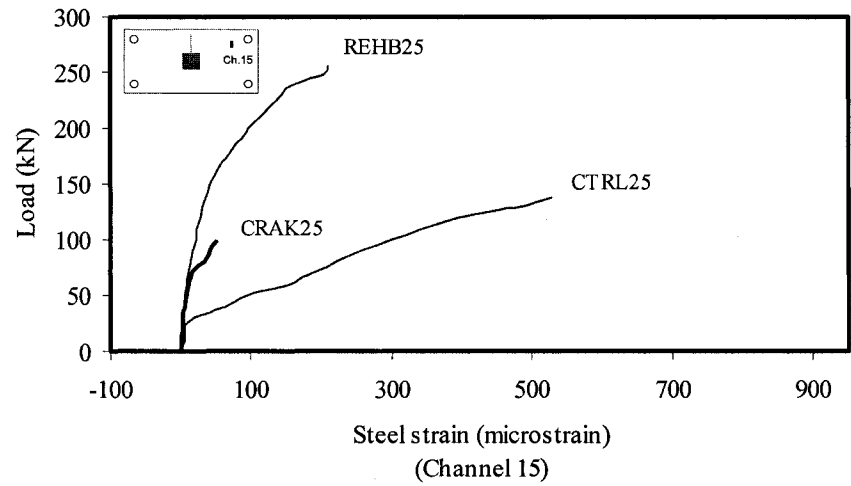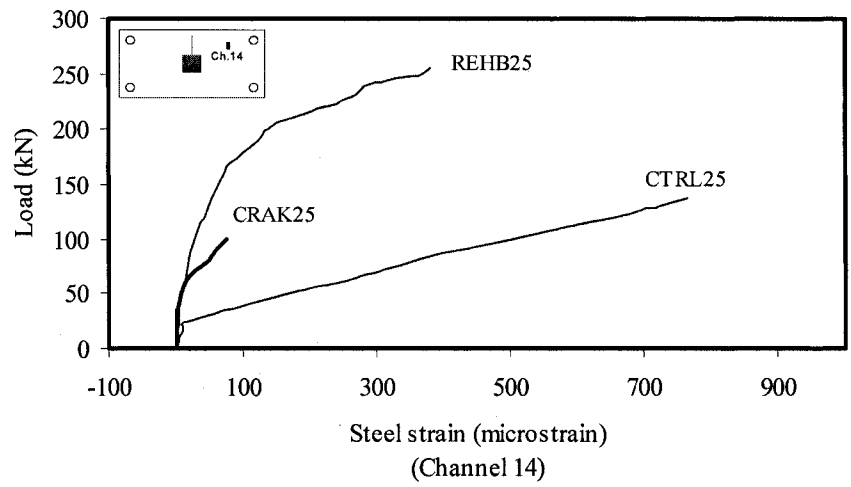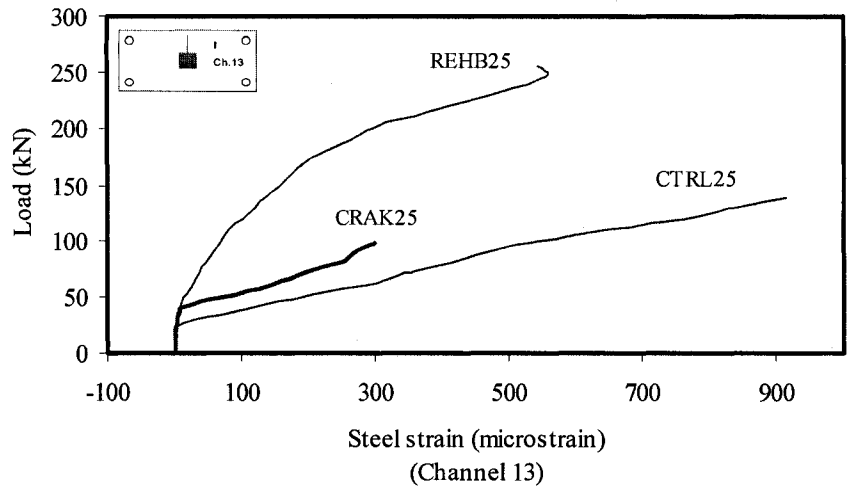
Fig. 4-64: Load versus tension short direction steel strain
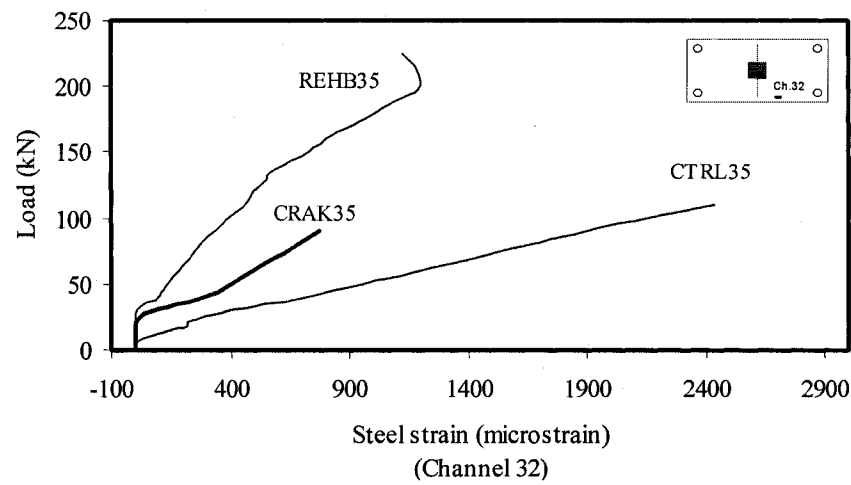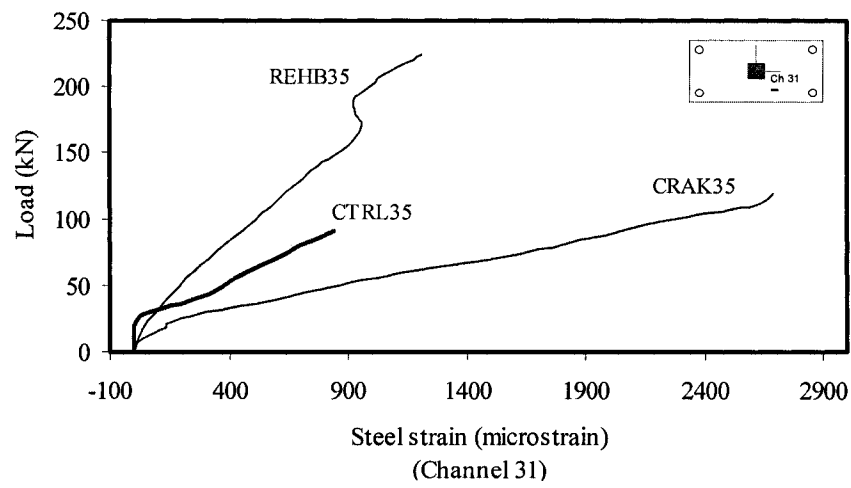
235
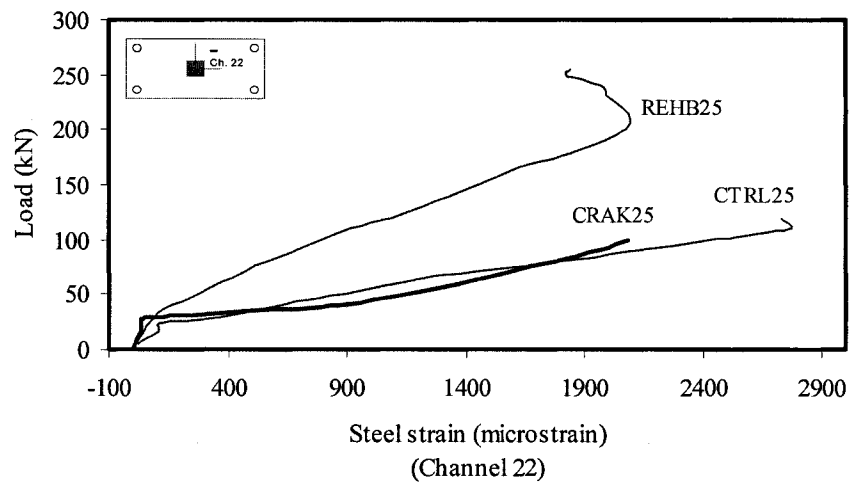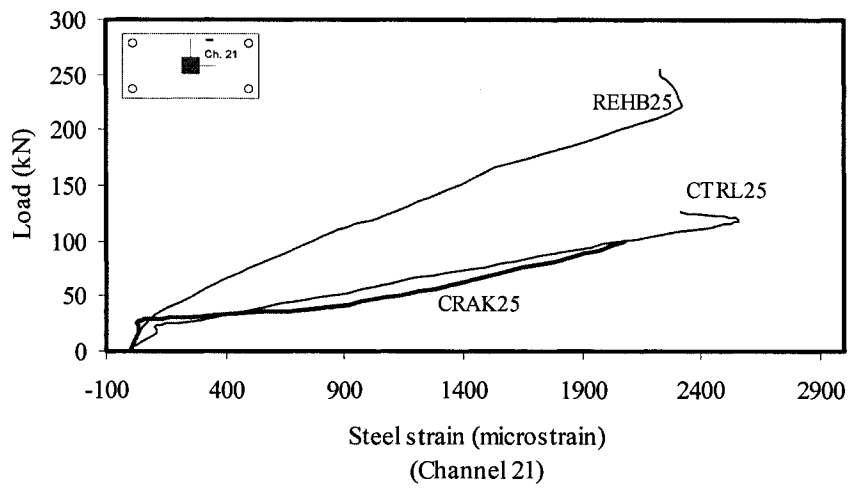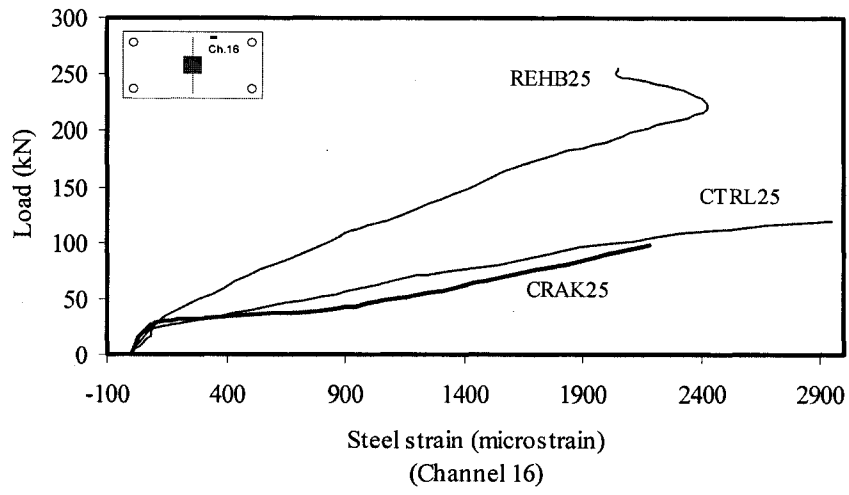
Fig. 4-65: Load versus tension long direction steel strain
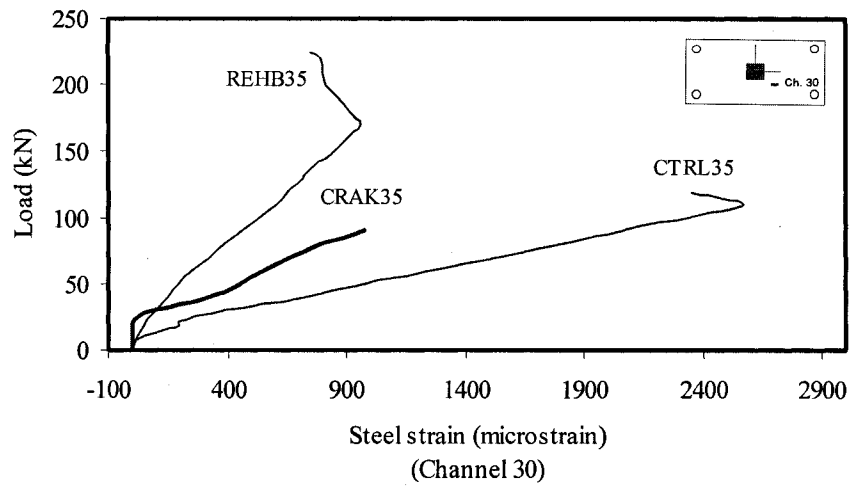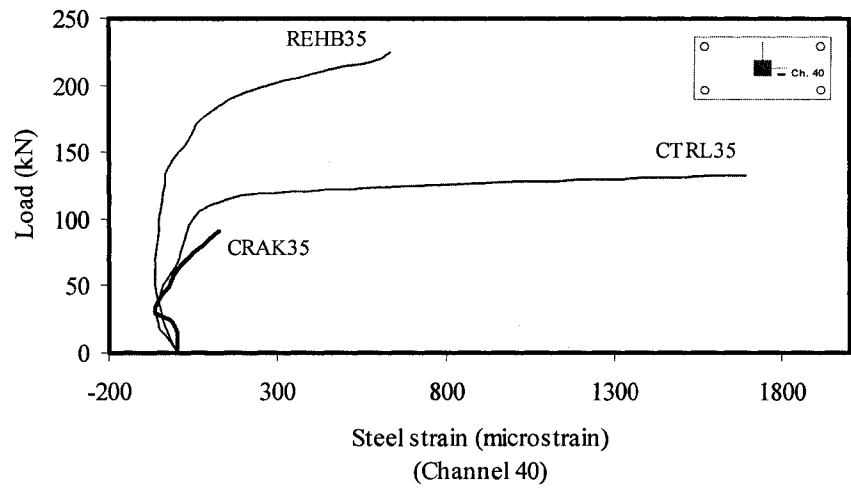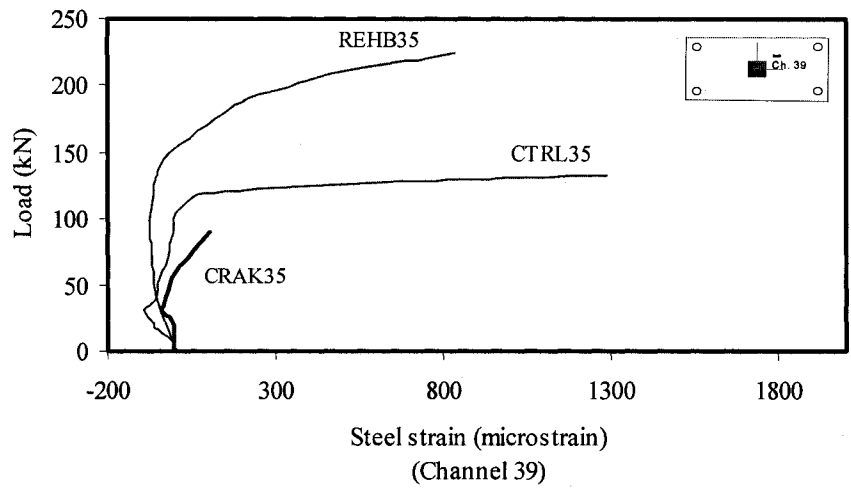
236
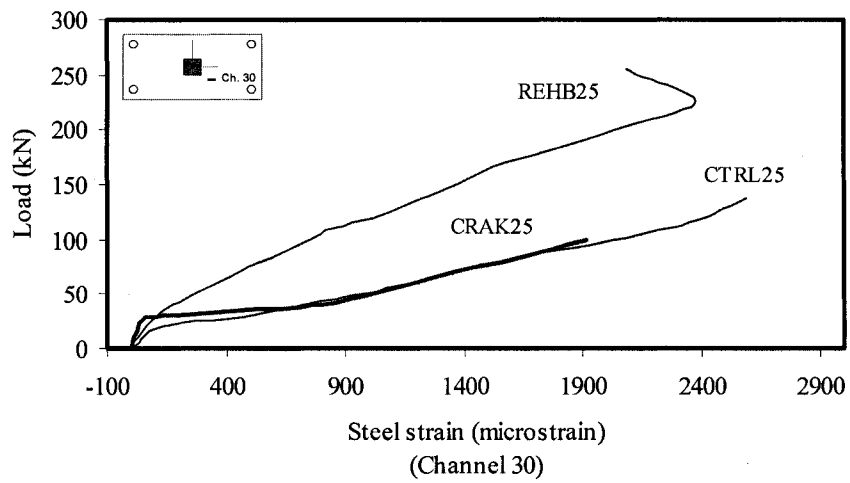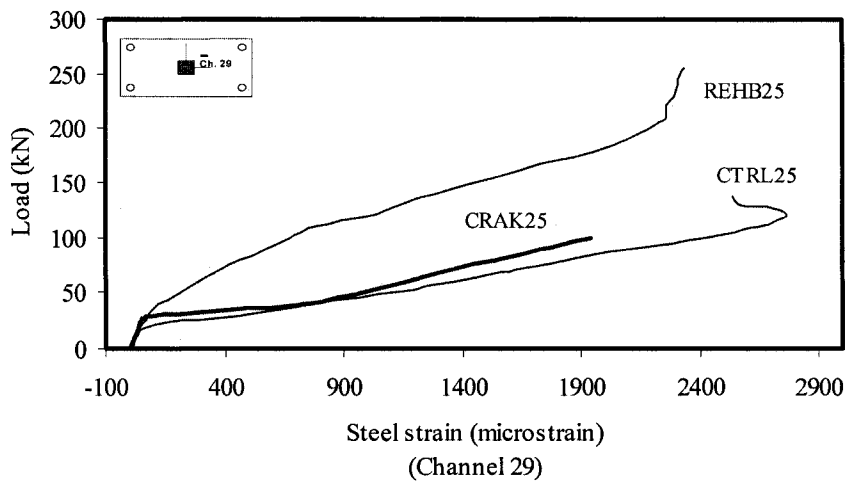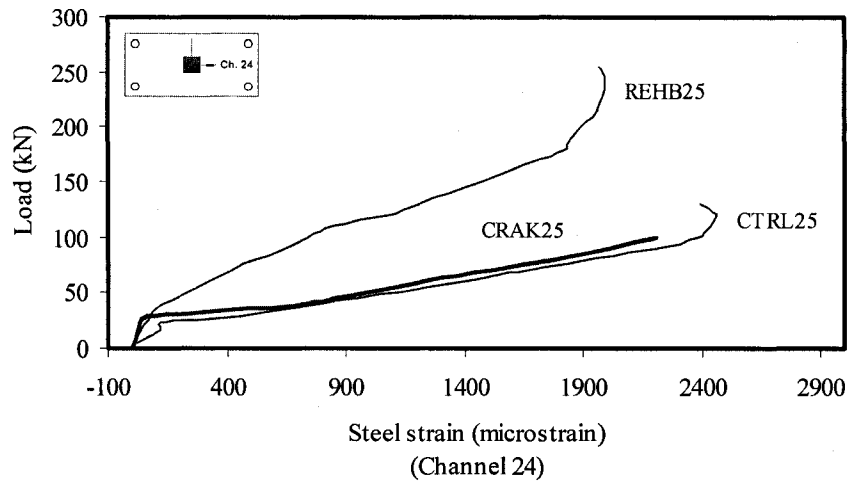
Fig. 4-66: Load versus tension long direction steel strain

237
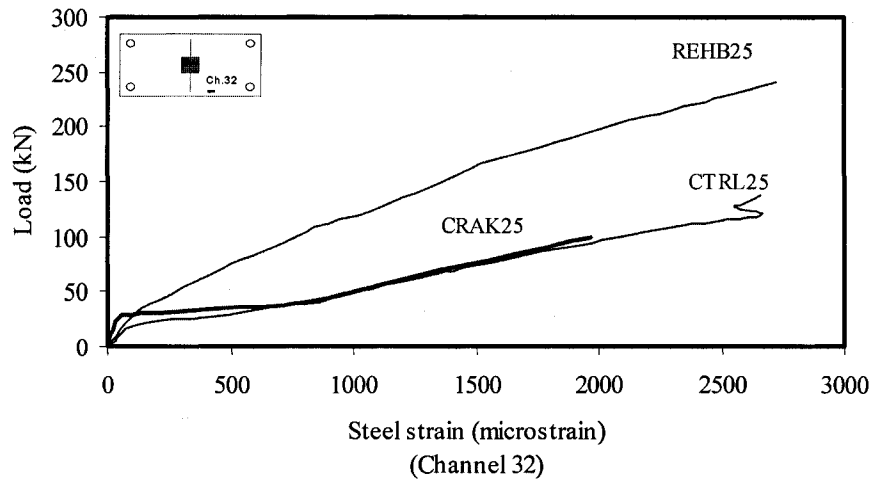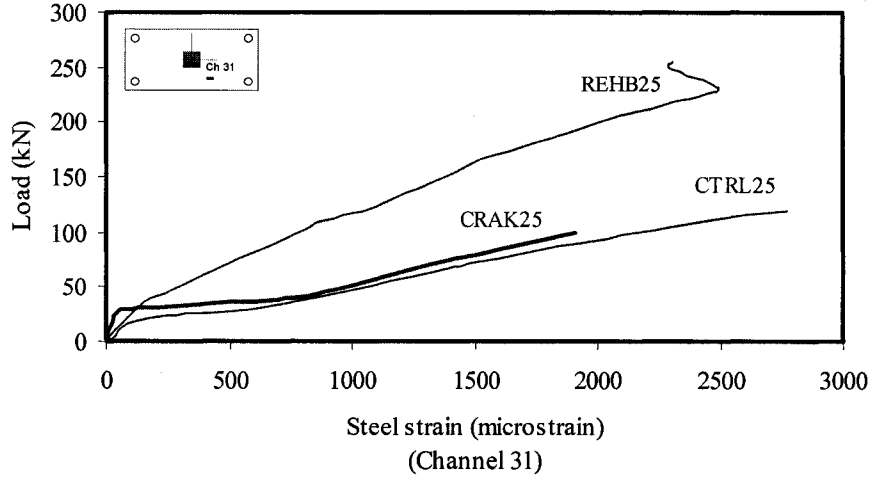
Fig. 4-67: Load versus tension long direction steel strain

238
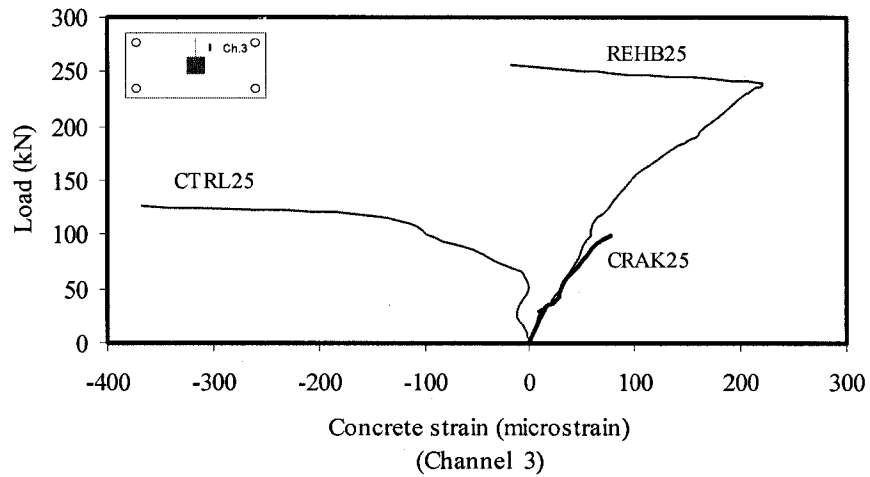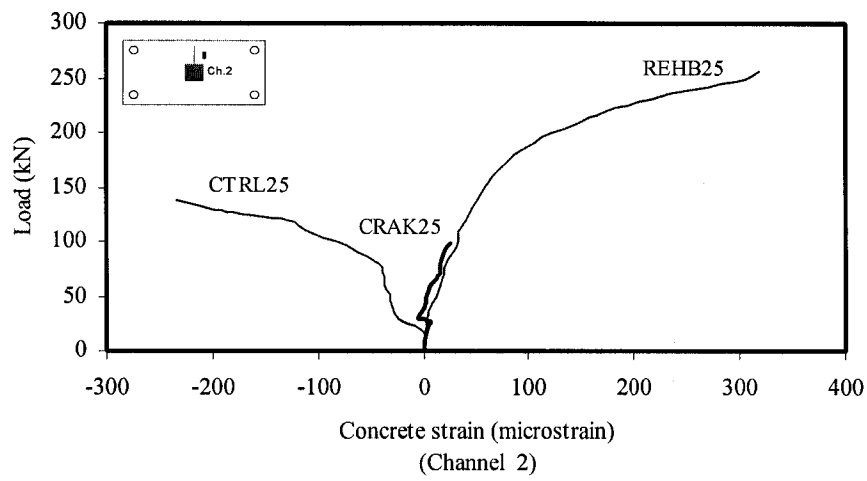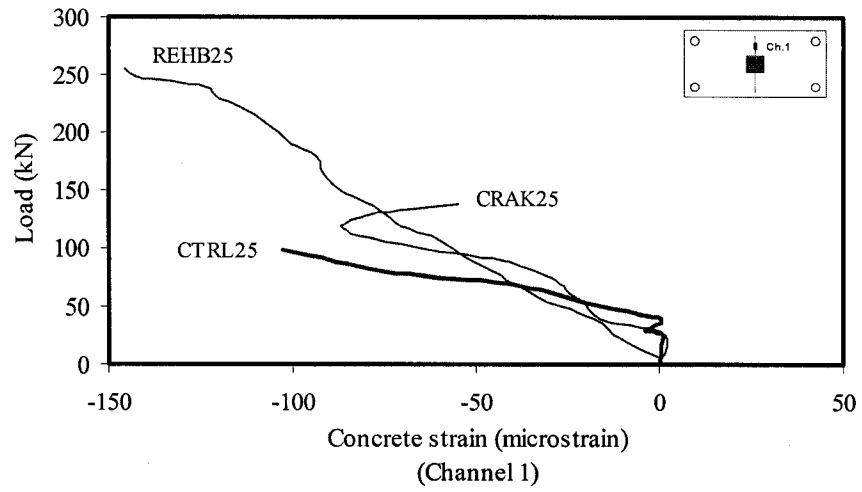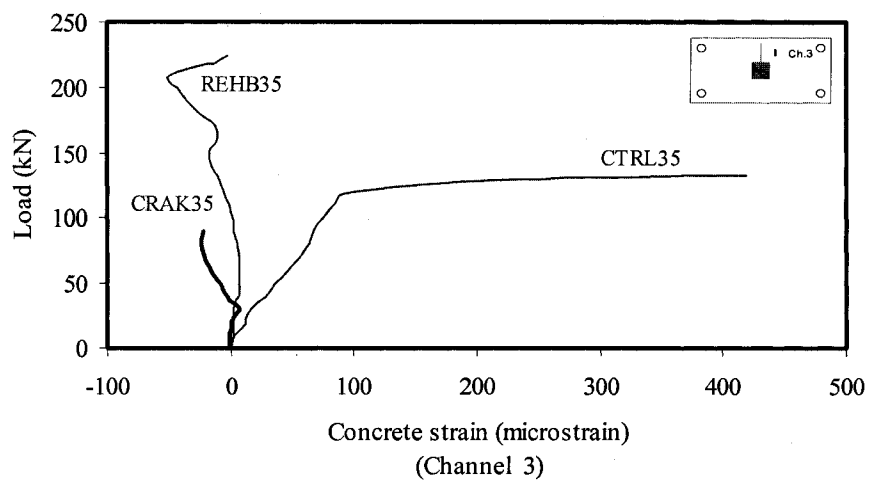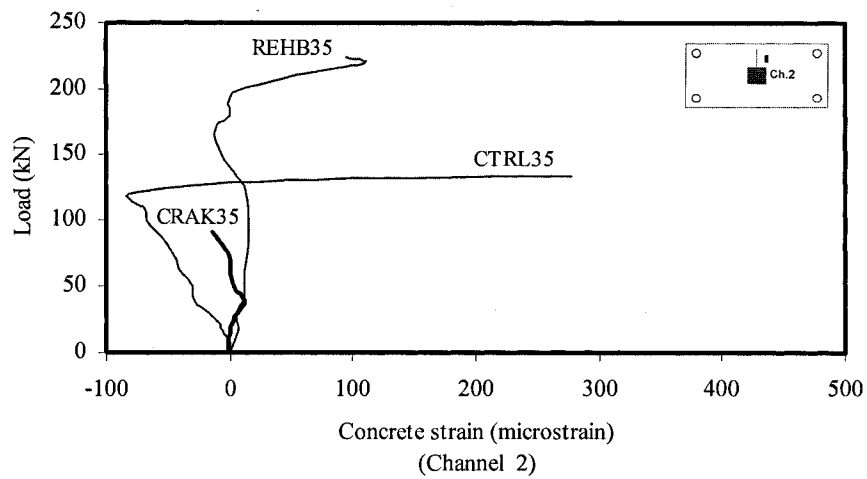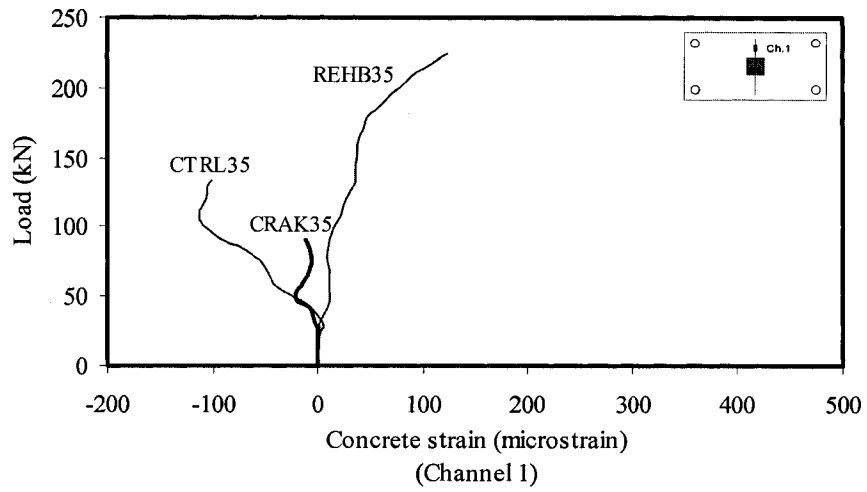
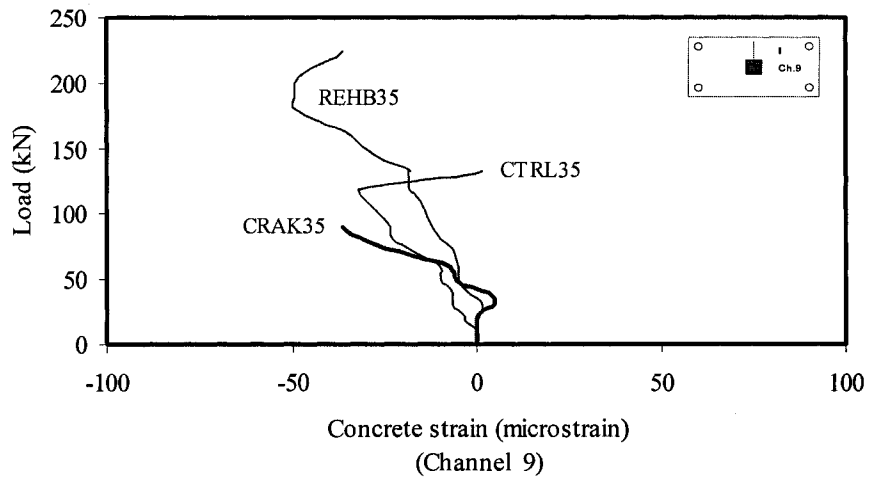Fig. 4-67: Load versus short direction concrete strain

239
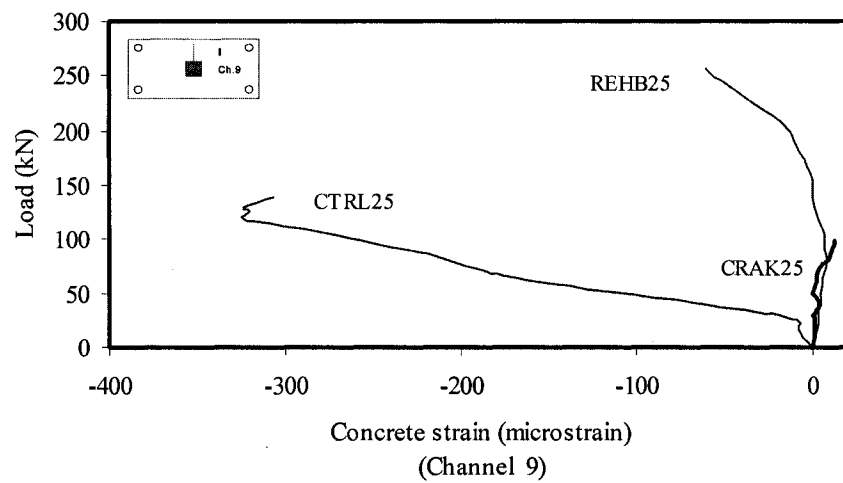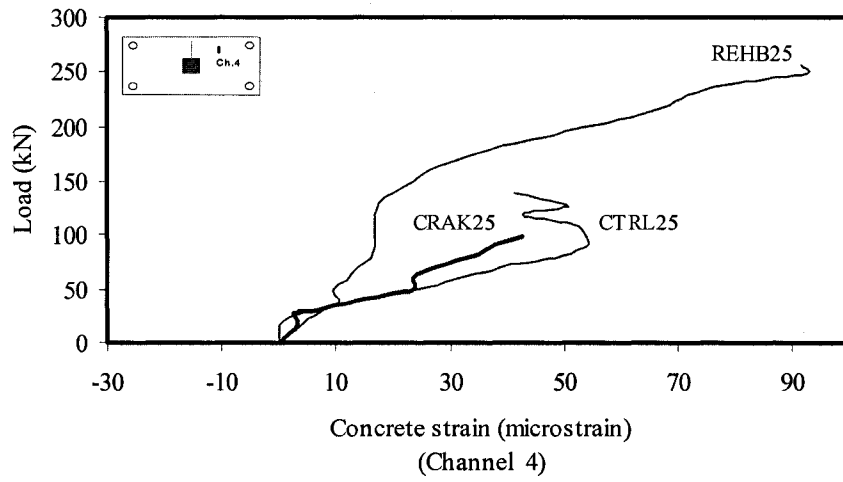
Fig. 4-68: Load versus short direction concrete strain

240
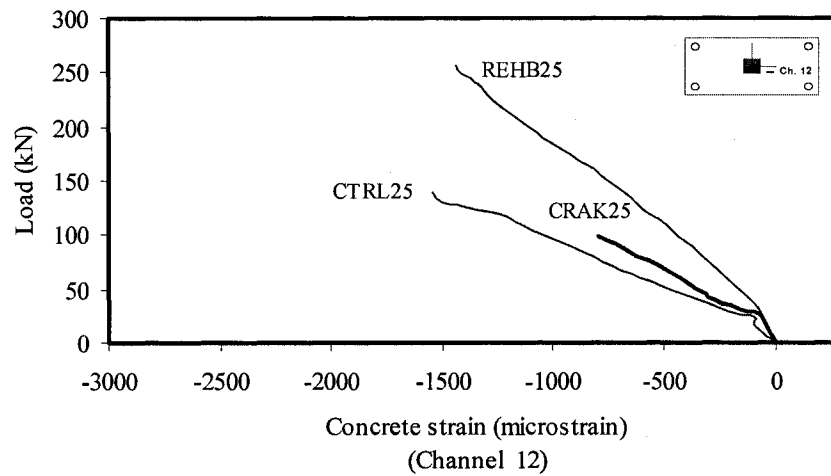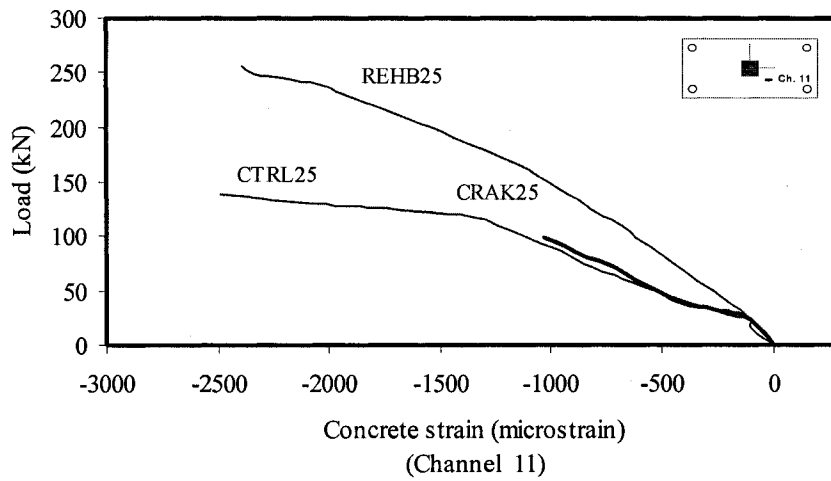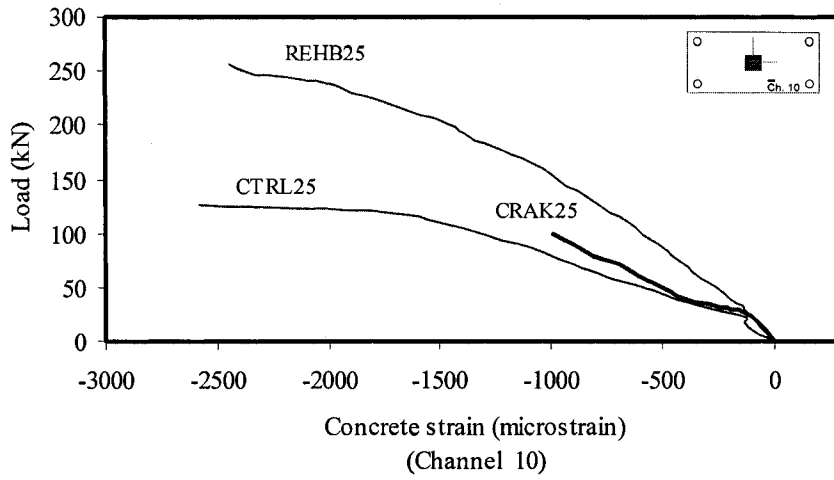
Fig. 4-69: Load versus compression long direction concrete strain

241
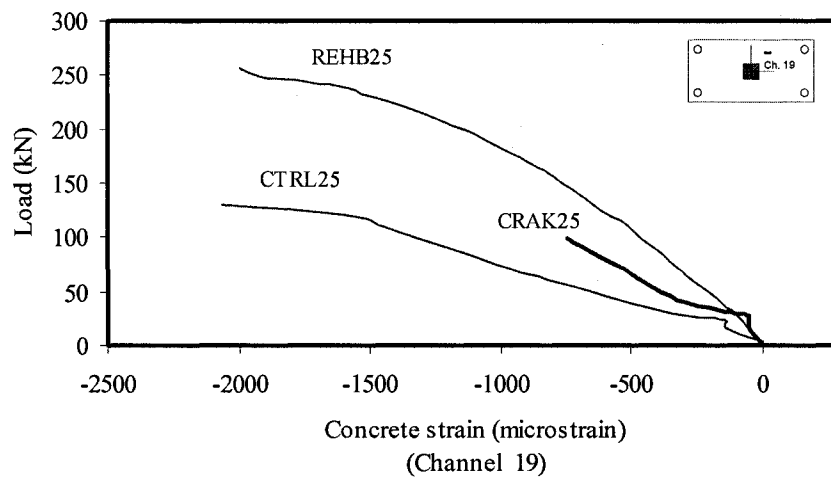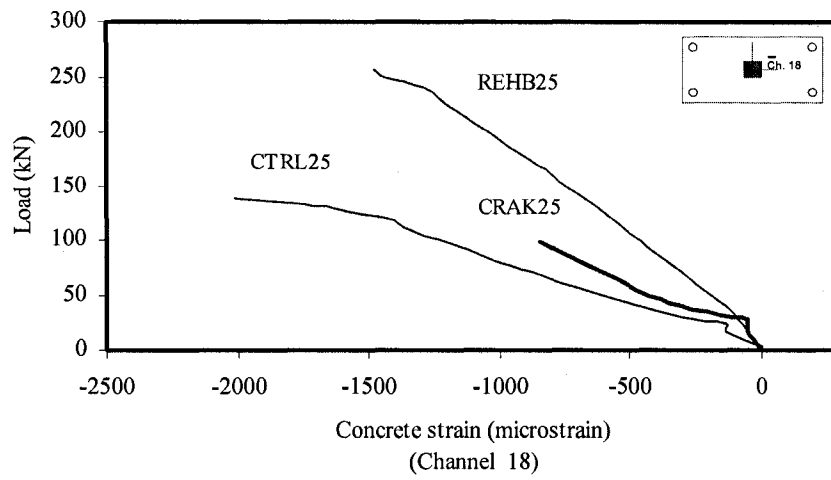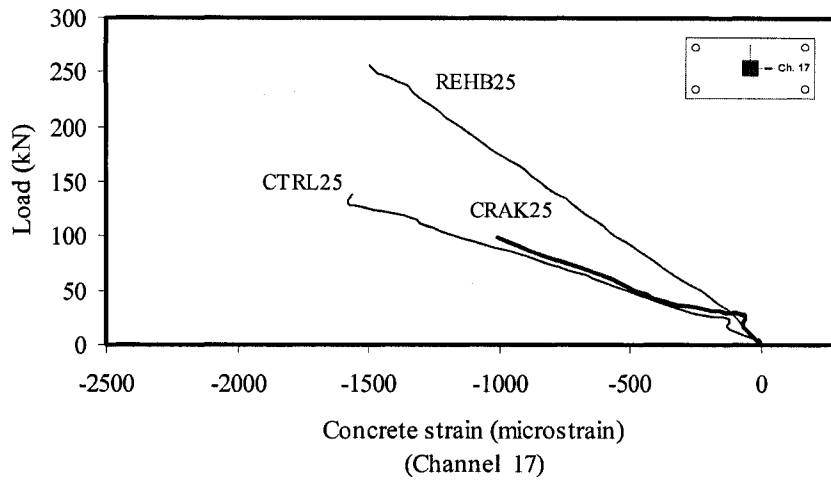
Fig. 4-70: Load versus compression long direction concrete strain

242
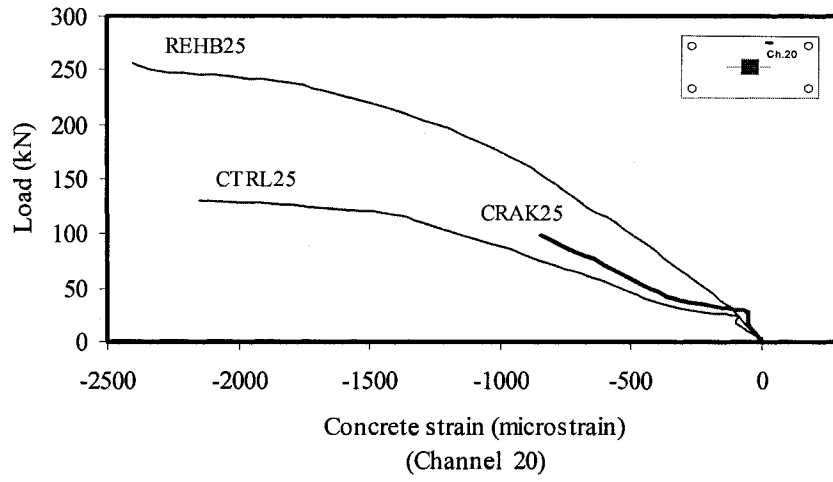
Fig. 4-71: Load versus compression long direction concrete strain

243
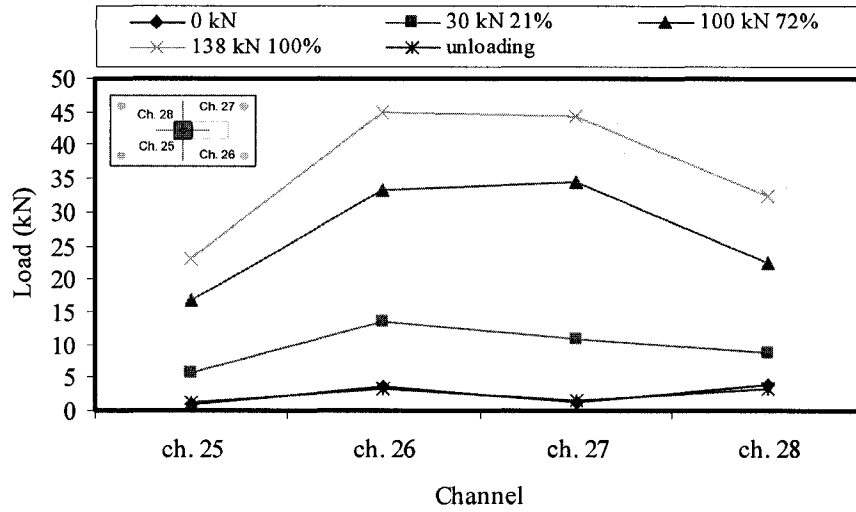
Fig. 4-72: Load distribution on each reaction for the control specimen (CTRL25)
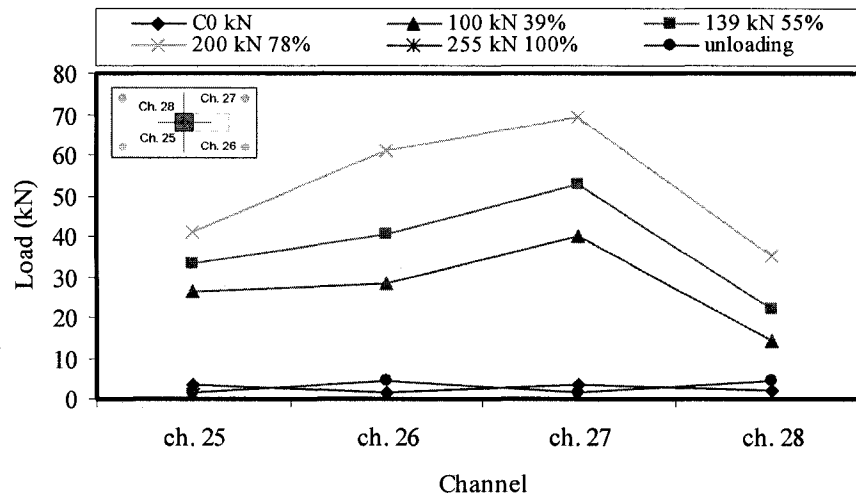
Fig. 4-73: Load distribution on each reaction for the rehabilitated specimen (REHB25)

244
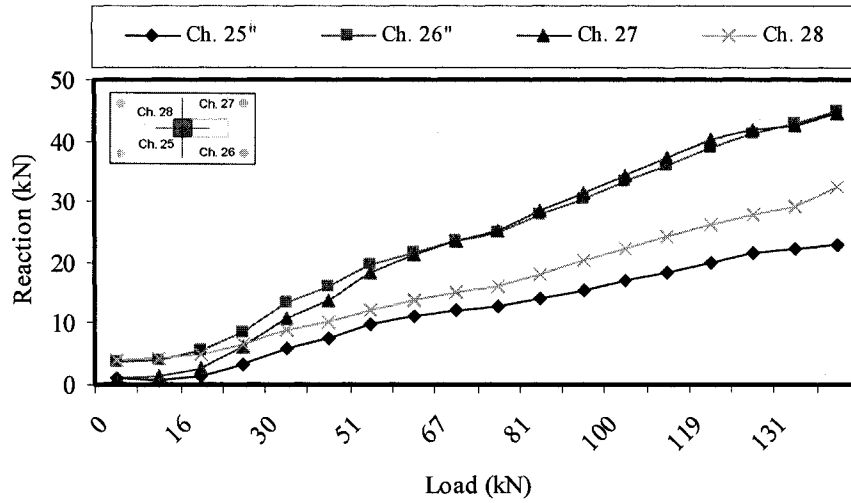
Fig. 4-74: Reaction distribution for the control specimen (CTRL25)
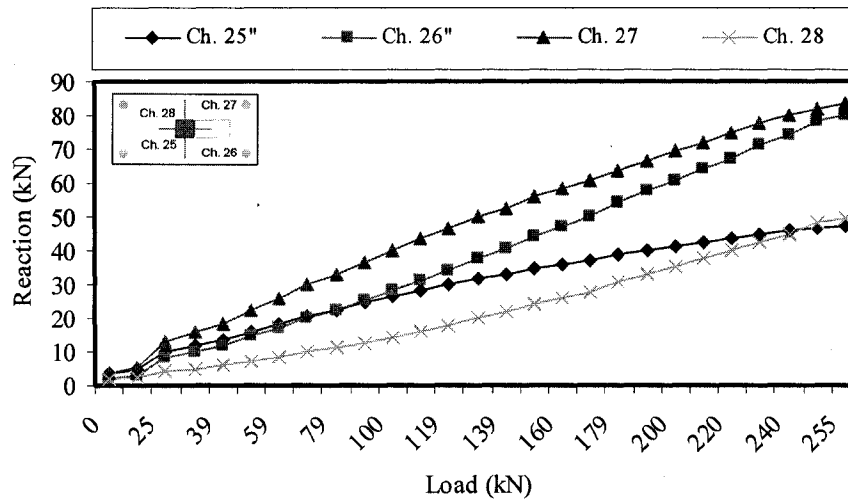
Fig. 4-75: Reaction distribution for the rehabilitated specimen (REHB25)

245
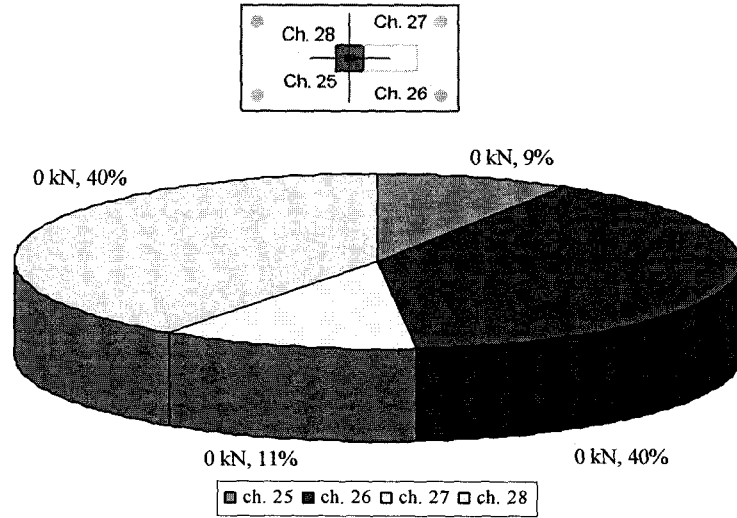
Fig. 4-76: Percentage of load on each reaction before loading (CTRL25)
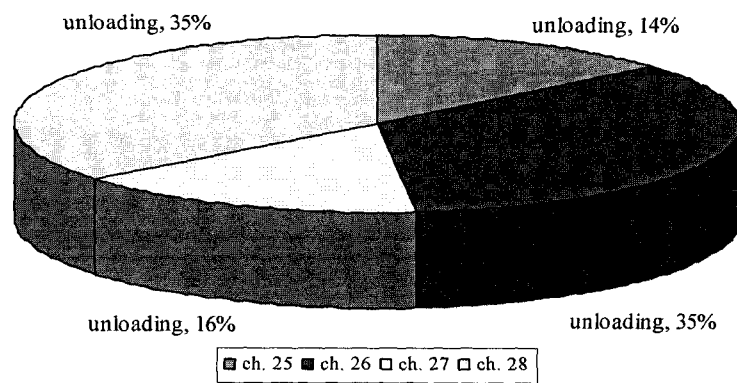
Fig. 4-77: Percentage of load on each reaction after unloading (CTRL25)
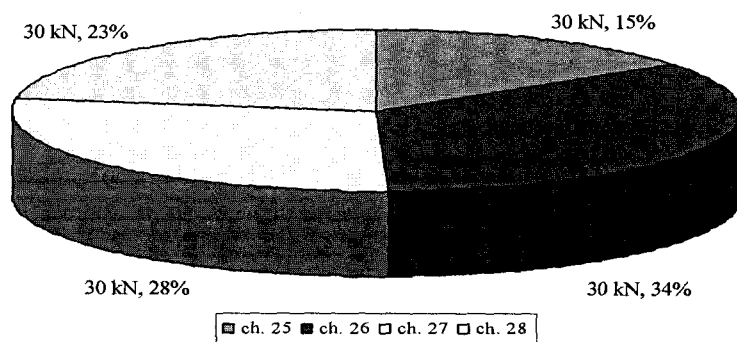
Fig. 4-78: Percentage of load on each reaction at cracking load (CTRL25)

246

100 kN, 21%   100 kN, 16%

100 kN, 32%   100 kN, 31%

ch. 25   ch. 26   ch. 27   ch. 28
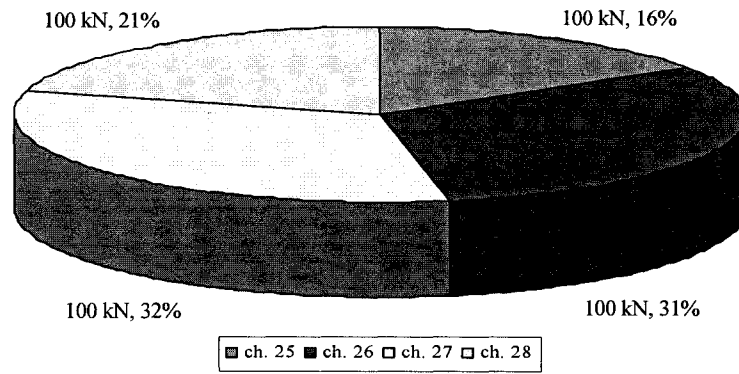
Fig. 4-79: Percentage of load on each reaction at steel yielding (CTRL25)

138 kN, 22%   138 kN, 16%

138 kN, 31%   138 kN, 31%

ch. 25   ch. 26   ch. 27   ch. 28
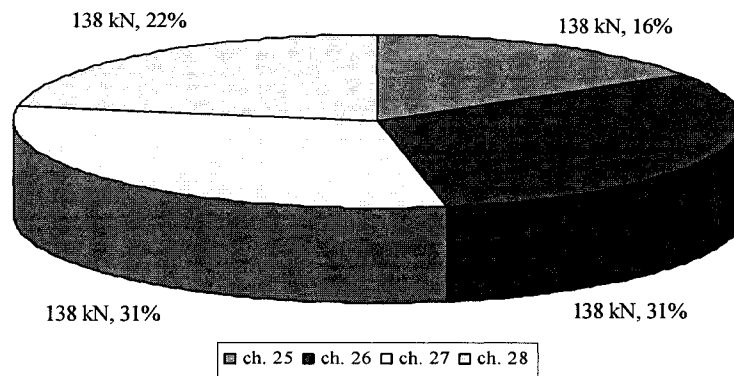
Fig. 4-80: Percentage of load on each reaction at ultimate load (CTRL25)

0 kN, 19%   0 kN, 33%

0 kN, 32%   0 kN, 16%

ch. 25   ch. 26   ch. 27   ch. 28
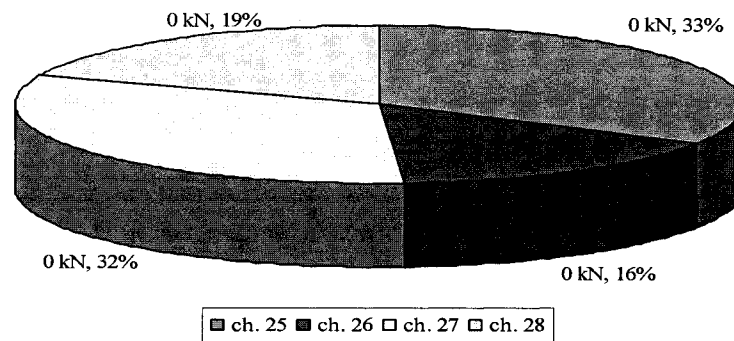
Fig. 4-81: Percentage of load on each reaction before loading (REHB25)

247
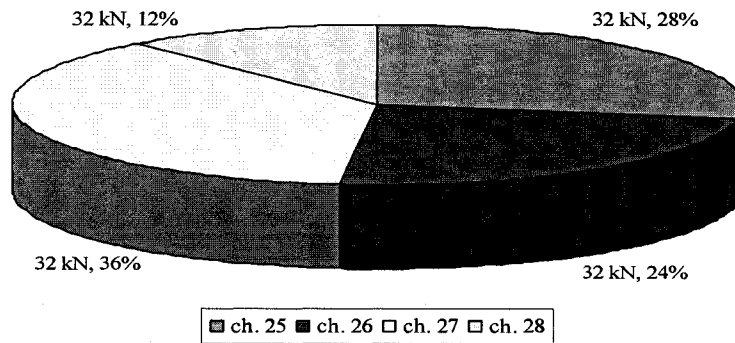
Fig. 4-82: Percentage of load on each reaction at 32 kN (REHB)
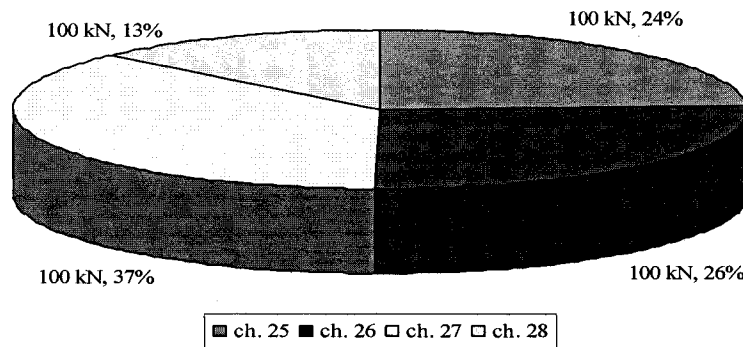
Fig. 4-83: Percentage of load on each reaction at 100 kN (REHB25)
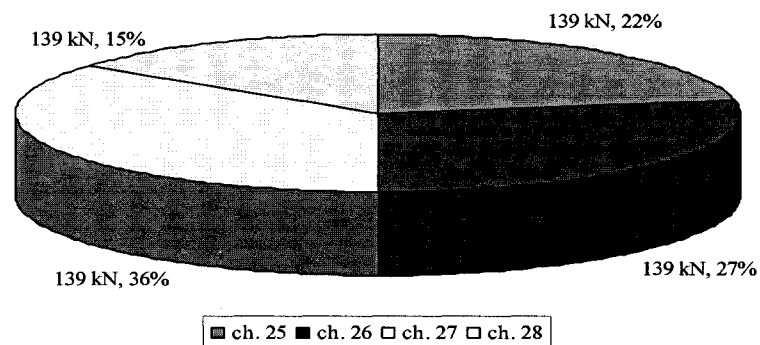
Fig. 4-84: Percentage of load on each reaction at 139 kN (REHB25)

248
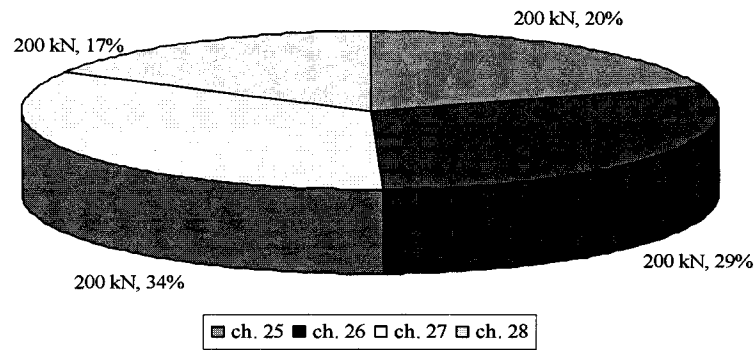
Fig. 4-85: Percentage of load on each reaction at tension steel yielding for

the rehabilitated specimen (REHB25)
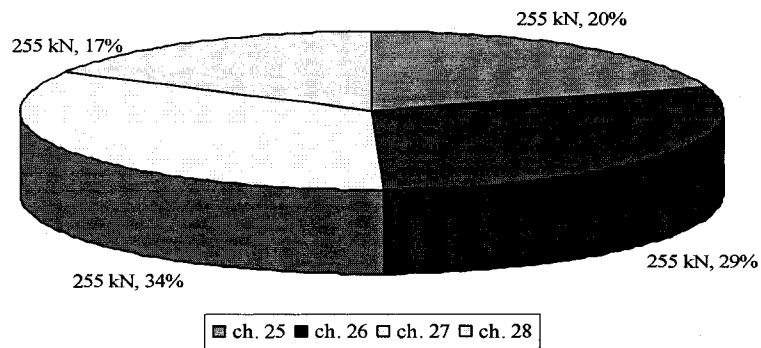
Fig. 4-86: Percentage of load on each reaction at ultimate load for

the rehabilitated specimen (REHB25)

249
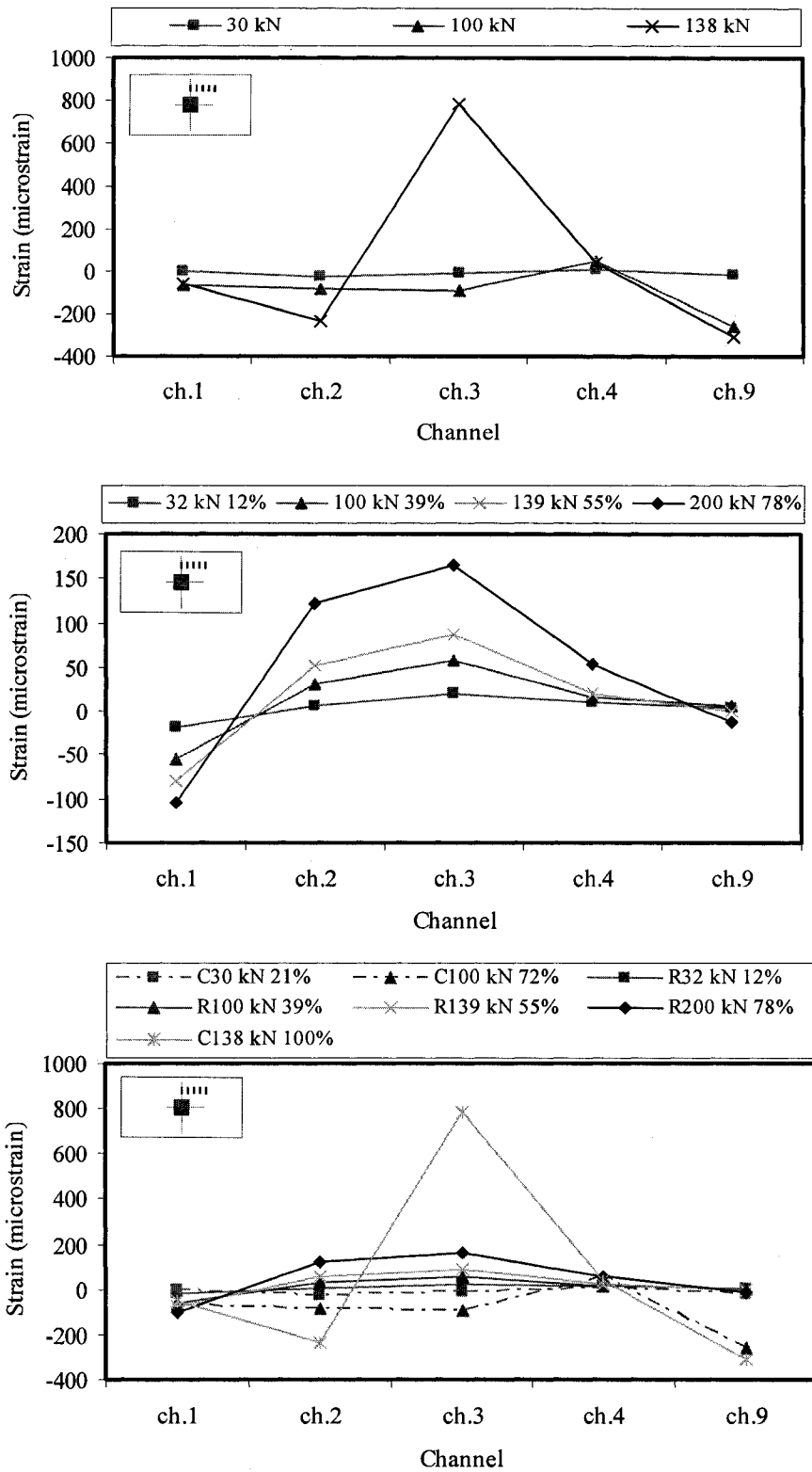
Fig. 4-87: Load versus short direction concrete strain CTRL25(C), REHB25(R) and C&R

250
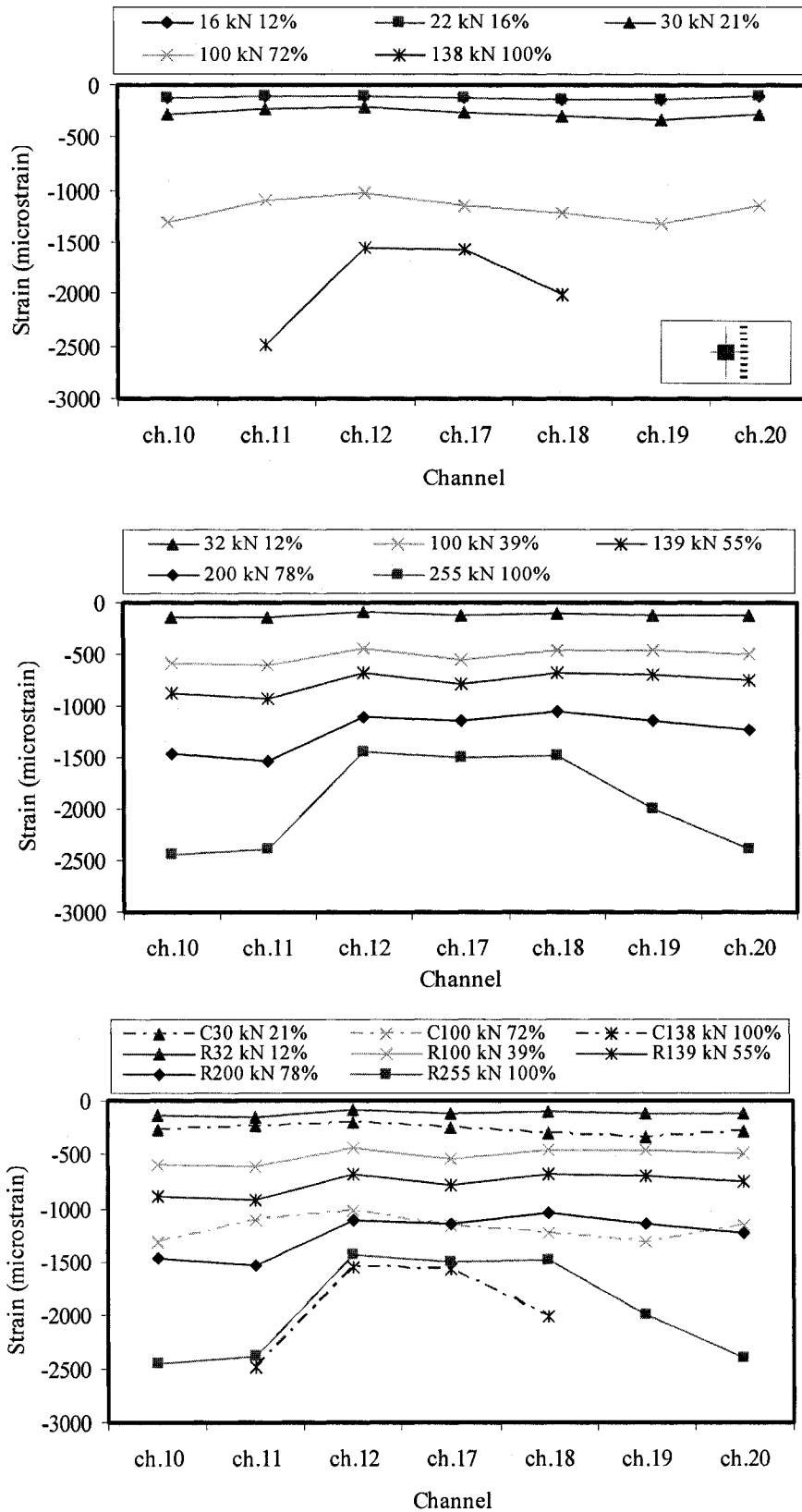
Fig. 4-88: Load versus long direction concrete strain CTRL25(C), REHB25(R) and C&R

251
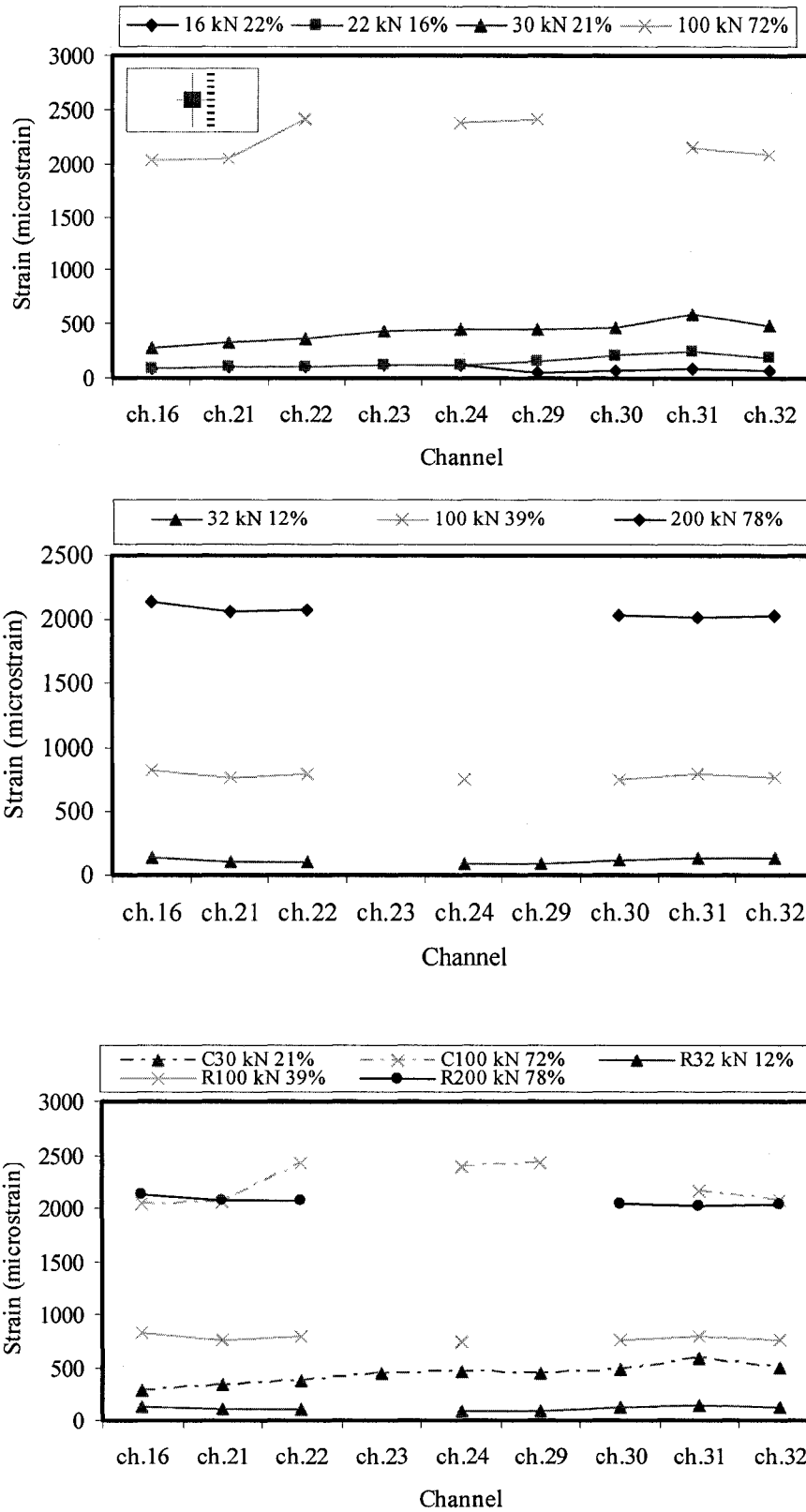
Fig. 4-89: Load versus long direction steel strain CTRL25(C), REHB25(R) and C&R

252
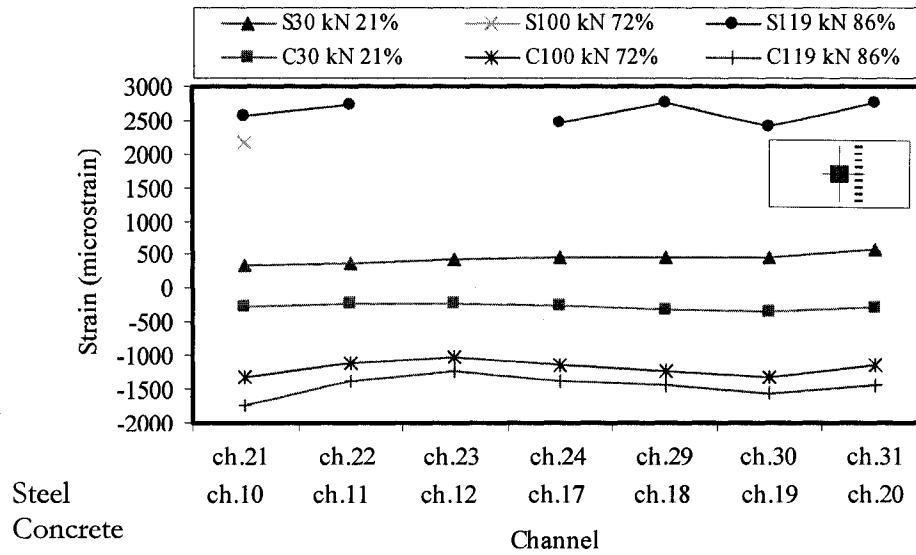
Fig. 4-90: Concrete and Steel strain readings on the long direction

Control specimen (CTRL25)
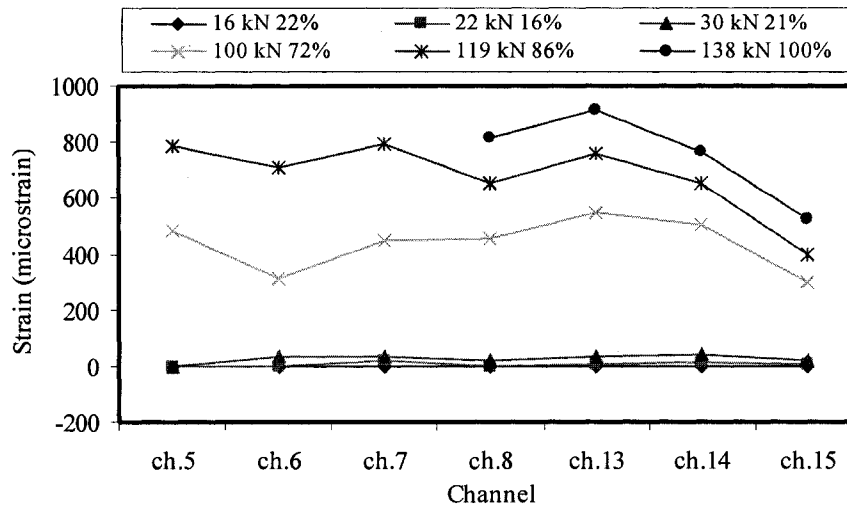
Fig. 4-91: Load versus short direction steel strain

Control specimen (CTRL25)

253
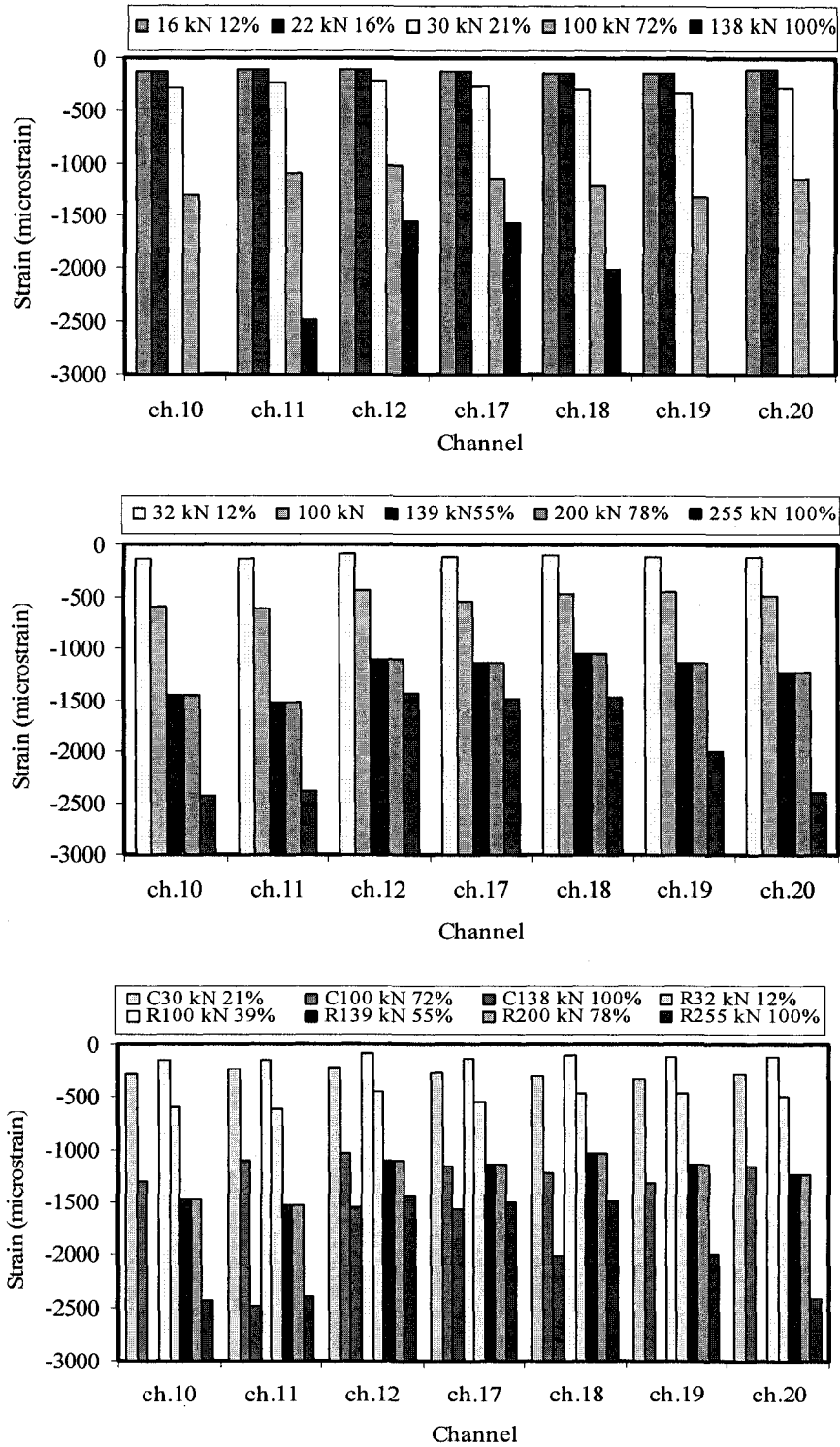
Fig. 4-92: Concrete strain response on the long direction for

CTRL25(C), REHB25(R) and for both specimens together

(Dominance of one-way slab)

254
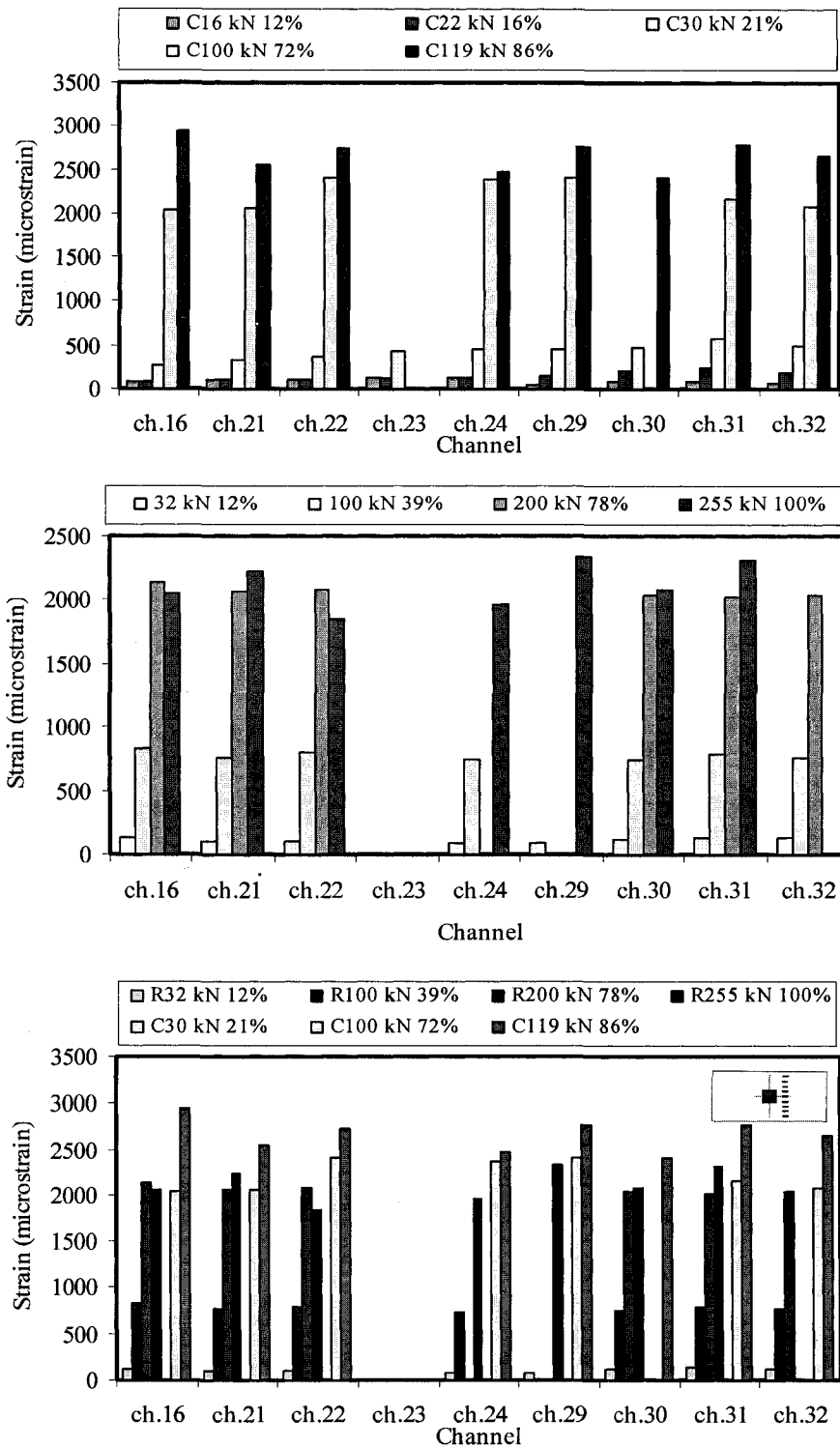
Fig. 4-93: Steel strain response on the long direction for

CTRL25(C), REHB25(R) and for both specimens together

(Dominance of one-way slab)

255
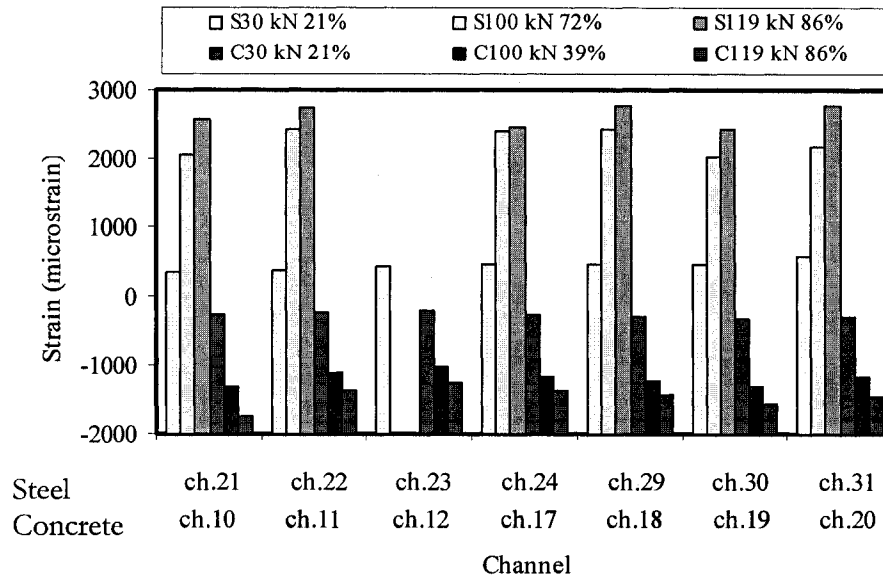
Fig. 4-94: Concrete and Steel strain response on the long direction

control specimen (CTRL25)

(Flexural failure)
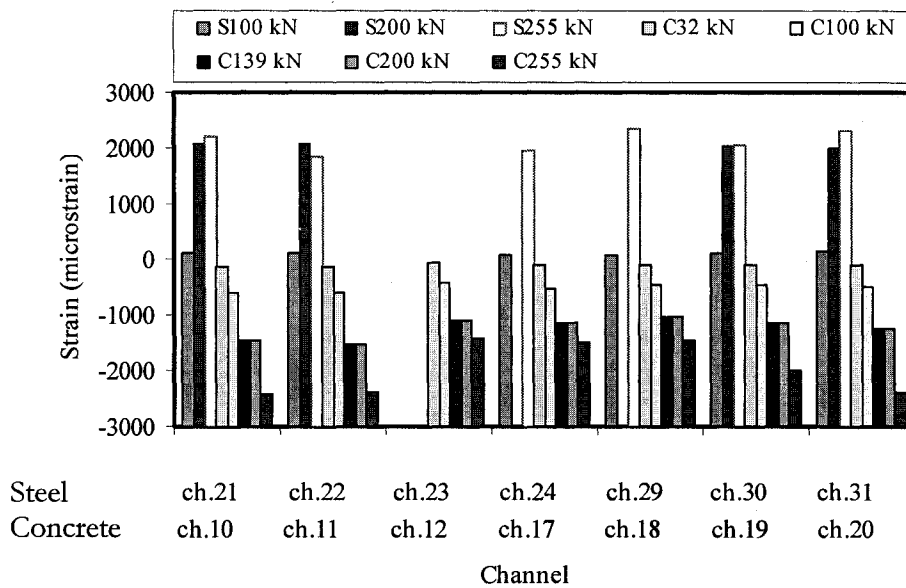
Fig. 4-95: Concrete and Steel strain response on the long direction

Rehabilitated specimen (REHB25)

256

GROUP III FIGURES

(Specimens with 350 mm eccentricity)

LOAD

350mm
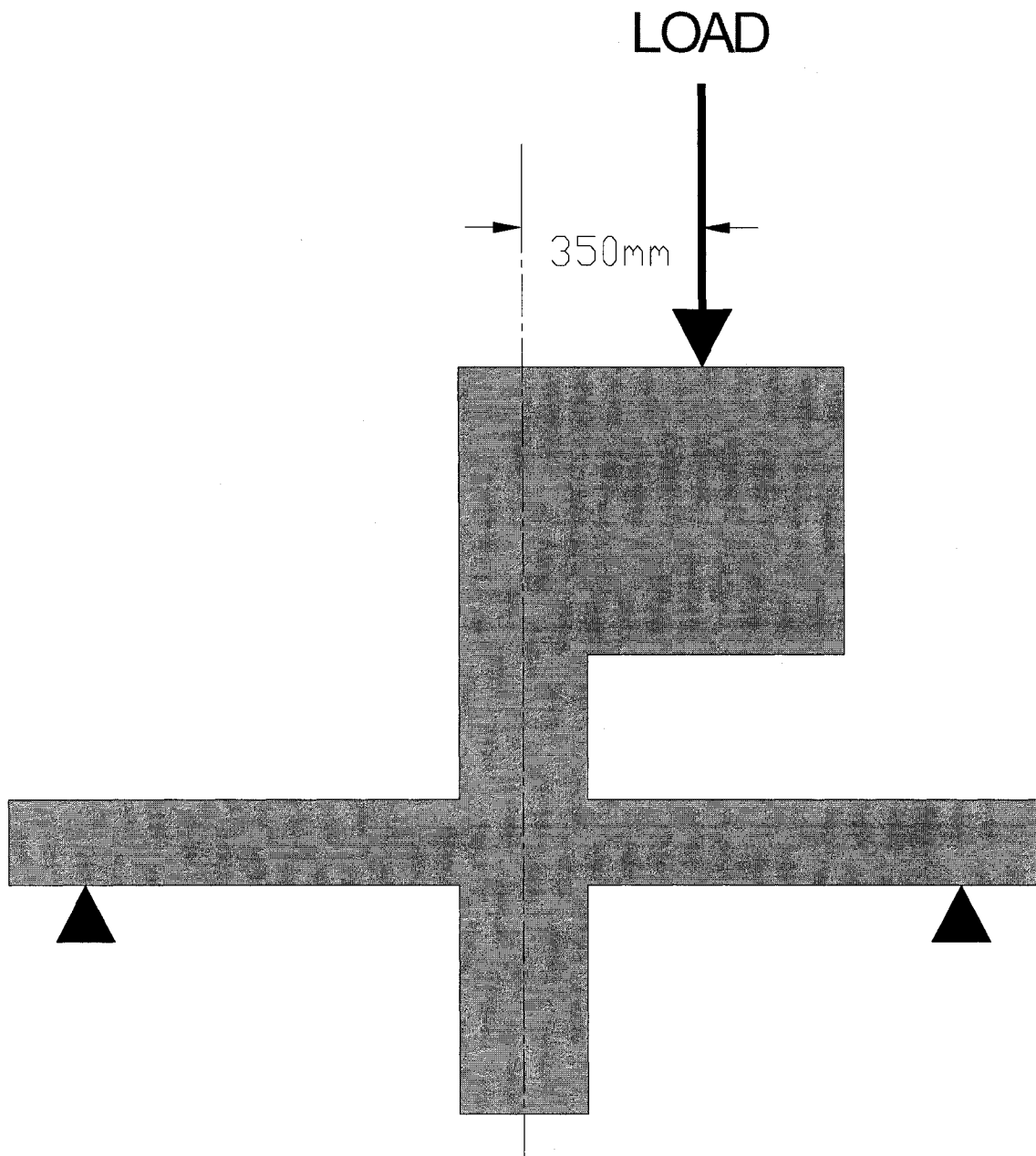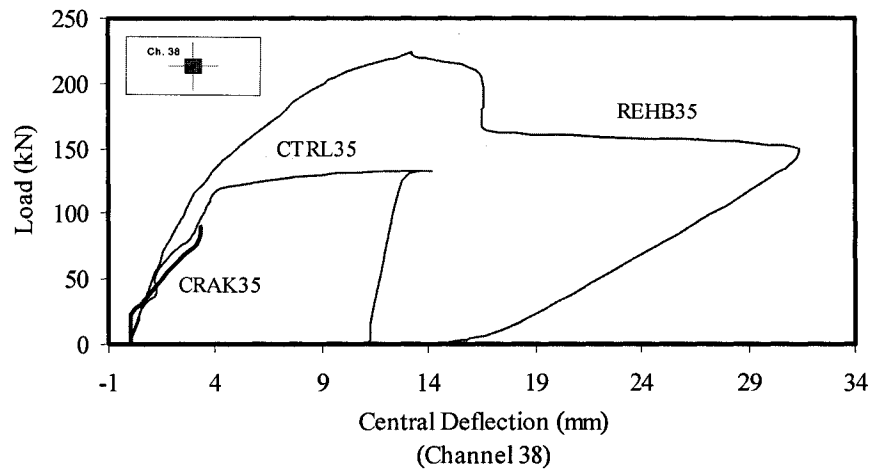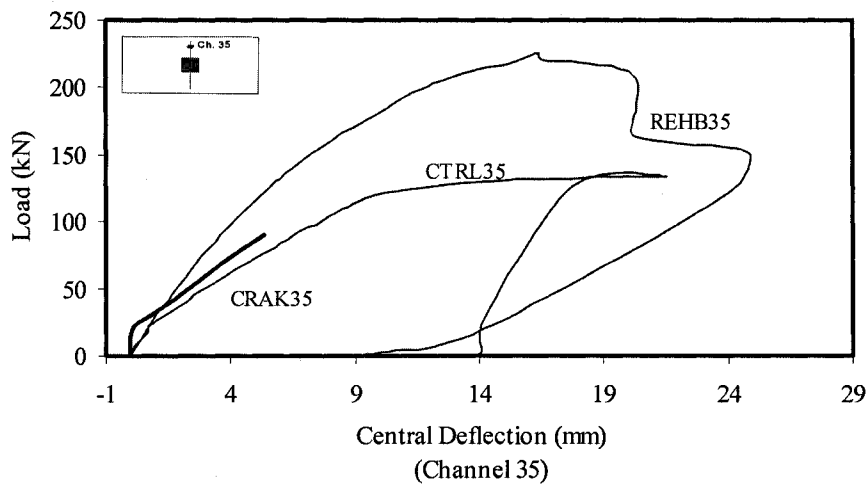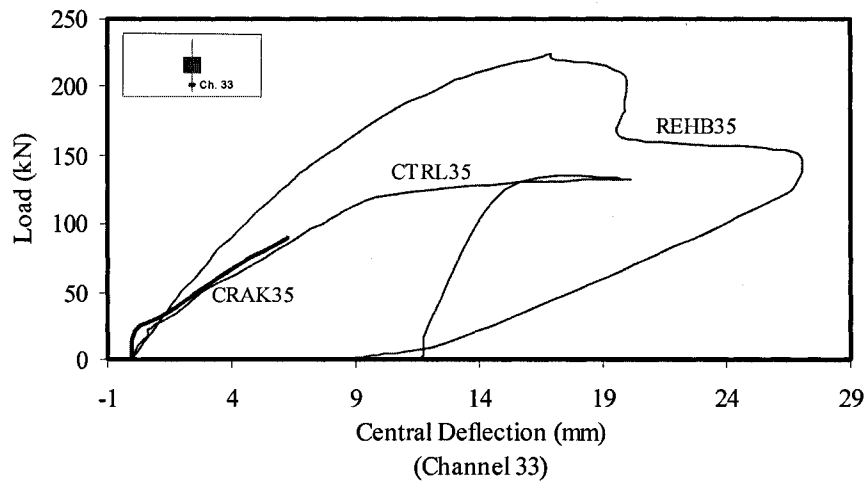
Fig. 4-96: Load versus central short direction deflection

258
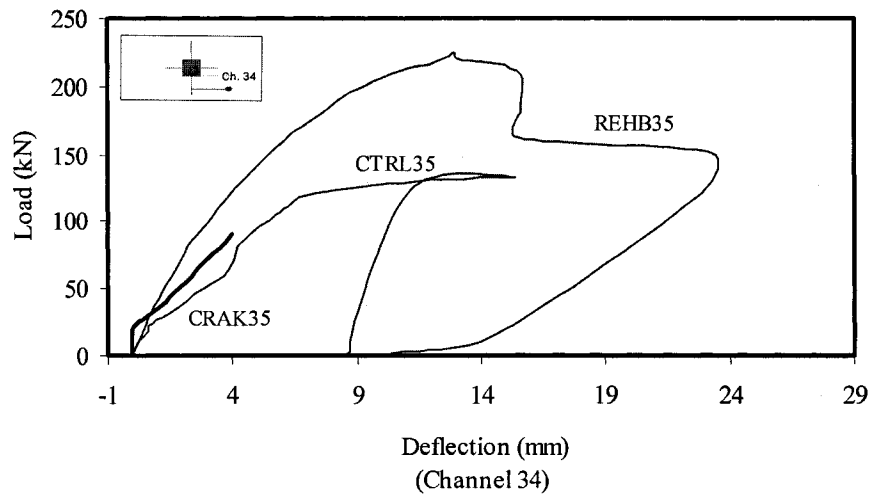
Fig. 4-97: Load versus east long direction deflection
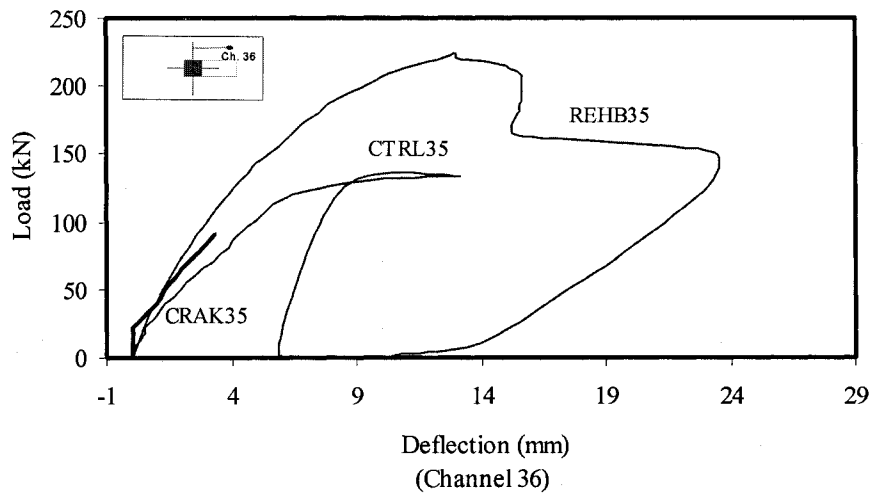
Fig. 4-98: Load versus west long direction deflection

259
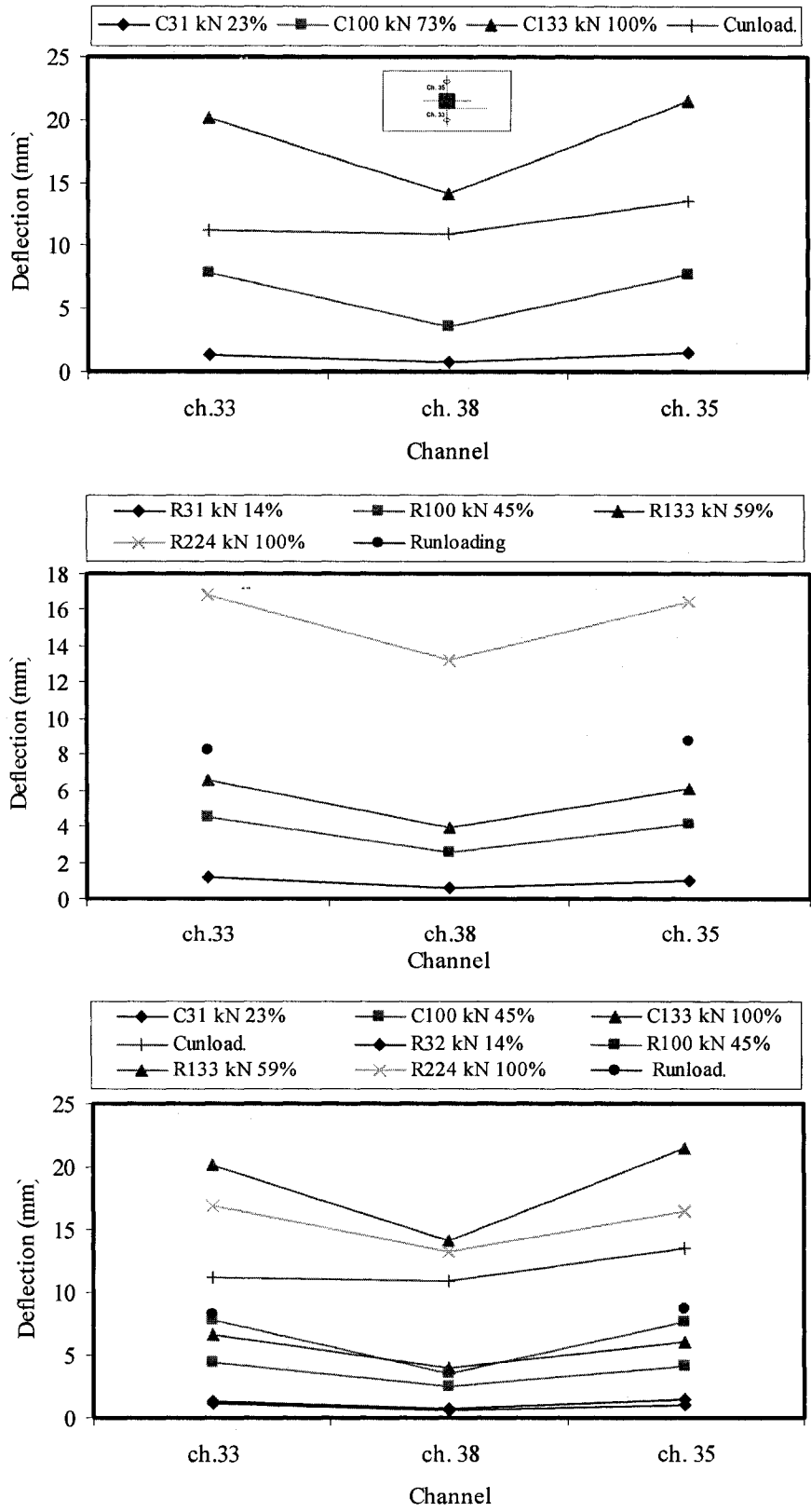
Fig. 4-99: Deflection on the east long direction for CTRL35(C), REHB35(R) and C & R

260
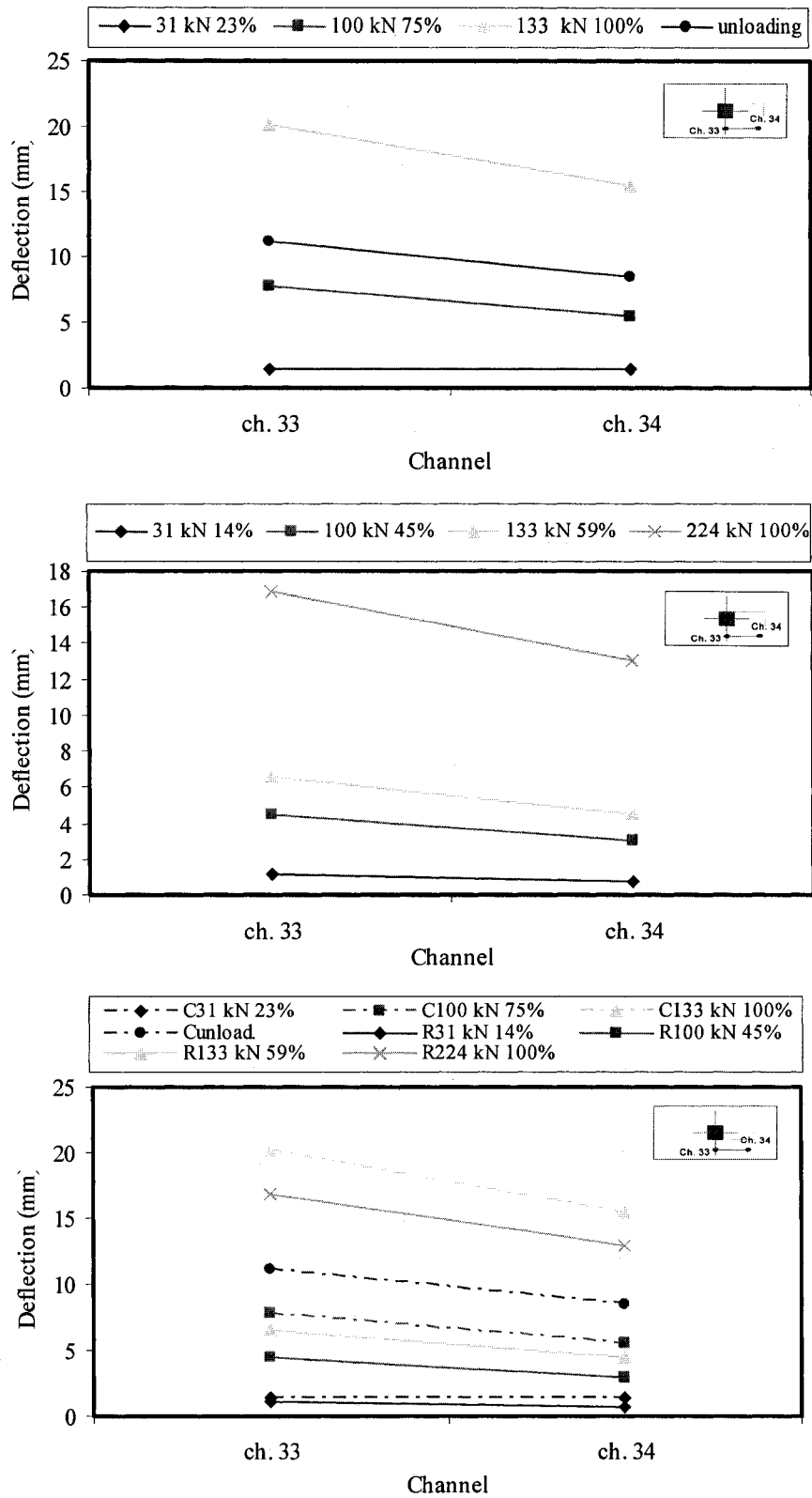
Fig. 4-100: Deflection on the east long direction for CTRL35(C), REHB35(R) and C & R

261
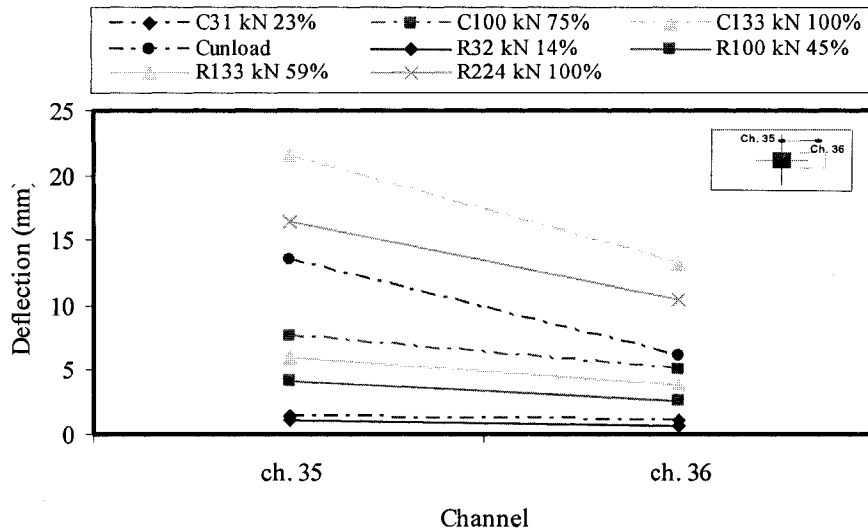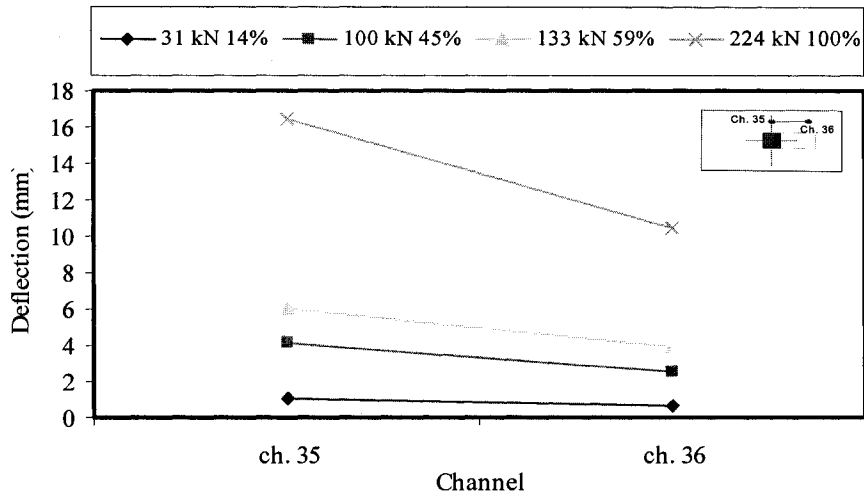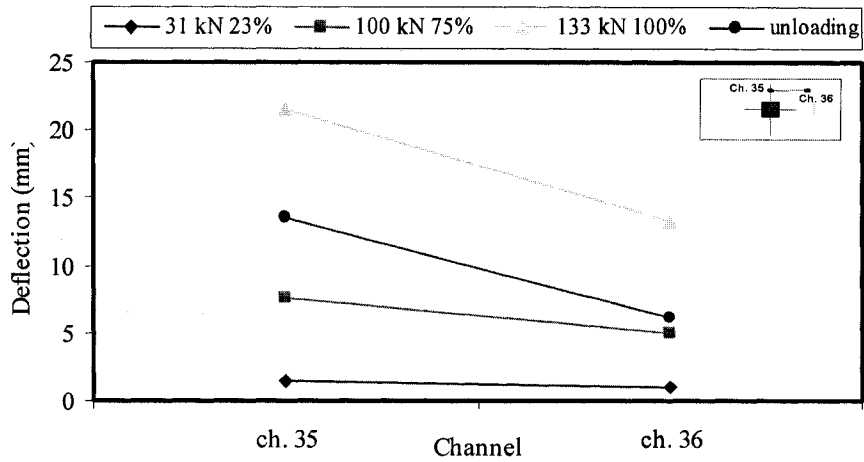
Fig. 4-101: Deflection on the west long direction for the control specimen

CTRL35(C), rehabilitated specimen REHB35(R), and both specimens together

262
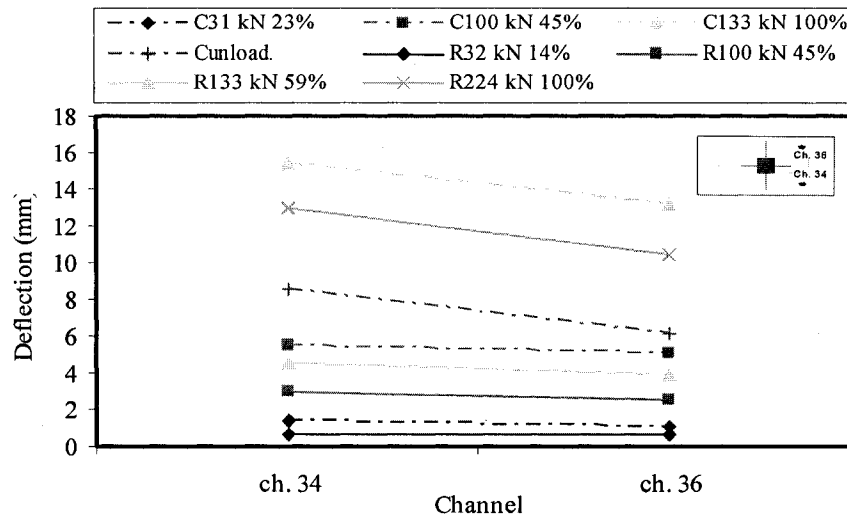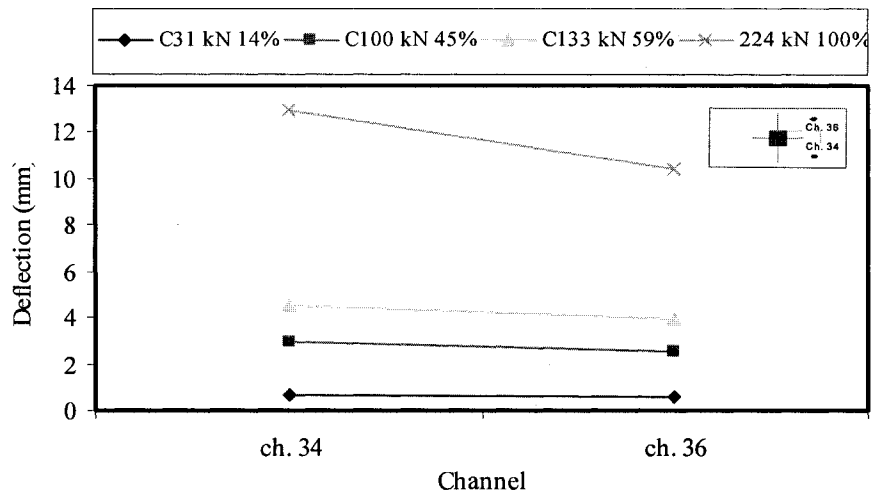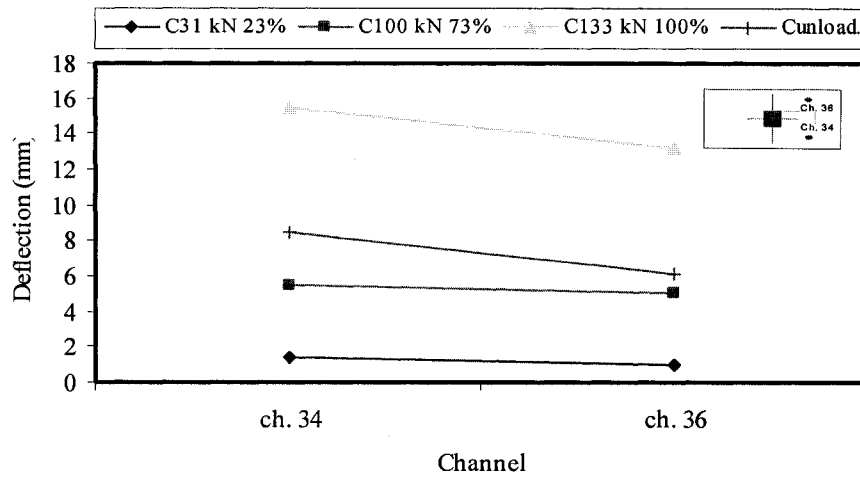
Fig. 4-102: Deflection on the north short direction for the control specimen

CTRL35(C), rehabilitated specimen REHB35(R), and both specimens together

263
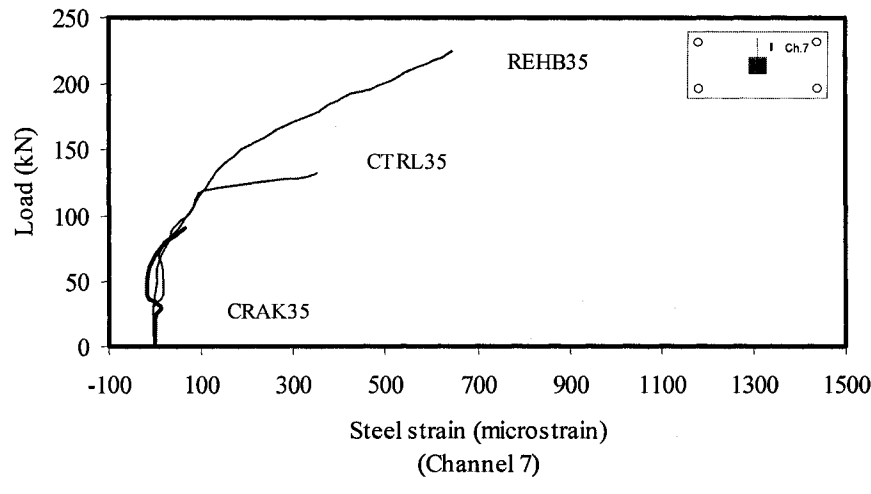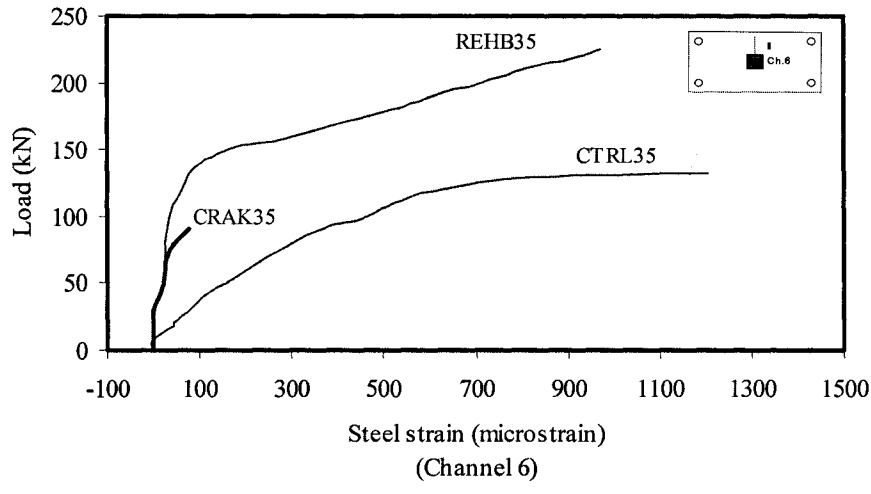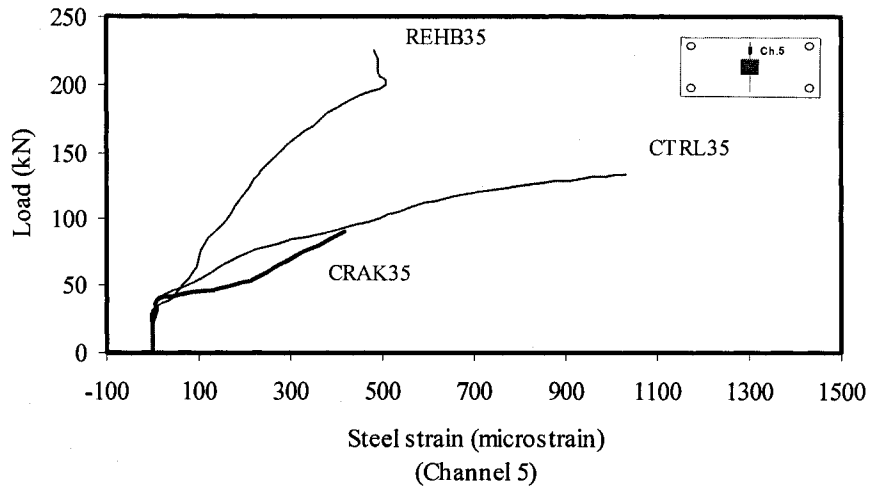
Fig. 4-103: Load versus tension short direction steel strain

264
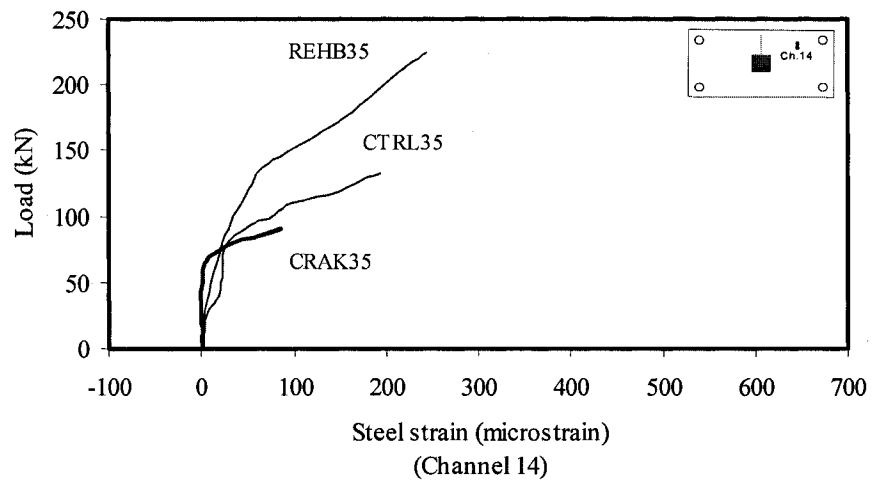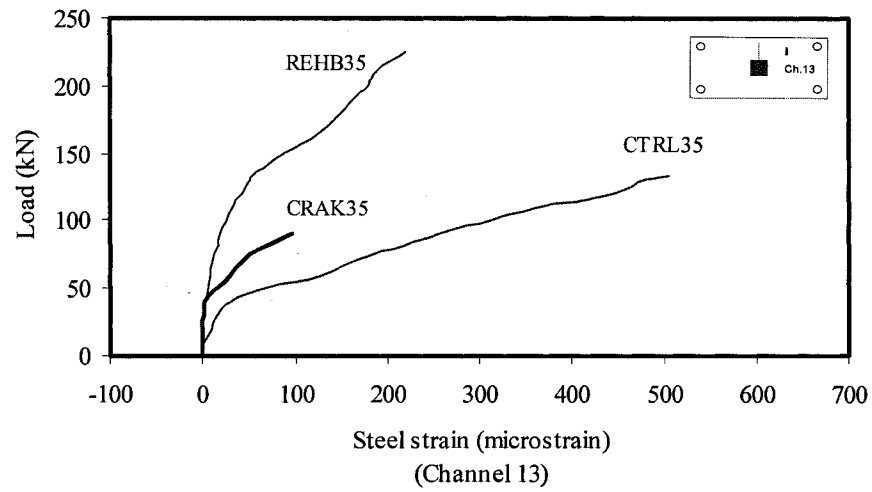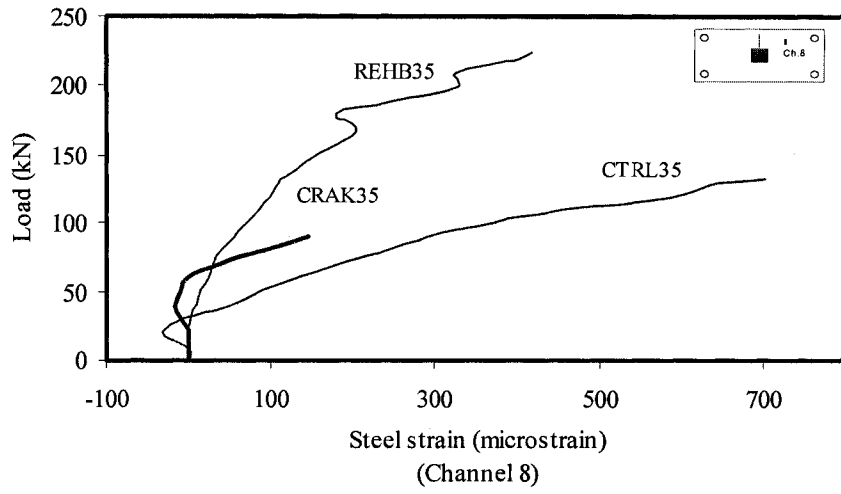
Fig.4-104: Load versus tension short direction steel strain

265
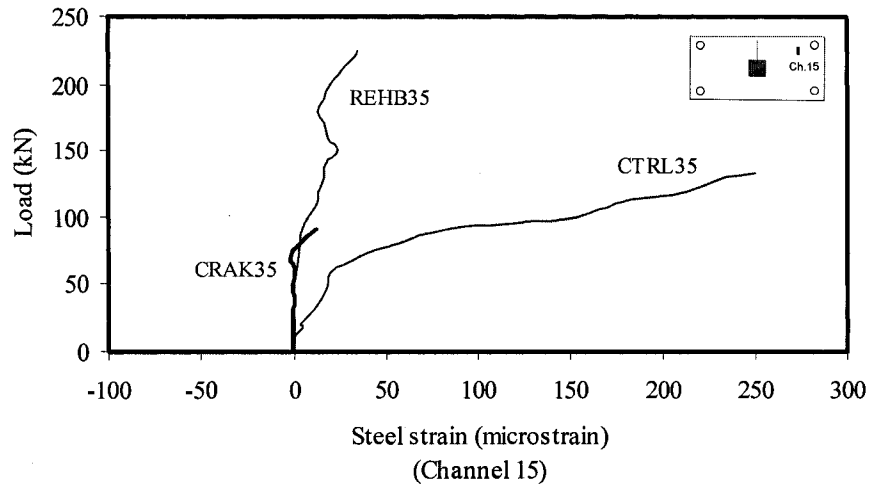
Fig.4-105: Load versus tension short direction steel strain

266
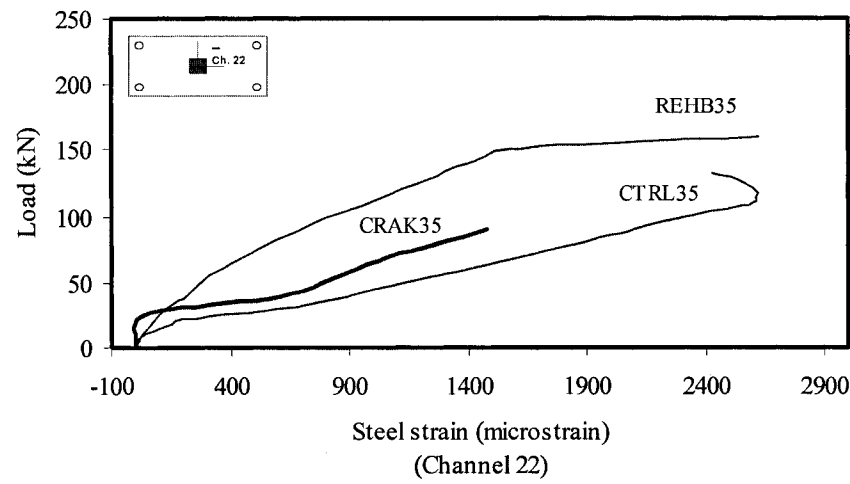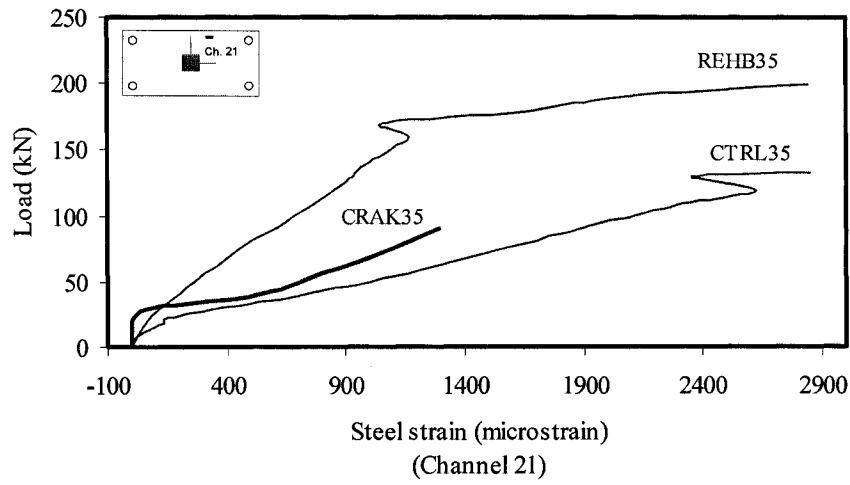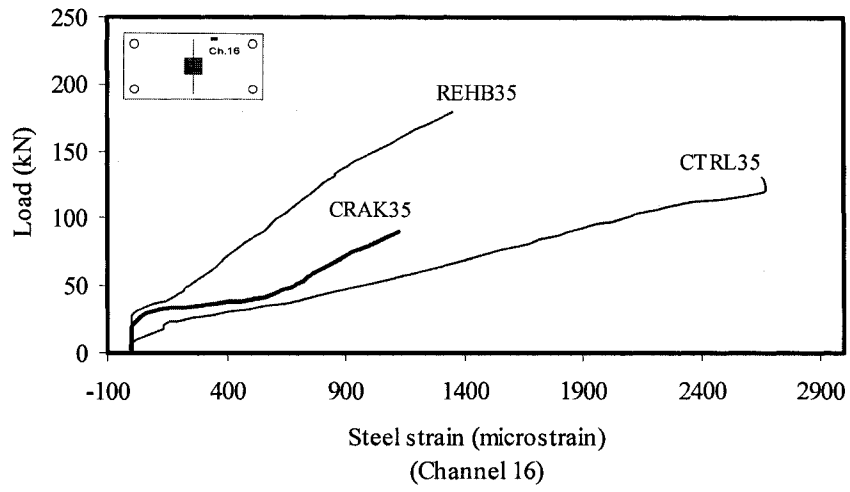
Fig. 4-106: Load versus tension long direction steel strain

267
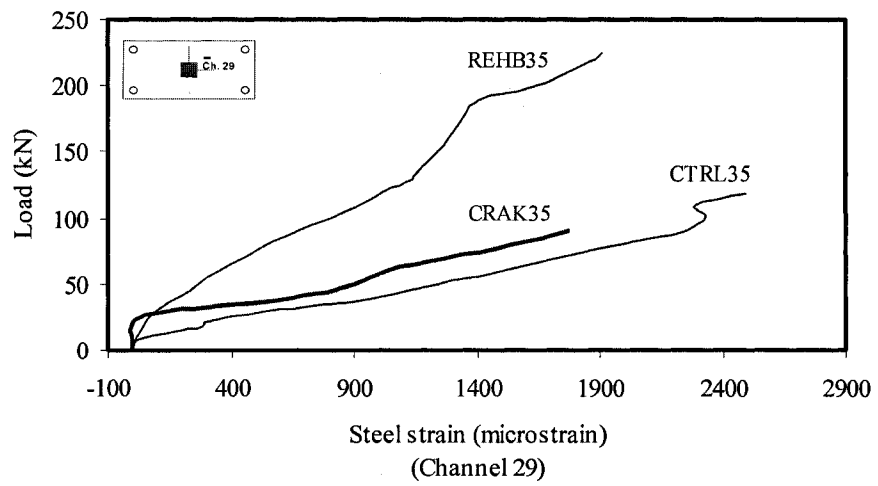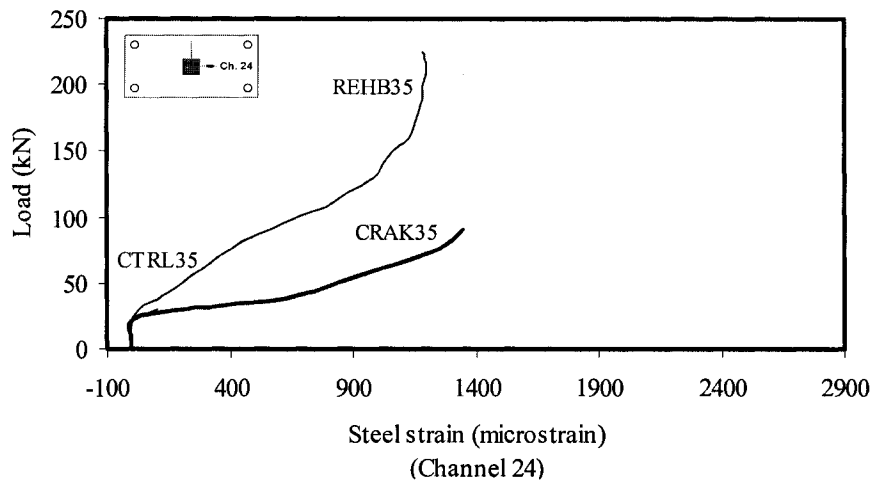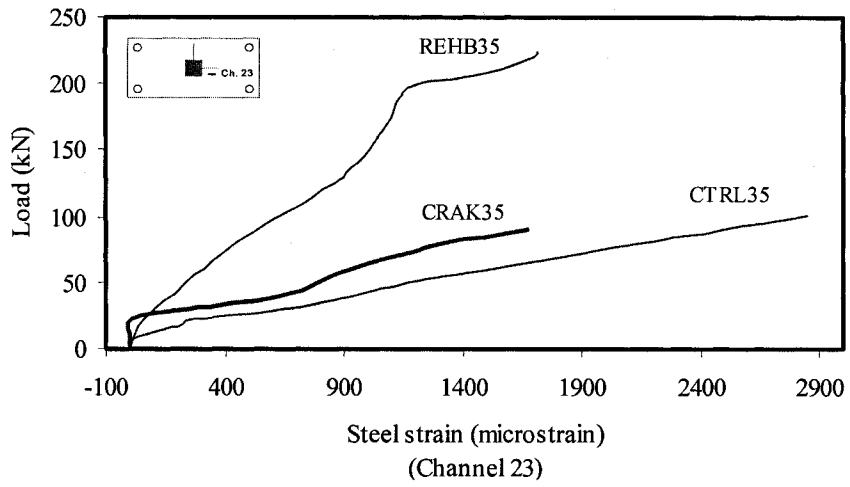
Fig. 4-107: Load versus tension long direction steel strain

268

Fig. 4-108: Load versus tension long direction steel strain

269

Fig. 4-109: Load versus compression long direction upper layer steel strain

270

Fig. 4-110: Load versus short direction concrete strain

271
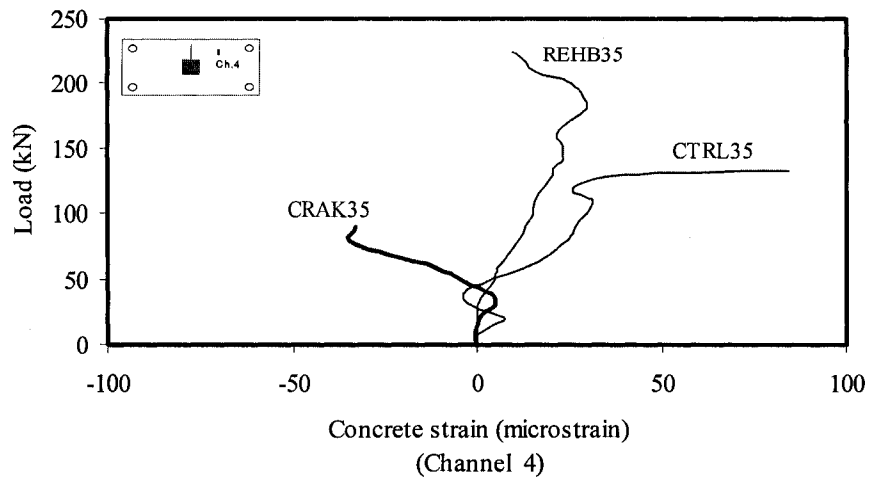
Fig. 4-111: Load versus short direction concrete strain

272
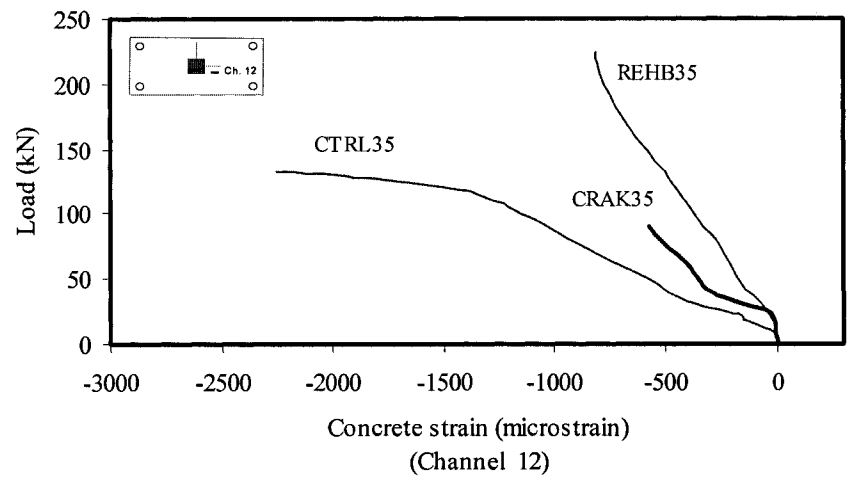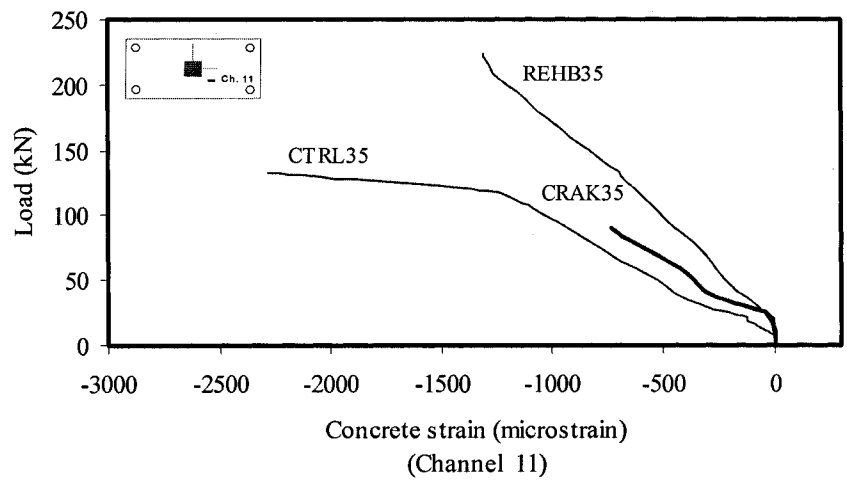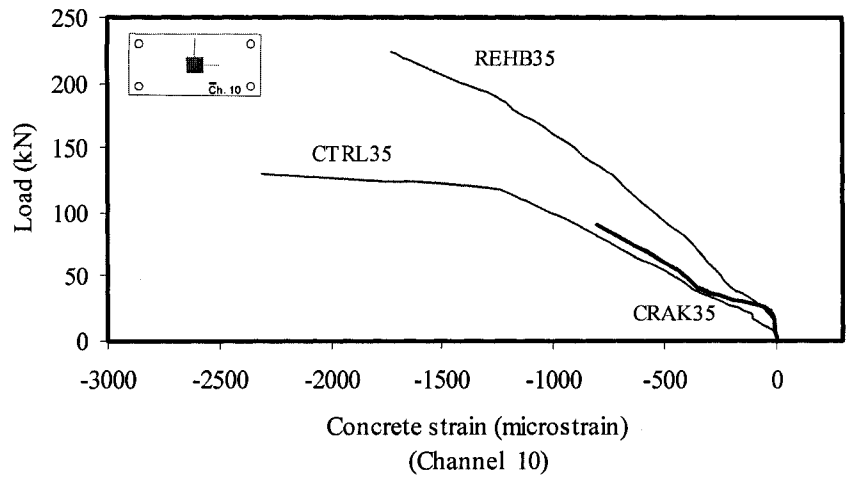
Fig. 4-112: Load versus long direction concrete strain

273
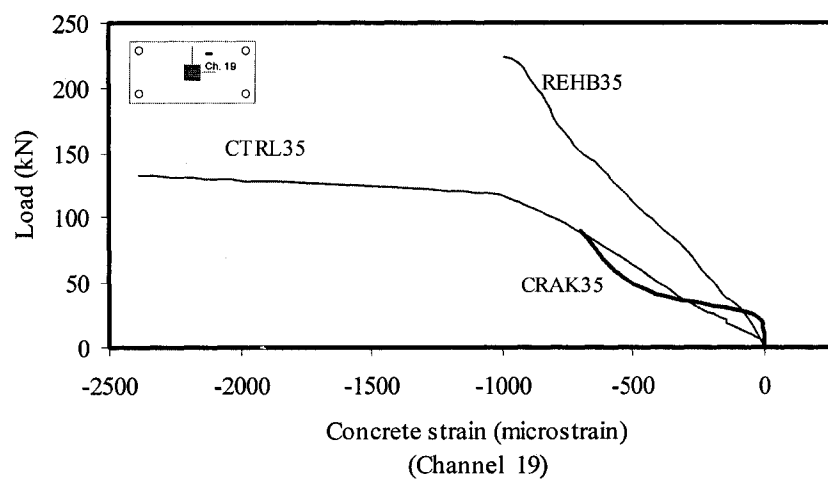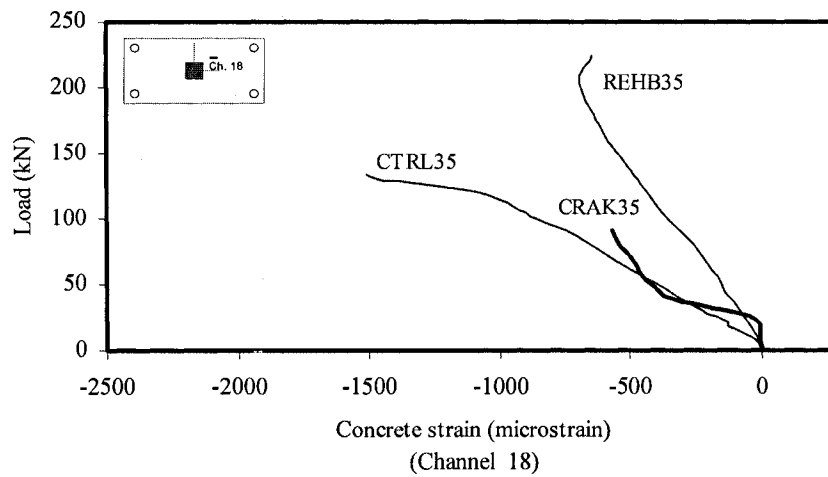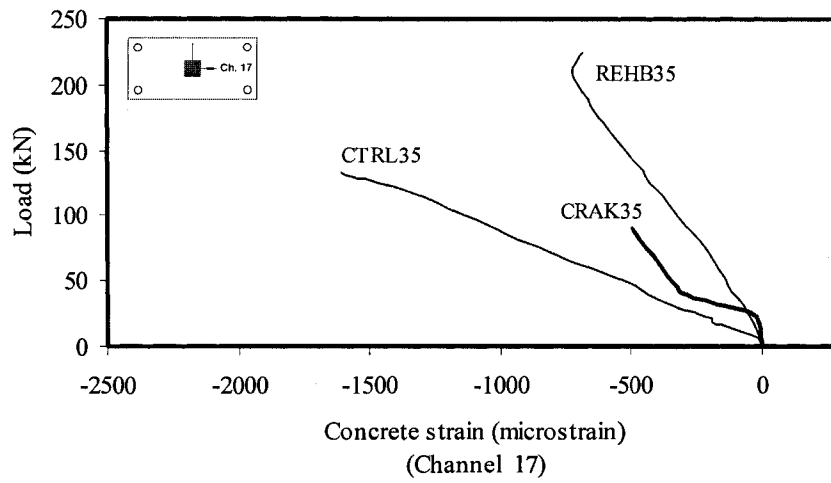
Fig. 4-113: Load versus long direction concrete strain

274
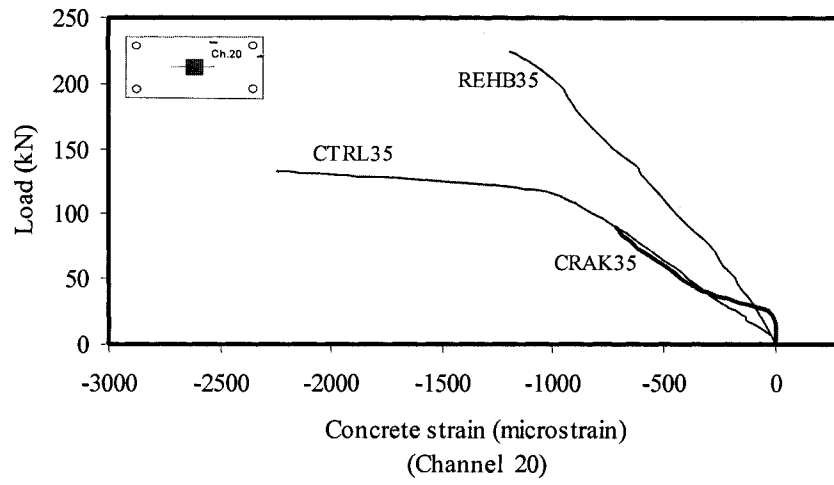
Fig. 4-114: Load versus long direction concrete strain

275
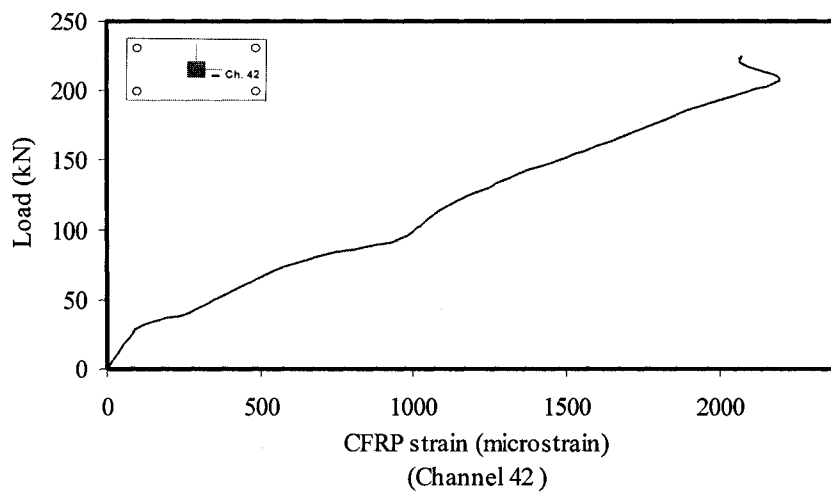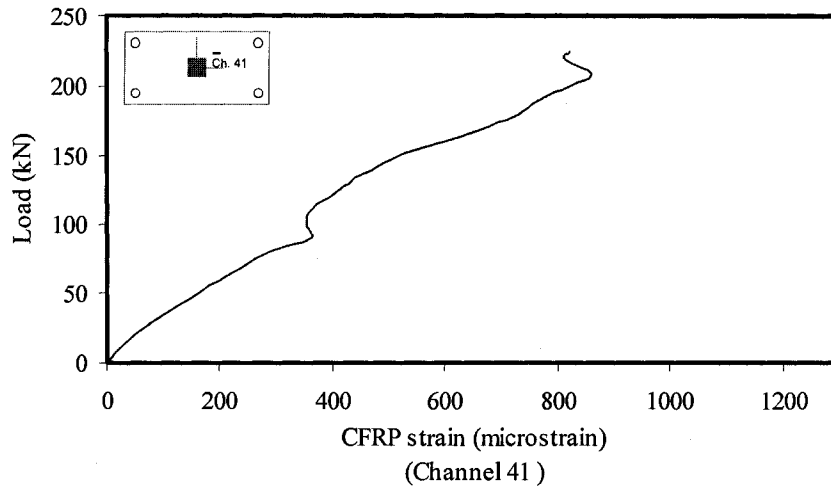
Fig. 4-115: Load versus tension long direction CFRP strain
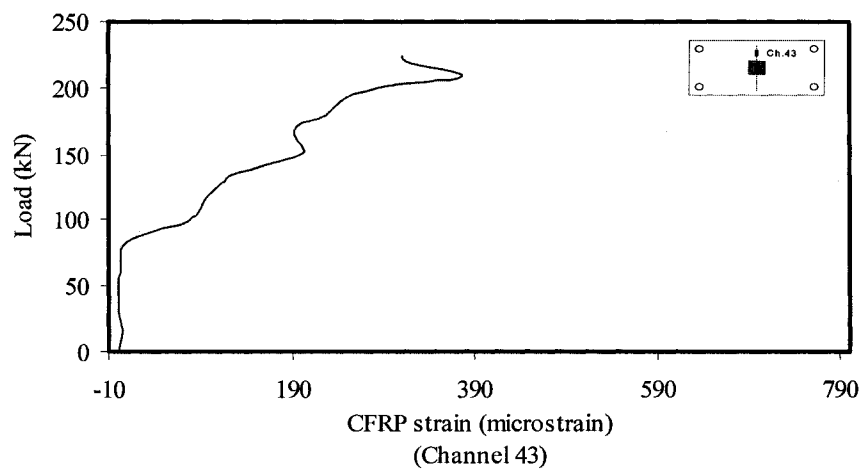
Fig. 4-116: Load versus tension short direction CFRP strain

276
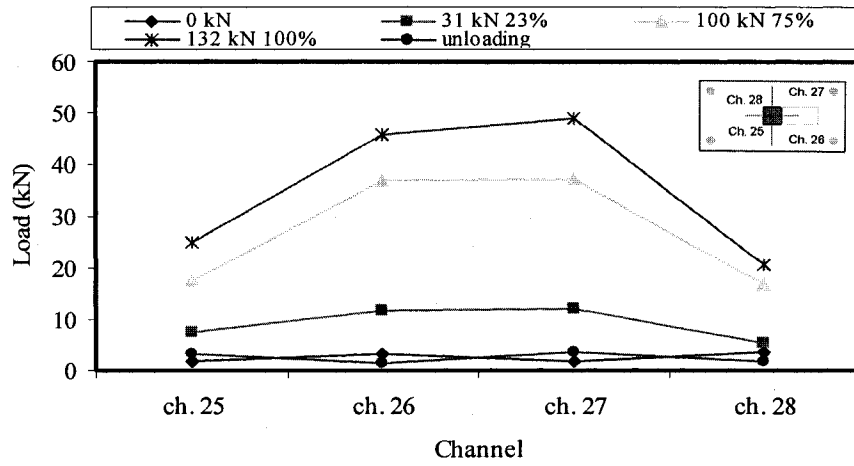
Fig. 4-117: Load distribution on each reaction for the control specimen (CTRL35)
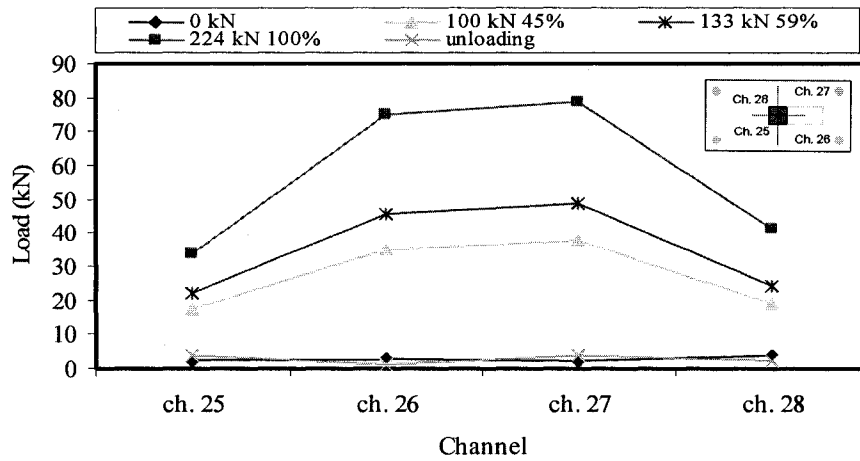
Fig. 4-118: Load distribution on each reaction for the rehabilitated specimen (REHB35)
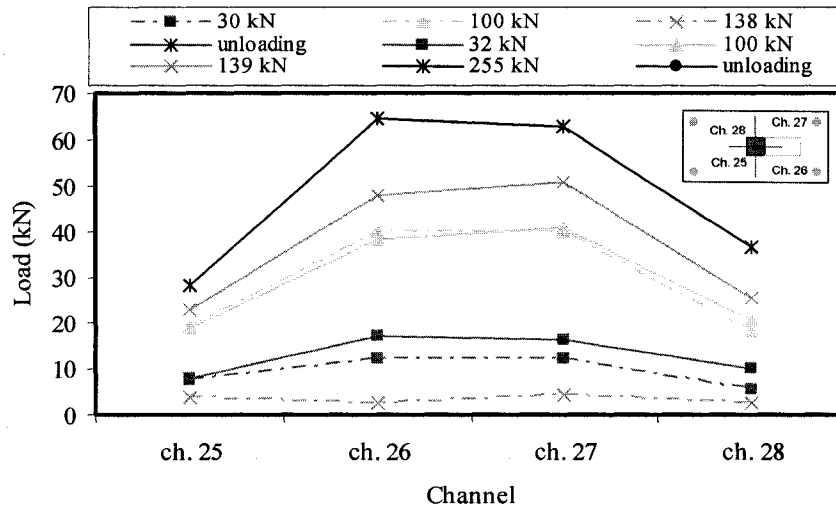
Fig. 4-119: Load distribution on each reaction for (CTRL335) and (REHB0)

277
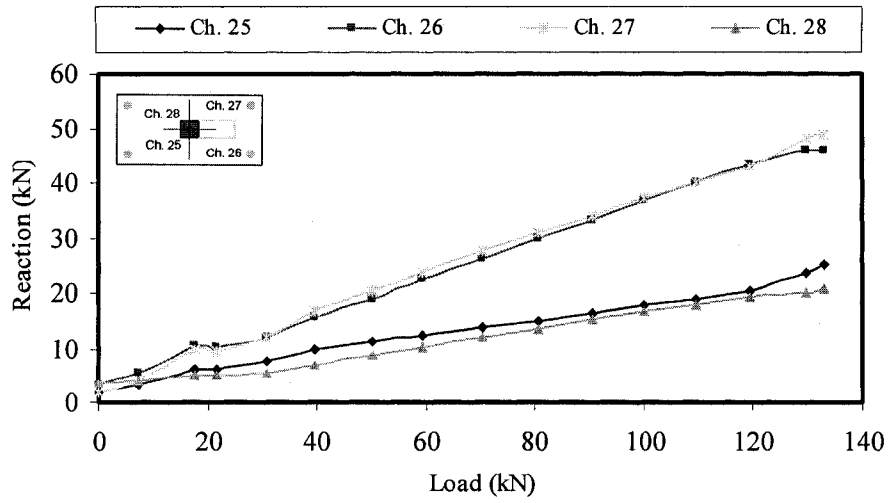
Fig. 4-120: Reaction distribution for the control specimen (CTRL35)
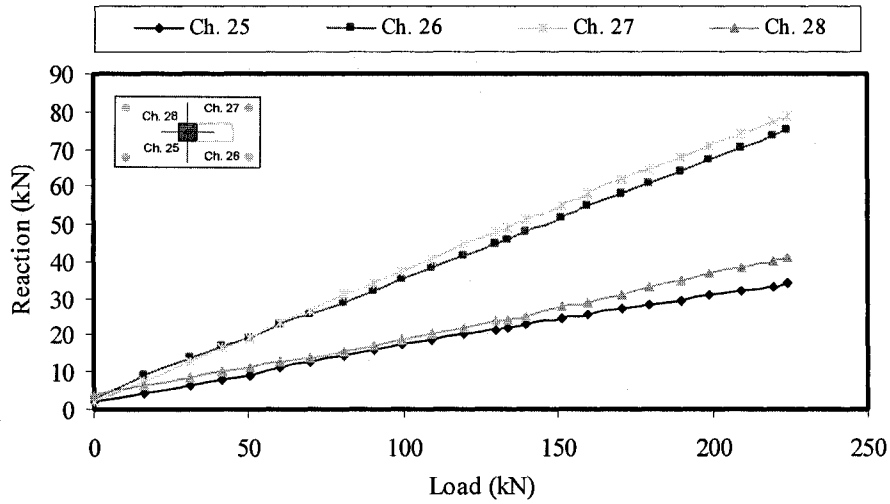
Fig. 4-121: Reaction distribution for the rehabilitated specimen (REHB35)

278

Ch. 28 | Ch. 27

Ch. 25 | Ch. 26

0 kN, 34%   0 kN, 18%

0 kN, 17%   0 kN, 31%

ch. 25 ch. 26 ch. 27 ch. 28
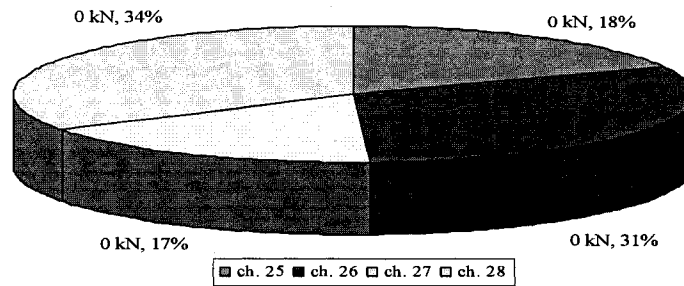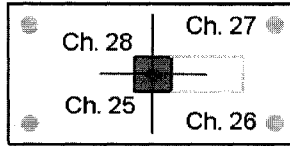
Fig. 4-122: Percentage of load on each reaction at 0 kN (CTRL35)

31 kN 23%,   31 kN 23%,
15%   20%

31 kN 23%,   31 kN 23%,
33%   32%

ch. 25 ch. 26 ch. 27 ch. 28
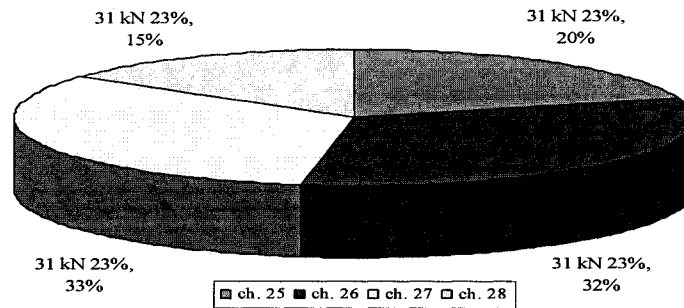
Fig. 4-123: Percentage of load on each reaction at 31 kN (CTRL35)

100 kN 75%,   100 kN 75%,
15%   16%

100 kN 75%,   100 kN 75%,
34%   35%

ch. 25 ch. 26 ch. 27 ch. 28
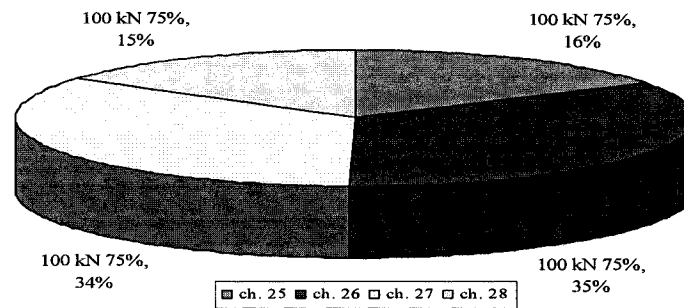
Fig. 4-125: Percentage of load on each reaction at 100 kN (CTRL35)

Control specimen

279
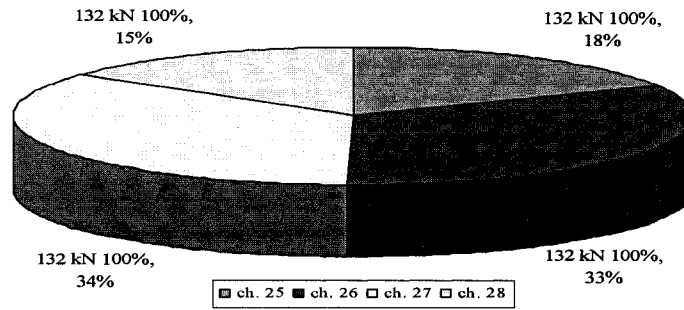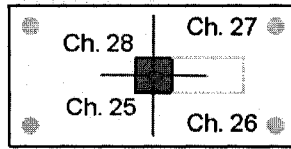
Fig. 4-126: Percentage of load on each reaction at ultimate load for

the control specimen (CTRL35)
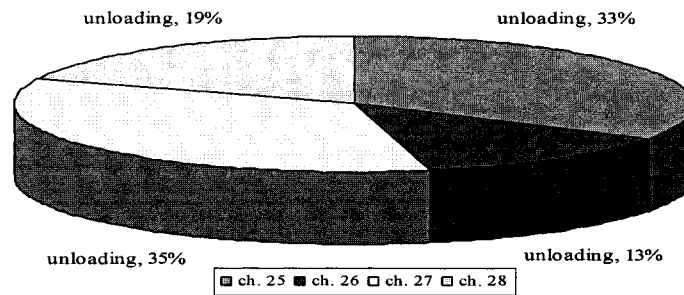
Fig. 4-127: Percentage of load on each reaction after unloading for

the control specimen (CTRL35)

280
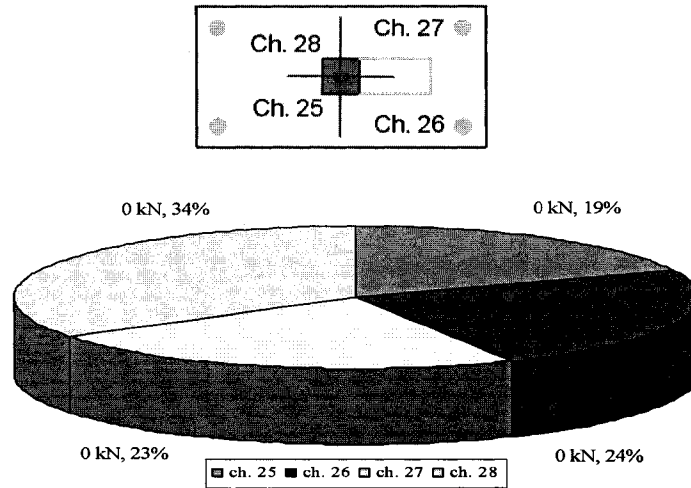
Fig. 4-128: Percentage of load on each reaction at 0 kN (REHB35)
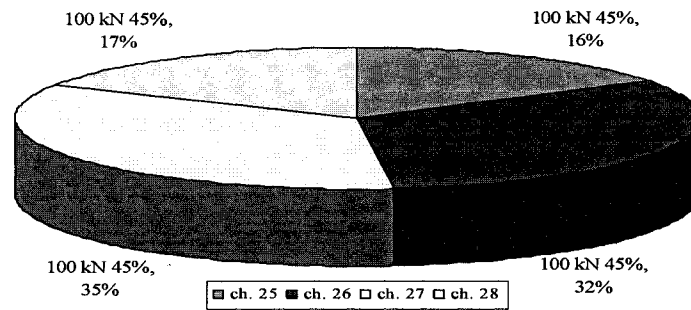
Fig. 4-129: Percentage of load on each reaction at 100 kN (REHB35)
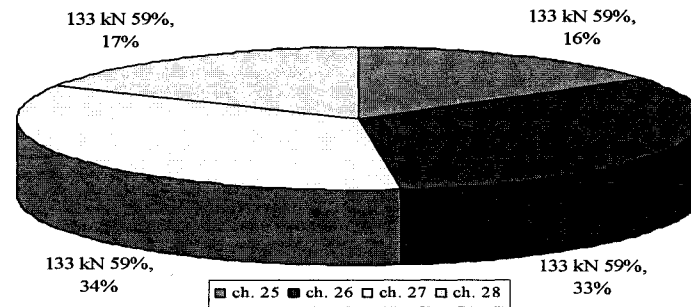
Fig. 4-130: Percentage of load on each reaction at 133 kN (REHB35)
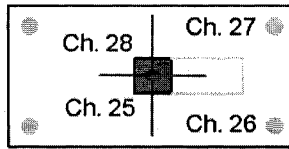
Rehabilitated specimen

281
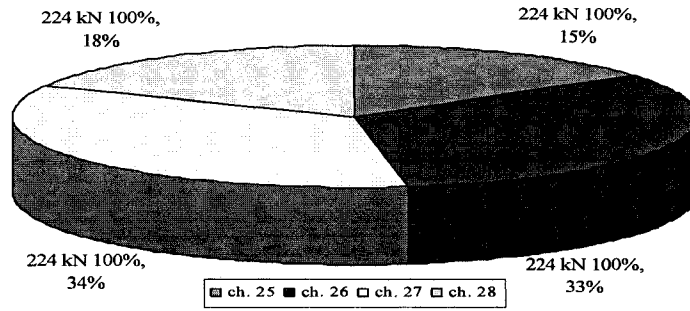
Fig. 4-131: Percentage of load on each reaction at ultimate load for

the rehabilitated specimen (REHB35)
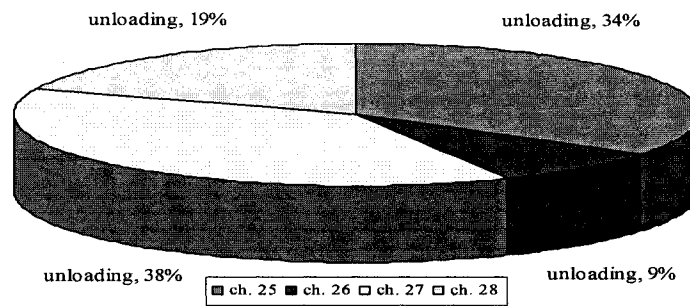
Fig. 4-132: Percentage of load on each reaction after unloading for

the rehabilitated specimen (REHB35)

282
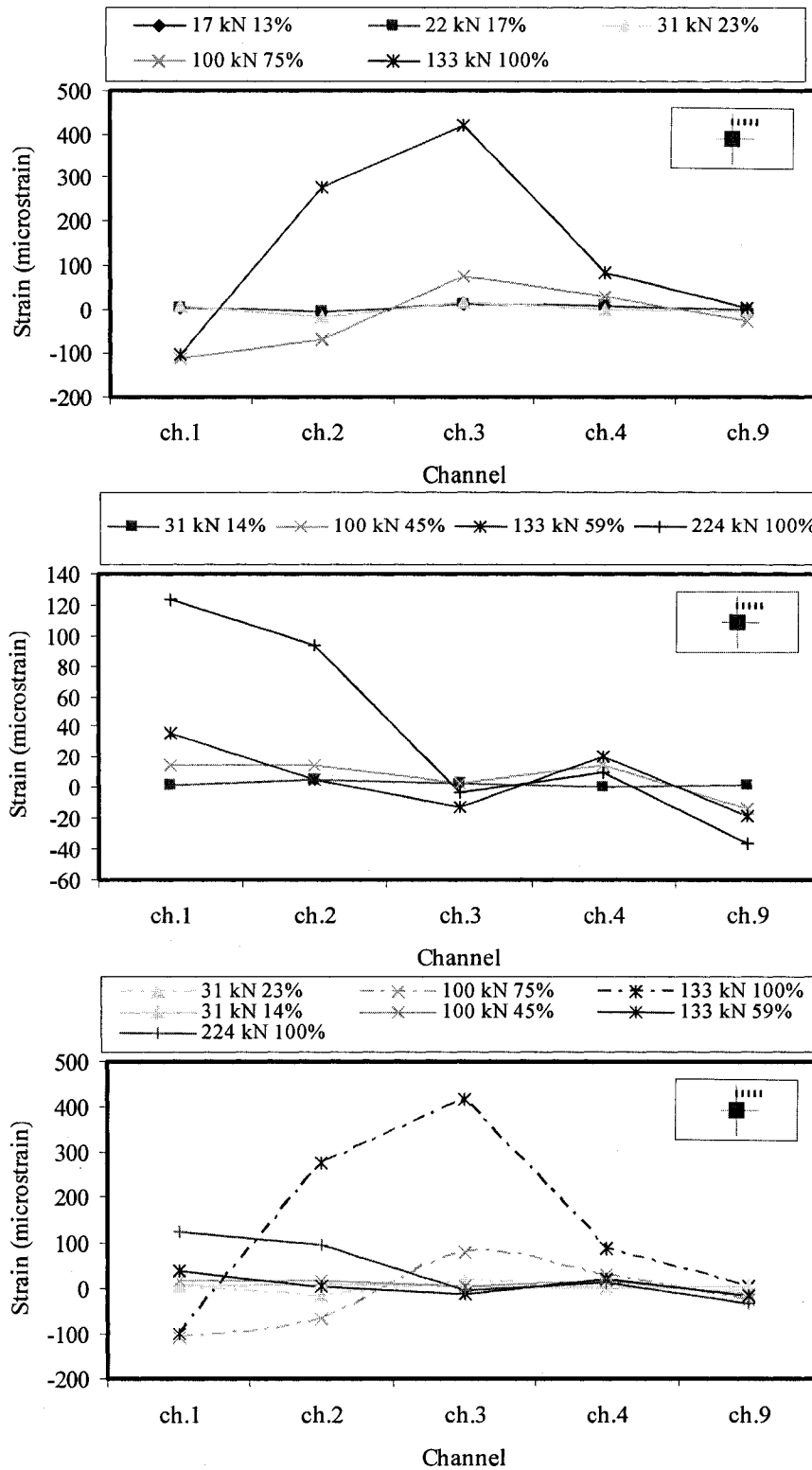
Fig. 4-133: Load versus short direction concrete strain

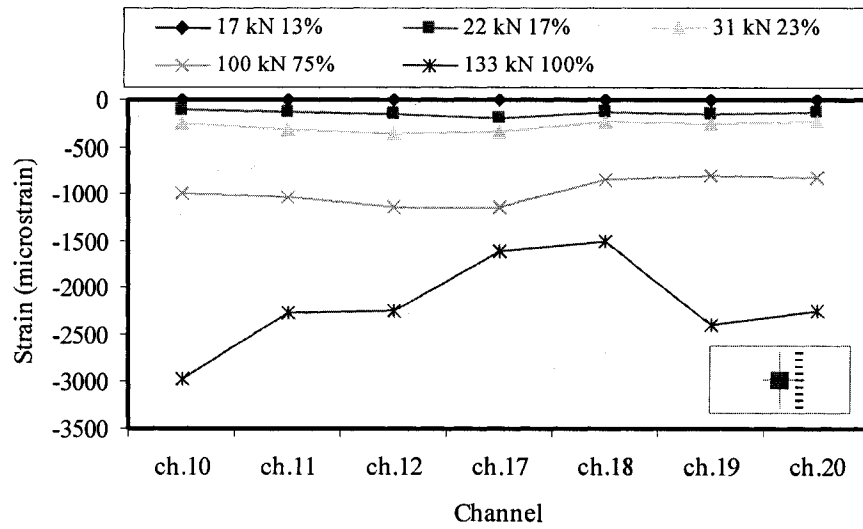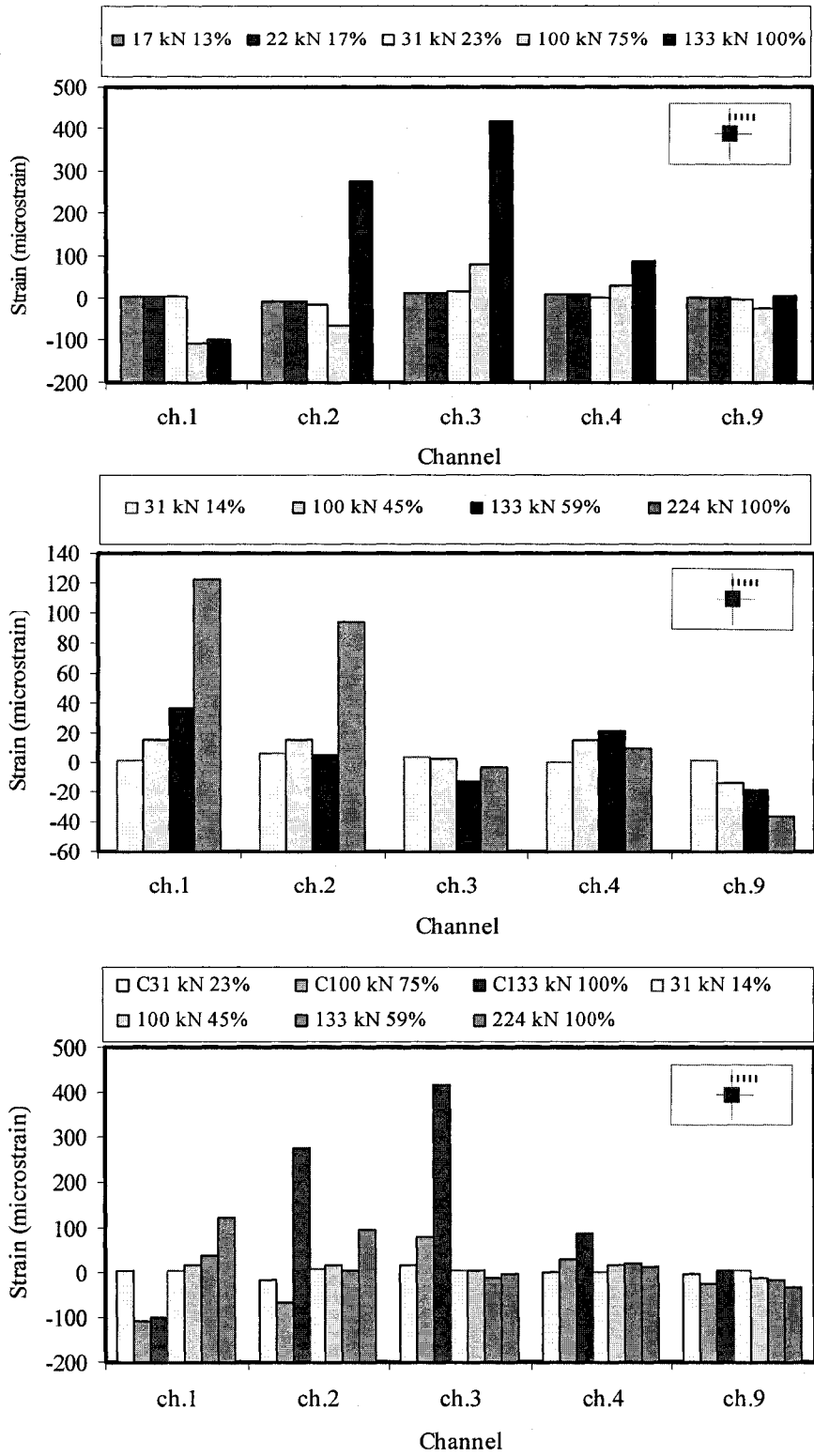Control specimen CTRL35(C), rehabilitated specimen REHB25(R), and both together
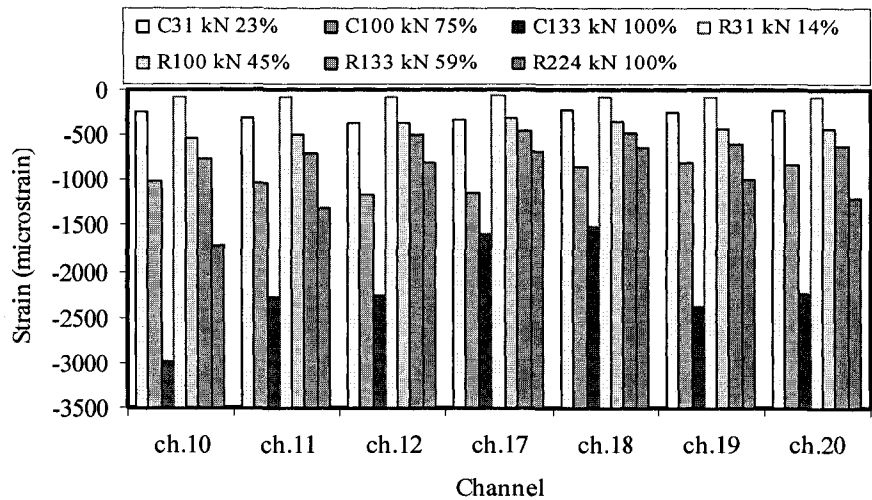
283
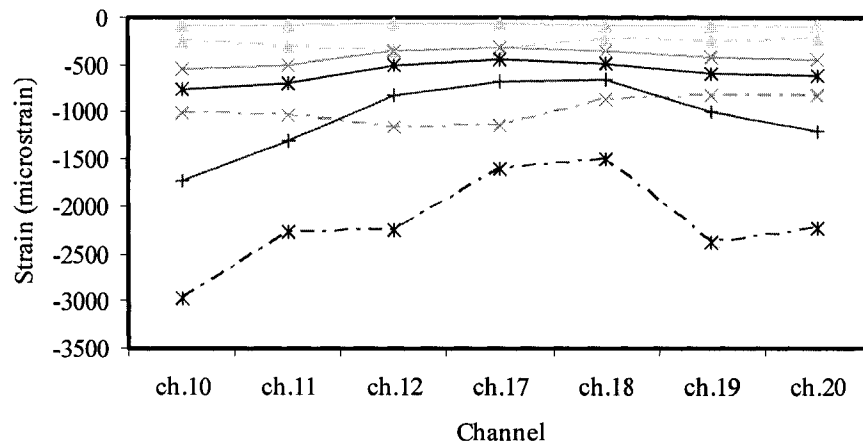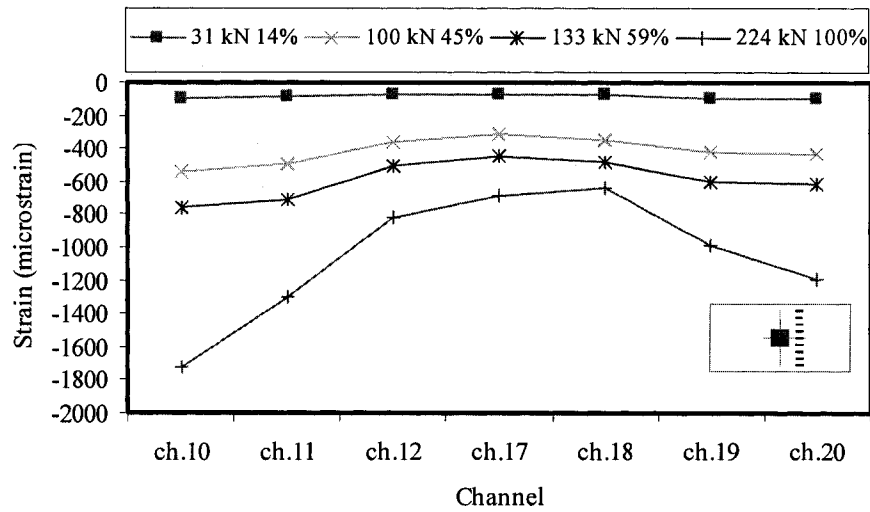
Fig. 4-134: Load versus long direction concrete strain

Control specimen CTRL25(C), rehabilitated specimen REHB25(R), and both together

284

Fig. 4-135: Load versus short direction concrete strain

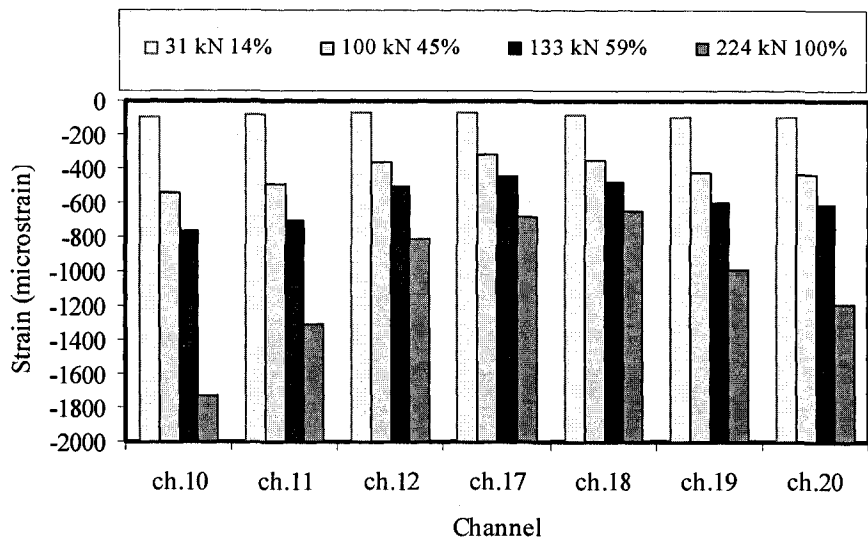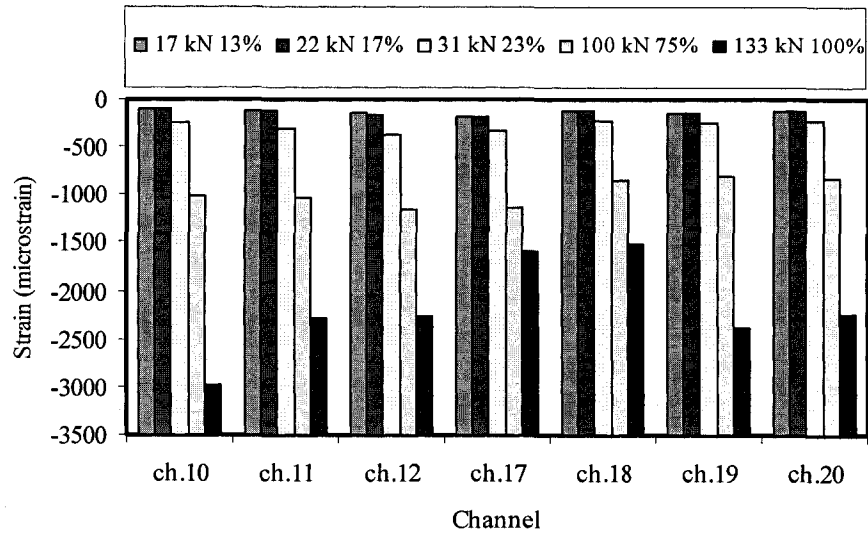Control specimen CTRL25(C), rehabilitated specimen REHB25(R), and both together

285

Fig. 4-136: Load versus long direction concrete strain

Control specimenCTRL35(C), rehabilitated specimen REHB35(R), and both together
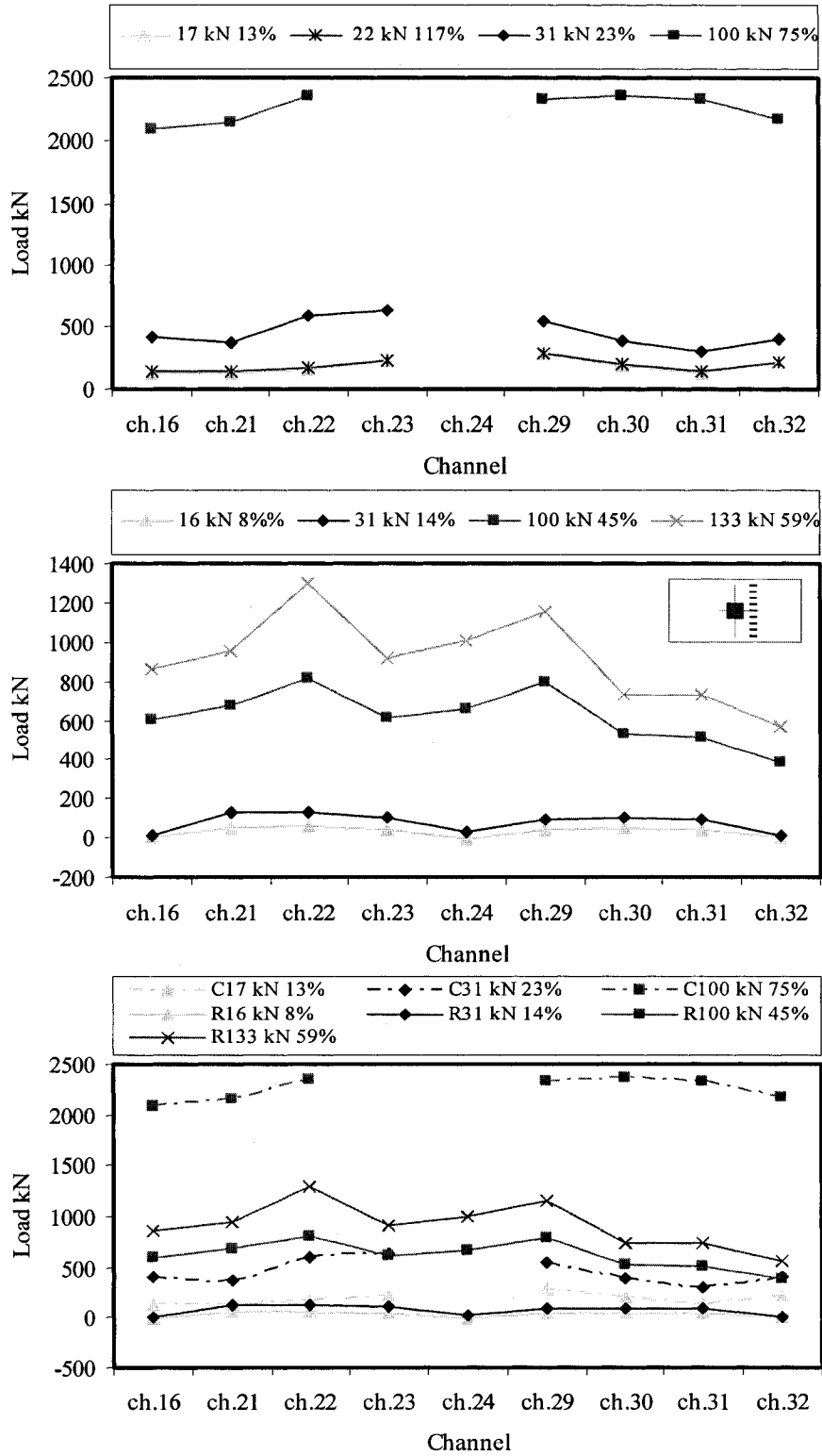
286

Fig. 4-137: Load versus long direction steel strain

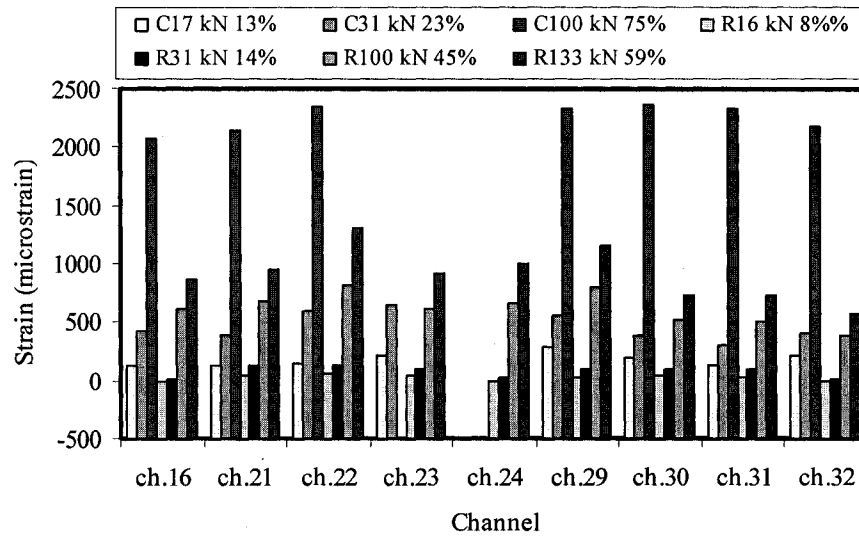Control specimen CTRL35(C), rehabilitated specimen REHB35(R), and both together
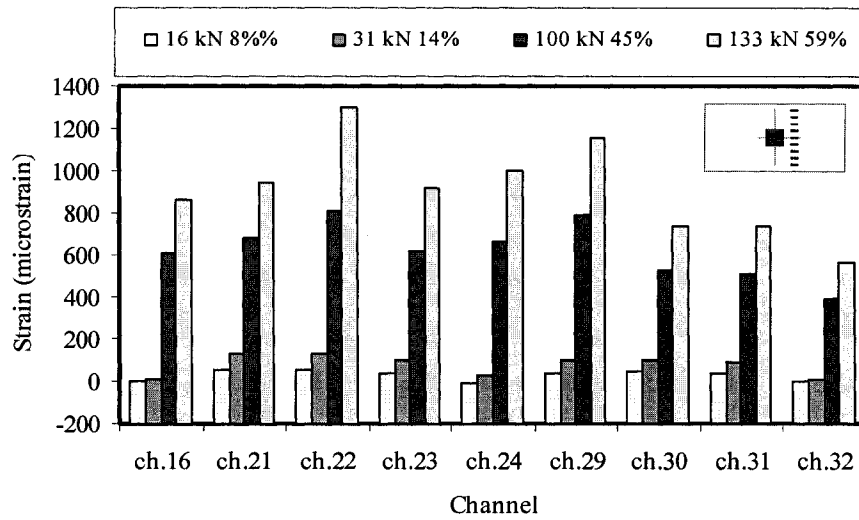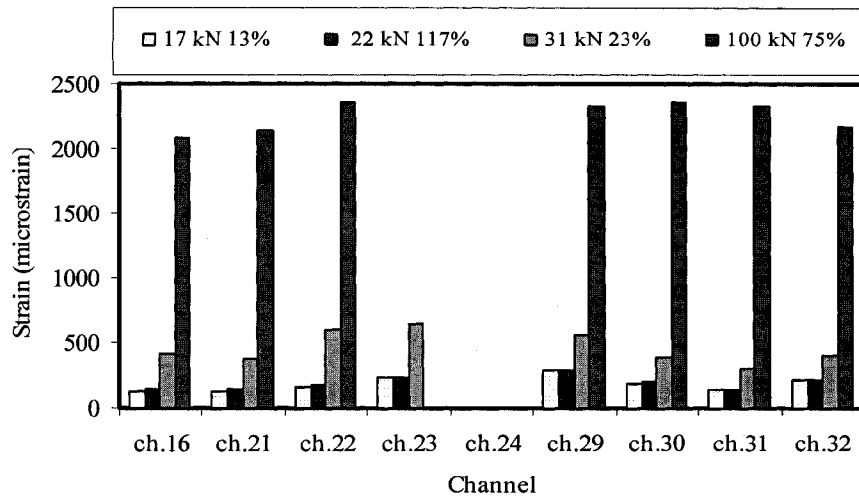
287

Fig. 4-138: Load versus long direction steel strain

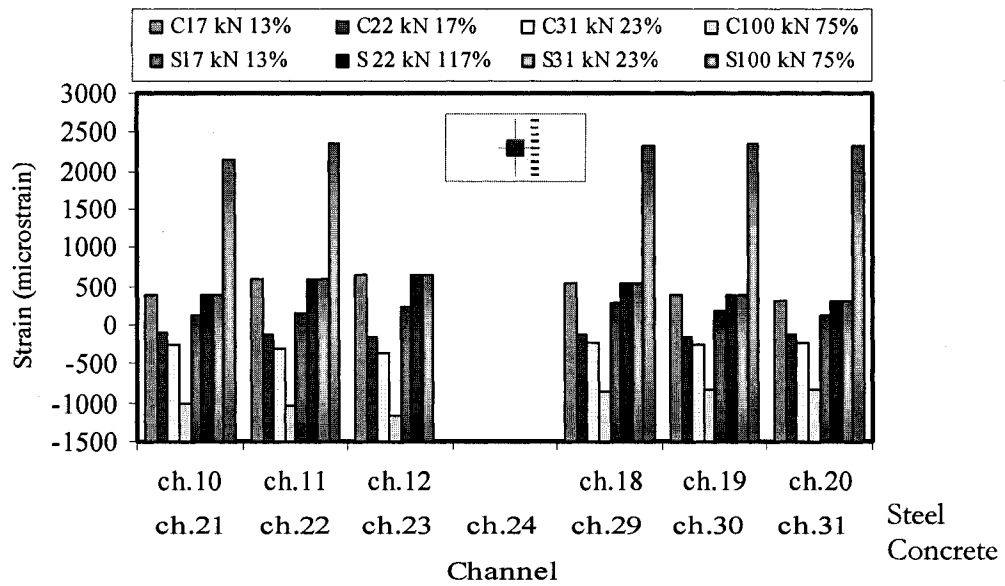Control specimen CTRL25(C), rehabilitated specimen REHB25(R), and both together

288

Fig. 4-139: Concrete and Steel strain response on the long direction
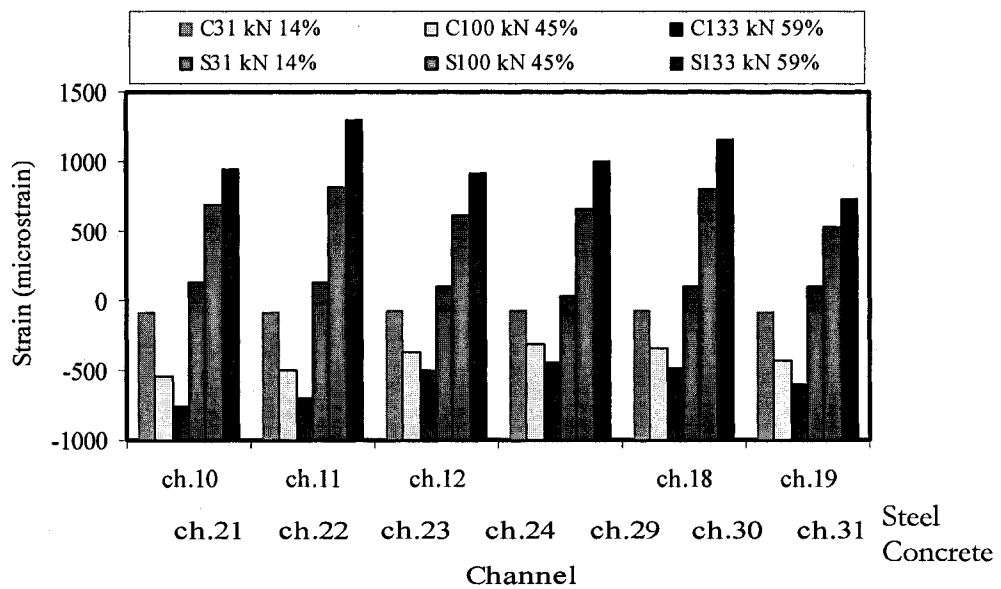
Control specimen (CTRL35)

Fig. 4-140: Concrete and Steel strain response on the long direction

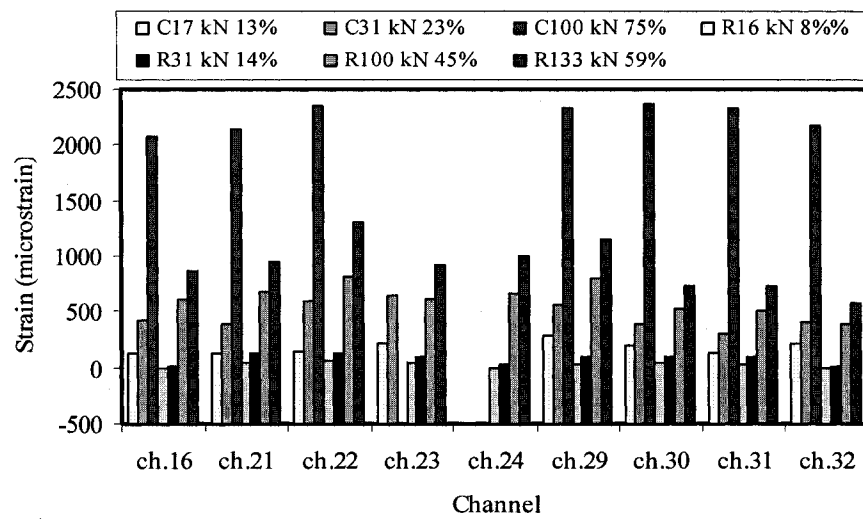Rehabilitated specimen (REHB35)

(Flexural failure)

289
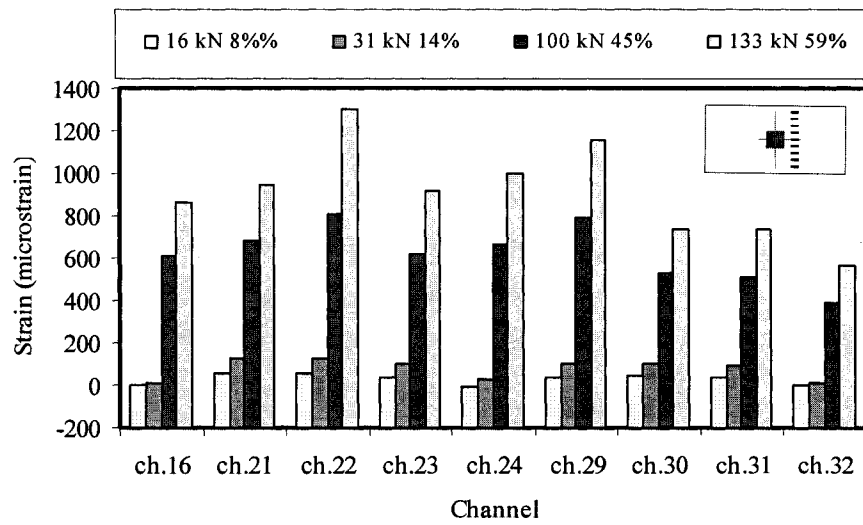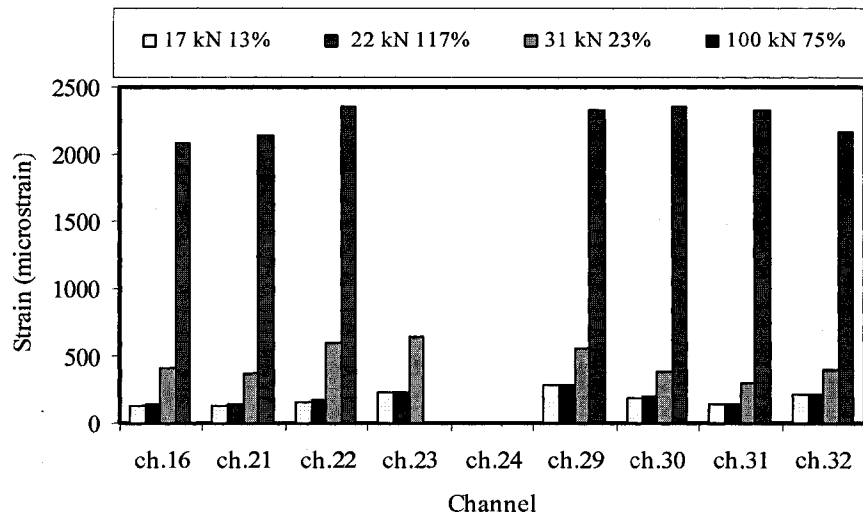
Fig. 4-141: Load versus long direction concrete strain

Control specimen CTRL35(C), rehabilitated specimen REHB35(R), and both together

290
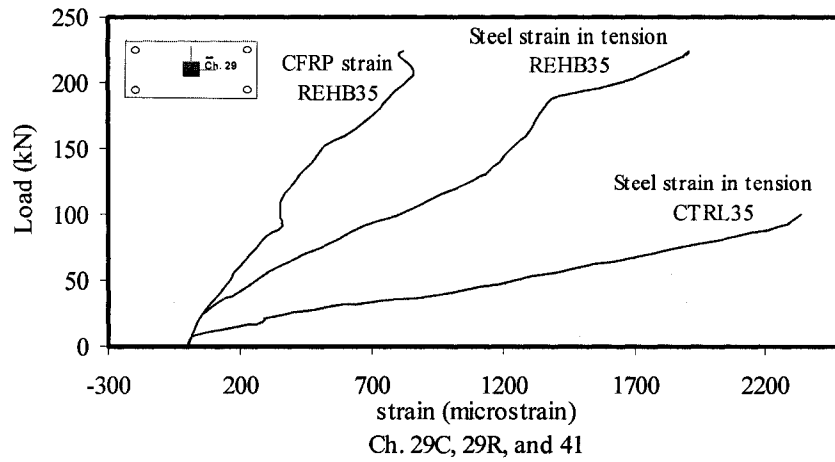
Fig. 4-142: Load versus tension long direction strain on the same cross-section for

Steel and CFRP

Control specimen (CTRL35), and rehabilitated specimen (REHB35)
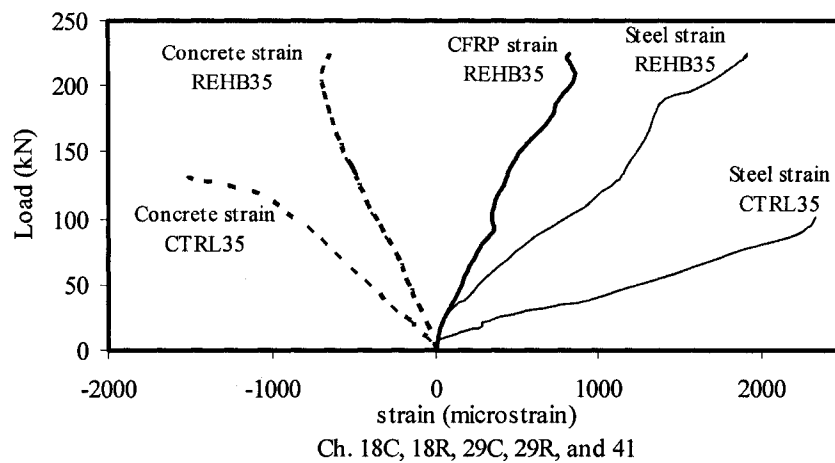
Fig. 4-143: Load versus tension long direction strain on the same cross-section for

Steel, Concrete and CFRP

Control specimen (CTRL35), and rehabilitated specimen (REHB35)

291
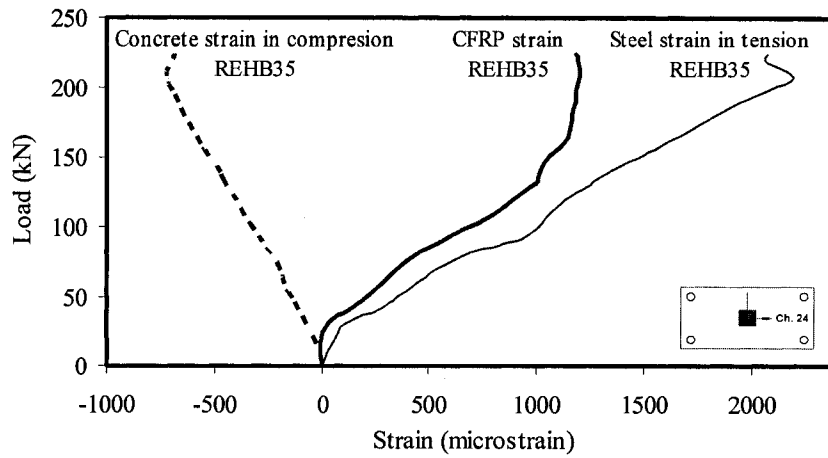
Fig. 4-144: Load versus tension long direction strain for

Steel, CFRP, and concrete in compression for the same cross-section

Rehabilitated specimen (REHB35)
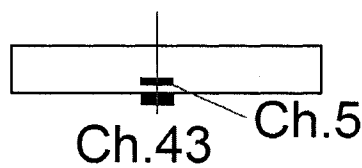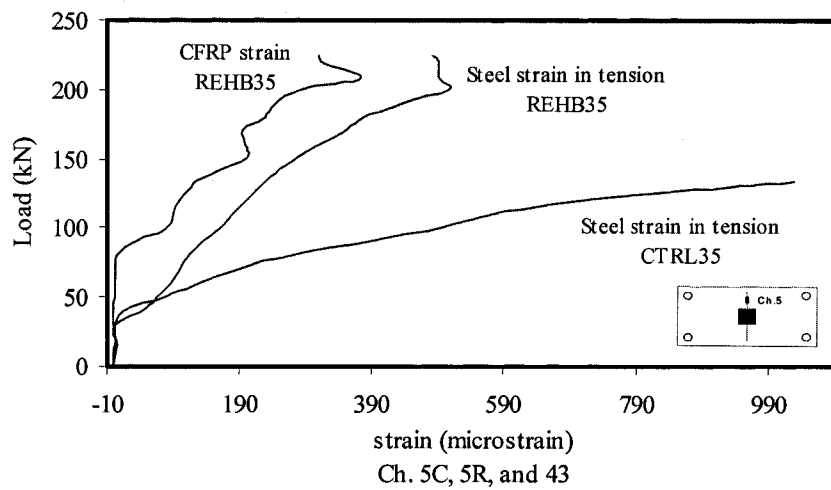
Fig. 4-145: Load versus tension strain short direction strain for CFRP and Steel

Control specimen (CTRL35), and rehabilitated specimen (REHB35)

292
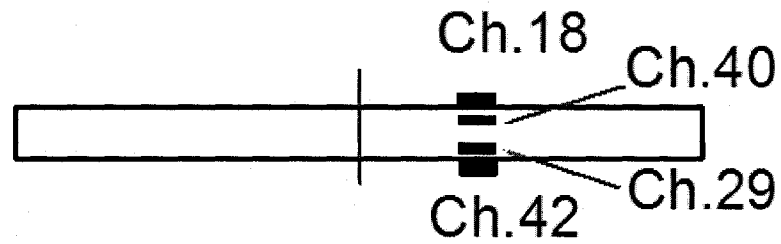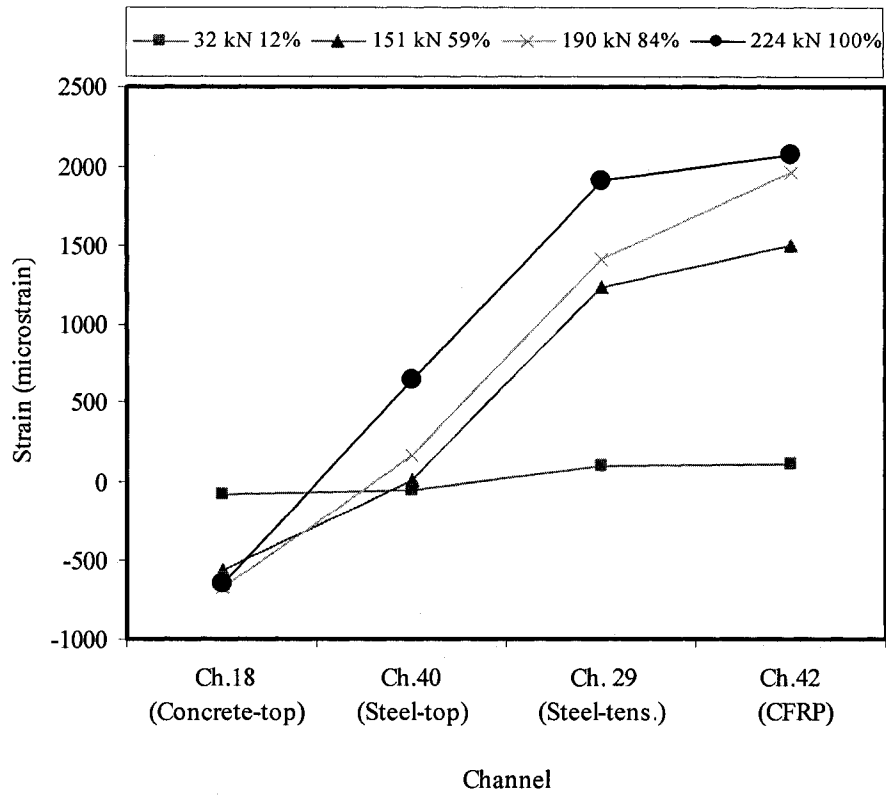
Fig. 4-146: Long direction strain response for concrete, steel and CFRP for the rehabilitated specimen (REHB35) on the same cross-section

293
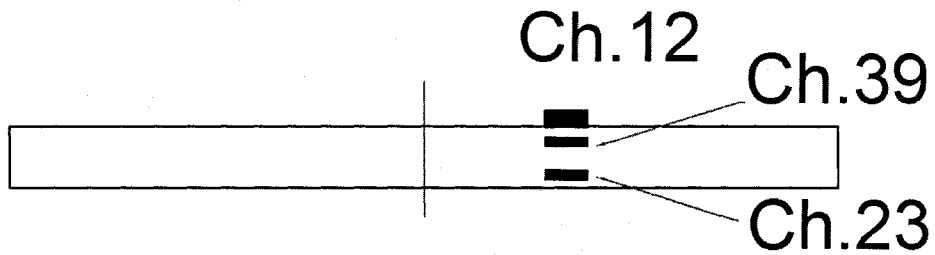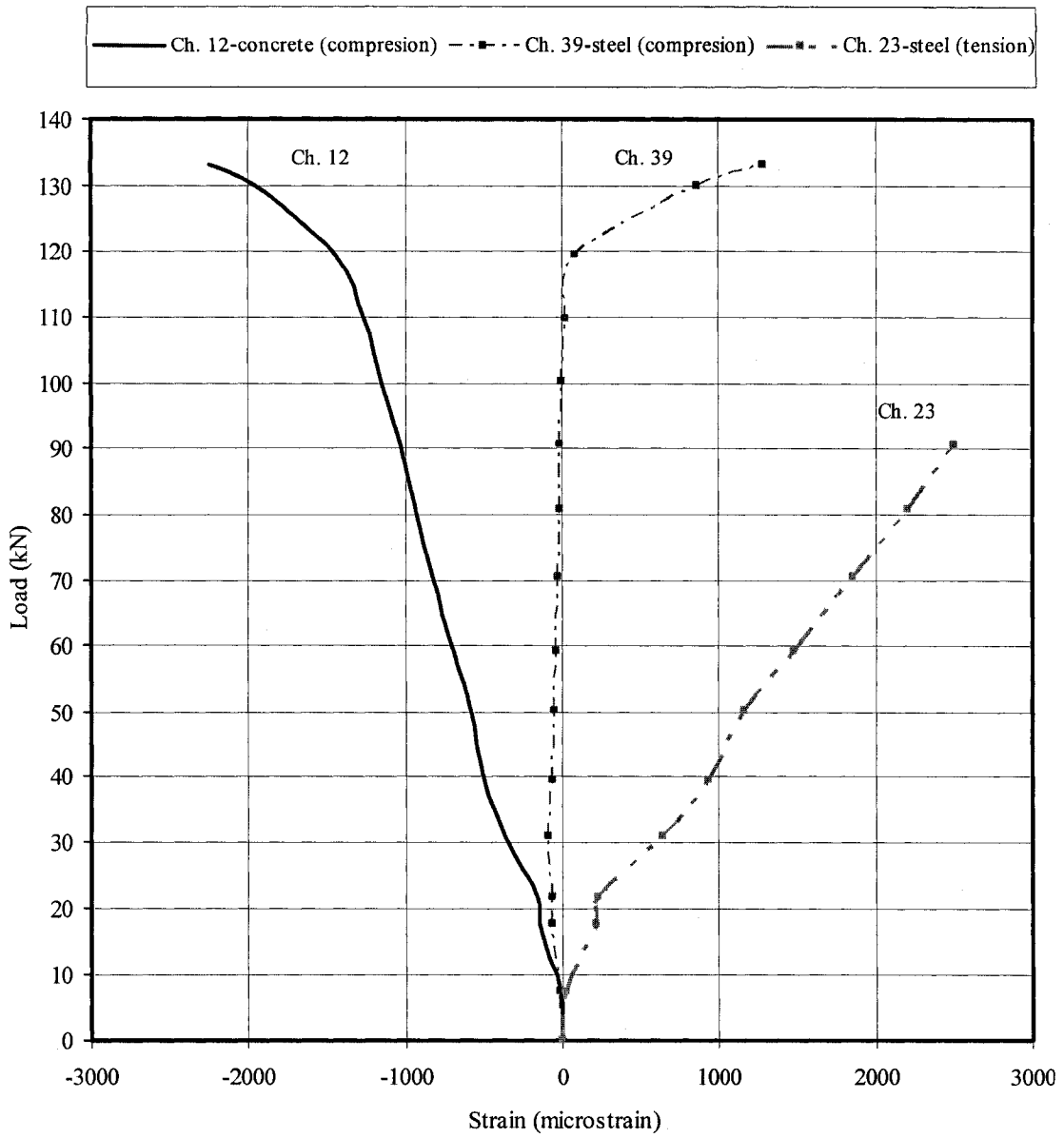
Fig. 4-147: Load versus long direction strain for the

control specimen (CTRL35) on the same cross-section

294
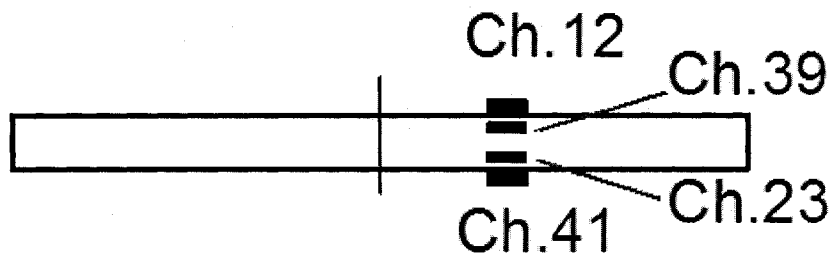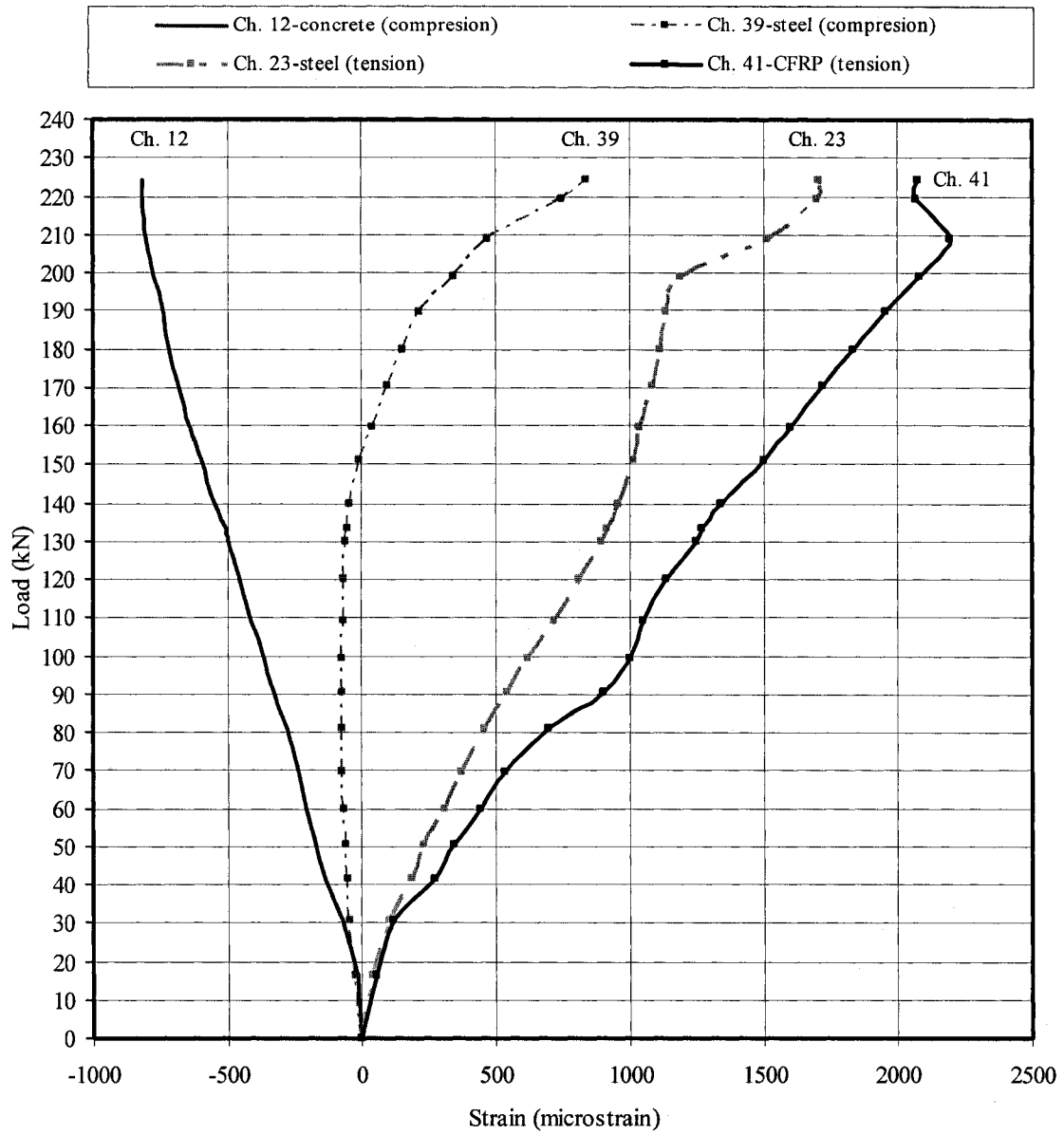
Fig. 4-148: Load versus long direction strain for the rehabilitated specimen (REHB35)

295

BEHAVIOUR OF THE THREE GROUPS

Central Deflection (Channel 33)
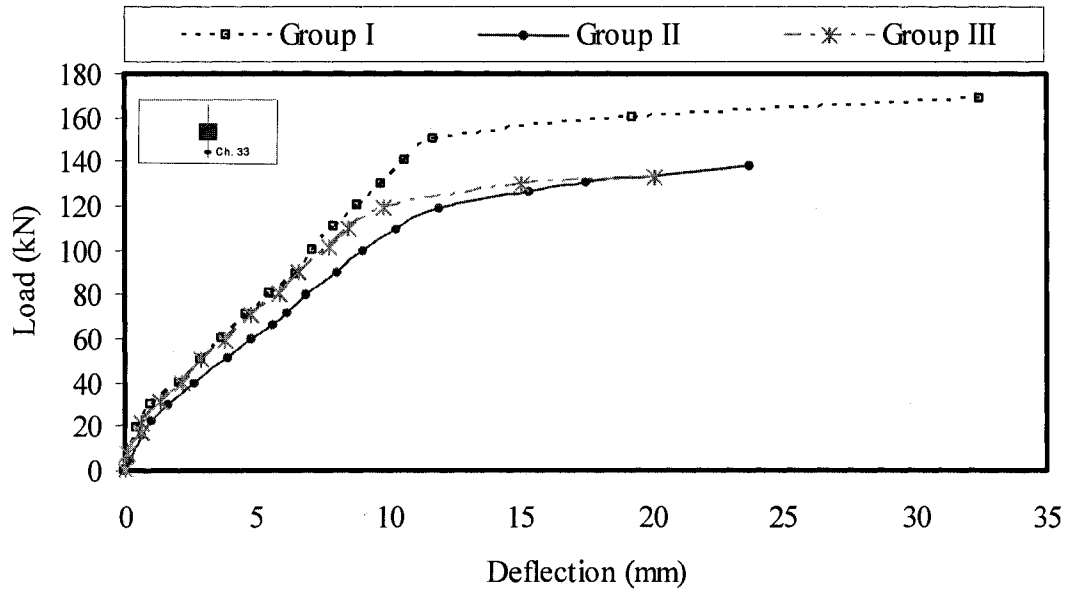
Fig. 4-149: Effect of the eccentricity on the central deflection for the

control specimens (CTRL)
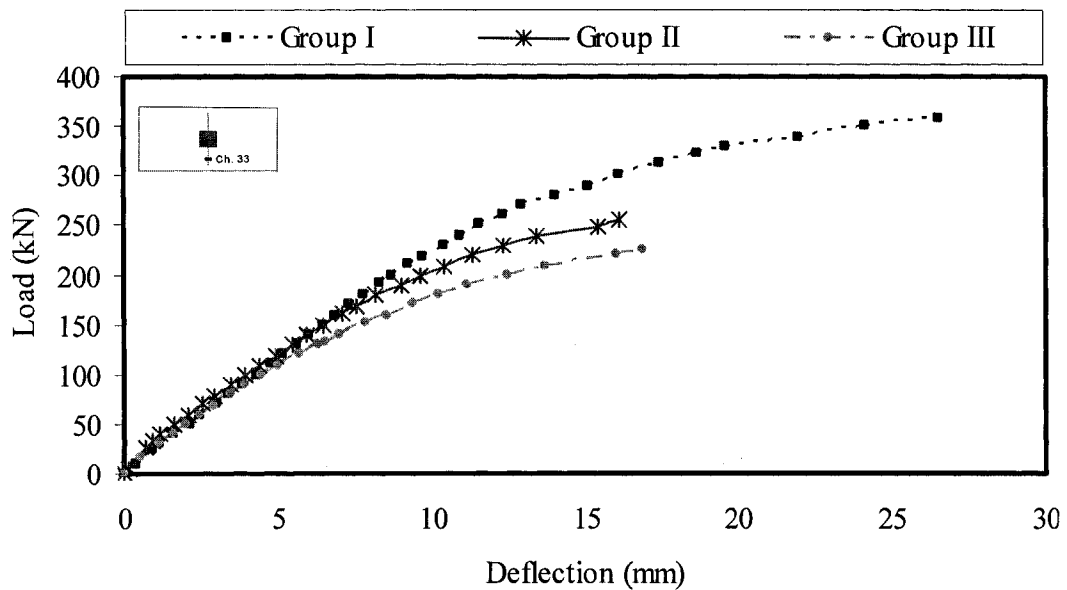
Fig. 4-150: Effect of the eccentricity on the central deflection for the

rehabilitated specimens (REHB)

Central Deflection (channel 33)
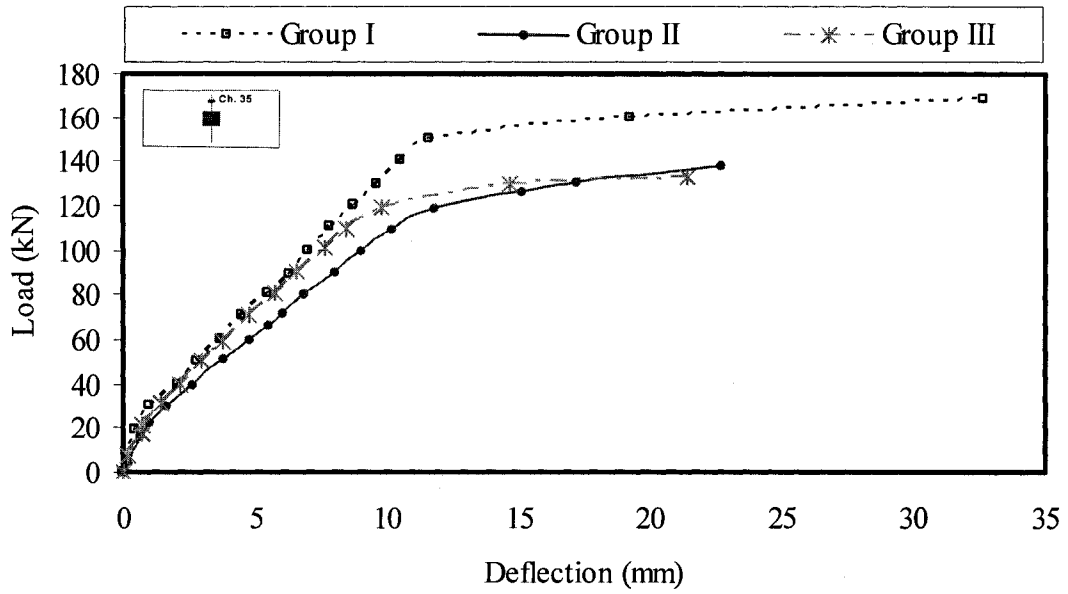
Fig. 4-151: Effect of the eccentricity on the central deflection

Control specimens (CTRL)
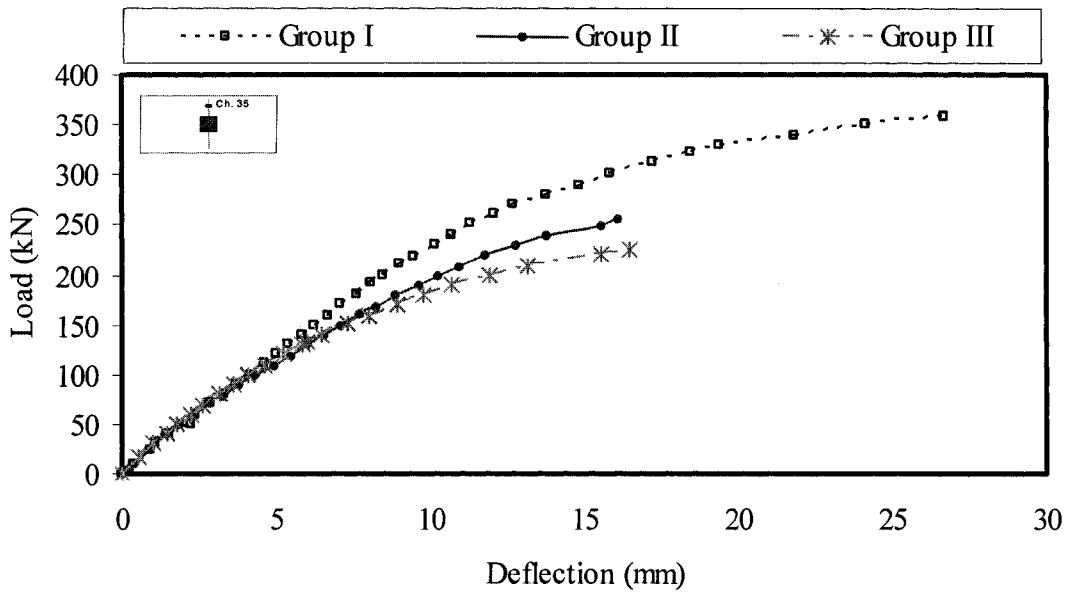
Fig. 4-152: Effect of the eccentricity on the central deflection

Rehabilitated specimens (REHB)

297

Concrete Strain (channel 12)
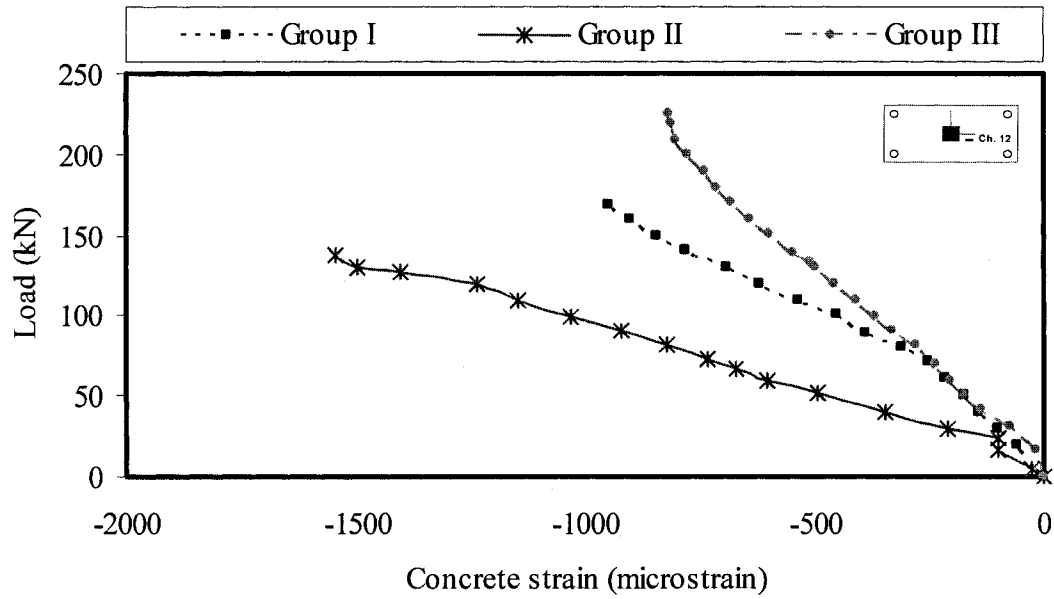
Fig. 4-153: Effect of eccentricity on the long direction concrete strain

Control specimens (CTRL)
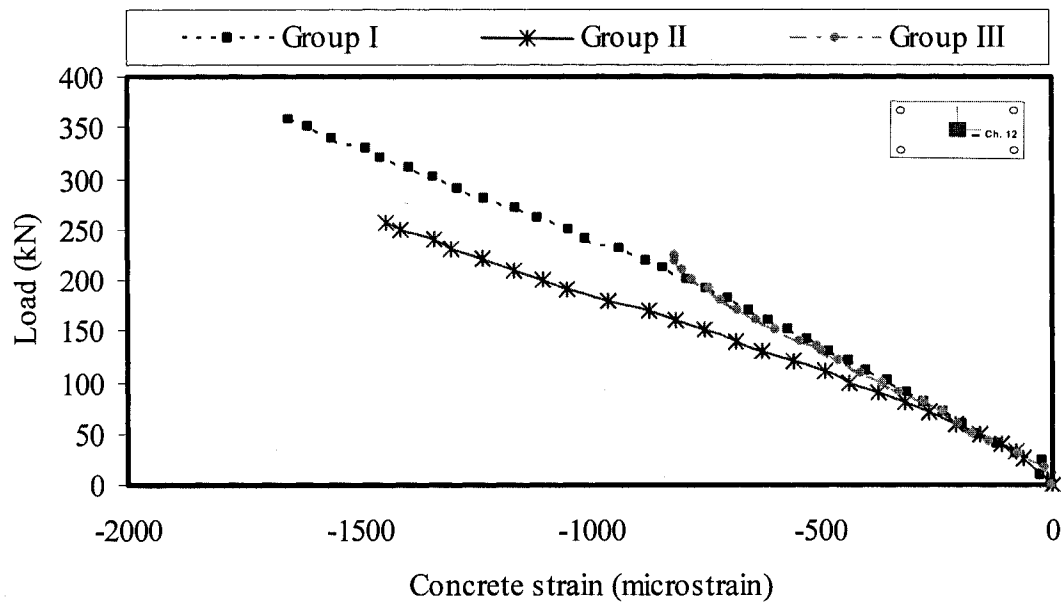
Fig. 4-154: Effect of eccentricity on the long direction concrete strain

Rehabilitated specimens (REHB)

298

Steel Strain (channel 23)
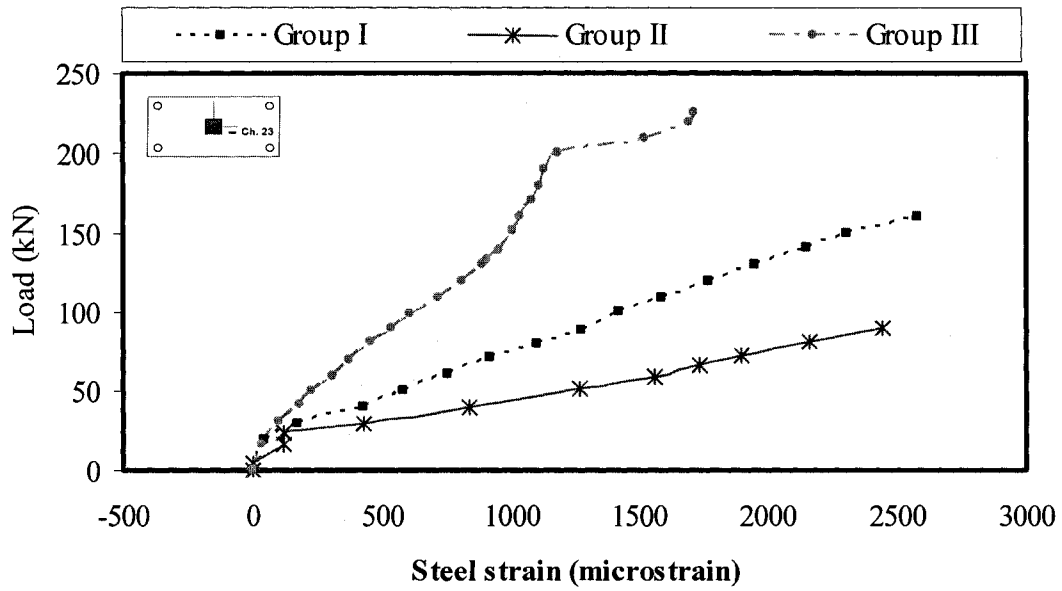
Fig. 4-155: Effect of eccentricity on the long direction steel strain for

Control specimens (CTRL)
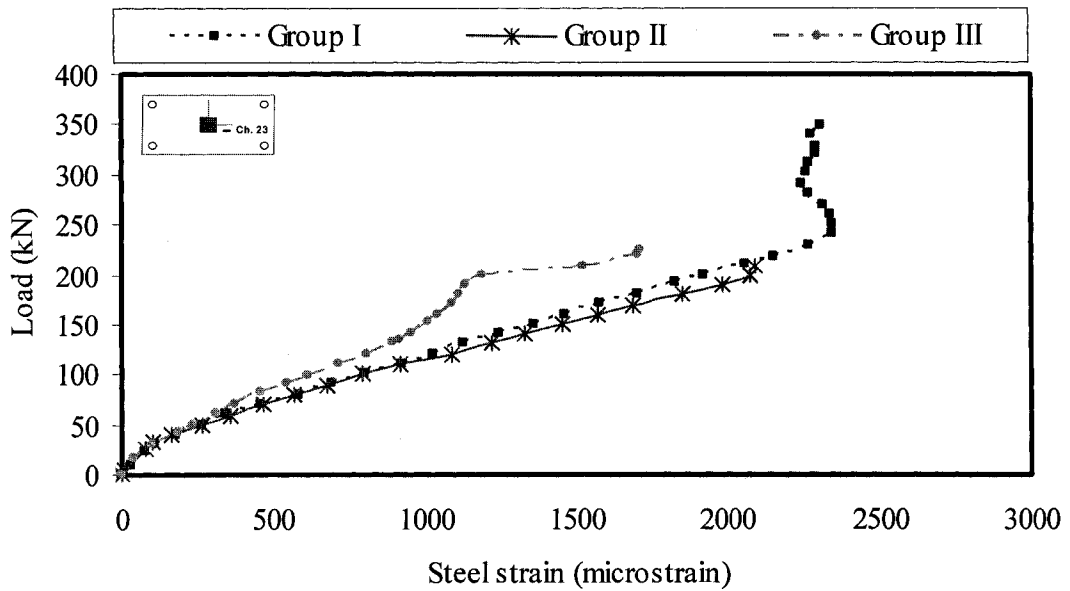
Fig. 4-156: Effect of eccentricity on the long direction steel strain for

Rehabilitated specimens (REHB)

299

	I	II	III
CTRL specimens	3.1	2.6	2.6
REHB specimens	2.1	1.7	1.5

Group
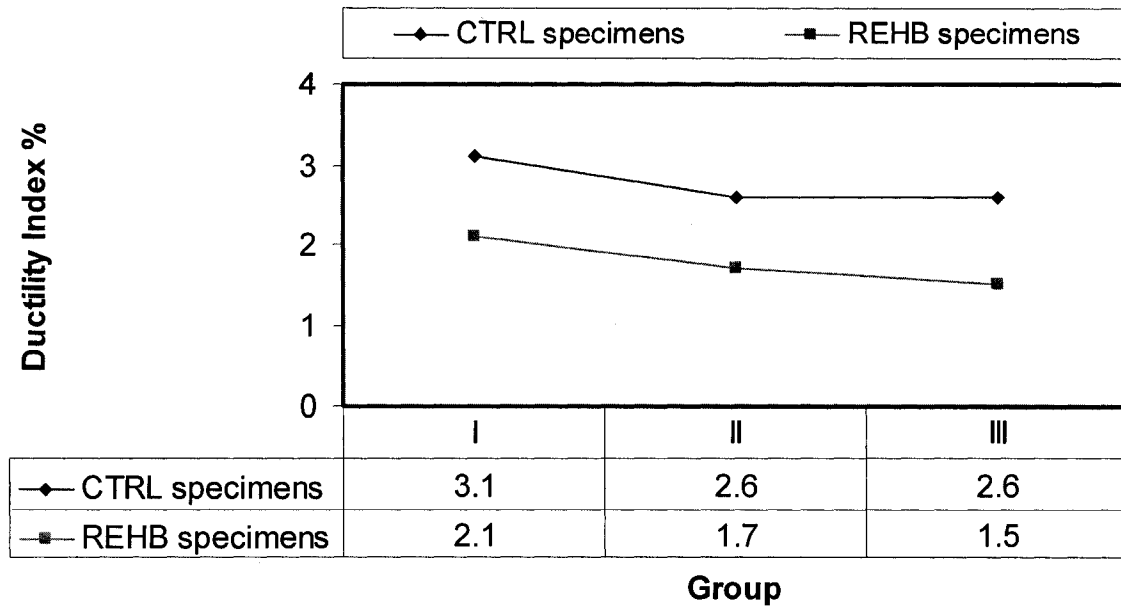
Fig. 4-157: Effect of eccentricity on the Ductility Index
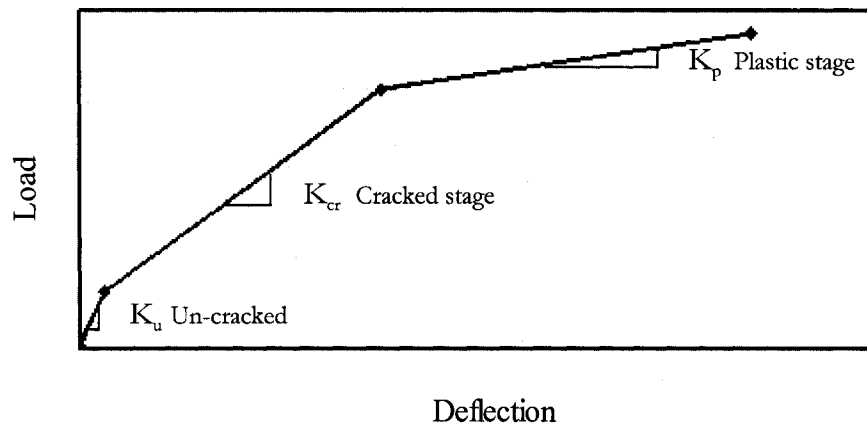
Fig. 4-158: Idealized load-deflection behaviour of a reinforced concrete member

300
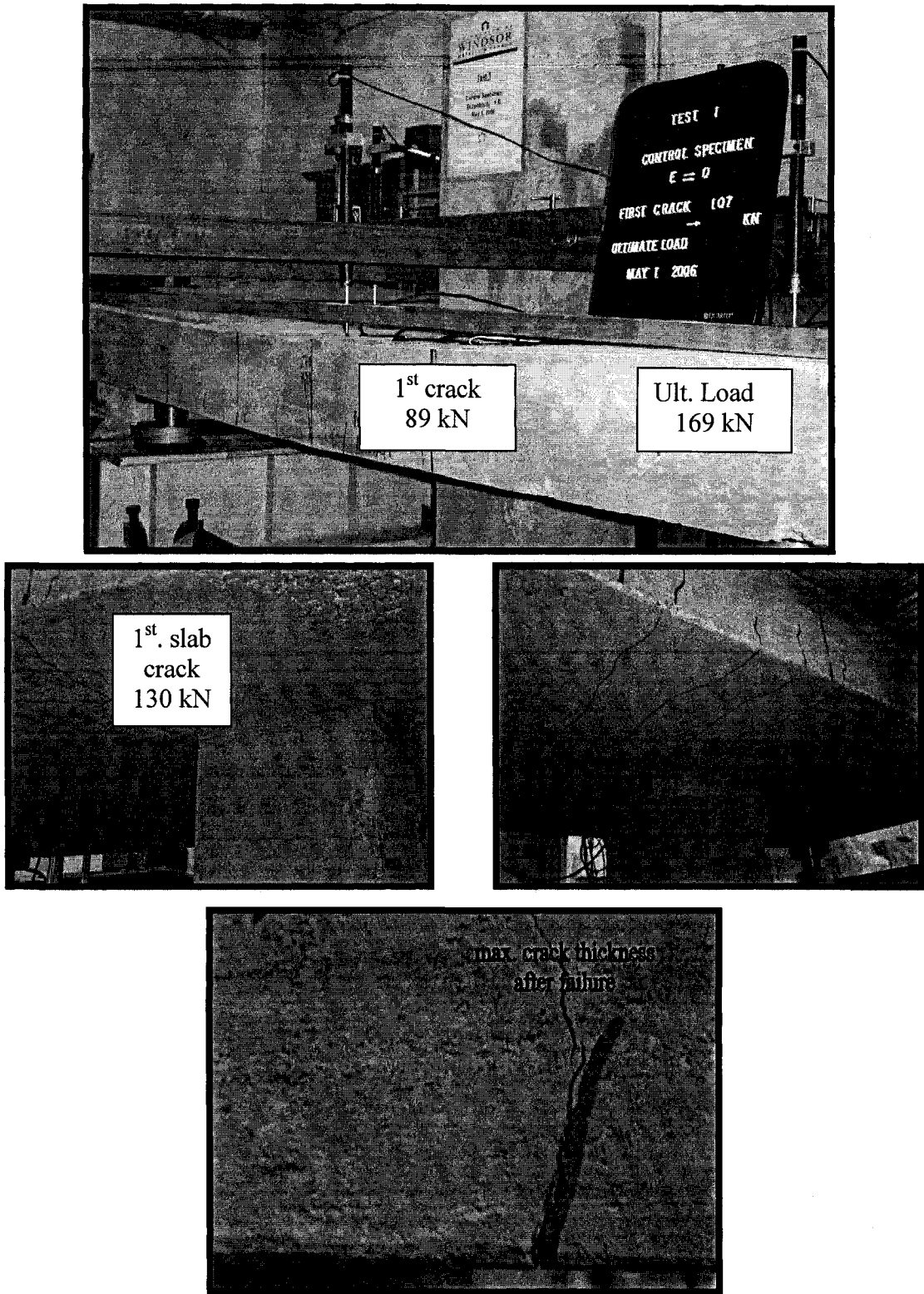
Fig. 4-159: The control specimen (CTRL0) during different sages of loading

301

1st crack
89 kN
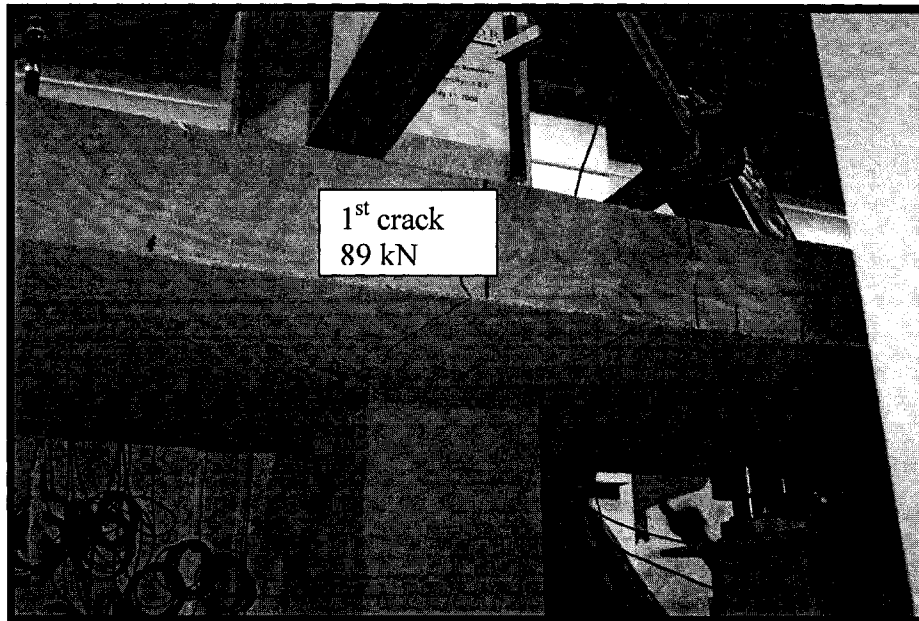
Fig. 4-160: The cracked specimen (CRAK0) during loading
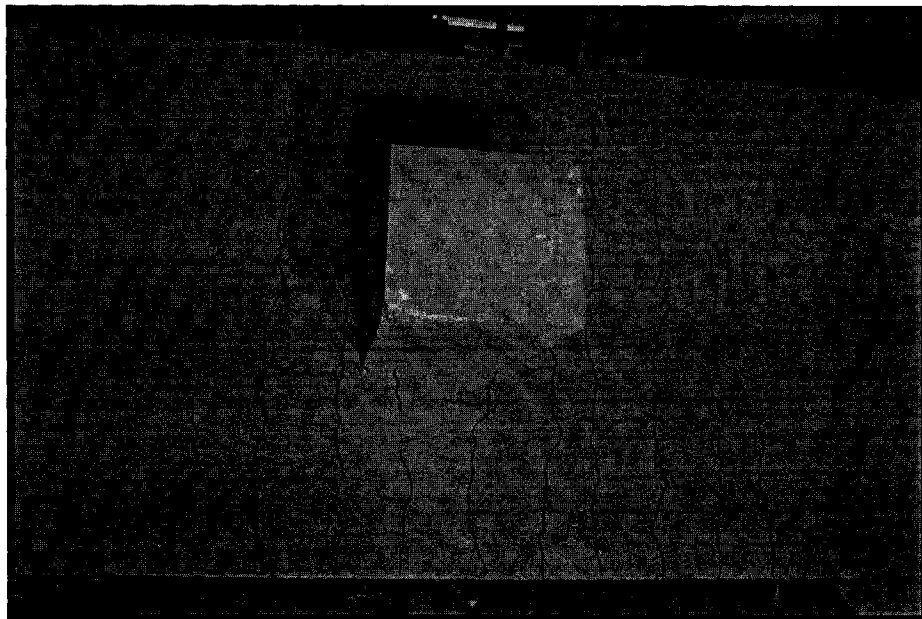
Fig. 4-161: The cracked specimen (CRAK0) after loading and transferring

302
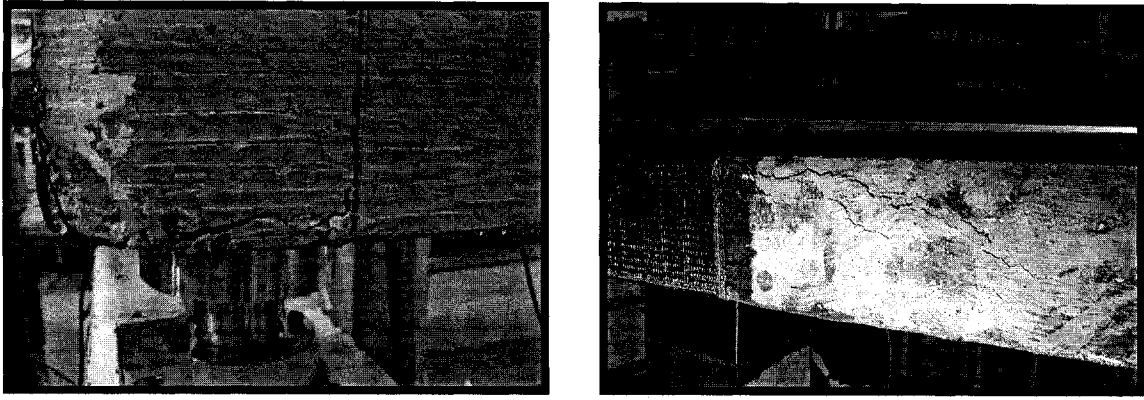
Fig. 4-162: The Rehabilitated specimen (REHB0) during loading
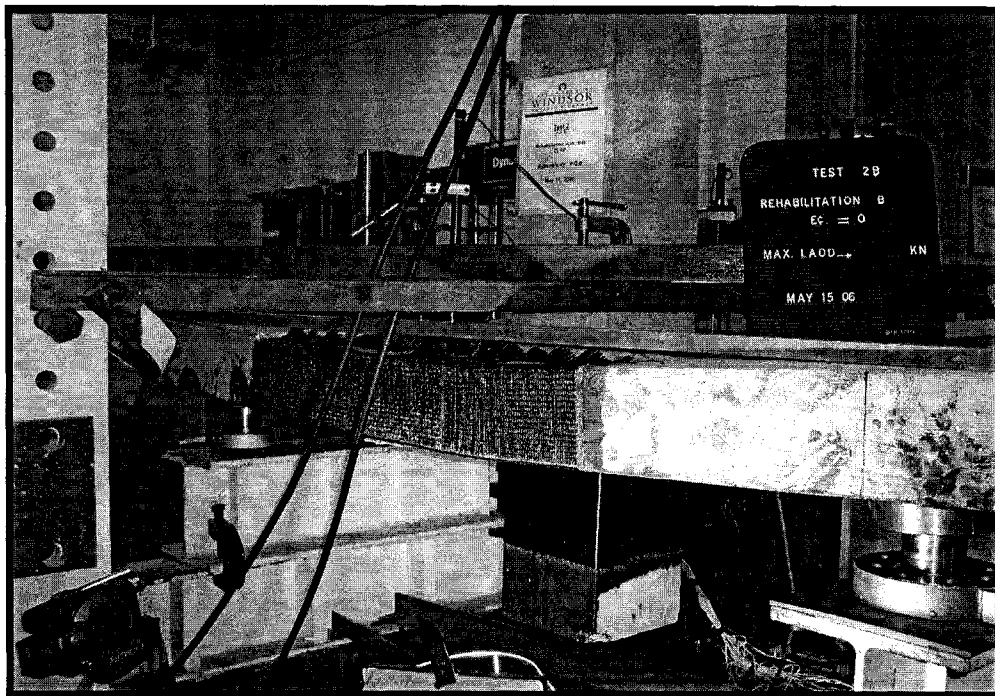
Fig. 4-163: The rehabilitated specimen (REHB0) after failure

303
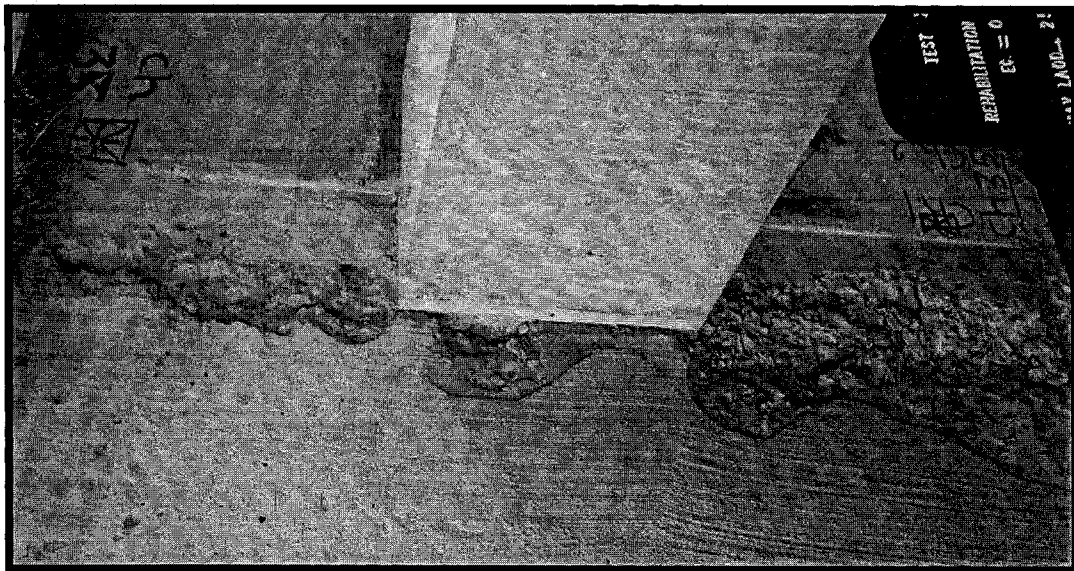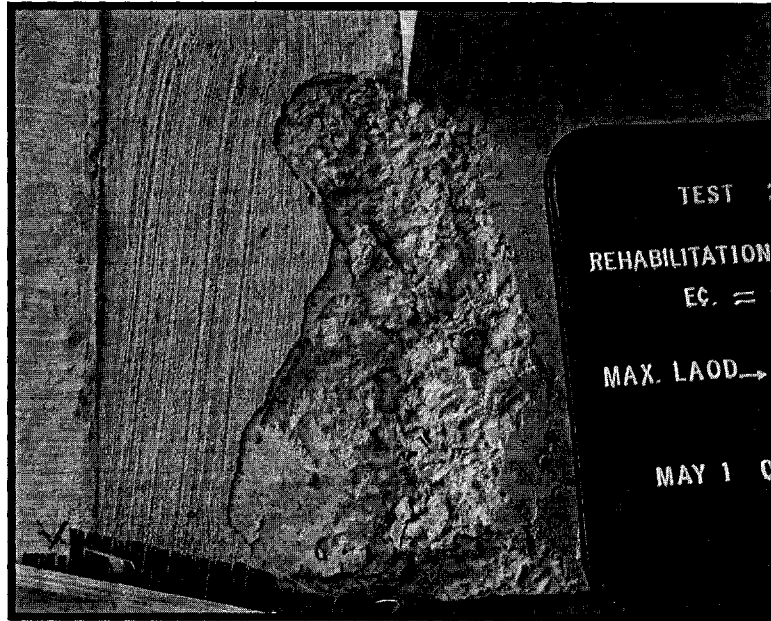
Fig. 4-164: The rehabilitated specimen (REHB0) after failure and moving

304
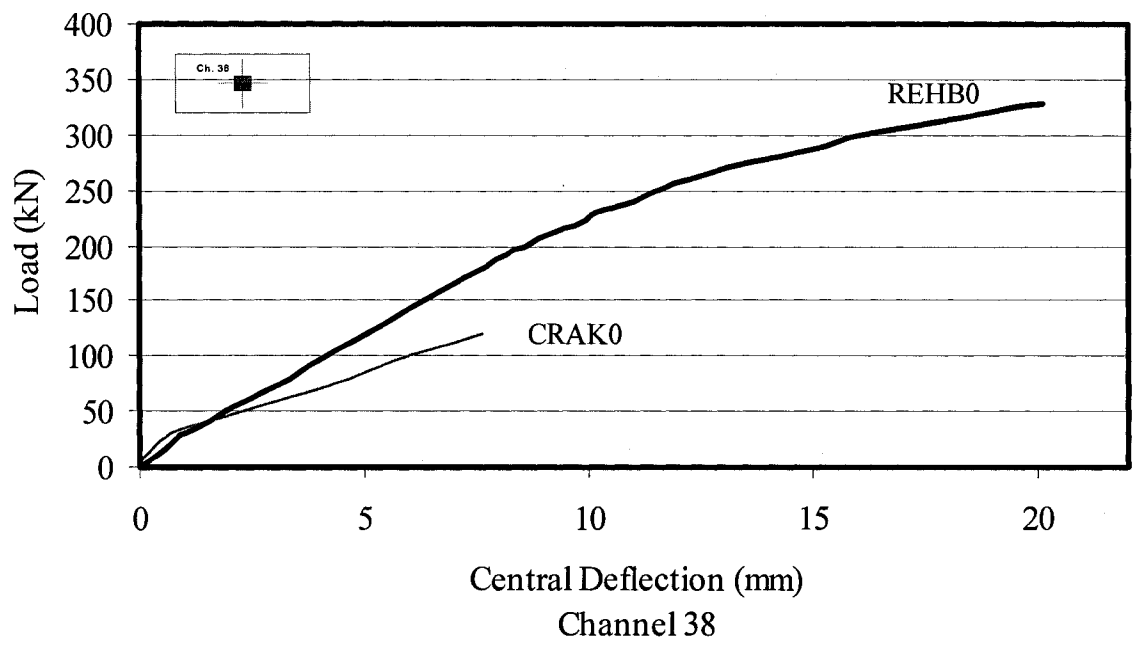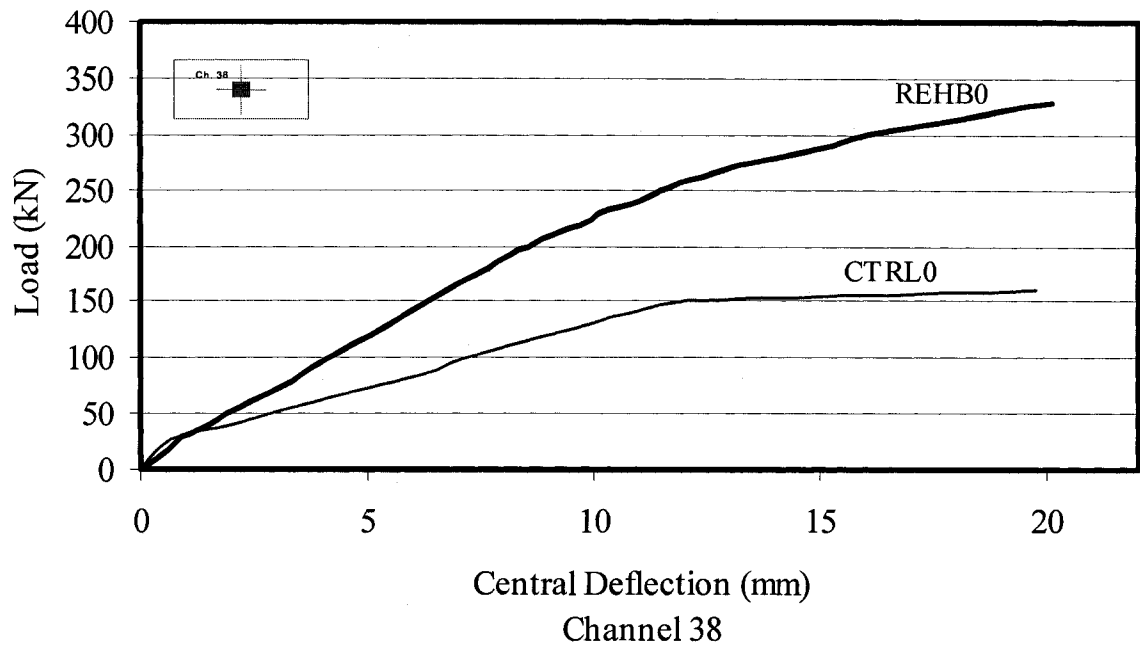
Fig. 4-165: Load versus central deflection for group I specimens (Ch. 38)

305
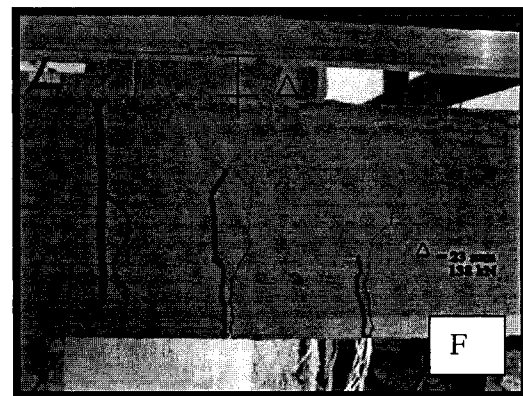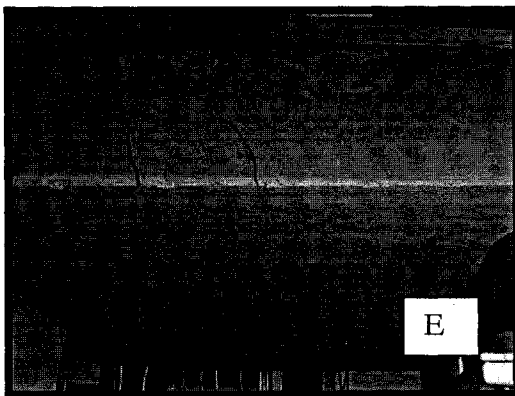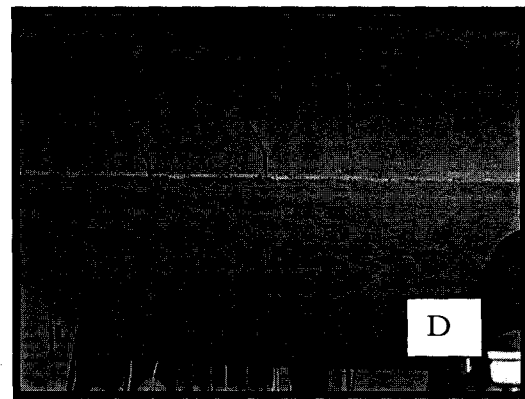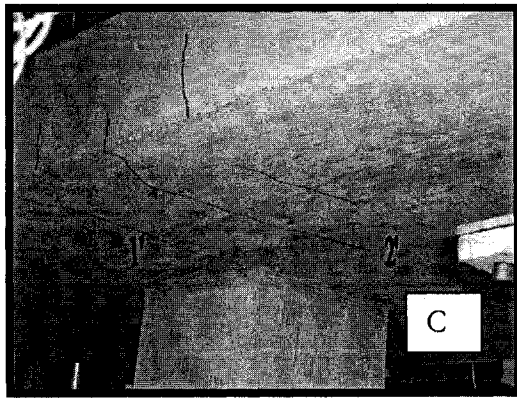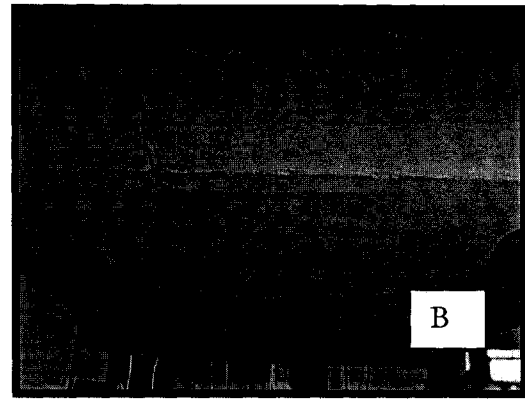
Fig. 4-166: The control specimen (CTRL25) during different stages of loading

306
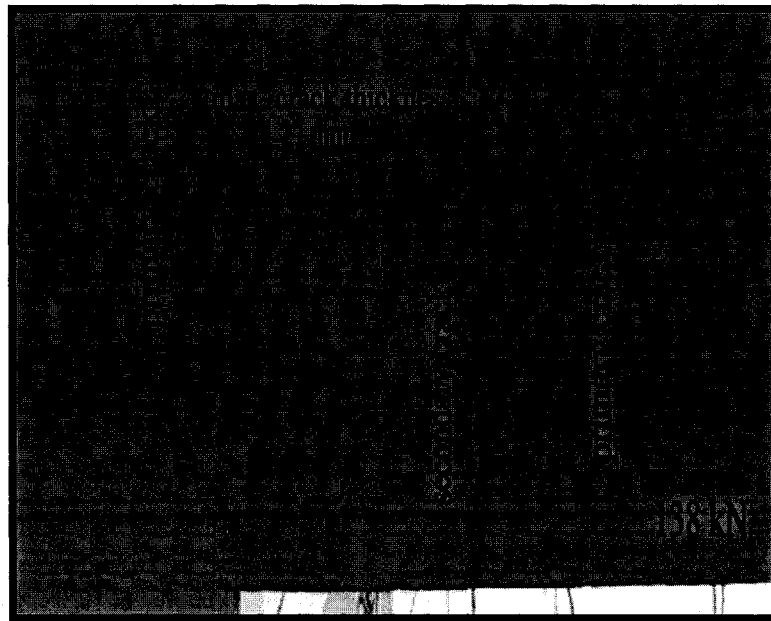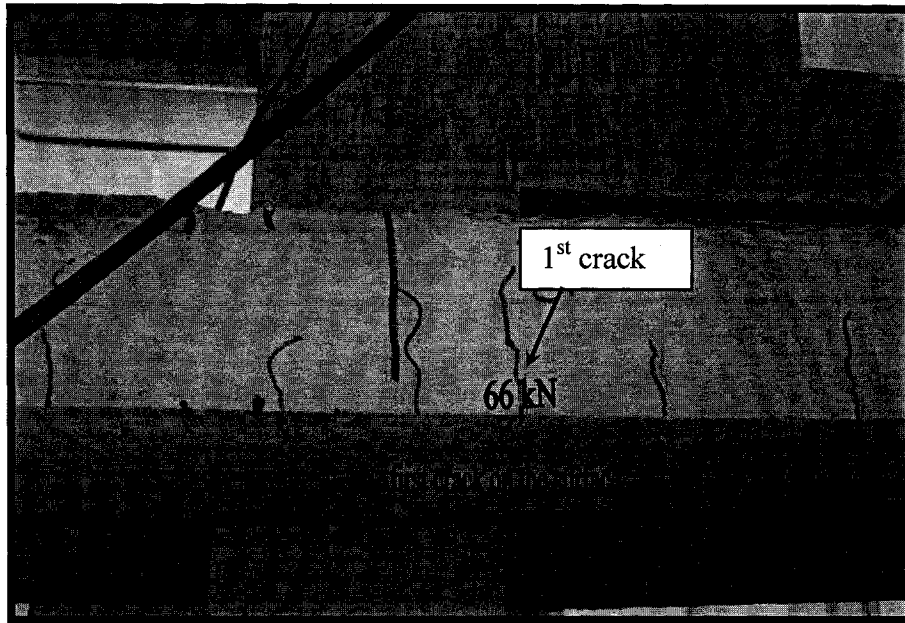
Fig. 4-167: The control specimen (CTRL25) after failure

307
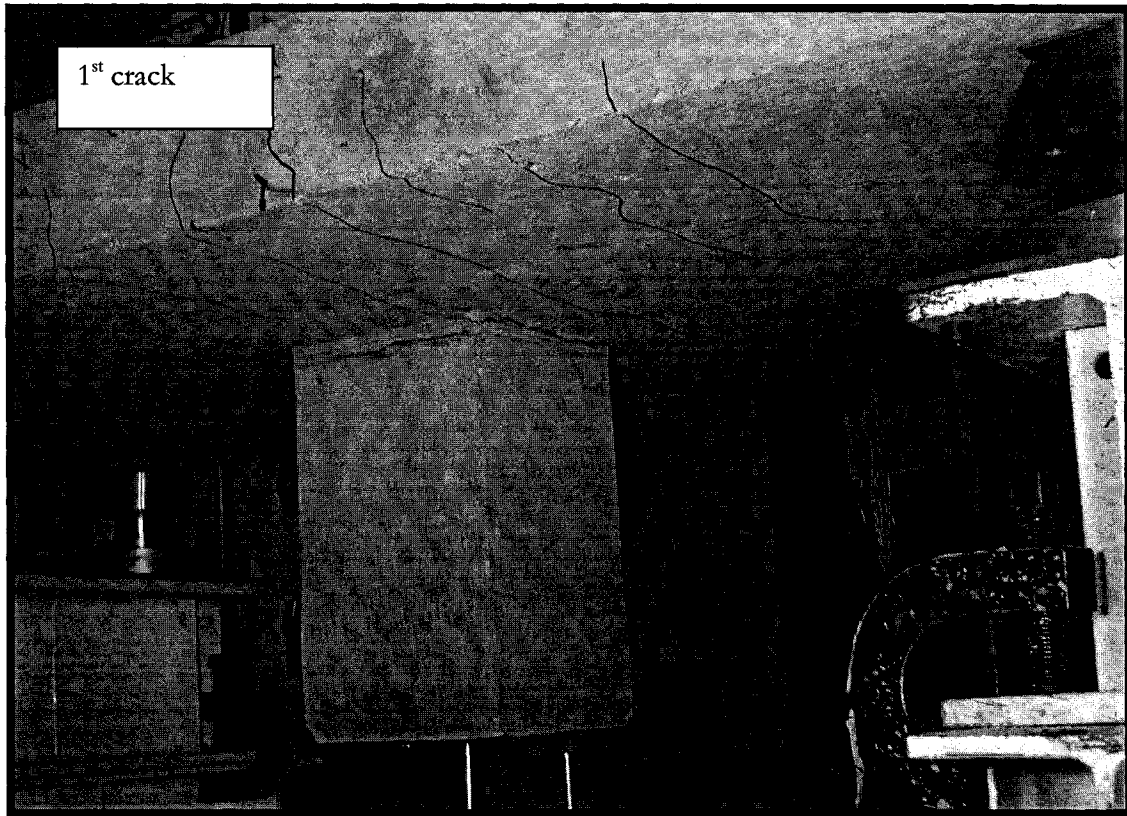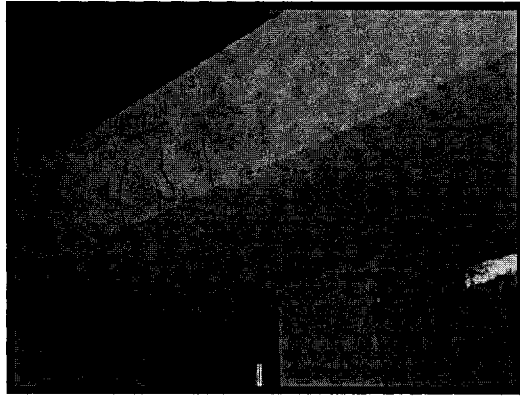
Fig. 4-168: The cracked specimen (CRAK25) during different stage of loading

308
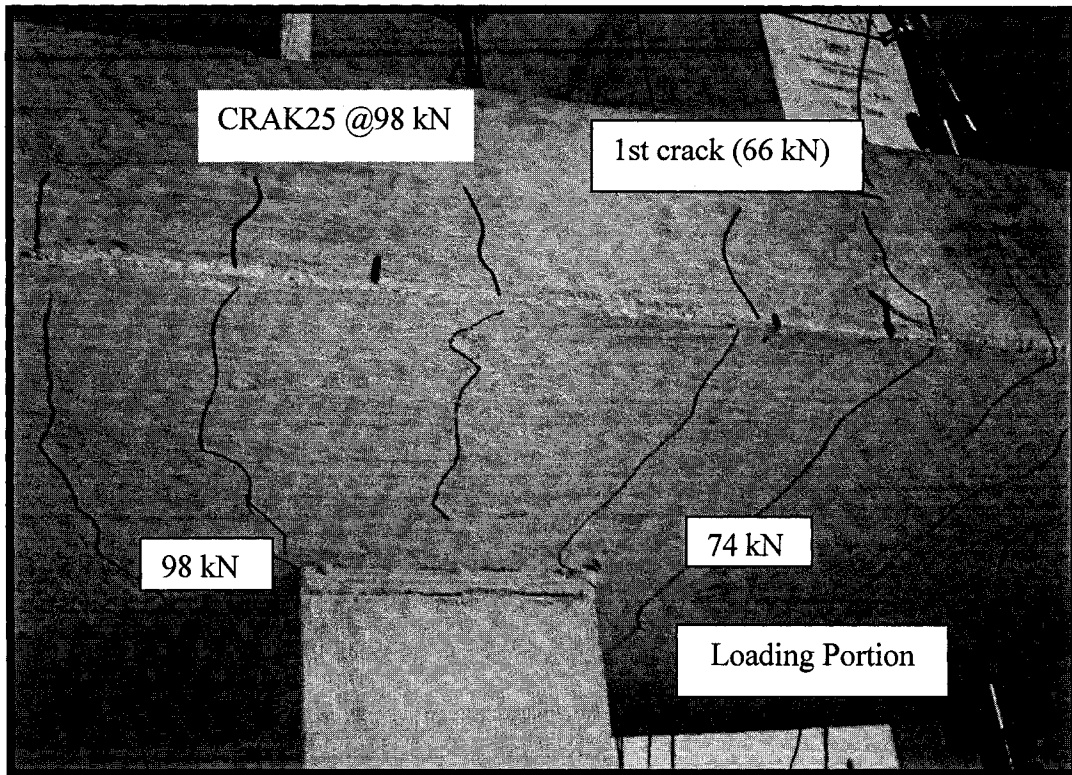
Fig. 4-169: The cracked specimen (CRAK25) at 99 kN applied jacking load
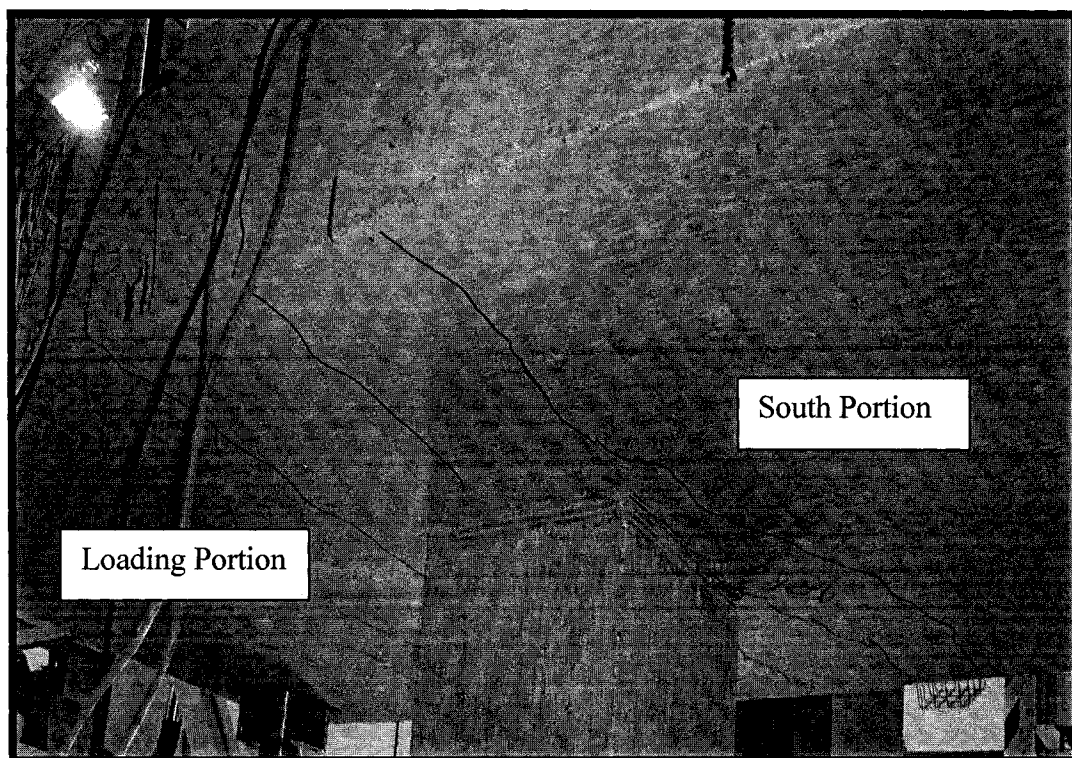
Fig. 4-170: South-west portion of the racked specimen (CRAK25)

309
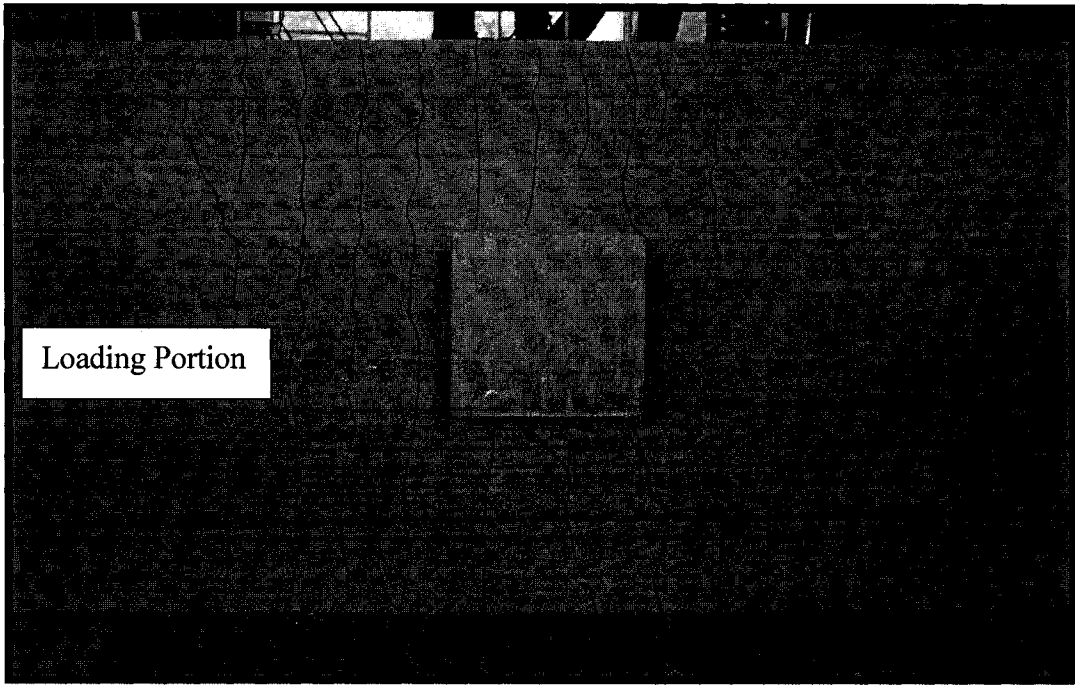
Fig. 4-171: The cracked specimen (CRAK25) after releasing the load and transferring
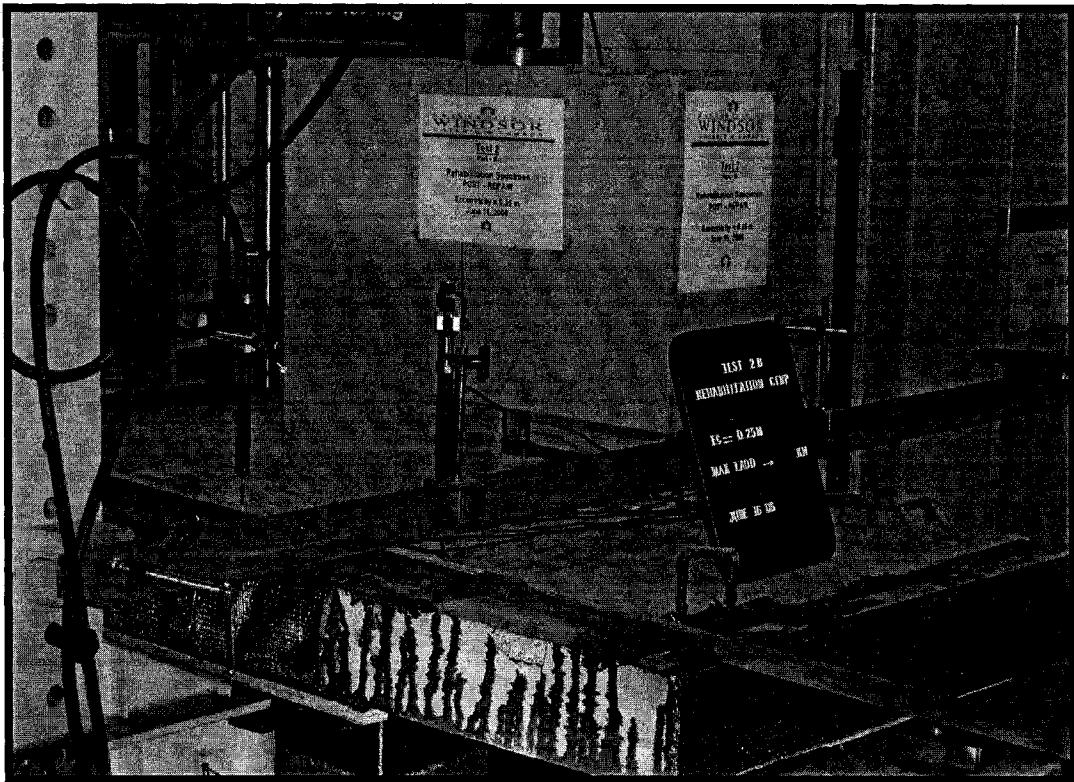
Fig. 4-172: The rehabilitated specimen (REHB25) during loading

310
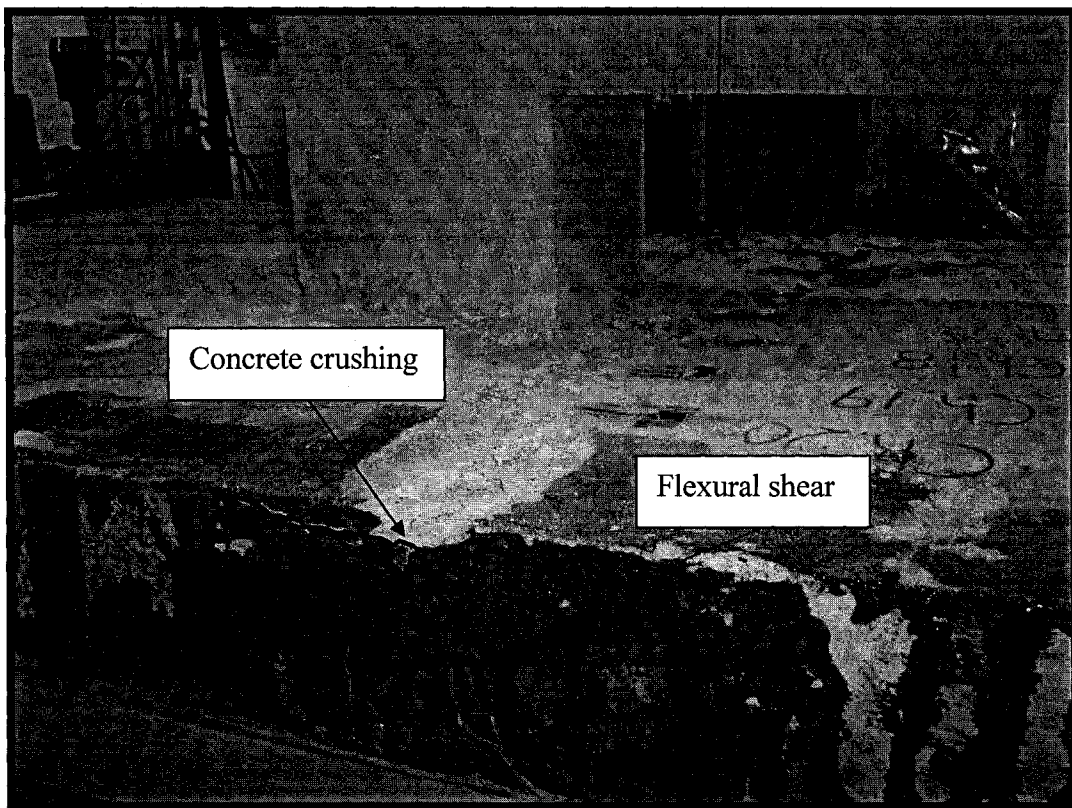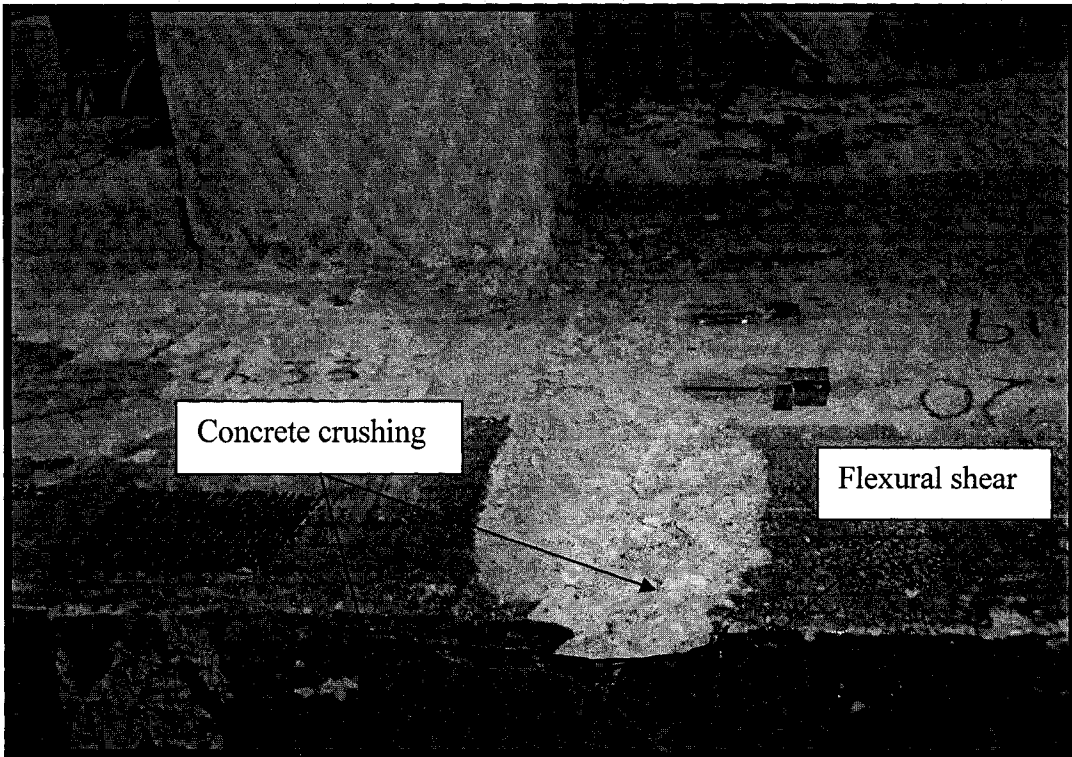
Fig. 4-173: The rehabilitated specimen (REHB25) after failure and transferring

311
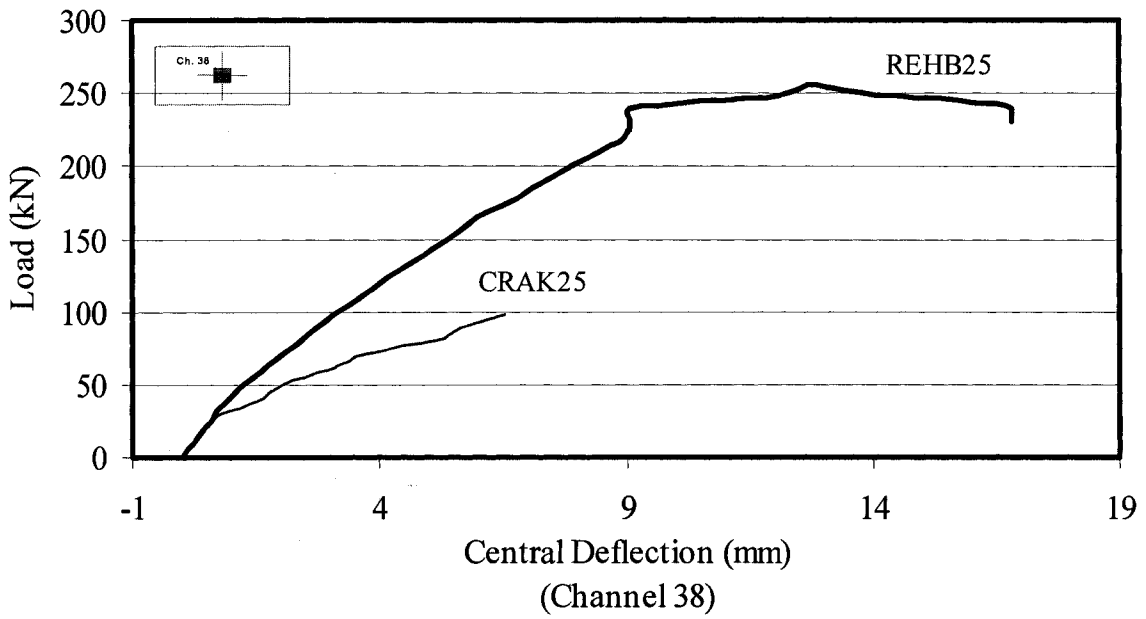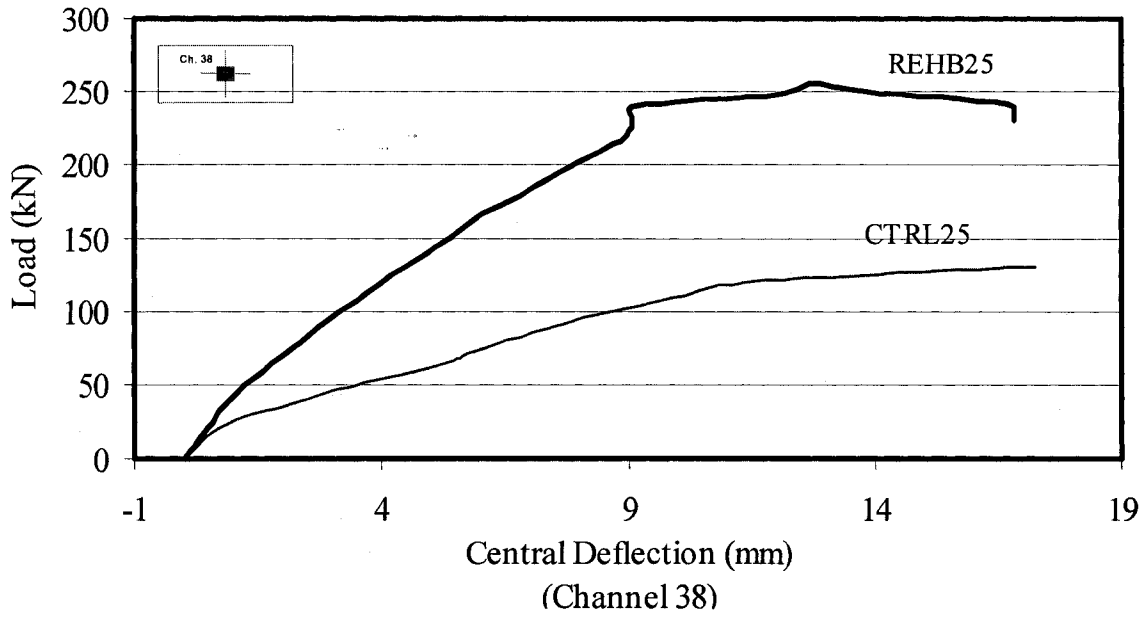
Fig. 4-174: Load versus central deflection for group II specimens (Ch. 38)

312
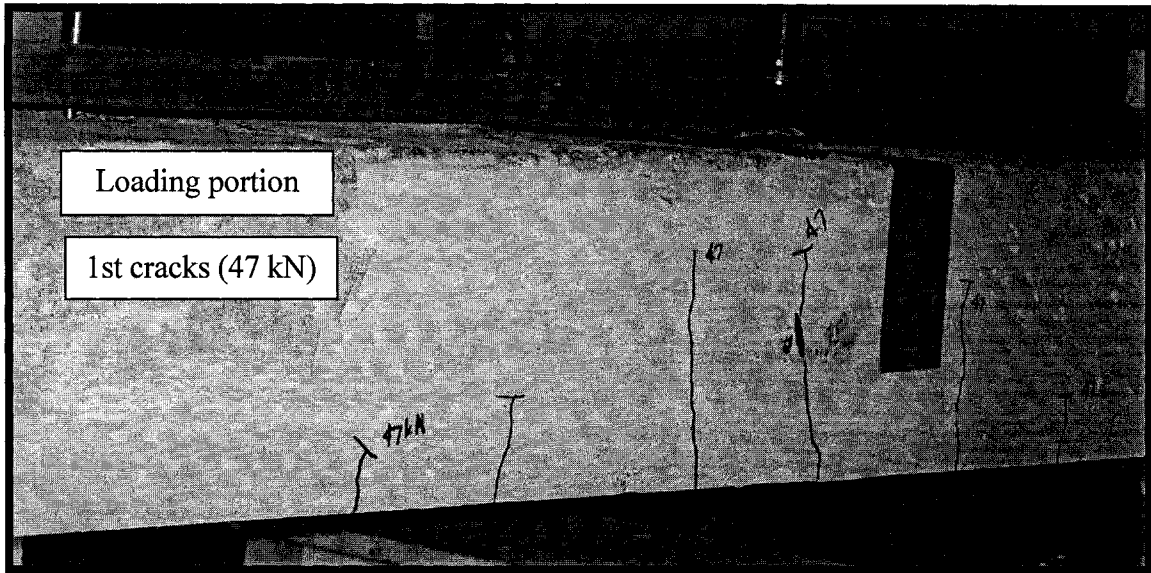
Figure 4-175: The control specimen CTRL35 at first visible cracks (47 kN)
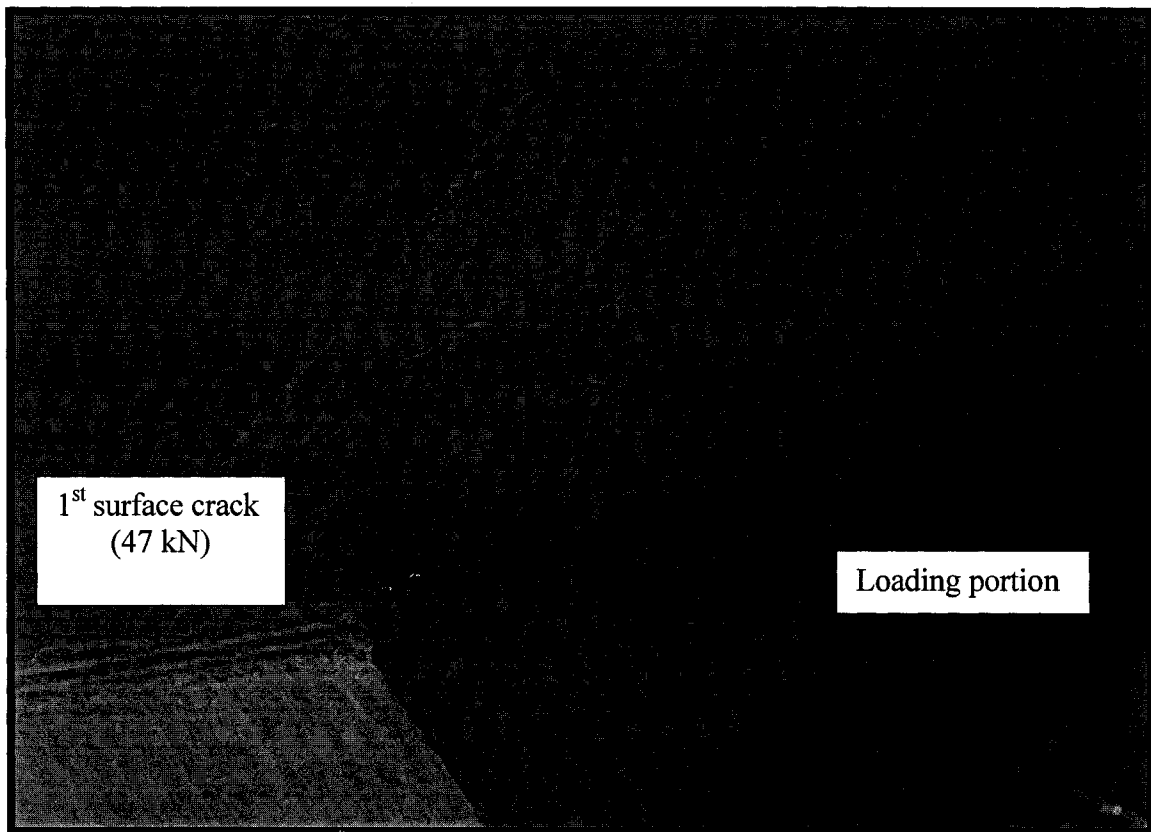
Fig. 4-176: The control specimen CTRL35 at jacking load of 80 kN

313
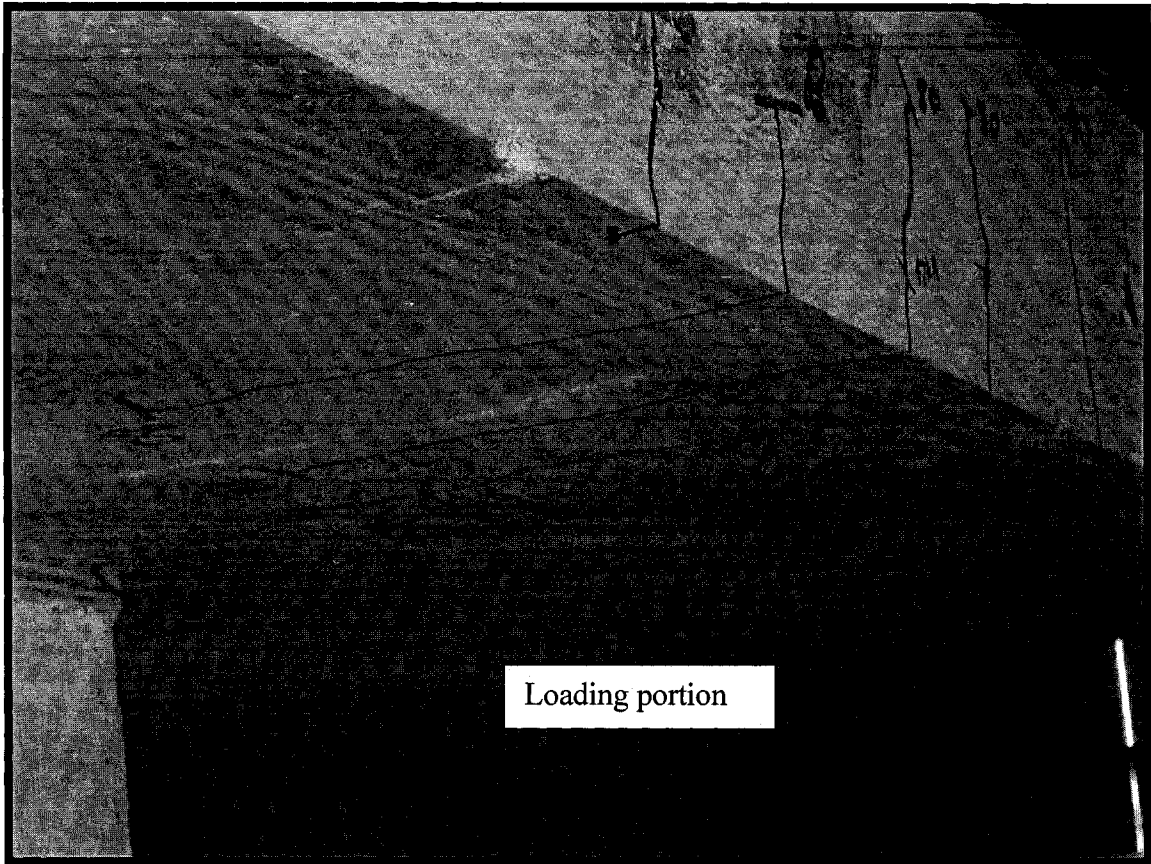
Fig. 4-177: The tension surface of control specimen CTRL35 at jacking load of 80 kN
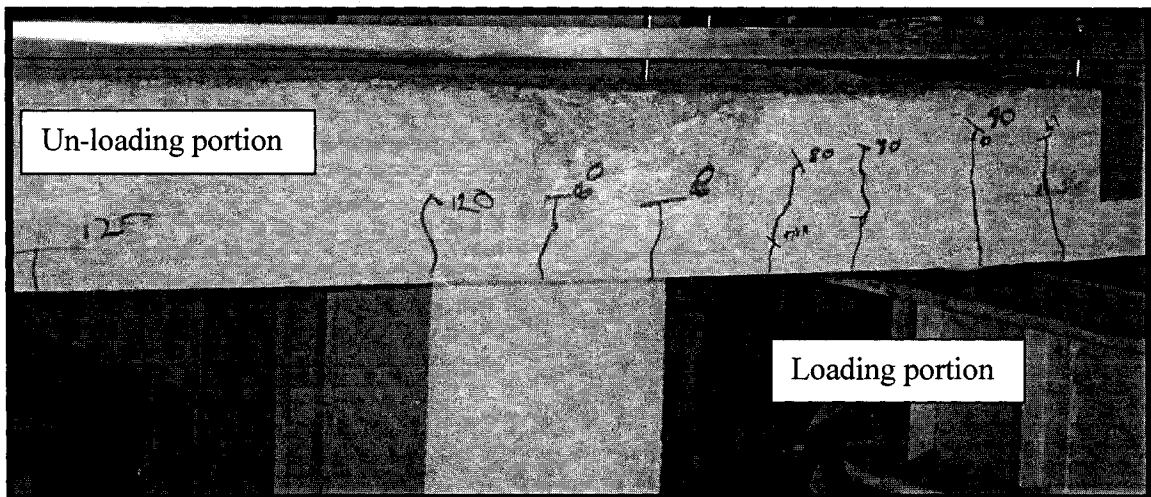
Fig. 4-178: The control specimen CTRL35 at jacking load of 120 kN

314
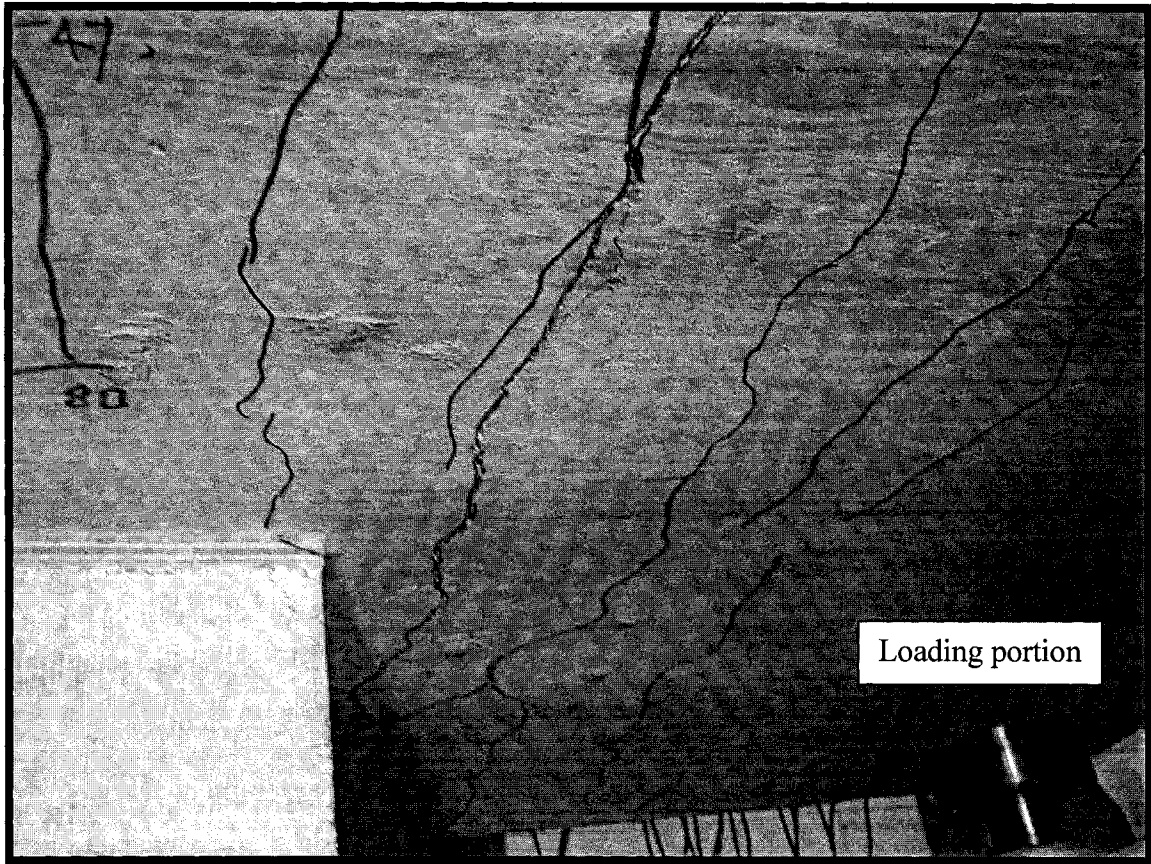
Fig. 4-179: The control specimen CTRL35 after failure

315
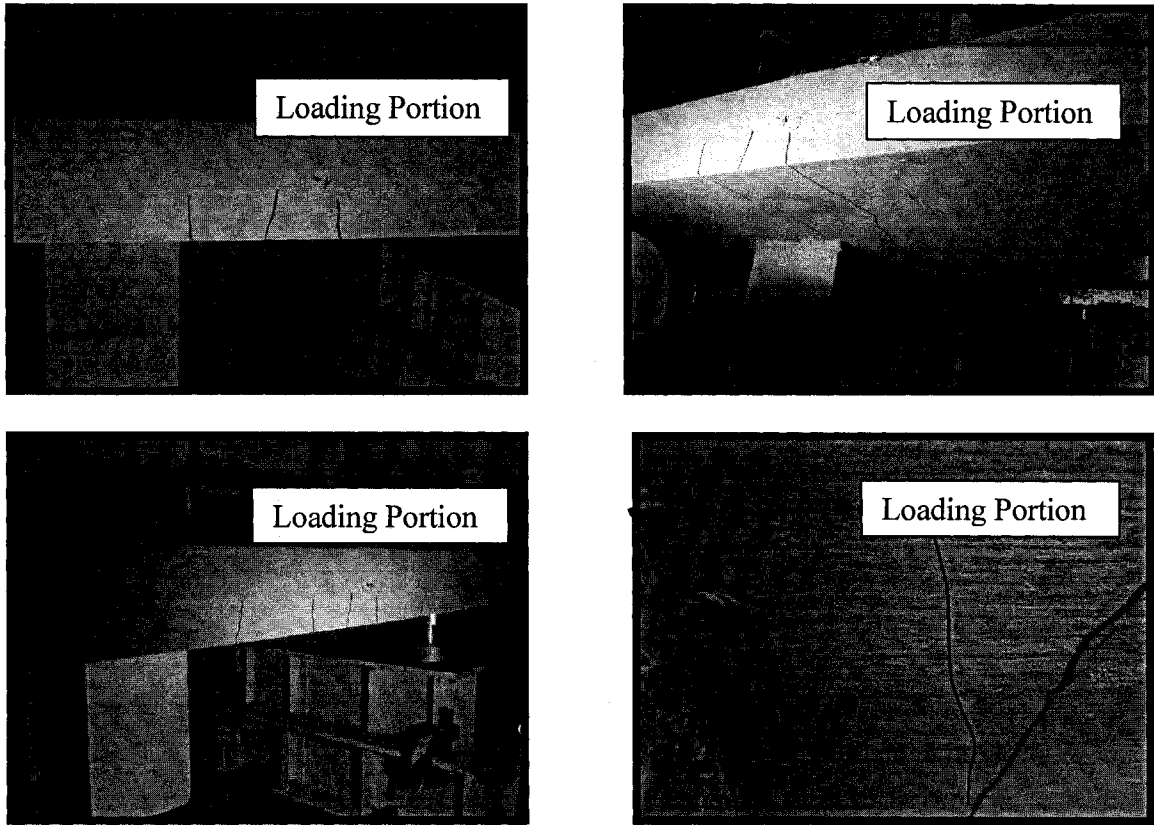
Fig. 4-180: The cracked specimen CRAK35 during different stage of loading
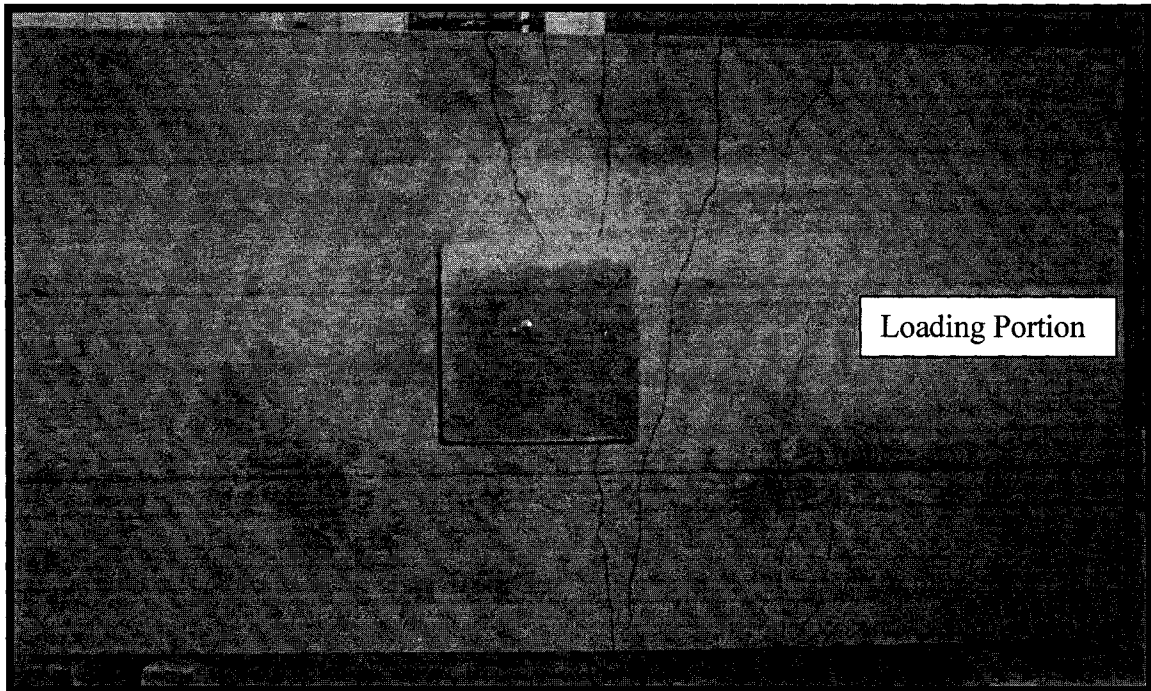
Fig. 4-181: The cracked specimen CRAK35 after failure and transferring

316
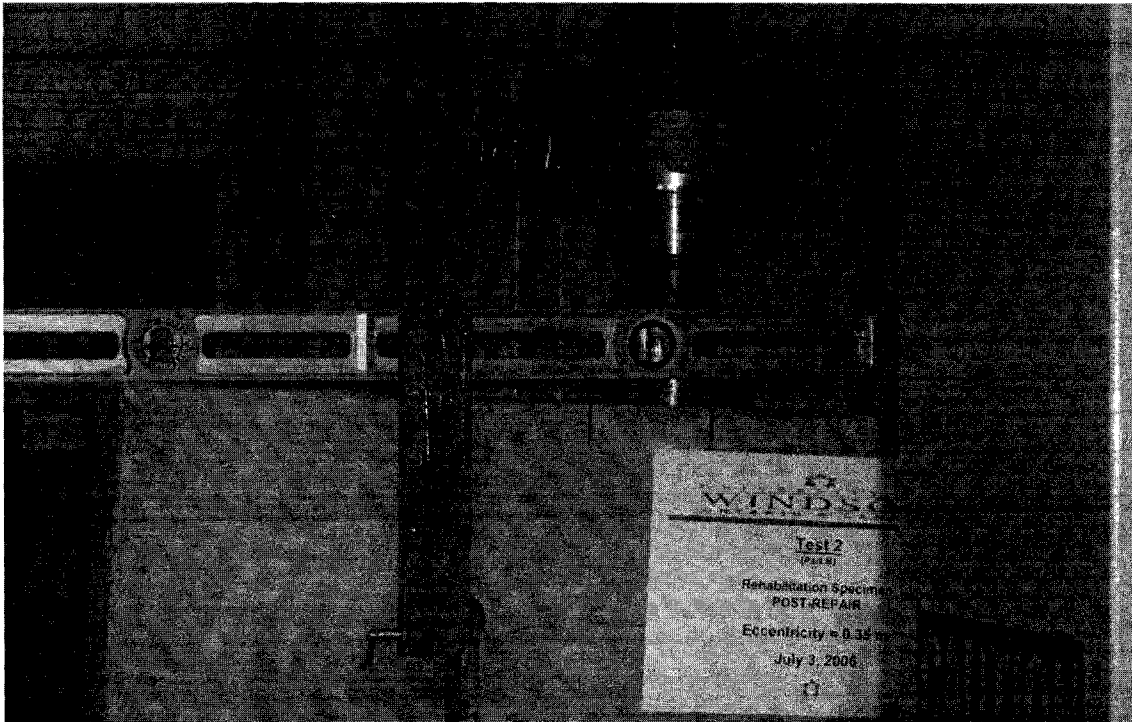
Fig. 4-182: The inclination of the upper part of Rehabilitated specimen
REHB35 before failure
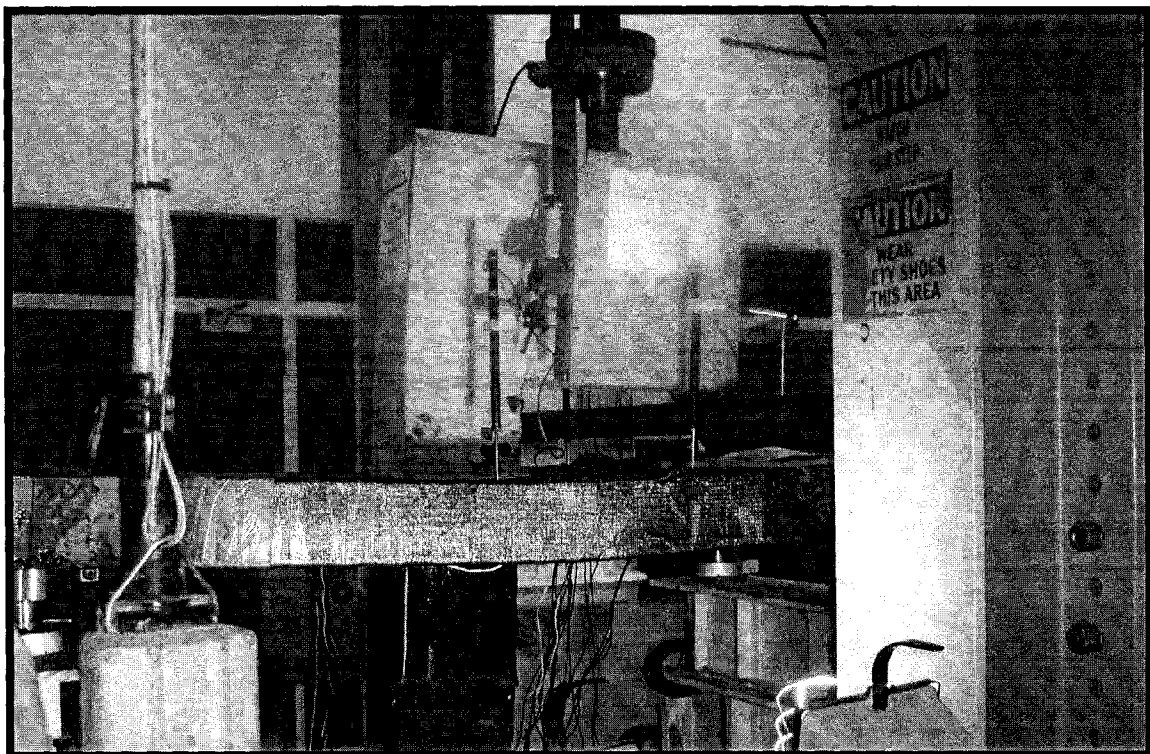
Fig. 4-183: Deflection of the rehabilitated specimen REHB35 before failure

317
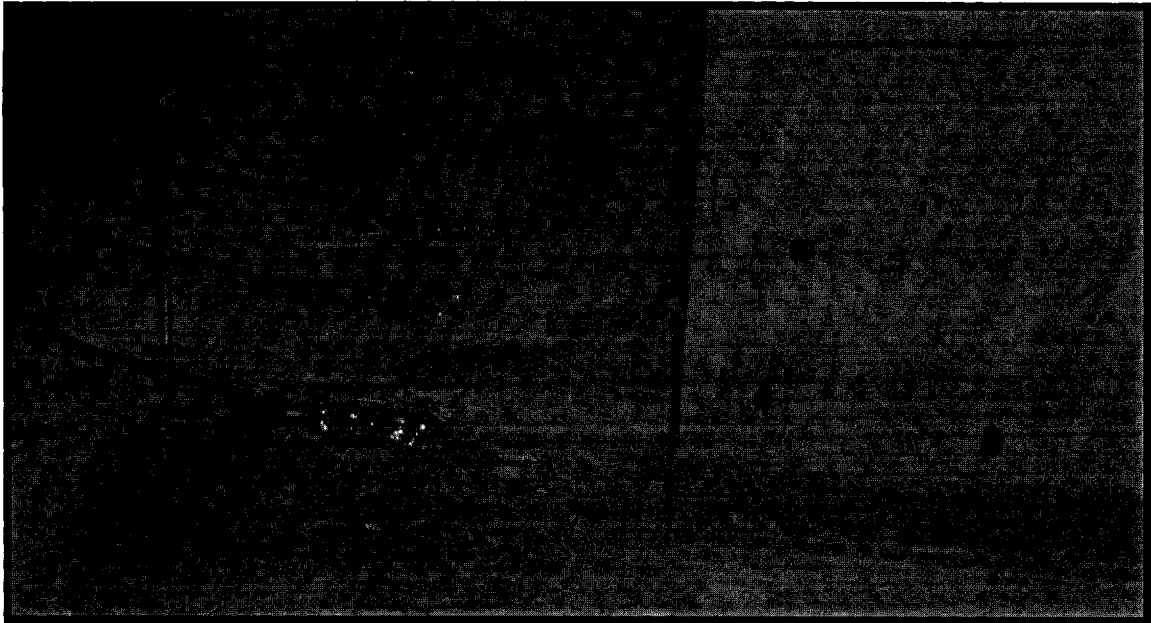
Fig. 4-184: Concrete crushing on the west side of rehabilitated specimen REHB35
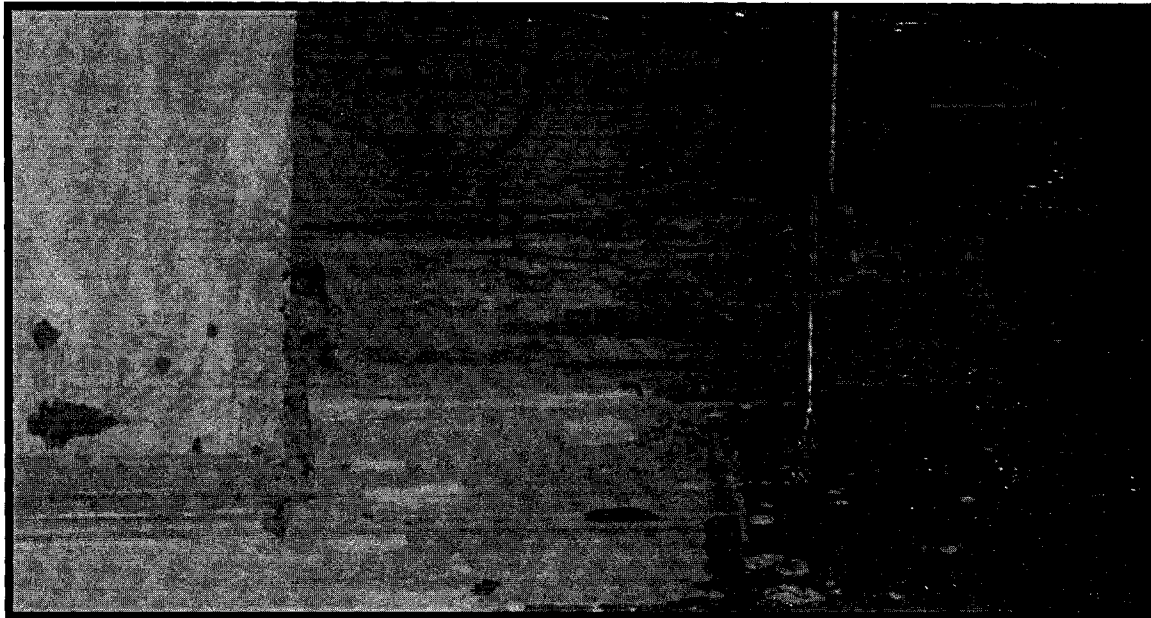
Fig. 4-185: Concrete crushing on the east side of the rehabilitated specimen REHB 35
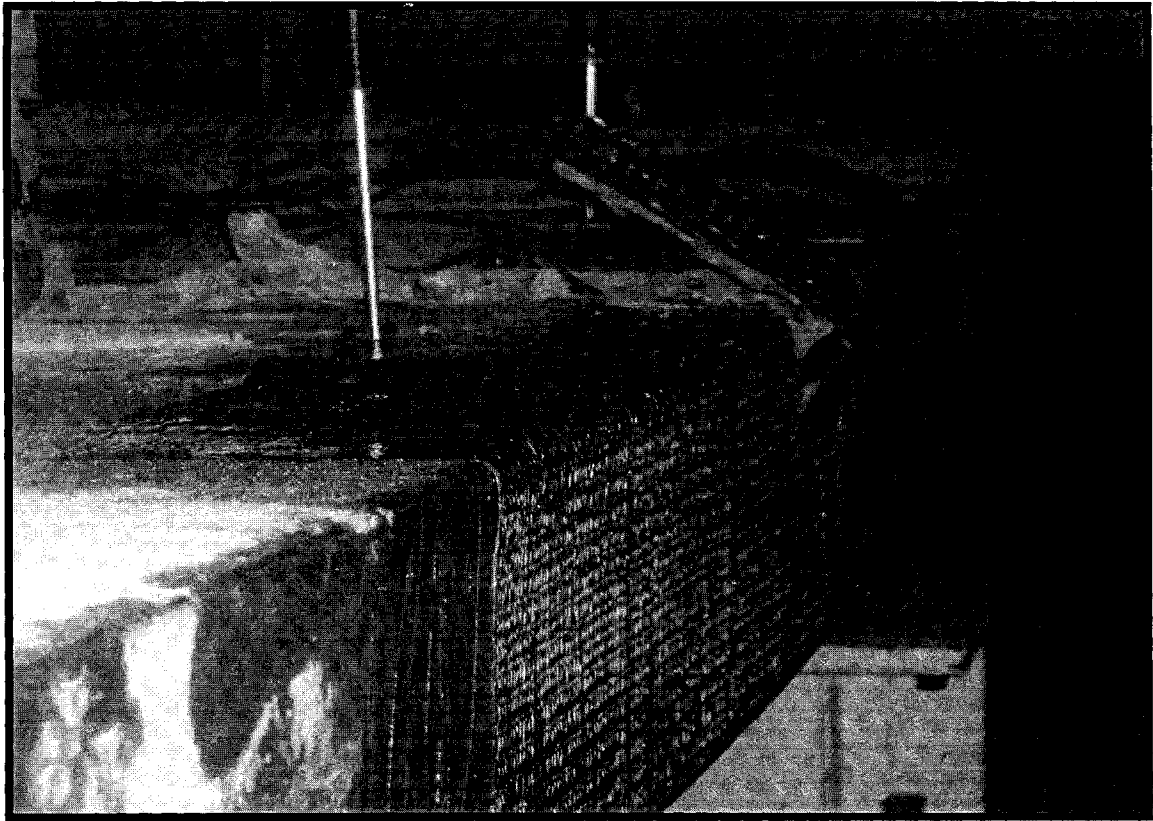
Fig. 4-186: Concrete crushing on the east side of the rehabilitated specimen REHB35
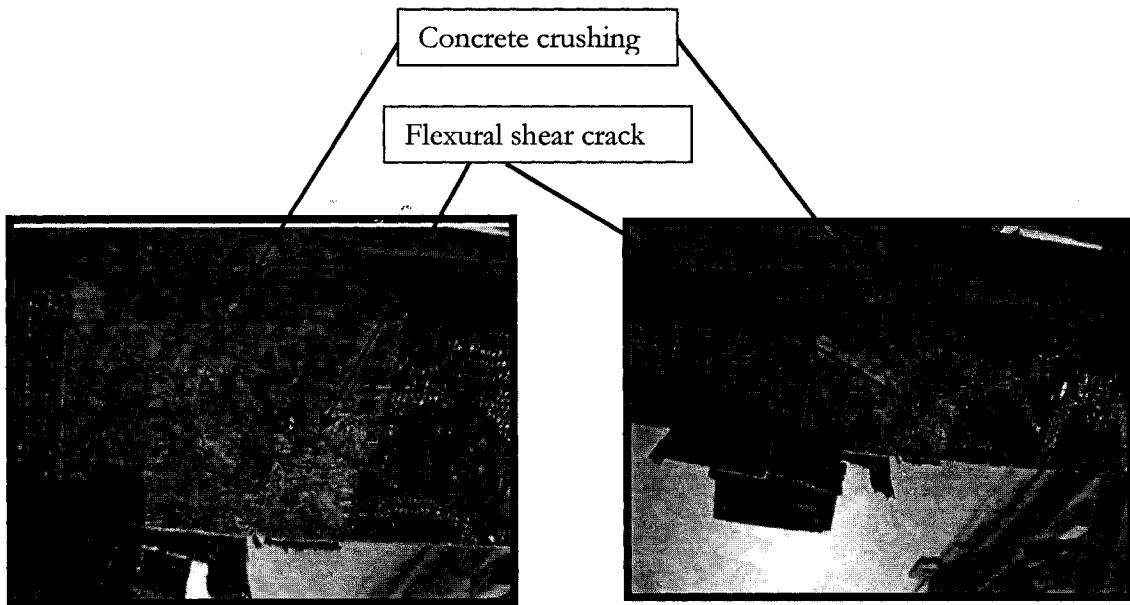
Fig. 4-187: Combination of flexural shear and concrete crushing failure after partial removing CFRP sheet from the east side of the rehabilitated specimen REHB 35

319
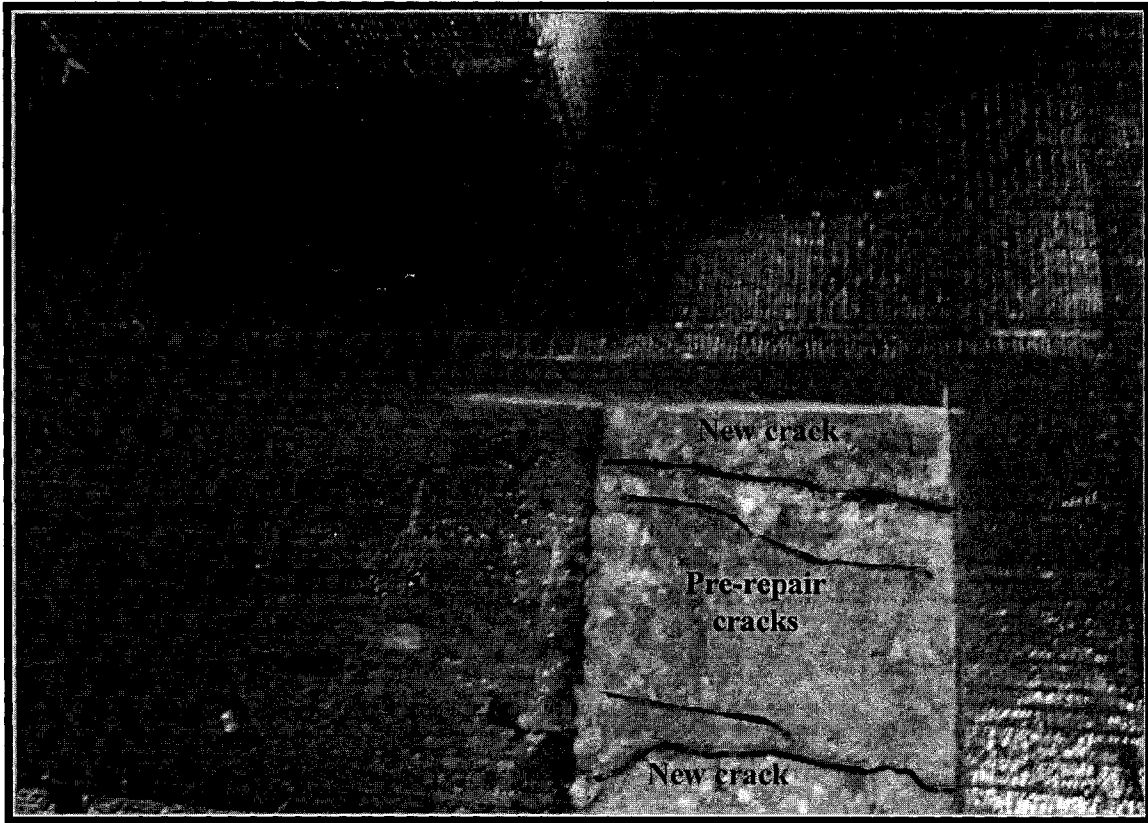
Fig. 4-188: Pre-rehabilitation and post-rehabilitation cracks after releasing the load and partial removing CFRP sheet from the tension zone (bottom surface) of the rehabilitated specimen REHB 35
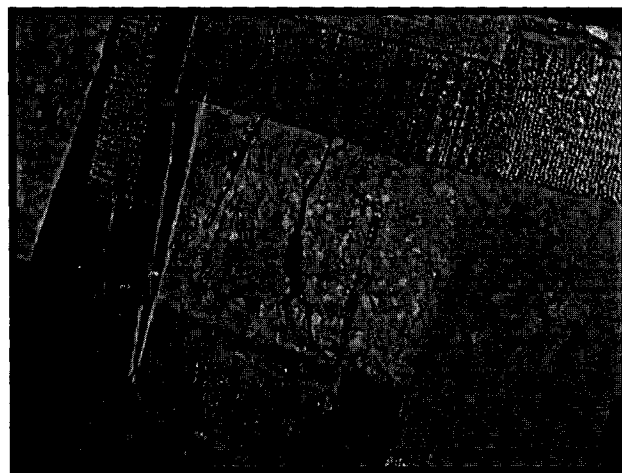
Fig. 4-189: The flexural shear crack after removing the fragile concrete from the surface

320
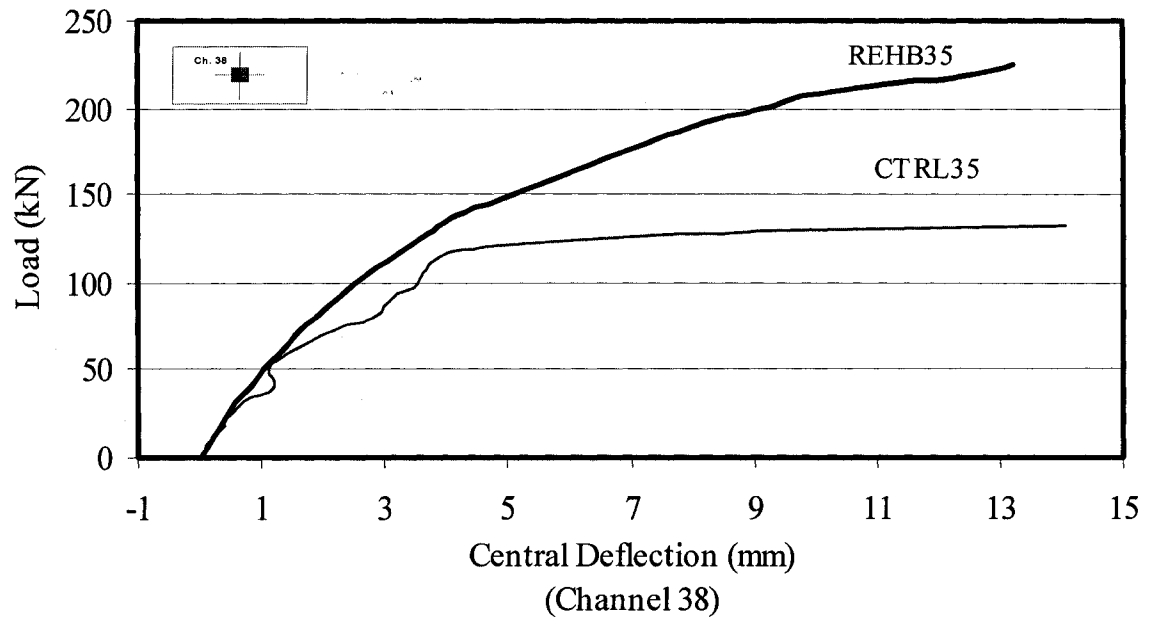
Fig. 4-190: Load versus central deflection for group III specimens (Ch. 38)

321

Axis of zero strain

M   M

y
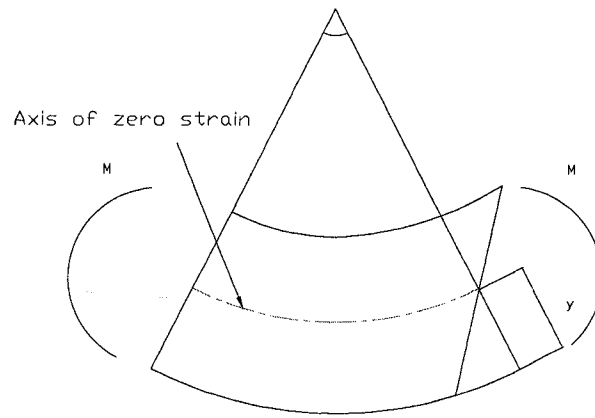
The deformed slab segment

73

58,56   As'

102

114

At yielding load

366

As'

Shifting of N.A
with crack propagation

N.A

40,29

616

1000

At cracking load
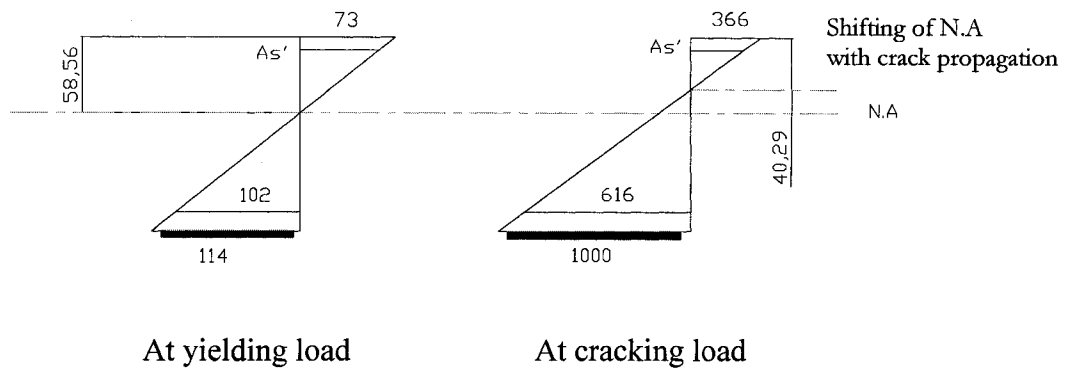
Fig. 4-191: Distribution of strain in the rehabilitated slab (REHB35) with 350 mm

eccentricity

322

CHAPTER V

CONCLUSIONS AND RECOMMENDATIONS

5.1 Conclusions

5.1.1 General

This research is an investigation of the feasibility and the effectiveness of bonding CFRP sheets to the cracked tension surface of a deficient RC flat-plate slab-column connection as a rehabilitation method. The result of six specimens, and nine tests with and/or without CFRP sheets have been reported in details. The purpose of the rehabilitation was to improve the function and performance of the structure, restore and increase the strength and stiffness, improve the appearance of the concrete surface, and improve the overall durability of the structure.

The unidirectional CFRP sheets used as an external tension reinforcing material were successful in restoring and upgrading the load carrying capacity and stiffness of the system. This technique led to a redistribution of the strains and stresses in both concrete and steel reinforcement. The redistribution of the stresses depends on the nature and efficiency of the CFRP bonding with concrete surface.

5.1.2 Conclusions of the experimental and analysis results:

1. Based on the overall evaluation of the test results, the rehabilitation technique proposed using CFRP sheets as tension reinforcement around the slab-column connection area proved to be an effective and competitive rehabilitation technique in increasing the strength and post-cracked stiffness of the flat-plate slab-column connection subjected to monotonic transfer of shear and unbalanced moment.

323

2. Increase in the moment/shear ratio (eccentricity) decreases the cracked load, yielding load, and ultimate load capacity of the system for all specimens. Moreover, the decrease was more evident when the unbalanced moment (eccentricity) was applied compared to the concentrated load than the increase in the degree of eccentricity when the eccentric load was applied.

3. The maximum allowable deflection for rehabilitated specimens was reached at a higher load than the control specimens. These deflections were recorded on the east turn point of the central line for the control and rehabilitated specimens. The percentage of increase of the load corresponding to the allowable deflection at the same position mentioned is 75%, 80%, 61% for group I, II, and III, respectively. Furthermore, and after rehabilitation the deflection at the yield load of the control specimen of each group decreased by 43%, 57%, 42% for group I, II, and III, respectively; and at the ultimate load of the control specimen of each group decreased by 77%, 75%, 67% for group I, II, and III, respectively,

4. The ductility of the structure decreased after the use of CFRP. The experimental results show that the eccentricity has a negative effect on the ductility. The ductility index was decreased by 32%, 34%, and 42% for group I, II, and III respectively.

5. The ultimate load of the rehabilitated specimen increased by an average of 88%. The average concrete and steel strain readings in specimens with CFRP were smaller than in the control specimens throughout all stages of loading. Suggesting that CFRP sheets contributed efficiently in supporting the structure.

5.2 Recommendations for Future Research

1. The experimental investigations reported herein confirmed that the failure mode of rehabilitated structure started with debonding of CFRP sheets at the tension surface followed by flexural-shear failure. Future studies should be concentrated on improving the bonding between CFRP sheets and concrete surface.

2. Further experimental and analytical investigations are needed to examine and verify the effectiveness and suitability of this technique to use with various types of loading like lateral or dynamic loading.

3. The full strength of the CFRP was not fully exploited, and their use was not economical. Further analytical study is required to optimize the design of this composite material.

4. Numerical simulation of such complex structure should give insight on the stress distribution and efficiency of each component. The numerical simulations are ideal tools to optimize designing these structures.

REFERENCES

Abou El-Enein, H. (2004). "*Strengthening Reinforced Concrete Column-Slab Connection Using CFRP Sheets.*" Master's thesis, University of Windsor, Windsor, Ontario, Canada.

ACI Committee 311 (1967). "Manual of Concrete Inspection." Publication SP-2, 167, *American Concrete Institute.*

ACI Committee 352 (1988). "Recommendations for design of slab-column connections in monolithic reinforced concrete structures." *American Concrete Institute* Volume 85, Issue 6.

ACI Committee 318 (1996). "Building Code Requirements for Structural Concrete." ACI 318R-95, *American Concrete Institute*

ACI Committee 440 (1996). "State-of-the-Art Report on Fiber Reinforced Plastic (FRP) Reinforcement for Concrete Structures." ACI 440R-96, *American Concrete Institute.*

ACI Committee 224 (1984). "Causes, Evaluation, and Repair of Cracks in Concrete Structures." Voulme 81, Issue 3, pp.211-230, *American Concrete Institute.*

ACI Committee 224 (1971). "Cracking, Deflection, and Ultimate Load of Concrete Slab Systems." Publication SP-30, 197, American Concrete Institute.

ASTM (2002). "Standard Test Method for Tensile Properties of Polymer Matrix Composite Materials." *Annual Book of ASTM Standards*, ASTM D 3039.

A. Ghobarah & T. El-Amoury. (2005). "Seismic rehabilitation of deficient exterior concrete frame joints." *ASCE Journal of Composites for Construction*, Volume 9, Issue 5, pp. 408-416.

Aiello, M. A. & Ombres, L. (2004). "Cracking and deformability analysis of reinforced concrete beams strengthened with externally bonded carbon fiber reinforced polymer sheets." *ASCE Journal of Materials in Civil Engineering*, Volume 16, Issue 5, pp. 392-399.

Alagusundaramoorthy, P., Harik, I. E., & Choo, C. C. (2003). "Flexural behavior of R/C beams strengthened with carbon fiber reinforced polymer sheets or fabric." *ASCE Journal of Composites for Construction*, Volume 7, Issue 4, pp. 292-301.

Allen, R. T. L., Edwards, S. C., & Shaw, J. D. N. (1993). "The repair of Concrete Structures." Second edition, Glasgow, UK.

Antonopoulos, C. P., & Triantafillou, T. C. (2002). "Analysis of FRP-strengthened RC beam-column joints." *Journal of Composites for Construction*, Volume 6, Issue 1, pp. 41-51.

Arduini, M., & Nanni, A. (1997). "Behavior of precracked RC beams strengthened with carbon FRP sheets." *Journal of Composites for Construction*, Volume 1, Issue 2, pp. 63-70.

Bakis, C. E et al. (2002). "Fiber-reinforced polymer composites for construction---state-of-the-art review." *Journal of Composites for Construction*, Volume 6, Issue 2, pp. 73-87.

Baluch, M. H., Rahman, M. K., & Al-Gadhib, A. H. (2002). "Risks of cracking and delamination in patch repair." *ASCE Journal of Materials in Civil Engineering*, Volume 14, Issue 4, pp. 294-302.

Bianchini, Albert C., Kesler, Clyde E., and Lott, J. L. (1966). "Cracking of reinforced concrete under external load." Causes, Mechanisms, and Control of Cracking in Concrete, ACI, Publication SP-20, Mar., pp. 73-85.

Binici, Baris (2005). "Upgrading of slab-column connections using fiber reinforced polymers." *Journal of Structural Engineering*, Volume 27, Issue 1, pp. 97.

Bischoff, P. H. (2003). "Tension stiffening and cracking of steel fiber-reinforced concrete." *ASCE Journal of Materials in Civil Engineering*, Volume 15, Issue 2, pp. 174-182.

Bizindavyi, L., & Neale, K. W. (1999). "Transfer lengths and bond strengths for composites bonded to concrete." *Journal of Composites for Construction*, Volume 3, Issue 4, pp. 153-160.

Bonacci, J. F., & Maalej, M. (2001). "Behavioral trends of RC beams strengthened with externally bonded FRP." *Journal of Composites for Construction*, Volume 5, Issue 2, pp. 102-113.

Borges, R. F. (2004). "Crack patterns of reinforced concrete slab." *Journal of Composites for Construction*, Volume 8, Issue 3, pp. 229-240.

Branson, D. E. (1977). *"Deformation of Concrete Structures."* Advanced book program, McGraw-Hill international book company.

Brena, S. F., & Macri, B. M. (2004). "Effect of carbon-fiber-reinforced polymer laminate configuration on the behavior of strengthened reinforced concrete beams." *Journal of Composites for Construction*, Volume 8, Issue 3, pp. 229-240.

Brena, S. F., & Macri, B. M. (1965). "Crack width and crack spacing in reinforced concrete members." *Journal ACI*, pp. 1237-1255.

Broms, Fengt B. (1965). "Stress distribution in reinforced concrete members with tension cracks." Journal ACE, pp. 1095-1108.

Buyukozturk, O., & Hearing, B. (1998) "Failure behavior of precracked concrete beams retrofitted with FRP." *Journal of Composites for Construction*, Volume 2, Issue 3, pp. 138-144

Camata, G., Spacone, E., Al-Mahaidi, R., & Saouma, V. (2004). "Analysis of test specimens for cohesive near-bond failure of fiber-reinforced polymer-plated concrete." *Journal of Composites for Construction*, Volume 8, Issue 6, pp. 528-538

Carolin, A., Taljsten, B., & Hejll, A. (2005). "Concrete beams exposed to live loading during carbon fiber reinforced polymer strengthening." *Journal of Composites for Construction*, Volume 9, Issue 2, pp. 178-186

Chahrour, A., & Soudki, K.(2005). "Flexural response of reinforced concrete beams strengthened with end-anchored partially bonded carbon fiber-reinforced polymer strips." *Journal of Composites for Construction*, Volume 9, Issue 2, pp. 170-177

Cheng, J. J. R., Hutchinson, R. & Rizkalla, S. H. (1997). "Rehabilitation of concrete bridges for shear deficiency using CFRP sheets." *International SAMPE Symposium and Exhibition,* Volume 42, Issue 1, pp. 325-335.

Crasto, A. S., Kin, R. Y., Mistretta J. P., & Dougherty, M. (1997). "Rehabilitation of concrete bridge beams with fiber-reinforced composites." *International SAMPE Symposium and Exhibition*, Volume 42, Issue 1, pp. 77.

Cruz,Jose Manuel de Sena, & de Barros,Joaquim Antonio Oliveira. (2004). "Bond between near-surface mounted carbon-fiber-reinforced polymer laminate strips and concrete." *Journal of Composites for Construction*, Volume 8, Issue 6, pp. 519-527.

CSA-A23.3-94. (1995). "Concrete Design Handbook." *Concrete Standards Association*, Ontario, Canada.

DANSK STANDARD (2004), "Repair of Concrete Structures To EN 1504." *Danish Standards Association.* Elsevier Butterworth-Heinemann, Oxford, UK.

Duthinh, D., & Starnes, M. (2004). "Strength and ductility of concrete beams reinforced with carbon fiber-reinforced polymer plates and steel." *Journal of Composites for Construction*, Volume 8, Issue 1, pp. 59-69.

El-Ghandour, A. W., Pilakoutas, K., & Waldron, P. (2003) "Punching shear behavior of fiber reinforced polymers reinforced concrete flat slabs: Experimental study." *Journal of Composites for Construction*, Volume 7, Issue 3, pp. 258-265.

El-Mihilmy, M. T., & Tedesco, J. W. (2000). "Analysis of reinforced concrete beams strengthened with FRP laminates." *Journal of Structural Engineering*, Volume 126, Issue 6, pp. 684-691.

El-Salakawy, E., Soudki, K., & Polak, M. A. (2004). "Punching shear behavior of flat slabs strengthened with fiber reinforced polymer laminates." *Journal of Composites for Construction*, Volume 8, Issue 5, pp. 384-392.

El-Tawil, S., Ogunc, C., Okeil, A., & Shahawy, M.(2001). "Static and fatigue analyses of RC beams strengthened with CFRP laminates." *Journal of Structural Engineering*, Volume 5, Issue 4, pp. 258-267.

Engindeniz. (2005). "Repair and strengthening of reinforced concrete beam-column joints." ACI structural journal , Volume 102 ,Issue 2 , pp. 187.

Fanning, P. J., & Kelly, O.(2001). "Ultimate response of RC beams strengthened with CFRP plates." *Journal of Composites for Construction*, Volume 5, Issue 2, pp. 122-127.

Farhey,Daniel N.; Adin,Moshe A.; Yankelevsky,David Z. (1995). "Repaired RC flat-slab-column subassemblages under lateral loading." *Journal of Structural Engineering*, Volume 121, Issue 11, pp. 1710-1720.

Ferguson, P. M. (1965) "*Reinforced Concrete Fundamentals*" Second Edition.

Francois, R., & Arliguie, G. (1998). "Influence of service cracking on reinforcement steel corrosion." *ASCE Journal of Materials in Civil Engineering*, Volume 10, Issue 1, pp. 14-20.

Francüois Buyle-Bodin. (2004). "Use of carbon fibre textile to control premature failure of reinforced concrete beams strengthened with bonded CFRP plates." *Journal of Industrial Textiles*, Vol. 33, No. 3, pp.145-157 .

George Lubin (Editer) (1982). "*Handbook of Composites*". Sponsored by the Society of Plastics Engineers, Van nostrand reinhold company,

Green,Mark F.; Debaiky,Ahmed S.; Hope,Brian B. (2002). "FRP corrosion rehabilitation of reinforced concrete columns." Canadian research SAMPE Journal, Volume 38, Issue 5, pp. 36.

Harajli, M. H., & Soudki, K. A. (2003). "Shear strengthening of interior slab--column connections using carbon fiber-reinforced polymer sheets." *Journal of Composites for Construction*, Volume 7, Issue 2, pp. 145-153.

Hassan, T., & Rizkalla, S. (2003). "Investigation of bond in concrete structures strengthened with near surface mounted carbon fiber reinforced polymer strips." *Journal of Composites for Construction*, Volume 7, Issue 3, pp. 248-257.

Hassoun, M. Nadim (2002). *"Structural Concrete Theory and Design."* Second Edition, New Jersey, USA.

High-performance Composites. (2006) "Composites technology." Langhorne, PA USA.

Karantzikis, M., Papanicolaou, C. G., Antonopoulos, C. P., & Triantafillou, T. C. (2005). "Experimental investigation of nonconventional confinement for concrete using FRP." *Journal of Composites for Construction*, Volume 9, Issue 6, pp. 480-487.

Kodur V. K. R.Bisby L. A. Green M. F. (2004). "Fire endurance of FRP-strengthened reinforced concrete columns." National Research Council, NRCC-46633, Quebec Canada. p.12.

Lamanna, A. J., Bank, L. C., & Scott, D. W. (2004). "Flexural strengthening of reinforced concrete beams by mechanically attaching fiber-reinforced polymer strips." *Journal of Composites for Construction*, Volume 8, Issue 3, pp. 203-210.

Lee, T., Pan, A. D. E., & Ma, M. J. L.(2004). "Ductile design of reinforced concrete beams retrofitted with fiber reinforced polymer plates." *Journal of Composites for Construction*, Volume 8, Issue 6, pp. 489-500.

Lee, Y. J., Boothby, T. E., Bakis, C. E., & Nanni, A.(1999). "Slip modulus of FRP sheets bonded to concrete." *Journal of Composites for Construction*, Volume 3, Issue 4, pp. 161-167.

MacGregor, J. G., & Bartlett, F. M. (2000). *"Reinforced Concrete Mechanics and Design."* First Canadian Edition, Prentice Hall, New Jersey, USA.

Mailvaganam, N. P. (1991). "Repair and protection of concrete structures." Institute for Research in Construction, National Research Council of Canada, Ottawa, Ontario, Canada.

Mailvaganam, N. P. (2001)."Concrete repair and rehabilitation." Issues and trends. *The Indian Concrete Journal.*

Malvar, L. J., Joshi, N. R., Beran, J. A., & Novinson, T. (2003). "Environmental effects on the short-term bond of carbon fiber-reinforced polymer (CFRP) composites." *Journal of Composites for Construction*, Volume 7, Issue 1, pp. 58-63.

Mansur, M. A., Ahmad, I., & Paramasivam, P. (2001). "Punching shear strength of simply supported ferrocement slabs." *Journal of Materials in Civil Engineering*, Volume 13, Issue 6, pp. 418-426.

Mel M. Schwartz, (1983). *"Composite Materials Handbook."*.

McMullin, P. W., Pantelides, C. P., & Reaveley, L. D.(2003). "CFRP composite connector for concrete members." *Journal of Composites for Construction*, Volume 7, Issue 1, pp. 73-82.

Minoru, K., Toshiro, K., Yuichi, U., & Keitetsu, R. (2001). "Evaluation of bond properties in concrete repair materials." *ASCE Journal of Materials in Civil Engineering*, Volume 13, Issue 2, pp. 98-105.

Moran, D. A., & Pantelides, C. P. (2002). "Stress-strain model for fiber-reinforced polymer-confined concrete." *Journal of Composites for Construction.*, Volume 6, Issue 4, pp. 233-240.

Moran, D. A., & Pantelides, C. P. (2002). "Variable strain ductility ratio for fiber-reinforced polymer-confined concrete." *Journal of Composites for Construction*, Volume 6, Issue 4, pp. 224-232.

Mosallam, A. S. (2000). "Innovative systems for seismic repair & rehabilitation of structure." Design & application, Proceedings of second conference on seismic repair and rehabilitation of structures (SRRS2).

NAHB Research Center, Inc. (2002). "Testing and assessment of epoxy injection crack repair for residential concrete stem walls and slab-on-grade." http://www.quakewrap.com.

Nguyen, D. M., Chan, T. K., & Cheong, H. K.(2001) "Brittle failure and bond development length of CFRP-concrete beams." *Journal of Composites for Construction*, Volume 5, Issue 1, pp. 12-17.

Perkins, P. H. (1997). *"Repair, Protection and Waterproofing of Concrete Structures."* Third edition, Chapman & Hall, London, UK.

Quattlebaum, J. B., Harries, K. A., & Petrou, M. F. (2005). "Comparison of three flexural retrofit systems under monotonic and fatigue loads." *Journal of Bridge Engineering*, Volume 10, Issue 6, pp. 731-740.

Rahimi, H., & Hutchinson, A. (2001). "Concrete beams strengthened with externally bonded FRP plates. *Journal of Composites for Construction*, Volume 5, Issue 1, pp. 44-56.

RSIC, Reinforcing steel institute of Canada (1996). "Manual of Standard Practice." Third ecition, Richmond Hill, Ontario, Canada.

Reis, Elmer E., Mozer, John D., Bianchini, A. C., and Kesler, C. E. (1965). "Causes and control of cracking in concrete reinforced with high- strength steel bars- a review of research." Engineering Experiment Station, Bulletin 479, pp. 1-61.

Robertson, I. N., & Johnson, G. (2004). "Repair of slab--column connections using epoxy and carbon fiber reinforced polymer." *Journal of Composites for Construction*, Volume 8, Issue 5, pp. 376-383.

Roesler, J. R., Lange, D. A., Altoubat, S. A., Rieder, K., & Ulreich, G. R.(2004). "Fracture of plain and fiber-reinforced concrete slabs under monotonic loading." *ASCE Journal of Materials in Civil Engineering*, Volume 16, Issue 5, pp. 452-460.

Saadatmanesh, H., & Malek, A. M. (1998). "Design guidelines for flexural strengthening of RC beams with FRP plates." *Journal of Composites for Construction*, Volume 2, Issue 4, pp. 158-164.

Saiidi, M. S., Sureshkumar, K., & Pulido, C. (2005). "Simple carbon-fiber-reinforced-plastic-confined concrete model for moment-curvature analysis." *Journal of Composites for Construction*, Volume 9, Issue 1, pp. 101-104.

Savoia, M., Ferracuti, B., & Mazzotti, C. (2005). "Creep deformation of fiber reinforced plastics-plated reinforced concrete tensile members." *Journal of Composites for Construction*, Volume 9, Issue 1, pp. 63-72.

Soudki, K., & Sherwood, T. (2003). "Bond behavior of corroded steel reinforcement in concrete wrapped with carbon fiber reinforced polymer sheets." *Journal of Materials in Civil Engineering*, Volume 15, Issue 4, pp. 358-370.

Spadea, G., Bencardino, F., & Swamy, R. N. (1998). "Structural behavior of composite RC beams with externally bonded CFRP." *Journal of Composites for Construction*, Volume 2, Issue 3, pp. 132-137.

Tamuzs, V., & Tepfers, R. (2004). "Strengthening of concrete structures with advanced composite materials: Prospects and problems." *Journal of Materials in Civil Engineering*, Volume 16, Issue 5, pp. 391.

Tan, K. H., & Zhao, H. (2004). "Strengthening of openings in one-way reinforced-concrete slabs using carbon fiber-reinforced polymer systems." *Journal of Composites for Construction*, Volume 8, Issue 5, pp. 393-402.

Tavakkolizadeh, M., & Saadatmanesh, H. (2003). "Repair of damaged steel-concrete composite girders using carbon fiber-reinforced polymer sheets." *Journal of Composites for Construction*, Volume 7, Issue 4, pp. 311-322.

Teng, J. G., Lam, L., Chan, W., & Wang, J. (2000). "Retrofitting of deficient RC cantilever slabs using GFRP strips." *Journal of Composites for Construction*, Volume 4, Issue 2, pp. 75-84.

Thanoon, W., Jaafar, M., Kadir, A., & Noorzaei, J. (2005). "Repair and structural performance of initially cracked reinforced concrete slabs." *Construction building materials*, Volume 19, Issue 8, pp. 595.

Thomsen, H., Spacone, E., Limkatanyu, S., & Camata, G. (2004). "Failure mode analyses of reinforced concrete beams strengthened in flexure with externally bonded fiber-reinforced polymers." *Journal of Composites for Construction*, Volume 8, Issue 2, pp. 123-131.

Tripi, J. M., Bakis, C. E., Boothby, T. E., & Nanni, A. (2000). "Deformation in concrete with external CFRP sheet reinforcement." *Journal of Composites for Construction*, Volume 4, Issue 2, pp. 85-94.

Ueda, T., Yamaguchi, R., Shoji, K., & Sato, Y. (2002). "Study on behavior in tension of reinforced concrete members strengthened by carbon fiber sheet." *Journal of Composites for Construction*, Volume 6, Issue 3, pp. 168-174.

Uomoto, T., Mutsuyoshi, H., Katsuki, F., & Misra, S. (2002). "Use of fiber reinforced polymer composites as reinforcing material for concrete." *ASCE Journal of Materials in Civil Engineering*, Volume 14, Issue 3, pp. 191-209.

Vatovec, M., Kelley, P. L., Alkhrdaji, T., & Nanni, A. (2002). "Evaluation and carbon fiber reinforced polymer strengthening of existing garage." Case study. *Journal of Composites for Construction*, Volume 6, Issue 3, pp. 184-193.

Wang, C., Shih, C., Hong, S., & Hwang, W. (2004). "Rehabilitation of cracked and corroded reinforced concrete beams with fiber-reinforced plastic patches." *Journal of Composites for Construction*, Volume 8, Issue 3, pp. 219-228.

White, T. W., Soudki, K. A., & Erki, M. (2001). "Response of RC beams strengthened with CFRP laminates and subjected to a high rate of loading." *Journal of Composites for Construction*, Volume 5, Issue 3, pp. 153-162.

Wu, Z., Yuan, H., Asakura, T., Yoshizawa, H., Kobayashi, A., & Kojima, Y., et al. (2005). "Peeling behavior and spalling resistance of bonded bidirectional fiber reinforced polymer sheets." *Journal of Composites for Construction*, Volume 9, Issue 3, pp. 214-226.

Yang, X., Wei, J., Nanni, A., & Dharani, L. R. (2004). "Shape effect on the performance of carbon fiber reinforced polymer wraps." *Journal of Composites for Construction*, Volume 8, Issue 5, pp. 444-451.

Zaghloul, A. (2002). *"Behaviour and strength of CFRP reinforced flat plate interior column connections subjected to shear and unbalanced moment."* Master thesis, Carleton University, Ottawa, Ontario, Canada.

VITA AUCTORIS

NAME: Wafa Habib Polies Asmaro

PLACE OF BIRTH: Mosul, Iraq

YEAR OF BIRTH: 1966

EDUCATION: Kourtoba High School, Mosul, Iraq
                              1981-1984

                              University of Mosul, Iraq
                              1984-1988   B.Sc. Science Civil Engineering

                              University of Windsor, Windsor, Ontario
                              2004-2007   M.Sc. Candidate, Science Civil Engineering

335